DEVELOPMENT OF TOOLS TO PREDICT ROCKBURST POTENTIAL USING MICROSEISMIC AND GEOTECHNICAL DATA: A CASE STUDY OF KONKOLA MINE NO.1 SHAFT, ZAMBIA.

By

DONALD CHISHIMBA

A thesis submitted to the University of Zambia in fulfillment of the requirements for the award of the Degree of Doctor of Philosophy in Mining Engineering

THE UNIVERSITY OF ZAMBIA

LUSAKA

2023

COPYRIGHT DECLARATION

DECLARATION

I, Donald Chishimba, declare that the said work was produced by me. I also declare that to the best of my knowledge; this work has never been done or previously been submitted for the award of a degree at the University of Zambia or any other University. All other works done by other researchers have been duly acknowledged and cited.

I, therefore, declare that this thesis was written according to the rules and regulations governing the award of the degree of Doctor of Philosophy at the University of Zambia.

Signed: …….

Date……

CERTIFICATE OF APPROVAL

This thesis of Donald Chishimba has been approved as fulfilling the requirements for the award of the degree of Doctor of Philosophy in Mining Engineering by the University of Zambia.

Supervisor …….

Signature ……

Date …….

Internal Examiner 1 …….

Signature …….

Date …….

Internal Examiner 2 …….

Signature …….

Date …….

External Examiner …….

Signature …….

Date …….

Chairperson Board of Examiners …….

Signature …….

Date …….

ABSTRACT

Since 1995, Konkola Mine No.1 Shaft in Zambia has been experiencing increased seismic activity, leading to more rockburst incidents, which could present significant safety and production challenges at deeper levels.

This study aimed to develop tools to predict rockburst from microseismic and geotechnical data. The specific objectives were to review and compile the global factors or conditions that cause rockburst, determine the site-specific rockburst indicators at Konkola Mine No. 1 Shaft, develop the tools that can be used to predict rockburst potential based on the determined rockburst indicators and validate the predictive tools on rockburst data from other mines.

Seventeen rockburst case histories were collected from different mines around the world and analysed to identify contributing factors to rockbursts. Next, 40 rockburst events captured by the microseismic (MS) monitoring system at the Konkola Mine No.1 Shaft were back analyzed. The 3D modelling software, Leapfrog Geo and Surpac, were used to analyse and visualise the rockburst events and to estimate hypocentral distances from the stopes, respectively.

The study found that the global contributing factors to rockburst included geological structures, mining depth, rockmass strength, stress conditions, mining methods and MS. The analysis results revealed that the mines with an orebody dip of 61^0 to 85^0 had a higher risk of rockbursts. Additionally, the study found that open stoping and cut and fill mining methods had a higher risk of rockbursts than other mining methods.

The study found significant correlations between rockburst at Konkola Mine No.1 Shaft and rock quality designation (RQD), tangential stress (σ_θ), uniaxial compressive strength (σ_c), uniaxial tensile strength (σ_t), linear elastic energy (W_{et}), and principal in-situ stress (σ_1). The results further showed that rockburst patterns were confined by fault zones in the south and north, most rockbursts occurred in excavations within a distance of 0 to 53 m from the ore shale or stopes, and argillaceous sandstone (AGSST), porous conglomerate (PC), footwall sandstones (FWSS), and ore shale (OS) rock types were more susceptible to rockbursts.

The study then developed two rockburst predictive tools (RPTs) to forecast rockburst potential based on geotechnical and MS data. The geotechnical-based RPT used RQD,

σ_θ, σ_c, σ_t, W_{et}, and σ_1, while the MS-based tool used M_L, E, and P factors. Sixteen rockburst cases from a different mine (Mufulira Mine) were used to independently validate the RPTs. The results showed that the MS factor-based RPT had an accuracy of 94 percent, while the geotechnical factor-based RPT had an accuracy of 87.5 percent.

Keywords: Rockburst, geotechnical factors, MS factors, RPT, validation, accuracy

DEDICATION

This thesis is dedicated to my children and wife, my late father and Mum.
To my beloved children, I embarked on this journey to rekindle your determination in your future endeavours.

To my beloved wife, to demonstrate that milestones are achieved either too late or too early, and both bear the benefits. However, the benefits may be different.

To my father and mum, you were my great teachers who trained me to become a valuable model to children and society.

- Donald Chishimba

ACKNOWLEDGEMENTS

I would like to express my sincere gratitude to Dr. Bunda Besa, my main supervisor, and Prof. Emmanuel Chanda, my co-supervisor, for their endless effort and guidance in ensuring that my thesis met acceptable standards, resulting in practical applications for the mining fraternity.

Special thanks go to the technical team at the Konkola Underground Mine and the Institute of Mine Seismology (IMS) for their help and for providing the microseismic database for the Konkola Mine.

I would like to acknowledge Mr. Herbert Kalume, Rock Mechanics Superintendent at Mopani Copper Mines, for providing Mufulira Mine rockburst data and Mr. Charles Mulenga, Geological Officer at Konkola Mine, for assisting me with geological data during the data collection phase.

I am deeply indebted to Konkola and Mopani Copper Mines plc for consenting to use the data for the thesis.

I appreciate the effort of my family and friends for their continuous encouragement and valuable contributions. To my wife, thank you so much for your encouragement and for being with me throughout this challenging undertaking.

Finally, I thank Almighty God for unwaveringly guiding me through this challenging journey and providing me with the light and strength to overcome all obstacles.

TABLE OF CONTENTS

LIST OF TABLES

LIST OF FIGURES

LIST OF APPENDICES

LIST OF ABBREVIATIONS AND ACRONYMS

Abbreviation	Description
AGSST	Argillaceous Sand Stone
AI	Artificial Intelligence
ANN	Artificial Neural Networks
AVM	Automated Valuation Models
BAS	Basement Schist
BC	Basal Conglomerate
BP	Back Propagation
BPI	Burst Potential Index
BSR	Bursting Potential Ratio
CAV	Cumulative Apparent Volume
CSIRO	Commonwealth Scientific and Industrial Research Organisation
DDA	Distance Discriminant Analysis
DRC	Democratic Republic of Congo
DSLAM	Digital-Subscriber-Line-Access-Multiplexer
EI	Energy Index
ERR	Energy Release Rate
ESS	Excess Shear Stress
FSWT	Frequency Slice Wavelet
FWC	Footwall Conglomerate
FWQ	Footwall Quartzite
FWST	Footwall Sand Stone
G_RPT	Geotechnical Based Rockburst Predictive Tool
GRNN	General Regression Neural Network
GRZ	Government Republic of Zambia
GUI	Graphical User Interface
HWA	Hangingwall Aquifer
HWQ	Hangingwall Quartzite
IMS	Institute of Mine Seismology
ISS	Integrated Seismic System
KCM	Konkola Copper Mines Plc
KMRL	Konkola Mineral Resources Ltd

KNN	K- Nearest Neighbor
LDA	Linear Discriminant Analysis
LERD	Local Energy Release Density
LERR	Local Energy Release Rate
LOMP	Life of Mine Plan
LPC	Lower Porous Conglomerate
LR	Linear Regression
MAE	Mean Absolute Error
MCC	Mathews Correlation Coefficient
ML	Machine Learning
MS	Microseismic
MS_RPT	Microseismic Rockburst Predictive Tool
MSE	Mean Square Error
Mtpa	Million Tonnes per year
NB	Naïve Bayes
NetADC	Net Analogy Digital Converter
NetSP	Network Seismological Processor
NN	Neural Network
OS	Ore Shale
PC	Porous Congregate
PNN	Probabilistic Neural Network
RL	Linear Regression
RMR	Rock Mass Rating
RMSE	Root Mean Square Error
RPT	Rockburst Predictive Tools
RQD	Rock Quality Designation
SLOS	Sublevel Open Stoping
SPR	Sill Pillar Recovery
SVM	Support Vector Machine
SWG	Shale With Grit
TRC	Tunnel Classification Chart
UCS	Uniaxial Compressive Strength
URD	Upper Roan Dolomite

LIST OF SYMBOLS

Symbol	Description	Unit of Measure
σ_1	Major principal stress	MPa
σ_2	Intermediate principal stress	MPa
σ_3	Minor principal stress	MPa
σ_c	Uniaxial compressive stress	MPa
σ_t	Uniaxial tensile strength	MPa
σ_θ	Tangential stress	MPa
e	Energy rate	J/s
E	MS energy	J
n	Event rate	n/s
v	Apparent volume	m^3
W_{et}	Linear elastic energy	J/m^3
W_{sp}	Strain energy retained	J
W_{st}	Strain energy dissipated	J

CHAPTER 1: INTRODUCTION

1.1 Chapter Overview

In this Chapter, an overview is provided of the study area's description and location. This includes information on the mineral resources, geological settings, structural geological features and hydrogeological settings. Additionally, the Chapter covers the background of the study, problem statement, research gaps, research objectives, and significance of the study. This chapter also outlines the theoretical framework, scope, limitations of the study, operational definitions as well as the organization of the thesis.

1.2 Description and Location of the Study Area

The primary study case is the Konkola No.1 shaft, located near Chililabombwe on the Zambian Copperbelt at coordinates 12° 22' 46" S and 27° 49' 42" E. The altitude of the site is about 1333 meters above mean sea level. The shaft is south of the border with the Democratic Republic of the Congo (DRC) and approximately 430 km north of Lusaka, the capital city of Zambia (Figure 1.1).

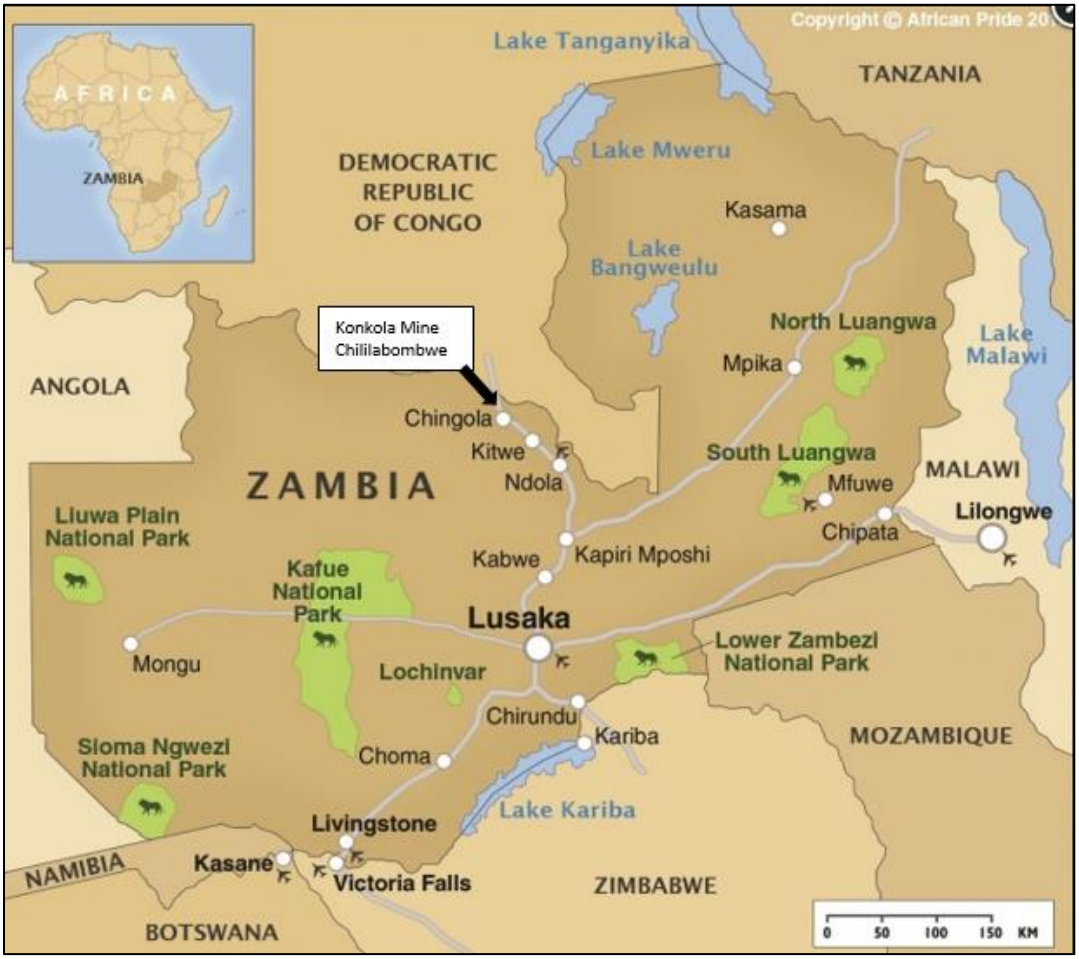

Figure 1.1: Location map of Konkola Underground Mine (Google Earth, 2021)

The mine has been in operation since 1957 (Sakala, 1996). Konkola Minerals Resources Limited (KMRL), a subsidiary of Konkola Copper Mines plc (KCM), is the current owner and operator of the mine. KCM is a major integrated copper producer in Africa and is majority-owned by Vendetta Resources plc, which holds 79.4 percent of shares. The Government of the Republic of Zambia (GRZ) owns the remaining 20.6 percent of shares.

1.2.1 Geological Settings

Konkola Mine No.1 shaft is located on the southern side of the Kirilabombwe Anticline. The orebody is about 9 m thick and dips between 35^0 and 70^0. The Kirilabombwe deposit has two orebodies separated by a barren gap, both traced to a depth of 2000 m. The barren zone, which spans nearly 1.5 km, is continuous below a depth of 720 m from the surface. This renders a strike length of around 10 km of resource at a cut-off grade of one percent Cu. The mineral deposit's strike length at the Konkola mine is approximately 11 km. The orebody is split into two limbs: the North and the West. The North limb and West limb are 3 km and 4 km long, respectively. The Kirilabombwe deposit has 268 mt of mineral resources with an average copper grade of 3.6 percent Cu, reaching depths of 1350 mL at the No.1 shaft in the north limb, 1350 mL for Konkola Flats and Extensions, and 1150 mL for Konkola East at No. 3 shaft in the west limb (as shown in Figure 1.2).

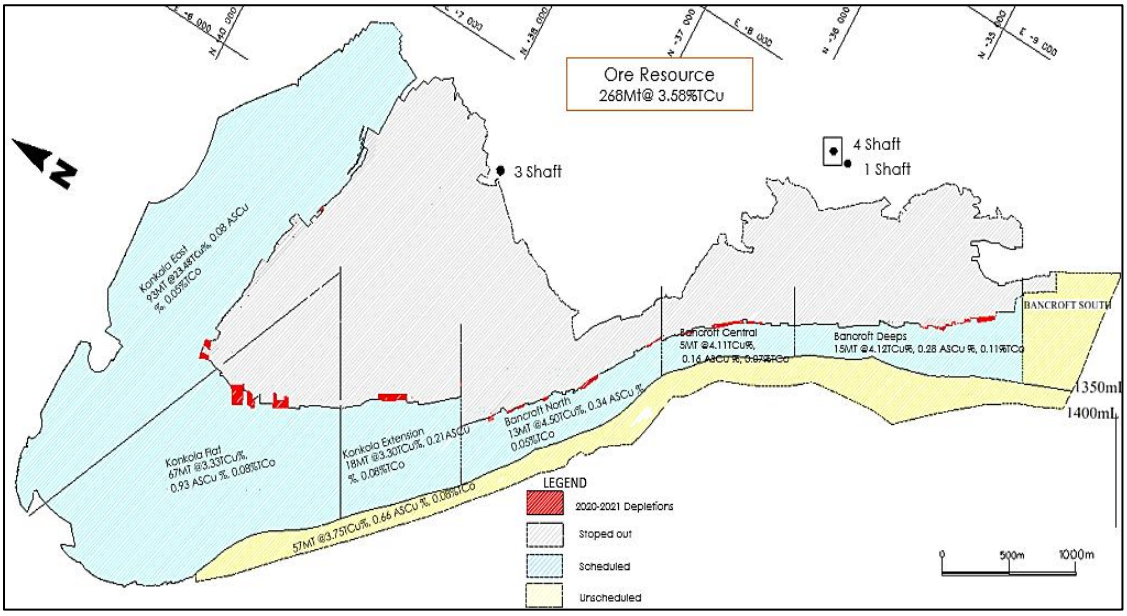

Figure 1.2: Ore resources and reserves at Konkola Mine (Manyika, 2022)

Based on the available ore resources, there are two schedule categories as seen in Figure 1.2. The scheduled areas are the areas that are currently planned and designed as per the life of mine plan (LOMP). Generally, the scheduled areas are primarily above 1350 m

level both on the west and north limbs of the mine. The unscheduled areas lie between the 1350 m and 1400 m levels. The areas also lie above 1350 m level in the Bancroft south. Mineralisations are disseminated in the matrix of the host rock mainly as chalcocite, chalcopyrite, bornite, and carrollite (Sweeney et al., 1986). The rock formations are of sedimentary deposition and some metamorphosed rocks categorised in the Katanga system. The geological setting of the Konkola Mine No.1 Shaft is shown in the Lithostratigraphic table (Table 1.1).

Table 1.1: Konkola Mine No.1 Shaft Lithostratigraphic table

(Modified after Torremans et al., 2012)

Super-Series	**Group**	**Formation**	**Thickness-m**	**Lithology**
Kundelungu	Kundelungu Lower	Kundelungu Shales	Undefined	Shales, minor Dolomite
		Trade-off	250	Limestone Dolomite
Mine series	Upper Roan	Mwanshia Shales	300 - 500	Finely banded and lensed Dolomitic Siltstones and Shales in places, massive Dolomite, Gabbro intrusive Conglomerate and breccia
		URD	100 - 450	Dolomitic interbedded Sandstone and Shale
	Lower Roan	SWG	40 - 165	Siltstone and Grit bands
		HWA	15 - 75	Massive Dolomite at top interbedded siltstones, sandstones
		HWQ	30 - 150	Quartzite with Argillite bands
		OS	5 - 20	Siltstones with carbonate bands
		FWC FWSS PC	20 - 40	Feldspathic Sandstones with Conglomerate bands
		AGSST	400+	Interbedded Argillaceous and Sandstones
		FWQ		
		LPC	30	
		PC	30 - 40	Coarse Quartzite Conglomerate leached and porous at top
		BC	100 - 300	Coarse Boulder Conglomerate
Basement		BAS	Undefined	Schist Granite and Porphyry

Economic copper mineralization is generally restricted to the ore shale formation and adjacent parts of formations above and below the ore shale unit (Torremans et al., 2012). The ore shale has a variable thickness of 5 to 20 m and is divided into five ore horizons (A, B, C, D, and E). Unit A is the lowest geological unit of the orebody with a variable thickness of 0.5 to 1.2 m, which increases with steepening of the dip. It is finely bedded and frequently weathered to brown micaceous clay and is the weakest geological unit of the orebody. Unit A acts as a stress relief valve and sometimes causes rib pillars to breach. The Hangingwall Quartzite (HWQ) formation lying immediately above the Ore Shale degrades to a weak and, in places, Kaolinised band towards the ore shale contact. The propensity for bedding separation because of the tensile zone is higher for thinly bedded, laminated ore shale than the more massive quartzite formation. The stability of the back of stopes is influenced by the characteristics of the hangingwall rock mass remaining in the immediate roof. The permanent structures (shafts and haulages) are positioned in the Footwall formations, as the formations are generally competent. The footwall formations comprise Footwall Conglomerate (FWC), Footwall Sandstone (FWSS), Porous Conglomerate (PC), Argillaceous Sandstone (AGSS), Footwall Quartzite (FWQ), Pebble Conglomerate (PC,) and the Boulder Conglomerate (BC). The basement gneisses and schist formations underlie all these. The main footwall aquiver units are FWC, FWSS, PC and AGSS.

1.2.2 Major Structural Features

The two main fold structures that influence the shape of the Kirilabombwe North and South orebodies are the Kirilabombwe anticline with a Northwest-Southeast trend and the Lubengele fault with an east-west trend crossing the anticline obliquely, as shown in Figure 1.3.

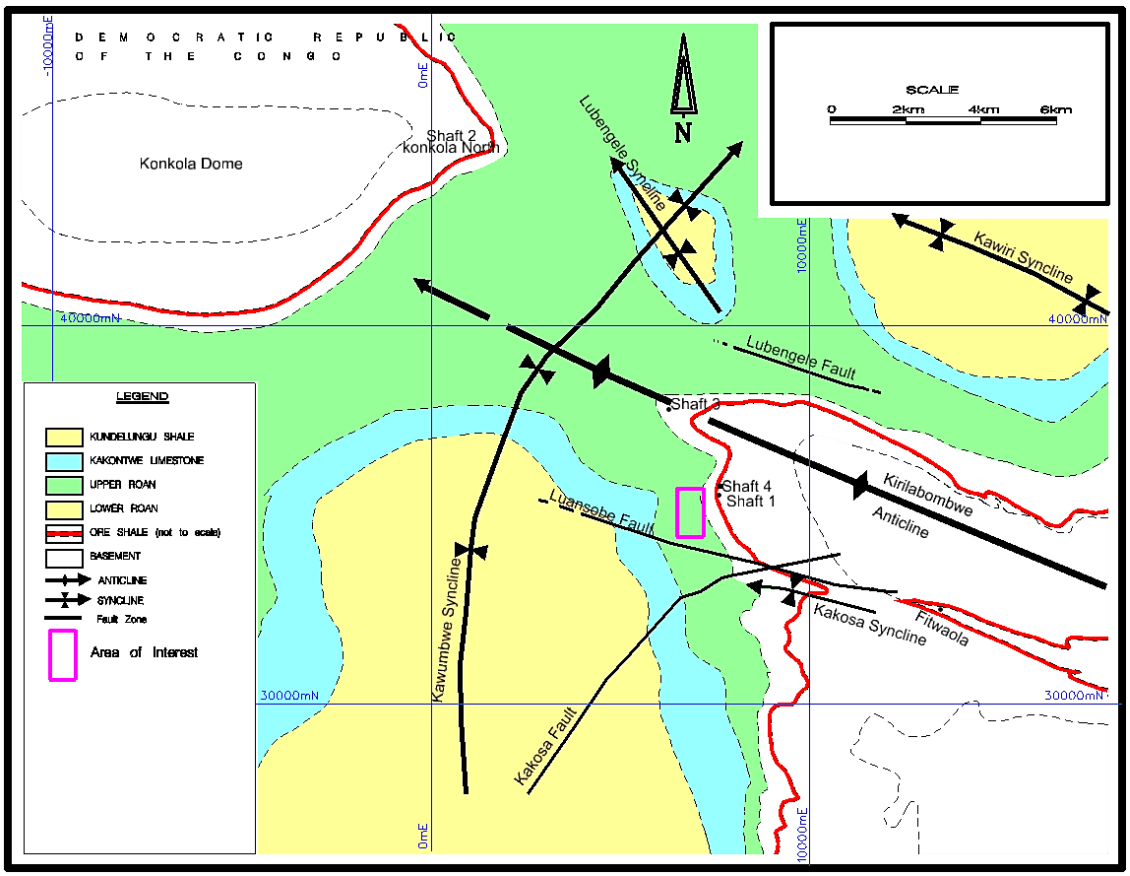

Figure 1.3: Map of structural features associated with the Konkola ore deposit (KMRL, 2019)

A structural saddle is formed by the Kirilabombwe anticline and the Kawumbe syncline between the Konkola and the Kirilabombwe basement (Torremans et al., 2012). The fault zones occur to the north and south ends of the deposit i.e., the Lubengele fault zone, comprising faults dipping 79^0 to the south and the Luansobe fault zone with faults dipping 82^0 to the North (Mulenga et al., 1992). Faults have been identified as major regional structures at No. 1 Shaft. They occur in groups on the southern limb of the anticline, one at 2200 mN and the other at 2700 mN local coordinate system ranging in width from 40 m to 60 m. Each group is bounded by two major fault planes with several secondary faults lying parallel in between. The dip averages 75^0-85^0 to the north, and trends in the east-west direction. The fault openings contain very weak materials of highly weathered to soft clay material, breccia, and angular rock fragments. The disturbance and weakening in the adjacent ground, are more pronounced within the orebody than in the waste footwall formations, making ground conditions within the ore formation unbearable (Katongo, 2004). Within the footwall formations, the fault planes are characterised by sharp edges and are slickensided, with little or no gouge material. In general, the two fault zones are characterised by extensive fracturing and leaching, resulting into weak ground. The rock

mass rating (RMR) in the fault zones range from 25 to 54. Thus, placing of the excavations in these zones can be extremely difficult and challenging. The presence of the pervasive faults at No. 1 Shaft has influenced the setting of the development layouts, stoping sequence, and support conditions within the zones. Where there are numerous displacements, the portion of the ore body was left unmined.

1.2.3 Hydrogeological Settings

Konkola Mine is amongst the wettest mines in the world, pumping about 400,000 m^3 per day. There are three water-bearing horizons at the Konkola Mine property: the Hangingwall aquifer (HWA), the footwall aquifer (FWA) and the lower porous conglomerate (LPC). The HWA is a massive dolomite interbedded by siltstone, sandstone, and dolomite. It provides about 35 percent of the mine's water release (190 000 cubic meters per day) and 70 percent of the No. 3 Shaft's water because of its proximity to the anticlinal structure and the cross fault at 3850 mN location. These features have led to tensional joints and a fissure that connects the dolomitic horizons, the Lubengele fault zone and the Kafue River. Before production can begin, the water table must be lowered below the cave line (65°). This is achieved by drilling dewatering holes. The FWA comprises the footwall conglomerate (FWC), footwall sandstone (FWSS) and porous conglomerate (PC). It accounts for 40 percent of the Mine's water release, both No. 1 and 3 Shafts. It is recharged by underground water systems. The FWA can also be drained off because of its high porosity and permeability. Pilot holes are drilled from the drain drives at a lower elevation than the footwall haulage. Footwall haulages are mined well before production, sometimes about two years in advance, thus providing an effective means of advance dewatering. The pebble conglomerate is not connected to the two aquifers and therefore does not require dewatering.

1.3 Background

In 1995, an unexpected rockburst occurred at Konkola Mine No.1 Shaft, affecting the southern region of the mine from 380 mS to 550 mS (Mutale, 2004). A rockburst is a dynamic failure and instability phenomenon of rock mass, which usually accompanied with violet expulsion of rock fragments from an underground excavation. (Zhao et al., 2020a).

At the time, the mining method employed was sublevel open stoping (SLOS) with mechanised draw points. The active seismic zones were identified as 3150 mL 300 mS and 3150 mL 155 mN, and the seismicity primarily consisted of shakedown events or face

bursts. These events caused more significant damage to crosscuts than to the Orebody and Footwall drives. The sketch to illustrate the crosscuts and the footwall excavations of the SLOS is shown in Figure 1.4.

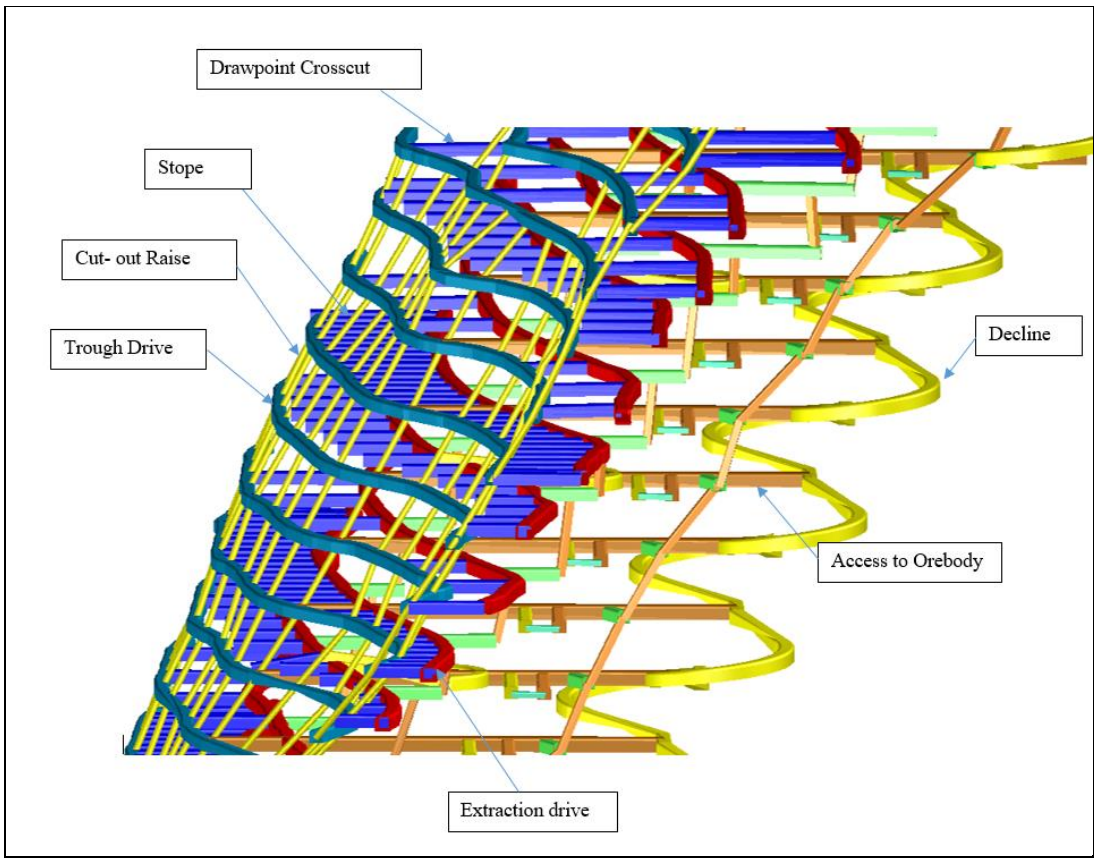

Figure 1.4: SLOS mining layout at Konkola Mine No.1 Shaft

In response, Konkola mine adopted the Integrated Seismic System (ISS) in 1995 to monitor microseismic activity. In 2015, the Institute of Mine Seismology (IMS) system replaced the ISS system because the IMS system provides more detailed seismic data such as the time and location of the event, event magnitude, energy index, apparent volume, potency, and energy ratios.

Mining activities at Konkola Mine No.1 Shaft have progressed to a depth of 1040 mL, with plans to reach maximum depth of 1350 mL. However, there are concerns that mine-induced seismic activity, particularly rockbursts, may become more frequent and pose significant risks to safety and production at greater depths. Therefore, rockbursts resulting from mining-induced seismicity are a significant operational and planning concern at Konkola Mine No.1 Shaft. The seismic activity caused by mining at the mine poses a danger to personnel, equipment, and infrastructure, potentially disrupting production and hindering the achievement of production targets. To address these concerns, a

comprehensive study was needed to develop tools that can help predict rockburst potential using microseismic and geotechnical data at Konkola Mine. Furthermore, these tools could be valuable to other operating mines facing similar potential rockburst problems.

1.4 Statement of the Problem

Konkola Mine No.1 Shaft has been experiencing mining-induced seismicity resulting in rockbursts for more than 20 years. The rockbursts are a significant concern because they threaten the safety of personnel and equipment and negatively impact production. Previously non-seismic regions have now become seismic, with active seismic areas located on the northern sides of the 1020 mL and the 1040 mL between 300 and 500 mN in the Bancroft Deeps. Seismic events, as captured by IMS monitoring system, typically occur slightly above the 1020 mL or below the 1040 mL as shown in Figures 1.5a and 1.5b.

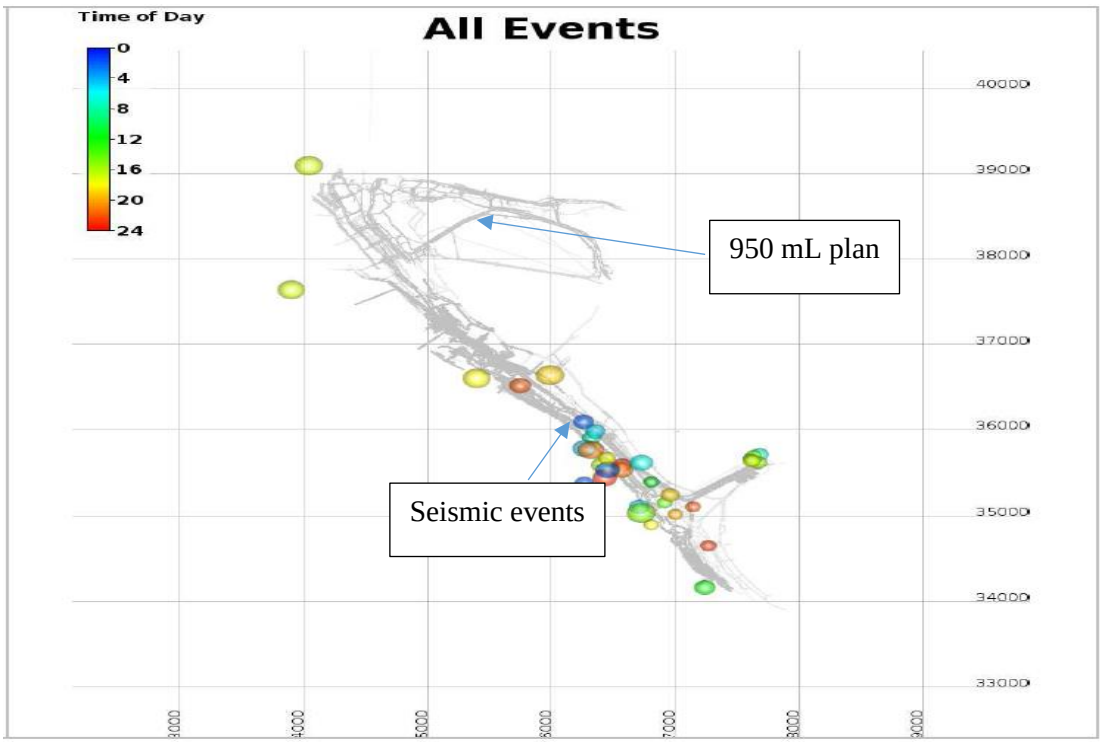

Figure 1.5a: Plan view of 950 mL showing the seismic events

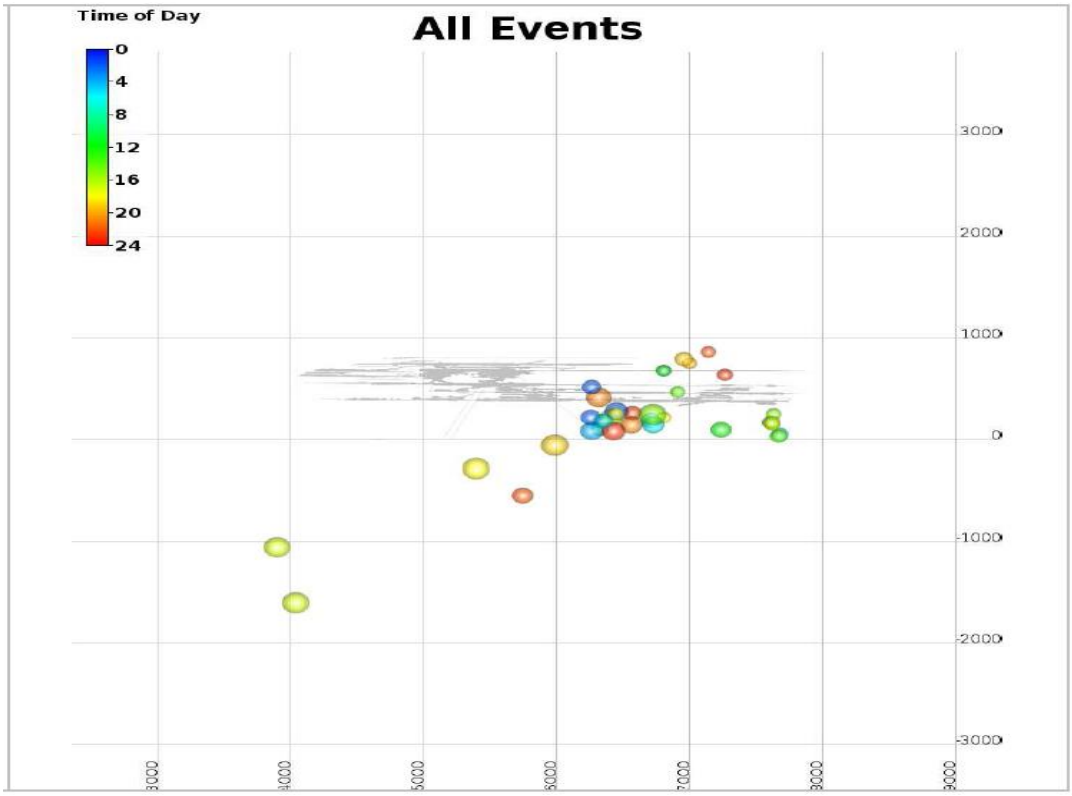

Figure 1.5b: Section view of 950 mL showing the seismic events below 1000 mL and above -1000 mL in the southern portion (Bancroft Deeps) of the Mine

Most of the seismic events are concentrated in the footwall formations comprising ore Shale, Footwall Conglomerate (FWC), Footwall Sandstone (FWSS), Porous Conglomerate (PC), Argillaceous Sandstone (AGSS), and Footwall Quartzite (FWQ). Only a few seismic events occur in the hangingwall formation such as the Hangingwall quartzite (HWQ).

There are also fault zones, within the vicinity, which occur to the north, and south ends of the deposit i.e., the Lubengele fault zone, comprising faults dipping 79^0 to the south and the Luansobe fault zone with faults dipping 82^0 to the North (Mulenga et al., 1992). Faults occur in groups, one at 2200 mN and the other at 2700 mN local coordinate system ranging in width from 40 m to 60 m.

To monitor the seismic events, the mine uses a microseismic (MS) system provided by the Institute of Mine Seismology (IMS). The system consists of three enclosures, each containing four triaxial and one uniaxial 4.5 Hz geophones, resulting in 12 sensors. The 12 sensors are installed on two main levels, 950 mL and 800 mL. The system has been

operating from 2015 to date. From this system, the collected seismic events have been plotted to show the trend as illustrated in Figure 1.6.

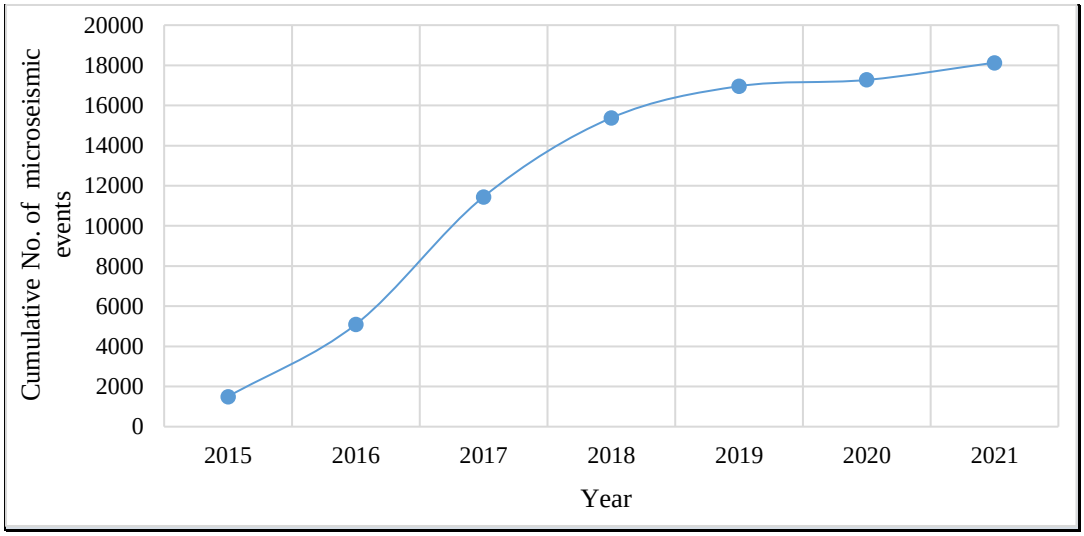

Figure 1.6: Increasing trend of the microseismic events at Konkola Mine No.1 Shaft

Figure 1.6 shows that from 2015 to 2021, the cumulative number (N) of seismic events has increased, highlighting the importance of continuous monitoring and management.

The operations have progressed to 1040 mL with plans to go even deeper to 1350 mL, as illustrated in Figure 1.7.

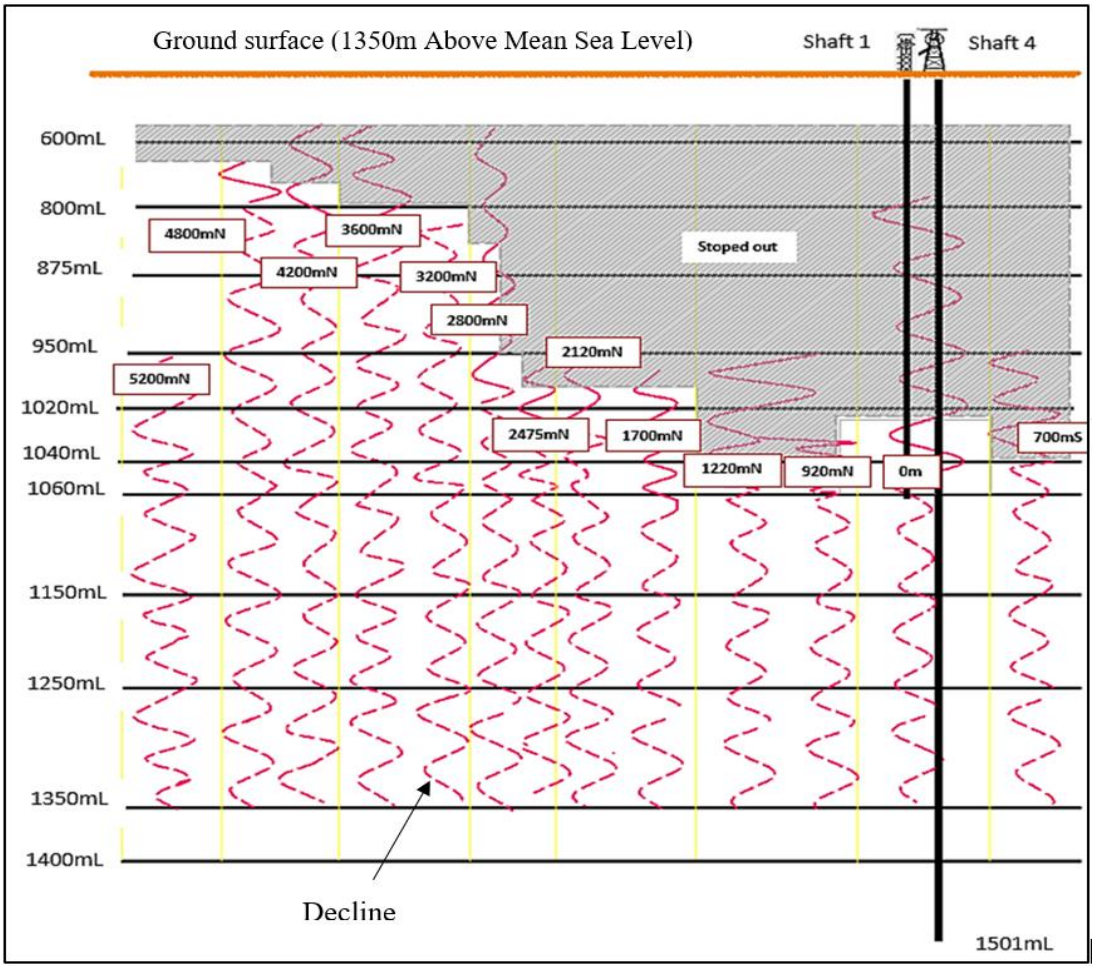

Figure 1.7: Longitudinal profile of Konkola Mine No.1 Shaft

The deeper mining levels could lead to more frequent mine-induced seismic activity based on the increasing trend of the microseismic events at Konkola Mine No.1 Shaft shown in Figure 1.6, posing safety and production challenges. To address these challenges, a study was conducted to develop tools that can predict rockburst potential at the mine based on back analysis and evaluation of previous rockbursts at Konkola Mine No.1 Shaft.

1.5 Research Gaps

Previous studies on the rockburst predictions conducted by various researchers are discussed in detail in Section 2. Table 1.2 summarizes prediction studies conducted at construction and underground mine sites

Table 1.2: Previous studies on the rockburst predictions

Authors	Location	Rockburst indicator	Prediction model
Hoek and Brown, 1980	-	Unconfined compressive strength, tensile strength, major principal stress	Empirical model
Pu et al., 2018a	Kimberlite underground Mine	Uniaxial compressive strength, uniaxial tensile strength, tangential stress, the elastic energy index	Decision Tree
Feng et al., 2019	Jinping hydropower project (China)	Cumulative number of MS events (N), cumulative MS energy (E), Cumulative MS apparent volume (V)	Optimised Probabilistic Neural Network (PNN)
Zeng et al., 2019	Qamchiq tunnel project	maximum tangential stress, rock uniaxial compressive strength ($\sigma_{c)}$, rock Brittleness coefficient, the uniaxial tensile strength of rock, the grade of groundwater condition, rock integrity coefficient	Back propagation (BP) Neural Network
Zhang et al., 2020a	Water diversion tunnels of Jiangbian hydropower station and Jinping secondary hydropower station (China)	Uniaxial compressive strength, stress coefficient, brittleness coefficient, elastic energy index, and integrity of rock mass	Comprehensive Weight and Extension methods
Ke et al., 2021	Underground projects	The maximum tangential stress, elastic energy index, uniaxial tensile stress	Naïve Baye (NB)
Liu et al., 2021	The Ashele Copper Mine (China).	Geological condition (lithology and geo-stress), mining process, microseismic data.	Cloud model
Farhadian, 2021		Tangential stress, elastic energy index (W_{et}), uniaxial compressive strengths	The Tunnel rockburst classification chart (TRC)

Table 1.2 displays various models and indicators, including artificial intelligence (AI) and empirical models. Indicators are classified into three categories: rock mechanical properties, stress, and microseismic factors. The mechanical properties include uniaxial compressive strength (σ_c), tensile strength (σ_t), and rock brittleness coefficient. Stress factors include tangential stress (σ_Θ) and geo-stress, while energy factors comprise the elastic energy index and microseismic (MS) energy. Identifying rockburst descriptive parameters is challenging due to hidden geological conditions.

To predict rockbursts successfully, it is necessary to forecast their time, location, and severity. While rockburst magnitude and location can be predicted, timing is tricky without a correlation between rockburst events and time. Predictive models analyse current and historical data, projecting what they learn onto a generated model to forecast likely outcomes, which makes time prediction even more challenging.

Previous studies on rockburst predictions used indicators developed at mines or construction sites that may not accurately reflect the conditions at the Konkola Mine No.1 shaft. Rockburst predictive models are complex and require site-specific determinations, so only a few studies have used a combination of indicators. To address this, the author analysed rockburst events at the Konkola No.1 Shaft Mine using a microseismic (MS) monitoring system to identify site-specific indicators. Each rockburst event was analysed to determine the geotechnical and MS site-specific factors.

From the studies represented in Table 1.2, no simple tools have been developed to predict the rockburst potential using geotechnical and microseismic data. To fill this gap, the author developed tools that use geotechnical and microseismic data to predict the likelihood of rockbursts at the mine. These tools, called Rockburst Predictive Tools (RPTs), were developed at Konkola and tested using external geotechnical and MS data from other rockburst-prone mines. Mufulira mine was the focus of the validation process because it has similar geological and geotechnical settings to Konkola mine, which helped to validate the models.

1.6 Main Research Objective

The main objective of this study is to develop tools to help predict rockburst potential based on microseismic and geotechnical data.

1.6.1 Specific Research Objectives

The specific objectives of this study are as follows:

- To review and compile the global factors or conditions that cause rockburst;
- To determine the site-specific rockburst indicators at Konkola No. 1 shaft;
- To develop the tools that can be used to predict rockburst potential based on the determined rockburst indicators; and
- To validate the predictive tools on rockburst data from other mines.

1.6.2 Research Questions

The fundamental research questions are:

- What are the conditions or factors that lead to rockbursts?
- What are the main evaluation indices for rockburst prediction?
- What methods or approaches are used to predict the potential rockbursts?
- What are the various methods or techniques that are used to validate the predictive models?

To answer these questions, first a thorough and comprehensive review of existing literature was conducted. The review delved into the factors and conditions that trigger rockbursts, the principal criteria utilised for evaluating rockburst prediction, the techniques or methods employed to forecast potential rockbursts, and the different approaches used to validate the predictive models.

1.7 Significance of the Study

The author created reasonable tools for predicting rockburst potential at Konkola Mine. These tools can assist in implementing site-specific measures to minimize rockburst risks, enhancing mining efficiency and operational safety. Furthermore, this study has added to the existing academic body of knowledge on rockburst prediction.

1.8 Theoretical Framework

This study utilised established theoretical frameworks to select parameters for developing rockburst prediction tools based on previous research and analyses of rockburst phenomena and predictive models.

To select parameters for developing rockburst prediction tools, the researcher used established theoretical frameworks cited by Dou et al., (2014) in their research titled, 'Research progress of monitoring, forecasting, and prevention of rockburst in underground coal mining in China.' These frameworks included energy theory (Cook, 1965), stiffness theory (Petukhov and Linko, 1979), strength theory (Li, 1985), rockburst tendency theory (Kidybinski, 1981), three-criterion theory, and system deformation stability theory (Zhang, 1987). The study also used other methods used, including energy methods such as the Elastic strain energy index (Kidybiński, 1981), Seismic energy (Spottiswoode and McGarr (1975), stress methods that included rock brittleness coefficient (Qiao and Tan, 1998), tangential stress criterion (Wang et al., 1988; Hoek and Brown, 1980), Russenes method (Russeness, 1974) and strength method (Hawkes, 1966).

The author utilised these theories to establish a strong base of fundamental concepts and current trends in the field, enabling the collection of critical parameters, data analysis, and interpretation of findings.

1.9 Scope and Limitation of the Study

Many researchers have explored rockburst, as evidenced by the extensive literature on the subject. This study specifically aimed to create tools that could reasonably predict the likelihood of a rockburst at the Konkola Mine No. 1 Shaft. The development of these predictive tools relied on historical data regarding previous rockburst incidents. The study identified factors contributing to rockburst and developed the tools to predict rockburst potential at the Konkola Mine. To test the predictive tools (RPTs), the author utilised data from other mines with a well-documented rockburst history. The research focused on Konkola Mine No.1 Shaft underground mine.

1.10 Operational Definitions

The definitions of the key terms used in this study:

Accuracy:	A performance metric refers to the percentage of correct predictions for test data. It can be calculated by dividing the number of correct predictions by the total number of predictions.
Predictive tool:	A technique used to forecast likely potential outcomes using historical and existing data. It works by analysing current and historical data to forecast likely outcomes.
Rockburst:	A dynamic failure and instability phenomenon of rock mass, which usually accompanied with violet expulsion of rock fragments from an underground excavation. (Zhao et al., 2020a).
Validation:	Part of the model development process that is undertaken in order to ensure that the model developed is sufficiently accurate for the purpose at hand (Tsioptsias et al., 2016).

1.11 Thesis Organisation

The thesis is organised into seven chapters as follows:

Chapter 1 discusses the study area, including mineral resources, geological settings, and structural geological features. It also covers the background to rockburst, problem statement, research gaps, research objectives, significance of the study, theoretical framework, scope and limitations of the study, operational definitions, and thesis structure.

Chapter 2 comprehensively reviews the rock burst phenomenon, including its contributing factors, evaluation criteria, prediction methods, and an overview of the validation methods used to test predictive models. Chapter 2 concludes by summarising the extensive research and identifying the areas or gaps where further research is needed.

Chapter 3 presents the methodology used to achieve the research objectives. The method covers research philosophy, research type, research strategy, research design, sampling, data collection, data analysis, limitations of the research and ethics.

Chapter 4 presents the analysis and the results of the gathered data. The study's objectives, including reviewing the rockburst case histories from other mines to determine contributing factors and determination of site-specific rockburst indicators at the Konkola No.1 Shaft mine, were addressed. Additionally, a summary of the data analysis and the results is provided.

Chapter 5 focuses on the last two objectives of the study, including developing tools to predict rockburst potential using microseismic (MS) and geotechnical factors, validating, and testing the predictive tools with rockburst data from Mufulira Mines.

Chapter 6 discusses the results of the significant contributing factors established through data analysis. A discussion summary is presented as an epilogue to this chapter.

Chapter 7 provides a compressive summary of the research study’s findings, including its conclusion, limitations, and recommendations for future research and contributions of the study to the field.

Five appendices are included in the thesis to store study-generated data and enhance readability.

CHAPTER 2: LITERATURE REVIEW

2.1 Introduction

Chapter 2 provides an overview of the rockburst phenomenon, the conditions or the factors that contribute to rockburst phenomenon, rockburst classification and source mechanisms, factors contributing to rockburst.

The indices that are used to evaluate the rockburst potential as well as classification of rockmass damage severity are presented.

Three methods or techniques that are used to predict the rockburst potential are reviewed. The methods that are used to validate the models and, the metrics that are used to evaluate the performance of the models are reviewed. The chapter ends with a summary of the literature review and significant findings.

2.2 Rockburst Phenomenon

Many scholars have defined rockburst differently, as illustrated in Table 2.1. Javed et al., (2019) observed that there is no precise and unified definition of a rockburst in the research community. Moreover, scholars have varying definitions of rockburst.

Table 2.1: Definitions of rockburst

Definition	Source
Mining activities induce a particular manifestation of seismic activity.	Brown ,1992
Damage to an excavation that occurs suddenly and violently and is associated with a seismic event.	Hedley, 1992; Kaiser et al., 1996
A seismic event that causes violent and significant damage to tunnels or excavations of a Mine.	Ortlepp,1997
A kind of sudden dynamic failure and instability phenomenon of rock mass, which usually associated, with violet expulsion of rock fragments from the surface of underground excavations.	Zhao et al., 2020
A dynamic rock mass failure occurring during underground mining under unfavourable stress conditions.	Wojtecki et al., 2021.

Rockbursts are a significant risk to mining operations because they can damage the mine's infrastructure and equipment, cause worker injuries, or even fatalities (Zhou and Wang, 2017; Cai and Kaiser, 2018). Rockbursts can be triggered by various factors, such as

distant seismic events, load transfers, or the failure of the rock mass itself (Gill and Aubertin, 1994). As mining depth and underground construction increase, stress-induced failure processes become more common near excavations and deep inside the rock mass (Kaiser, 1996; Javed et al., 2019). These failures can cause seismic events, slip along weak planes (e.g., faults) or a shear rupture, and strainburst damage to the excavations. Rockbursts can result from deep-seated rock mass failure, excavation failure, or a combination of these mechanisms.

Rockbursts typically occur in rock formations that are stiff, brittle and highly stressed. Therefore, understanding the stress distribution around underground mining excavations is crucial in predicting and preventing rockbursts. The theory of elasticity can be used to study the induced stresses and their impact on rockbursts in underground mines.

2.2.1 Mines with Rockburst Potential

Table 2.2 lists some of the mines that are at risk of rockbursts, with mining depths exceeding 900 m below the surface. On the other hand, Table 2.3 provides a list of countries with recorded rockburst events (Pu et al., (2018).

Table 2.2: Mines with rockburst potential

Mines	Depth below surface	Source
Mines in Australia	1000 m and 1650 m	Hudyma & Potvin, 2010
Canadian Mines	between and 2500 m	
Kolar gold (India)	Greater than 2400 m in depth	Wen et al., 2016
Iron ore field of Krivoy Rog (Russia)	Between 910 m and 1570 m	Wen et al., 2016
Mine in South Africa	3000m to 3800 m	Liu et al., 2018a
Konkola Mine No.1 Shaft (Zambia)	Between 900 m and 1040 m	Katunansa, 2021

Table 2.3: Mining countries with records concerning rockburst events (Pu et al., 2018).

Country	Source
Australia	Potvin et al., 2000
Canada	Blake and Hedley, 2003
Germany	Baltz and Hucke, 2008
South Africa	Gibowicz, 2009
China	Qiang et al., 2005; Li et al., 2016

According to Wu et al., (2022), the rockburst at the Altenberg tin mine in Germany in 1640 may be the earliest catastrophic rockburst, which resulted in shutting down of the mine for many years. In Canada, rockbursts have occurred in many Mines, including the Brunswick

lead–zinc Mine at Bathurst, the Lake Shore Mine, the Teck-Hughes Mine, the Wright-Hargreaves Mine, the Falconbridge nickel mine and the Macassa gold Mines at Kirkland Lake (Keneti and Sainsbury, 2018). From 1996 to 2003, rockburst was the second leading cause of fatal accidents in South Africa (Durrheim et al., 1998

2.3 Rockburst Classification

Rockburst was first classified in 1950 based on its origin (Colson, 1950). Russenes (1974) proposed a classification system based on the severity of the rockburst, which categorized it into four groups: none, weak, moderate, and severe. Hedley (1992) also proposed a classification system, dividing rockburst into three groups: inherent, induced, and fault-slip burst. However, this classification system has significant disadvantages because it does not adequately consider the geomechanical nature of rockbursts and cannot describe the rockburst process mechanism. Ortlepp and Stacey (1994) classified rockbursts into five groups based on the source and damage mechanisms. They categorized rockbursts based on the source mechanisms, which include first motion from seismic records and Richter magnitude. The five categories include strain bursting, buckling, face crush, shear failure and Fault – slip (Table 2.4).

Table 2.4: Classification of rockburst proposed by Ortlepp and Stacey (1994)

Seismic event	**Postulated source mechanism**	**First motion from seismic record**	**Richter magnitude, M_L**
Strain bursting	Spalling rockburst with a severe ejection of fragments	Usually undetected, it could be implosive	- 0.2 - 0
Buckling	Outward expulsion of pre-existing larger slabs parallel to the opening	Implosive	0 - 1.5
Face crush	Violent expulsion of rock from the tunnel face	Implosive	1.0 - 2.5
Shear failure	Violent propagation of shear fracture through the intact rock mass	Double-couple shear	2.0 - 3.5
Fault - slip	Severe renewed movement on existing fault	Double - couple shear	2.5 - 5.0

The classification of rockbursts divides them into five classes, with the first three classes (strain bursting, buckling, and face crush) having coincident locations and sources of

damage. However, the last two classes involve a shear failure on a plane that could reach hundreds of meters. This classification is beneficial because it clearly defines the type of rockburst based on the energy source and damage mechanisms (Zhou et al., 2018).

The energy source for a rockburst can be either the stored elastic energy in the rock or a seismic event. The location and source of damage may either coincide or not. When they coincide, a rockburst happens in an area where energy was stored. On the other hand, when they do not coincide, the energy that triggers the rockburst may originate from a seismic event. In such a case, the hypocenter's source may be some distance away from the damage location (Askaripour et al., 2022).

Rockbursts, a sudden and violent failure of rock, can be classified based on different mechanisms and their intensity. Kaiser et al., (1996) proposed a classification based on self-initiated and remotely triggered mechanisms, dividing rockbursts into minor, moderate and major groups. Tang (2000) classified rockbursts into three major types: strainburst, fault-slip burst, and the combination of the two mechanisms. Misich and Lang (2001) defined a classification based on the time between the unloading and the start of the rockburst. Kaiser (2009) proposed another classification based on the mechanisms of strainburst slip burst and pillar burst. He et al., (2015) classified rockbursts into two main types: strainburst and pillar burst, which occur in a high-stress environment, and fault-slip burst, which occurs in major geological structures far away from the location of underground excavation.

The classification proposed by Kaiser et al., (1996) is advantageous as it considers two significant mechanisms of rockburst and its intensity. Recent classifications by Tang (2000) and He et al., (2015) are based on the idea that rockburst events should be categorised based on the mechanism and severity. Li et al., (2017) provide a comprehensive classification of rockbursts, describing six classes of rockbursts based on their failure plane, type of cracking (tensile or shear), and amount of energy released. This classification provides an advantage as it presents a detailed description of different types of rockbursts based on their underlying mechanisms.

Li et al., (2017) provide one of the best rockburst classifications, which defines six classes of rockbursts and their mechanisms as follows:

- Tensile cracking and spalling;
- Tensile cracking and toppling;
- Tensile cracking and sliding;
- Buckling and braking;
- Tensile cracking and toppling; and
- Tensile cracking and sliding.

The classification was premised on the four characteristics i.e., structure of the rockmass, cracking property, failure plane and energy release. The advantage of the classification is that the different types of rockburst are described according to their failure plane, type of cracking (tensile or shear), and amount of energy released.

2.3.1 Classification of Rockburst Damage Severity

Classification of rockburst damage severity has been based on depth of failure and others on volume of rock displaced. Kaiser et al., (1996) suggested that the rockburst damage severity is best characterised by the depth and lateral extent of the rock involved in the failure process around an opening. This classification of damage severity considers primarily the depth of failure. It applies to opening sizes commonly found in underground hard rock mines, ranging in width and height from 3 and 6 m respectively. They stated that the severity levels depend on many other factors, including rock mass quality, support effectiveness, local mine stiffness, geological structures, opening size and orientation, and intensity of seismicity. They classified rockburst damage into three severity levels: minor, moderate, and major or severe, as shown schematically in Figure 2.2.

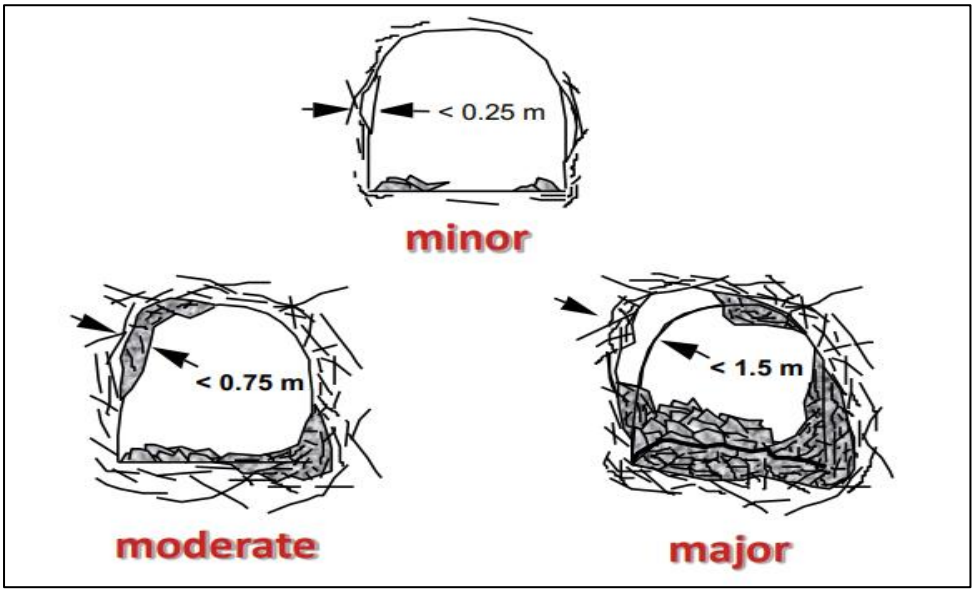

Figure 2.2: Rockburst damage severity (after Kaiser et al., 1996)

(a) Minor Damage

Damage of minor severity would commonly be described as rock spitting, spalling or shallow slabbing, as shown in Figure 2.3.

Figure 2.3: Minor rockburst damage involving shallow spalling (after Kaiser et al., 1996)

Minor damage can occur during the initial development of deep tunnels and drifts or in highly stressed moderately jointed rock at relatively large distances from fault-slip-type seismic events. This damage level can lead to dangerous situations, particularly when miners are nearby. Minor damage is typically shown by a shallow skin of fractured or loose rock, generally less than 0.25 m thick, and moderate new mesh bagging with a few broken wires. If the damage mechanism is rock bulking, observations show minor mesh bagging for a standard support system. If rock ejection is the mechanism involved, observations include spitting rock. If rockfall is the mechanism involved, then relatively minor falls of ground may occur, although the thickness (weight) of rock would be small enough that a standard support system should be capable of retaining this material in place.

(b) Moderate Damage

Moderate damage implies that the rock is heavily fractured and may have displaced violently. Mesh will be bagged at its capacity and is often torn or pulled over rock bolt plates. Many holding elements will have failed but the volume of broken rock is limited such that drifts are still accessible. Shotcrete would be heavily fractured Moderate damage

is generally characterized by fractured or loosened rock of 0.25 m to 0.75 m in thickness (Figure 2.4).

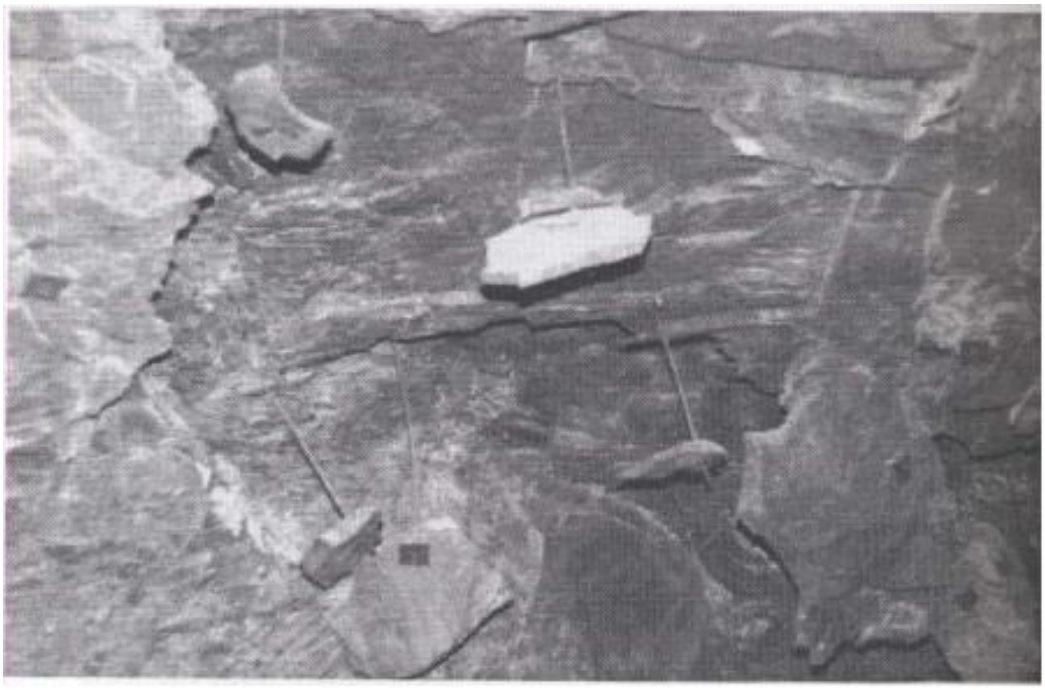

Figure 2.4: Moderate rockburst damage (after Kaiser et al., 1996)

The exact nature of the damage will depend on the specific rockburst mechanism involved; for example, rock bulking versus seismically induced rockfalls. For rock bulking, deformation of the rock surface would generally be restricted to between 50 and 150 mm.

(c) Major or Severe Damage

If a drift sustains major damage, it would be impassable due to substantial amounts of displaced rock. Most ground support components would be broken or damaged and shotcrete or other retaining elements would have lost their functionality, permitting unraveling of broken rock between holding elements. Major damage involves deep fracturing or the presence of damaged rock to a depth of more than 0.75 m around the opening as shown in Figure 2.5.

Figure 2.5: Major Rockburst damage resulting in closure of the drift (Kaiser et al., 1996)

The severity is best described by a measure of seismic energy release, i.e., the magnitude of the seismic event that is co-located with the damage (Cai and Kaiser, 2018).

2.3.2 Other Classifications

The severity of damage caused by rock displacement is classified as light, medium, or heavy depending on the volume of displaced rock and the area of damage. The Potvin (2009) rockburst damage scale (Table 2.5) considers the rock mass and the support system.

Table 2.5: Rockburst damage scale (Potvin, 2009)

Rockburst damage scale	Rock mass damage	Damage surface area	Rock support damage
R1	No damage, minor	0	No damage
R2	Minor damage, less than 1 ton displaced	< 1 m^2	Support system is loaded, loose in mesh, plate deformed, shotcrete cracked
R3	Minor damage, less than 1 ton displaced	< 10 m^2	Some broken bolts, mesh bulged, shotcrete fractured
R4	10 -100 tons displaced	10 -50 m^2	Major damage to support system, retention capacity severely compromised
R5	100+ tons displaced	> 50 m^2	Complete failure of support

Several researchers have come up with different methods to classify rockbursts. For instance, Tan (1992) identified four rockburst grades: weak, moderate, strong, and severe. The classification is based on the extent of damage and mechanical and acoustic characteristics of the rockburst. Russenes (1974) also divided rockbursting activity into four classes from 0 to 3. Class 0 indicates no rockbursting activity, while classes 1, 2 and 3 indicate low, moderate, and high rockbursting activity (Table 2.6).

Table 2.6: Standard rockburst classifications (After Zhou et al., 2016)

Classification	Class	Failure characteristics (Zhou et al., 2012)	Failure characteristics (Russenes 1974)
High	3	The surrounding rock bursts severely thrown out or ejected into the tunnel accompanied by a strong burst and a roaring sound, air spray, and storm phenomenon, with continuity. Rapid expansion to the deep surrounding rocks occurs	Severe rockfalls from roof and walls begin immediately after blasting. Slabs pop from the floor, or the floor may heave. Considerable over breaks and deforming of the periphery occurs. Rock noises of the gun strength may be heard
Moderate	2	The surrounding rock is deformed and fractured and a considerable number of rock chips are ejected. Loose and sudden destruction occurs, accompanied by crisp cracking often in the local cavern of surrounding rock	Considerable slabbing and loosening of rock occur and a deformed periphery tends to develop over time. Strong cracking noises from the rocks are head
Low	1	The surrounding rock is deformed, cracked, rib - spalled. There is a weak sound and no ejection phenomenon	Cracking and loosening of the rock occur, light noise and light noises emerge

2.4 Seismic Source Mechanisms

Although numerous related research works concerning the mechanism, characteristics or type, the cause of formation, critical conditions, and preventive methods of rockburst have been conducted, the research community has had no precise and unified definition of rockbursts (Afraei et al., 2018).

In mine seismology, two different types of mine seismic events are observed. The first types of events are the larger magnitude ones, which occur at some distance from mining activities and are generally associated with major geological discontinuities (Gibowicz and Kijko, 1994). This type of source, according to Brady and Brown (2006), is predominantly

associated with a shear-slip type mechanism, as is commonly recognised in earthquake seismology. The second type of seismic event occurs in or near the mining domain and is low to medium magnitude. The frequency of occurrence of these events is generally a function of mining activity (Gibowicz and Kijko, 1994). In hard rock mines, in addition to unstable material rupture involving shearing, splitting, or crushing of the intact rock, mine instability and seismicity may arise from unstable slip-on planes of weakness such as faults or low-strength contacts between dykes and the country rock.

A dominant role for unstable fault- slip as the source of rockbursts has been proposed by Spottiswoode (1984) and is supported by interpretation of field observations of rock mass deformation attending rockbursts reported by Ortlepp (1978) confirming the observations by Gay and Ortlepp (1979), who described in detail the character of faults induced by mining on which clear indications of recent shear displacement were expressed. Ryder (1987) has discussed the relation between rockbursts involving a crushing mode of rock mass deformation and those involving fault slip. Hasegawa et al., (1989) presented the six possible ways that mine-induced seismic events can occur in Figure 2.1 as cavity collapse (A), pillar burst (B), tensional fault (C), normal fault (D), thrust fault (E) and shallow thrust faulting (F).

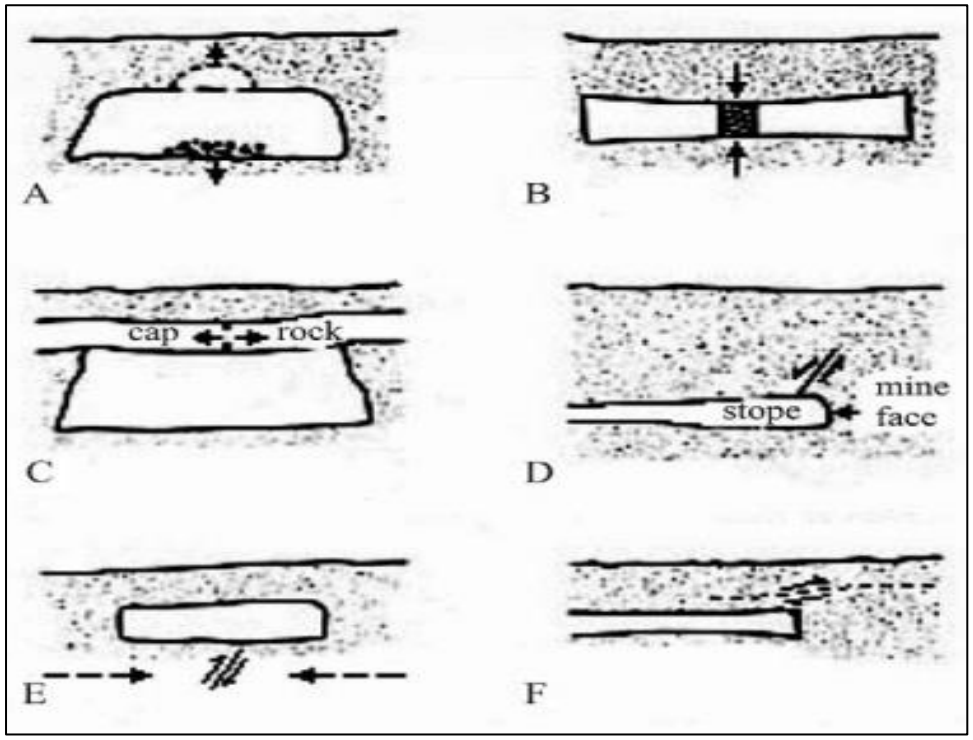

Figure 2.1: Six possible ways that Mine-induced seismic events can occur (after Hasegawa et al., 1989)

Three failure modes have the focal mechanism of a shear-slip type failure (thrust, normal, and reverse fault). In terms of a mechanical model, a double-couple focal mechanism can represent rock failures involving slip and shear rupture. Non-double-couple singularities represent the remaining three source mechanisms. These are a point force singularity, a dipole singularity and tensional faulting. Complex non-double-couple mechanisms may incorporate the simple double - couple and non-double-couple mechanisms (Gibowicz and Kijko, 1994).

Cai and Kaiser (2018) presented four dynamic damage mechanisms:

- Sudden stress-induced fracturing or strain bursting because of the tangential straining of the excavation;
- Rock ejection because of a high rock mass bulking rate during strain bursting;
- Rock ejection is by energy transfer from a remote seismic source; and
- Shake-downs or falls off the ground because of acceleration of forces elevated by the impact of ground motions from a remote seismic event.

2.5 Factors Contributing to Rockbursts

Researchers have extensively studied mining-induced seismicity and rockbursts over the past decades (Hasegawa et al., 1989; Spottiswoode, 1989; Gibowicz, 1990; McGarr et al., 2000; Gibowicz and Lasocki, 2001). The primary mechanism underlying mining-induced seismicity has been determined to be the readjustment of stresses because of the creation of vast openings underground as stopes (Cook, 1976) and the action of shear stress on fractures (Brady and Brown, 2006; Jaeger et al., 2007; Verdon et al., 2011). Seismicity in mines depends on depth, production rate, mining geometry, geological discontinuities, and ambient tectonic stress field. One or a combination of the above factors may contribute significantly to mining seismicity in any specific case (Gibowicz and Kijko, 1994; Mendecki, 1997). Driad-Lebeau, (2005) proposed that structurally complete rock combined with high horizontal tectonic stresses was responsible for rockbursts. Zhou et al., (2011) demonstrated that pre-existing cracks of rock masses were beneficial to abrupt energy release stored in rock masses coming into being rockbursts under certain conditions.

Lu et al., (2018) and Meng et al., (2017) showed that geological structures, such as faults and joints, increased stress sharply, easily leading to rockbursts. Yang et al., (2017) presented that high in situ stresses were the major factor that caused strain energy accumulation and gave rise to rockbursts in the strong rock. Zhu et al., (2010) stressed the

importance of rockbursts from the dynamic disturbance in underground mining. Wiles (2005) showed a strong link between rockmass strength and energy release density for inducing a rockburst. He also argued that knowledge of the loads (stress state) alone cannot assess stability. The stiffness of the loading system driving the failure process also needs consideration.

Many studies about the rockburst phenomena have resulted in a wide variety of theories, such as energy theory (Cook, 1965), stiffness theory (Petukhov and Linko, 1979), rockburst tendency theory (Kidybinski, 1981), strength theory (Li, 1985), three-criterion theory and system deformation stability theory (Zhang, 1987). The three criteria theory is more influential and is based on three factors internal factor, stress factor and structure factor.

Li et al., (2017) and Kaiser and Cai (2012) identified four factors that lead to rockburst: geotechnical, geology, mining, and seismicity (Figure 2.2).

Geotechnical factor	**Geology**	**Mining**	**Seismicity**
In situ stress (Magnitude and stress ratio) Rock strength Rock mass quality / joint fabric Rockmass brittleness	Rock type Foliation and bedding Geological structures (dykes, faults, and shears)	Mining-induced static stress (excavation spans, mining method) Local mine stiffness (extraction ratio, rock mass modulus) Excavation sequence (stress path) Production rate (blasting, cave loading) Destressing and hydro-fracturing	Seismically induced dynamic stresses and ground motions Event magnitude Distance to seismic source Source mechanism, e.g., fault slip or strain burst Rate of seismic energy release rate

Figure 2.2: Four factors that cause the rockburst phenomenon (After Li et al., 2017)

2.5.1 Geotechnical Factors

The in-situ stress increases with depth, so rockburst problems increase as mining migrates to deeper levels. Because of a large differential between the maximum and the minimum

principal stresses, high deviatoric stress produces high tangential stresses near the excavation boundaries. Hence, the in-situ stress magnitude and ratio define a mining block's overall stress level, and excavation geometries change this stress. The stress level, rock mass strength, and deformation behaviour all influence the strain energy stored and released during failure. Strong and stiff rocks can build up high stress and store much strain energy. The amount of releasable energy is determined by the peak strength and post-peak stiffness of the rock mass and the unloading stiffness of the surrounding rock. Joint fabrics weaken the self-supporting capability of the rock mass, elevating the risk of shakedowns and rock ejection.

2.5.2 Geology

Geological features, such as dykes, modify the mining-induced stresses and often produce local stress raisers. Faults promote stress concentrations and facilitate rock mass failure. They also alter the local mine system stiffness. Brittle hard rock tends to accumulate strain energy and it has the potential to fail violently with little warning. Faults that intersect excavations enhance the rock deformation, reduce the local loading system stiffness, and thus increase the amount of releasable energy. Foliations and beddings induce anisotropy in stress and strength and may alter failure mechanisms.

2.5.3 Mining

Mining disturbs the in-situ stress field, and the related stress changes lead to stress relaxation and stress concentration zones throughout a mine. Excavations alter the mine stiffness, leading to a lower mine stiffness at a higher extraction ratio. When the extraction ratio is high (typically greater than 80 percent), the remaining rock will be highly stressed and the mine system stiffness will be low, and as a result, the likelihood of rock bursting is increased (Kaiser and Cai, 2012). For example, the risk of rock bursting is high when recovering sill pillars. The excavation sequence determines the stress path and the rock failure process (Kaiser et al., 2001; Cai, 2008). Centre-out mining sequences in open stoping and transverse cut-and-fill stoping are widely practiced to reduce the rockburst risk. Stoping sequence retreating from faults or shears results in a more even seismic energy release (Hedley, 1992), reducing the risk of large rockbursts. The adopted mining method can therefore influence the rockburst damage potential and severity. For example, most mines that convert from cut-and-fill to long-hole stoping experience larger rockbursts (Blake and Hedley, 2003).

2.5.4 Seismicity

A strain burst can be triggered by a remote seismic event or occur without any dynamic disturbances. However, severe rockburst damage is often associated with a fault-slip seismic event because the associated dynamic disturbance causes dynamically loaded strain burst. The larger a seismic event is, the further away from the event the dynamic disturbance can be felt and the wider the strain burst trigger zone will be. On the other hand, the closer the seismic source to an opening is, the greater are the dynamic disturbances, stress pulses or ground motions, and therefore the rockburst potential. For this reason, large seismic events such as fault-slip events increase the area for potential rockburst damage and the severity of damage. Generally, the rockburst damage increases with the event magnitude. A large seismic event may also cause 'aftershocks', i.e., secondary events such as strainburst, and this may cause rockburst damages at multiple locations.

2.5.5 Combination of Factors

Rockburst damage is caused by several factors that determine the intensity of a dynamic disturbance and the vulnerability of excavation to such damage. When high stress, brittle rock, high extraction ratio, and faults are combined, a mine becomes highly prone to rockbursts. Significant seismic events can put excavations at risk, and severe damage is inevitable when the installed rock support system is ineffective. According to Durrheim et al. (1998), the source mechanism is frequently influenced by factors such as mine layout and regional structures, including faults, shears, and dykes, while local rock conditions and support systems mainly influence the location and severity of damage. In mines that experience rockbursts, it is common to observe severe damage in one area, while immediately adjacent locations remain unaffected.

Keneti and Sainsbury (2018) reviewed selected published case study data from around the world to establish and identify the contributing factors to rockburst to assist research associated with developing numerical modelling techniques to reproduce rock bursting. They identified the six key contributing factors, including unfavourable stress states, excavation geometry (size and orientation concerning the principal stresses) and rate and direction of advance (Figure 2.3).

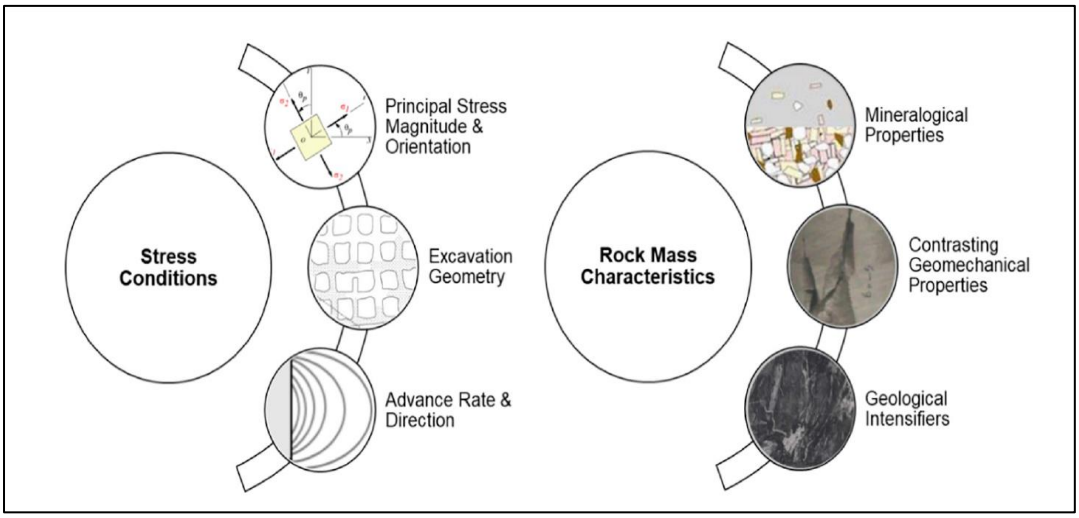

Figure 2.3. Contributing factors to rockburst (After Keneti and Sainsbury, 2018)

The identified factors also incorporated unfavourable rock mass characteristics that included mineralogy, contrasts in geomechanical properties, and geological intensifiers (dykes, faults). The first three factors (i.e., high and adversely re-oriented stresses by structures, excavation geometry, excavation rate and direction) relate to in situ and induced stresses. The last three (i.e., mineralogical properties, contrasting geomechanical properties and geological intensifiers affecting fracturing behaviour) relate to intrinsic rock properties (Sainsbury and Nurses, 2019). The main properties known to be associated with rockbursts are strength, stiffness, and brittleness (Keneti and Sainsbury, 2018). Strong, brittle, stiff, highly stressed rocks have significant potential for bursting (Blake and Hedley, 2009).

2.6 Evaluation Index Criteria for Rockburst Prediction

Rockburst prediction is a crucial task worldwide that significantly prevents and controls rock failure in underground excavations (Li et al., 2017). During the initial stages of construction, the empirical method is typically employed to assess the rock mass's quality and evaluate the rockburst risk, offering valuable design and support guidance (Wu et al., 2022). The empirical criterion is an index or criterion used to judge the occurrence and strength of rockbursts based on physical tests and engineering cases. It can be a single index criterion or a comprehensive index criterion. However, a single index criterion is one-sided and does not consider other factors influencing rockburst (Wu et al., 2022). While it can evaluate rockburst, it has the disadvantage of large deviations and low accuracy due to complex geological factors (Ma et al., 2018). Therefore, multi-indicators should be used to minimize deviations and improve accuracy. In practical engineering,

indicators are commonly adopted to assess burst liability and evaluate burst potential comprehensively. Some indicators reflect the rock mechanical property, such as uniaxial compressive stress (UCS) or uniaxial tension stress, while others reflect the environment stress condition, such as maximum tangential stress around an underground opening (Leveille et al., 2017; Lingga and Apel, 2018). Many factors influence rockburst, including stress level, physical and mechanical properties of rock, structure and fissure distribution of rock mass, excavation mode, temperature, and groundwater (Zhang et al., 2017; He et al., 2018). These factors vary under different geological conditions, making rockburst prediction a complex and indeterminate system question (Zhang et al., 2020a).

2.6.1 Stress Methods

According to Askaripour et al. (2021), several stress methods use predictor indices. The indices are the stress, strength and energy:

- Brittleness coefficient of rock (Qiao and Tian, 1998; Chen et al., 2013).
- Tao discriminant index (Tao,1988);
- Strength index (Hawkes,1966);
- Stress index (Yoon,1994);
- Tangential stress (Hoek and Brown,1980; Wang et al.,1998);
- Russenes method (Russenes,1974);
- Turchaninov method (Turchaninov et al., 1972).

2.6.1.1 Brittleness Coefficient of Rock

The rock brittleness coefficient is a widely used index to evaluate the likelihood of rockbursts. This coefficient is calculated by dividing the uniaxial compressive strength (UCS) by the tensile strength of the intact rock. According to the experimental results and site investigation, the rock brittleness coefficient is defined as the ratio of UCS to the tensile strength of intact rock is shown in Equation 2.1 (Qiao and Tian, 1998, Chen et al., 2013).

$$B_i = \frac{\sigma_c}{\sigma_t} \qquad (2.1)$$

Where:

B_i = Rock brittleness coefficient.

σ_c = Uniaxial compressive strength of the rock.

σ_t = Tensile strength of the rock.

The classification criteria based on the brittleness coefficient are presented in Table 2.7.

Table 2.7: Rockburst intensity based on the brittleness coefficient (Wang and Park, 2001)

Rock brittleness coefficient	Risk of violent rupture
$B_i > 40$	No rockburst
$26.7 < B_i < 40$	Weak rockburst
$14.5 < B_i < 26.7$	Moderate rockburst
$B_i < 14.5$	Strong rockburst

2.6.1.2 Tao discriminant index

The Tao discriminant index is based on the stress reduction factor in Q system (Barton's classification) and defined as the ratio of UCS of rock to the maximum principal in situ stress (Tao, 1998).The criterion is as shown in Equation 2.2.

$$\propto = \frac{\sigma_c}{\sigma_1} \tag{2.2}$$

Where:

$\propto$ = Tao discriminant index,

σ_c = Uniaxial compressive strength of the rock.

σ_1 = Maximum in situ stress.

Table 2.8 presents the rockburst classification based on the mean stress index.

Table 2.8: Rockburst intensity based on the Tao discriminant index (Tao, 1988)

Mean stress	Risk of violent rupture
$\alpha > 14.5$	No rockburst
$5.5 < \alpha \leq 14.5$	Weak rockburst
$2.5 < \alpha \leq 5.5$	Moderate rockburst
$\alpha \leq 2.5$	Strong rockburst

2.6.1.3 Strength index

Hawkes (1966) suggested a rock strength index (RS_i) as one of the empirical methods of rockburst prediction. The RS_i is as shown in Equation 2.3.

$$RS_i = \frac{3\sigma_1}{\sigma_c} \tag{2.3}$$

Where:

RS_i = Strength index.

σ_1 = Magnitude of maximum principal stress.

σ_c = UCS of rock.

The scale system (Table 2.9) shows the intensity of the rockburst based on RS_i.

Table 2.9: Rockburst intensity based on the strength index (Hawkes, 1966)

Strength index	Risk of violent rupture
$RS_i < 0.2$	Low
$0.2 < RS_i \leq 0.4$	Significant
$0.4 < RS_i \leq 0.6$	High
$0.6 < RS_i \leq 0.8$	Very high
$0.8 < RS_i \leq 1.0$	Dangerously high
$RS_i > 1.0$	Unstable

2.6.1.4 Stress index

The stress index (S_i) is defined as the ratio of the UCS of the rock to the vertical component of in situ stress (Yoon, 1994), which is shown in Equation 2.4.

$$S_i = \frac{\sigma_c}{\sigma_v} \tag{2.4}$$

Where:

S_i = Stress index.

σ_c = the UCS of the rock.

σ_v = the vertical component of in situ stress.

Table 2.10 shows the intensity of rockburst based on the stress index.

Table 2.10: Value of stress index for prediction of rockburst (Yoon, 1994**)**

Stress index	Risk of violent rupture
$S_i \leq 2.5$	Heavy rockburst
$2.5 < S_i \leq 5$	Mild rockburst

2.6.1.5 Tangential stress

The Tangential Stress Criteria is the ratio of tangential stress around excavation opening to rock's UCS, introduced by Wang et al., (1998) and Hoek and Brown (1980). The Tangential Stress Criteria is shown in Equation 2.5.

$$Ts = \frac{\sigma_\theta}{\sigma_c} \tag{2.5}$$

Where:

Ts = Tangential stress.

σ_c = UCS of the rock.

σ_θ = Tangential stress.

Table 2.11 presents the rockburst intensity based on the tangential stress.

Table 2.11: Tangential stress criterion (Wang et al., 1998)

Tangential stress	Risk of violent rupture
$Ts < 0.3$	No rockburst
$0.3 \leq Ts < 0.5$	Weak rockburst
$0.5 \leq Ts < 0.7$	Strong rockburst
$Ts \geq 0.7$	Violent rockburst

2.6.1.6 Russenes method

A new method for assessing the risk of rockburst was introduced by Russenes in 1974. This method involves measuring the relationship between the tangential stress and the strength of the rock. It is calculated by finding the ratio of the maximum tangential stress around the rock to the UCS of the rock. Table 2.12 displays the intensity of rockburst according to the Russenes criterion.

Table 2.12: Rockburst prediction value based on Russenes method (Russenes, 1974)

Russenes Method	Risk of violent rupture
$\sigma_\theta / \sigma_c < 0.2$	No rockburst
$0.2 \leq \sigma_\theta / \sigma_c < 0.30$	Light rockburst
$0.3 \leq \sigma_\theta / \sigma_c < 0.55$	Medium rockburst
$\sigma_\theta / \sigma_c \geq 0.55$	Violent rockburst

2.6.1.7 Turchaninov method

Turchaninov et al., (1972) defined a criterion to measure the rockburst intensity. The criterion is shown in Equation 2.6.

$$S = \frac{(\sigma_\theta + \sigma_1)}{\sigma_c} \tag{2.6}$$

Where:

S = Turchaninov index.

σ_θ = Tangential stress.

σ_1 = Major Principal stress.

σ_c = the UCS of the rock.

Table 2.13 represents the rockburst intensity based on the Turchaninov criterion.

Table 2.13: Rockburst prediction values (Turchaninov et al., 1972)

Turchaninov method	Risk of violent rupture
$S < 0.3$	No rockburst
$0.3 \leq S < 0.5$	Rockburst probably
$0.5 \leq S < 0.8$	Rockburst surely
$S \geq 0.8$	Violent rockburst

The method was later updated by replacing the major principal stress with the normal stress (Turchaninov and Markov, 1981; He et al., 2021). The method is shown in Equation 2.7.

$$T_m = \frac{(\sigma_\theta + \sigma_n)}{\sigma_c} \tag{2.7}$$

Where:

T_m = Turchaninov method.

σ_θ = Tangential stress.

σ_n = Normal stress.

σ_c = the UCS of the rock.

Table 2.14 represents the rockburst intensity based on the Turchaninov method.

Table 2.14: Rockburst prediction values (Turchaninov and Markov, 1981; He et al., 2021)

Turchaninov method	Rockburst Risk
$T_m < 0.2$	None
$0.2 \leq T_m < 0.4$	Low
$0.4 \leq T_m < 0.5$	Medium
$T_m \geq 0.5$	High

2.6.1.8 Uniaxial Compressive Strength

The rock's uniaxial compressive strength (UCS) is the rock specimen's maximum compressive stress before failure under uniaxial compression loading. According to Zhang et al., (2020), the UCS is a relatively intuitive factor in evaluating the possibility of rockburst, whose classification criteria are presented in Table 2.15.

Table 2.15: Classification criteria for uniaxial compressive strength of rocks (Zhang et al., 2020)

Rockburst grade	Classification	σ_c (MPa)
I	None	< 80
II	Weak	80 -120
III	Moderate	120 - 180
IV	Strong	>180

2.6.1.9 Rock Quality Designation

The RQD, or Rock Quality Designation, is a measure of the integrity of a rock mass. It can be used for predicting the likelihood of rockbursts and was developed by Tang in 2000. As per the RQD classification system, higher RQD values indicate a greater probability of rockbursts (Wang and Park, 2001). Table 2.16 provides a rockburst classifications based on RQD values.

Table 2.16: Rockburst occurrence based on the energetic rockburst indicator (Tang, 2000)

RQD	Risk of violent rupture
<25%	No
25% – 50%	Light
50% – 75%	Medium
75% – 90%	Strong
90% – 100%	Very strong

2.6.1.10 Energy Methods

Rock bursts occur when high amounts of energy are stored in the rock mass, which serves as the material basis for these events (Shang et al., 2013; Huang et al., 2014). Brittle rocks fail with a small strain in the elastic region, while ductile rocks experience significant plastic strain without losing their bearing capacity before failure (Zhang et al., 2016). Rock failure occurs when elastic energy accumulated in rocks is suddenly released (Xie et al., 2009; Peng et al., 2015; Hou et al., 2016; Wang et al., 2017).

Various energy methods are used to evaluate rockburst proneness, including the Elastic strain energy index (Kidybiński, 1981), Liner elastic energy (Wang and Park (2001), Rock mass integrity coefficient (Yoon, 1994), Seismic energy (Spottiswoode and McGarr (1975). Despite the multitudes of the energy theories, there are no widely accepted rockburst energy - based indices in rock mechanics.

2.6.1.11 Liner Elastic Energy

Wang and Park (2001) introduced the concept of linear elastic energy (W_{et}), which refers to the energy stored in a rock specimen before it reaches the point of failure, as cited by Askaripour et al., (2022). W_{et} is also known as the elastic energy as strain energy density (SED), first suggested by Kwasniewski et al. in 1994 as shown in Equation 2.8.

$$W_{et} = \frac{\sigma_c^2}{2E_u} \quad (2.8)$$

Where:

W_{et} = the linear elastic energy.

σ_c = the UCS of intact rock (MPa).

E_u = the elastic modulus.

The rockburst intensities based on the value of W_{et} are presented in Table 2.17.

Table 2.17: Rockburst intensity based on the linear elastic energy (Wang and Park, 2001)

Liner elastic energy	Risk of violent rupture
$W_{et} < 50$ kJ/m^3	Weak
50 kJ/m^3 < W_{et} < 100 kJ/m^3	Moderate
100 kJ/m^3 < W_{et} < 200 kJ/m^3	Strong
$W_{et} > 200$ kJ/m^3	Extra strong

2.6.1.12 Seismic Energy

Spottiswoode and McGarr (1975) introduced the concept of using microseismic monitoring to measure the radiated energy of rockbursts. They studied the correlation between the radiated energy and the intensity of the rockburst. As a result, they developed a new classification system for rockburst intensity based on the radiated energy, shown in Table 2.18 and evaluated using common logarithms.

Table 2.18: Rockburst classification based on the logarithm of radiant energy (Spottiswoode & McGarr, 1975)

Seismic method	Risk of violent rupture
Log(E/J) < 2	No
0 ≤ Log(E/J) < 2	Weak
2 ≤ Log(E/J) < 4	Moderate
4 ≤ Log(E/J) < 7	Intense
Log(E/J) ≥ 7	Extremely intense

2.7 Methods or Techniques to Predict Potential Rockbursts

According to Wu et al., (2022), Rockburst presents a complex problem for underground resource development and infrastructure construction due to the various factors contributing to its occurrence. Predicting the intensity and time of a Rockburst is a worldwide challenge, and accurate prediction is crucial for safety and planning measures. The literature review (Zhou et al., 2018; Li et al., 2022) categorized the four techniques used for Rockburst prediction: empirical, analytical, numerical modelling, experimental, and intelligent methods. Figure 2.4 illustrates the specific approaches for predicting potential rockbursts.

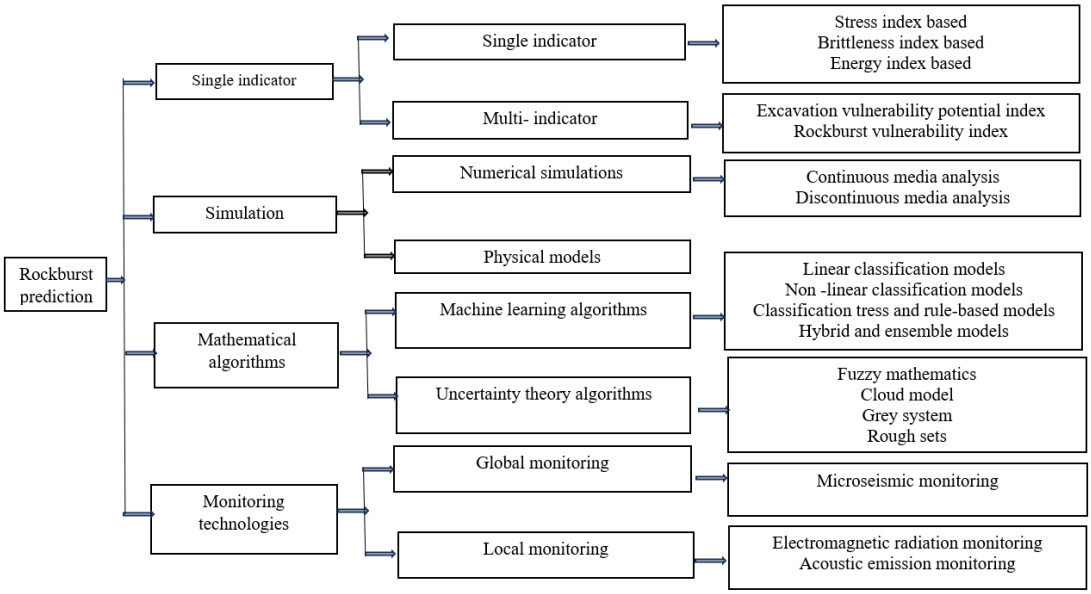

Figure 2.4: Approaches of different categories for rockburst prediction (Zhou et al., 2018)

The four classes of the rockburst prediction; empirical methods, simulation techniques, monitoring technology and mathematical or intelligent algorithms.

2.7.1 Empirical Methods

The empirical method for rockburst prediction includes single and multi-indicator indices. Single indicators include stress, brittleness, and energy-based indices, while multiple indices include the excavation vulnerability index and the rockburst vulnerability index. The most prominent advantage of the empirical models is their simple form and convenience for engineering applications. However, the models are often derived from the interpolation of curves and barely have physical meaning. The main weakness of the empirical models is their limited validity in some cases, giving rise to doubts concerning their effectiveness.

2.7.2 Numerical Simulation Techniques

Wang et al., (2021) summarized the numerical simulations, including the continuum, discontinued, and hybrid techniques for rockburst evaluation. The numerical simulation is economical, secure, and time saving. Nevertheless, choosing an appropriate constitutive model and simulation method is very important according to specific problems (Li et al., 2022).

Most numerical applications are challenged by poor availability of complete data sets regarding geologic, geometric, and geotechnical data, which include post-failure behavior and conditions of Rock masses (Maleki, 1981; Maleki, 1992; Maleki, 2015). Zhou et al., (2016) have highlighted a key issue in the field of rockburst classification. They noted that due to the lack of appropriate energy criteria, it is currently not possible to obtain an absolute classification of the rockburst energy provided by methods such as failure approach index (FAI) by Zhang et al., 2011, using excess shear stress (ESS) (Ryder, 1988), the local energy release density (LERD) (Wiles, 2002), the local energy release rate (LERR) (Wiles, 2002) or the energy release rate (ERR) (Salamon, 1984). Zhou et., (2016) suggested that this issue requires statistical analysis of several project examples in future research. Furthermore, they acknowledged that each numerical method has its own strengths and limitations. In addition, they emphasised the importance of estimating reliable model input parameter values, which can be a challenging task. They recommended that researchers should carefully consider the availability of realistic input data before applying sophisticated numerical methods.

Chen et al., (2021) through their review of ‘rockburst Precursors and the dynamic Failure mechanism of the deep tunnel project indicated that under the combined action of high static stress and dynamic disturbance, the uncertainty and complexity of mechanical behavior. The deformation and failure mechanism of rock engineering excavations become more prominent, which will certainly restrain the accuracy of numerical simulation and bring huge challenges to numerical methods.

2.7.3 Monitoring Technology

The rockburst prediction methods applied in engineering practice mainly include microseismic, microgravity, electromagnetic radiation, seismology, drilling cuttings, moisture, photo elasticity, rheological method, and rebounding (Jiang et al., 2003). The microseismic method can dynamically monitor the whole progressive rock mass failure process in real-time, effectively delineate the potential risk area of rockburst in the

monitoring area, and timely evaluate and predict the stability of surrounding rock (Li and Zhou, 2021). Real-time, mine scale seismic monitoring systems have been developed and installed in most of the deep underground projects in developed countries such as Canada, South Africa, the United States, and Australia and have been successfully applied in analyzing and determining the fracture distribution, damage state, and rockburst risk prediction (Mendecki, 1993; Mendecki, 1996). Recently, the microseismic monitoring technique has gained significant popularity in ensuring the safety of underground excavation engineering. Ma et al., (2021) in the research titled, 'Microseismic monitoring, analysis and early warning of rockburst, Geomatics, Natural Hazards and Risk', cited the applications of microseismic monitoring as presented in Table 2.19.

Table 2.19: Application of Microseismic (MS) Monitoring to forecast rockburst

Author	Application of MS monitoring
Jenkins et al.,1990	In 1940s, the United States Bureau of Mines began to apply the microseismic method to monitoring rockburst, which seriously threaten the safety of underground mines, but few successful cases have been reported so far.
Gibowicz.1990	Interpreted the research progress in seismicity induced by mining, which consists of improvement of microseismic monitoring system, understanding for induced seismicity mechanism and possibility of prediction and control of seismic hazards.
Senfaute et al., 1997	Characterized and analyzed the 2114 induced microseismic events during the mining operations in the Provence colliery, France to identify or establish criteria for the zones likely to generate rockburst.
Milev and Spottiswoode, 2000	used the accumulative seismic moment and volume of convergence to characterize the 300000 seismic events occurred at Deelkraal, Elandsrand, East Driefontein, Kloof and Leeudoorn mines in South Africa.
Urbancic and Trifu, 2000	Reviewed the progress of microseismic monitoring in mines of Canada, which mainly focused on characterize the types of source model by the S-wave energy to P-wave energy and rockburst prediction by vibration velocity and acceleration, and b value.
Luo et al., 2000	In Australia, the microseismic monitoring application began from 1994, which was well used in 13 mines until 2000.
Cai et al., 2001	Proposed a rock degradation model to quantitatively estimate the location, counts and propagation of cracks based on the microseismic data and associated source model.
Shen et al., 2008	Compared the stress, displacement and microseismic monitoring result during the caving of long wall working face in coal Australia, they, and mine found that microseismic indicators are more effective and sensitive than the stress and displacement information to reveal the caving process of roof. Scholars in South Africa.
He et al., 2010	Studied the characteristics of acoustic emissions during the fracture of rock mass, and proposed the catastrophe theory for rockburst based on acoustic emission monitoring.
Tang et al., 2010	First reported the successful application of microseismic monitoring to predict rockburst in deep-buried tunnel of the Jinping II hydropower station.
Ma et al., 2015	Studied the rockburst characteristics in tunnels of the Jinping II hydropower station and proposed four (4) rockburst criteria based on microseismic monitoring.
Xiao et al., 2016	Studied rock failure mechanisms during the evolution of strain-structure slip rockbursts in deep-buried tunnel using moment tensor analysis of microseismic events.

Microseismic monitoring technology can provide a comprehensive evaluation of the overall stability of the rock mass structure (Chen et al., 2021). This is achieved by monitoring the development and evolution of microfractures inside the rock mass so it can capture the precursor information of the macroscopic failure of the rock mass. Microseismic monitoring is used to identify potential failure zones in rock mass engineering, to achieve the early warning and forecast of rock mass damage (Dai et al., 2015; Xu et al., 2015; Zhang et al., 2020b). During the rock mass failure, the energy accumulated inside is released in the form of stress waves, causing microseismic signals (Ma et al., 2016; Zhang et al., 2020). By monitoring, analyzing, and processing the microseismic signals, the time, the spatial location, and the intensity of the microseismic signals can be obtained, and then qualitative and quantitative evaluations of regional rock mass stability can be made (Chen et al., (2021).

In most cases, episodes of joint- slip or rock material- fracture in a rock mass result in the radiation of some energy released as seismic waves, releasing strain energy and generating microseismic events (Cook, 1964). The elastic wave generated propagates outward through the surrounding medium and is received by sensors in the hole close to the rock wall. The sensor converts microseismic signals into electrical signals and sends them through cables to the signal acquisition instrument.

The microseismic events are analysed using waveform processing software, processed, and interpreted and applied in measuring the main parameters (i.e., seismic source location, seismic moment, Seismic energy, and magnitude) that characterise the event (Brady and Brown, 2006; Xiao et.al,.2016).

According to Mendecki (2013a), the four basic parameters of seismic sources are origin time, location, seismic potency, and radiated seismic energy. Information derived from the waveforms can also be used in characterising the failure mechanisms occurring at the seismic source. With good data quality, each located event can be solved for the source mechanism and interpreted in terms of whether the event is dominantly tensile opening, closing, or shear slip (Collins et al., 2014).

By means of the spatial distribution of microseismic events, the micro fracture area of rock mass can be effectively identified and the potential rockburst risk area can be predicted. The concentration area of microseismic events can be divided by analyzing the density and frequency of the spatial distribution of microseismic events (Li and Zhou, 2021).

Comprehensive early warning of rock burst based on microseismic monitoring has been carried out through the joint analysis of the microseismic spatial distribution characteristics, the microseismic energy-frequency distribution characteristics, and the b-value distribution before the shock occurs (Lai et al., 2022).

Microseismic monitoring technology is mainly used for rockburst early warning. Microseismic events can be obtained by analysing microfracture signals, the occurrence time and location (Gerard et al., 1995). Microseismic characteristic parameters such as the number of microseismic events, energy, apparent volume, and apparent stress can be used for rockburst prediction (Wu et al., 2022).

2.7.3.1 Apparent Stress

Apparent stress is a model independent measure of the stress change at a seismic source (Mendecki and van Aswegen, 2001). The apparent stress is defined as the ratio of the radiated seismic energy E to potency, P, which is a measure of the amount of radiated seismic energy per unit volume of inelastic deformation at source (Aki, 1966; Wyss and Brune, 1968). Originally proposed by Wyss and Brune (1968), apparent stress is defined as shown in Equation 2.9.

$$\sigma_a = \frac{\mu E}{M_O} \tag{2.9}$$

Where:

σ_a = Apparent stress.

μ = the shear modulus of rigidity of the source material.

E = Seismic energy.

M_o = Seismic moment.

Past work has shown that seismic events associated with increasing stress typically have a higher seismic energy than expected (van Aswegen and Butler, 1993; Simser et al., 2003). Instability analysis utilises this concept to identify regions of increasing and decreasing stress in an effort to identify unstable rockmass conditions that are potentially prone to large damaging seismic events (Mendecki et al., 1999).

2.7.3.2 Energy Index

The energy index (EI) is a parameter related to concentration and accumulation of stress in a rock mass. Previous studies have found that when an area with a structure (pillar, fault, or dyke) is accumulating stress the EI for related seismic events is greater than one (van

Aswegen and Butler, 1993). When that structure starts to fail, the EI for the related seismic events drops below one. Typically, EI is calculated as an average of a previous number of events to smooth out large variations.

2.7.3.3 Cumulative Apparent Volume

Cumulative apparent volume (CAV) is a measure of the rock mass deformation occurring at the time of a seismic event (Hudyma 2010). Previous studies have related CAV to measured rock mass deformation (Minney et al., 1997).

Generally, the stability of the rock mass subjected to mining can be related to its stiffness, i.e., its ability to resist deformation with increasing stress (Lynch et al., 2010). They stated that while the overall stiffness of the rock mass is being maintained, the seismic potency is expected to be proportional to the volume mined. Given these observations, searches for signs of the stress softening phase that precedes seismic instability reduces to analysis of the time histories of energy index and cumulative apparent volume, as proxies for seismic stress and strain, respectively (Lynch et al., 2010).

2.7.4 Mathematical or Artificial Intelligence Algorithms

The mathematical or artificial intelligent algorithms use machine learning (ML) algorithms and uncertainty theory (UT) algorithms based on Fuzz models (Wang et., 1998; Amoussou et al., 2011), cloud model, grey system, and rough system (Yang, 2010; Shi et al., 2010).

ML refers to using computer algorithms that support systems operation in training to automatically learn and enhance data to predict or classify the nature of such data using patterns. It is a subfield of artificial intelligence (AI) that allows systems to make decisions autonomously without external support (Racheal and Daramola, 2021). ML algorithms can be categorized into supervised, unsupervised, semi-supervised, and reinforcement learning, as well as parametric and non-parametric types (Jason, 2019; Burkov, 2019).

The primary advantage of using ML is that once an algorithm learns what to do with data, it can do its work automatically (Mahesh, 2019). The ML is based on the four models (i.e., linear classification, non-linear classification, classification trees and rule-based, hybrid method and ensemble models. Li et al., (2022) has indicated that with the blossom of artificial intelligence and big data, artificial intelligence algorithms are increasingly used to predict rockbursts. Compared to empirical, numerical, and experimental methods, the artificial intelligence model has high efficiency, good practicability and can foretell and prevent rockbursts in time. However, it requires high-quality data (Li et al., 2022).

In recent years, there has been significant interest in using machine learning to understand better the highly nonlinear relationship between rockburst, and it is influencing factors in geotechnical engineering (Zhang and Goh, 2016; Zhang et al., 2020c; Zhang and Wang, 2020; Huang et al., 2021; Napalai, 2021).

Yin et al., (2021) has shown that the application of ML in rockburst prediction was primarily conducted from two aspects: using rock mass properties and geological conditions as the input; and using field-monitoring data as the input. Li et al., (2021) cited the examples of case studies for prediction of the rockburst using rock mass properties, geological conditions, and MS monitoring as input in the prediction models.

The ML algorithms commonly used for rockburst classification include linear models (LM), decision trees (DT), artificial neural networks (ANN), k-nearest neighbour (KNN), Bayes classifiers, support vector machines (SVM), and ensemble models.

All classification algorithms have the same error rate when classifying previously unobserved points, according to the "No free lunch theorem" for machine learning (Wolpert, 1996). No algorithm is universally better than any other.

2.8 Methods or Techniques to Validate Predictive Models

The techniques are mainly K- fold validation and use of the dataset. These methods are also applicable in ML.

2.8.1 K- fold cross- validation

There are two additional techniques you can use to help find the sweet spot in practice: resampling methods to estimate model accuracy and hold back a validation dataset. The most popular resampling technique is K-fold cross-validation. It allows training and testing of the model k-times on different subsets of training data and builds up an estimate of the performance of an ML model on unseen data. The holdout method is inarguably the simplest model evaluation technique (Raschka, 2018).

2.8.2 Validation Dataset

A validation dataset is a subset of training data that is held back until the end of the project. Once ML algorithms have been selected and tuned on the training dataset, the learned model can be evaluated on the validation dataset to get an accurate idea of its performance on unseen data. Cross-validation is considered the gold standard for estimating model accuracy on unseen data in applied ML.

2.9 Model Evaluation Metrics

Evaluating ML algorithms is crucial to ensure their performance. After performing feature engineering and model training, testing on a separate dataset is essential to assess the model's effectiveness (Sharma and Mishra, 2020). A robust ML model should provide reasonable performance and error metrics (PFEMs) and capture the system's underlying physical mechanisms (Kingston et al., 2005). Kuhn (2016) suggests effective ML prediction models require deep problem knowledge, relevant data, and versatile algorithms.

Steurer and Hill (2020) recommended the fourth ingredient, the appropriate choice of performance metrics for model selection via cross-validation. The choice of metric for evaluating the predictive performance of ML methods is a potential source of confusion in the automated valuation models (AVM) literature. A number of metrics have been proposed, but there has been little attempt to undertake a systematic analysis of their properties. An essential approach to verify the robustness of the ML models is to perform parametric and sensitivity analyses (Alavi and Gandomi, 2011; Kuo et al., 2008). These types of analyses ensure that the ML predictions are in a sound agreement with the system's real behaviour and physical processes rather than being merely a combination of the variables with the best fit on the data. It is essential to have balanced dataset to avoid bias and performance evaluation is easier.

Raschka (2018) summarised the main objectives of evaluating the predictive performance of a model as:

- To estimate the generalization performance, the predictive performance of model on future (unseen) data;
- To increase the predictive performance by tweaking the learning algorithm and selecting the best performing model from a given hypothesis space; and
- To identify the ML algorithm that is best suited for the problem at hand by comparing different algorithms, selecting the best-performing one as well as the best performing model from the algorithm's hypothesis space.

Sharma and Mishra (2020) summarised the most common evaluation metrics in data science, including accuracy, recall, precision, specificity, f-beta score, f1-score, roc curve, Matthews's correlation coefficient (MCC), log loss, pr curve, root mean square error (RMSE), mean absolute error (MAE), mean square error (MSE) and Cohen's kappa. In

this thesis, the Author adopted accuracy as the measure of the performance of the prediction tools.

2.10 Previous Studies on Rockburst Prediction

Sun et al., (2009) employed the knowledge of fuzzy mathematics and neural network to build a rockburst prediction model that trained was with a backpropagation (BP) algorithm based on typical rockburst data. The model used fuzzy mathematics to improve comprehensive index and multi-index judgement. The model was used to predict rockburst in the Sanhejian coal mine in China reasonably.

Fu et al., (2010) used a Bayes discriminant analysis model to predict the possibility and classification of rockbursts in Dongyu Mine and Pingdingshan deep development opening. Yıldırım et al., (2011) used three different neural network (NN) models (feedforward networks, adaptive neural fuzzy inference system, and probabilistic NN) to discriminate between seismic events and quarry blasts. He found that the feedforward NN performed better than the other two NNs with a classification accuracy of 99 percent against 96 percent for adaptive NN and 97 percent for the probabilistic NN under the support of 175 seismic events data.

Zhao and Gross (2012) demonstrated how to use a support vector machine (SVM) to distinguish genuine microseismic from noise events. Sixteen input attributes were extracted from 71 original time-domain and frequency-domain features to train the SVM model based on a dimensionality reduction method (DRM) called neighborhood component analysis (NCA). Four different Kernel functions (Linear, Gaussian, Quadratic, Cubic) were embedded in the SVM model to compare accuracy.

Dong et al., (2016) compared the three machine learning models (Fisher classifier, Naive Bayesian classifier, and logistic regression) in differentiating seismic events and blasts that generate the seismic waveform. The results showed that the logistic regression model had the best discriminating performance in these three mines. However, databases from these three mines were used for training as well as testing. The generalization performance of the model was doubtful as the model only guaranteed empirical risk minimization instead of structural risk minimisation.

Zhou et al., (2012) employed a support vector machine (SVM) to determine the classification of long-term rockburst for underground openings. Two optimization methods namely genetic algorithm (GA) and swarm optimization algorithm (SOA) were

adopted to automatically determine the optimal hyper-parameters for SVMs. The results indicated that the heuristic algorithm of GA and PSO could speed up SVM's parameter optimization search.

Jia et al., (2013) proposed a rockburst prediction method based on the swarm optimization algorithm (SOA) and general regression neural network (GRNN). The characteristic of this model was to use the SOA to determine optimal parameters of GRNN to avoid the influences of human factors on GRNN. This model was employed in rockburst prediction in the Cangshanling highway tunnel and Dongguanshan Copper Mine in China.

Zhou et al., (2016) summarized 12 machine learning algorithms including artificial neural network (ANN), distance discriminant analysis (DDA), support vector machine (SVM), Bayes discriminant analysis (BDA), and Fisher linear discriminant analysis (LDA), in long-term rockburst prediction and compared their prediction accuracies. These algorithms used different rockburst indicators as input features and their training samples sizes were different. These applied machine-learning methods in rockburst prediction mainly focus on burst potential evaluation, which can be regarded as long-term rockburst prediction.

Shang et al., (2017) used a BP neural network to distinguish rock mass fracturing signals and blasting vibration signals. A combined method: frequency slice wavelet transform (FSWT) plus singular value decomposition (SVD) was adopted to extract relevant information from original microseismic signals as input parameters for BP neural network. The results showed that 87 percent of the signals could be precisely identified.

Zhou and Wang (2017) used a novel probabilistic neural network (PNN) based rockburst prediction model to determine whether rockburst would happen in the underground rock projects and how much the intensity of rockburst was. Some control factors, such as rocks' maximum tangential stress, rocks' uniaxial compressive strength, rocks' uniaxial tensile strength and elastic energy index of rock were chosen as the characteristic vector of the PNN. PNN model was obtained through training data sets of rockburst samples that came from underground rock projects domestic and abroad.

Zhao and Gross (2017) used a support vector machine to represent a nonlinear relationship between a rockburst and its factors. This model learned from case histories and then could be used for quick classification of a rockburst for similar conditions.

Su et al., (2018) proposed a new method based on K-Nearest Neighbor case reasoning technology. The results of the prediction of a mining-induced rockburst at a great depth in South Africa appeared to be reasonable with high precision. Yun et al., (2018) used a cloud model to classify and assess rock bursts using factors that influence rock bursts such as the uniaxial compressive strength (σ_c), the tensile strength (σ_t), the tangential stress (σ_θ), the rock brittleness coefficient (σ_c/σ_t), the stress coefficient (σ_θ/σ_c) and the elastic energy index (W_{et}), to establish the evaluation index system. The weights of these indicators were obtained by the rough set method based on 246 sets of domestic and foreign rockburst samples. The 10-fold cross-validation (10-fold CV) was used to obtain a higher generalization ability of models. The classification results of the RS-cloud model were compared with those of the Bayes, KNN and RF methods. The results showed that the RS-cloud model exhibits higher values of accuracy, Kappa and three within-class classification metrics (recall, precision, and the F-measure) than the Bayes, KNN and RF methods.

Pu et al., (2018a) used a decision tree method to predict rockburst potential in kimberlite at an underground diamond Mine. Three indicators including the ratio between uniaxial compressive strength (σ_c) and uniaxial tensile stress (σ_t), the ratio between maximum shear stress around the tunnel wall (σ_θ) and uniaxial tensile stress ($\sigma_{t)}$, and linear elastic energy (W_{et}) were chosen to evaluate rockburst liability (Leveille et al., 2017). Three indicators were chosen as partition attributes of the decision tree model to combine two fundamental conditions of rockburst occurrence namely, energy condition and rock mechanical condition. Additionally, four ranks were introduced for depicting the severity of rockburst (Cai et al., 2016) as follows, with increasing severity: no rockburst, moderate rockburst, strong rockburst and violent rockburst. Numbers 1, 2, 3 and 4 represent the different rockburst severity grades, respectively (1 – no rockburst, 2 – moderate rockburst, 3 – strong rockburst, 4 – violent rockburst).

Feng et al., (2019) carried out rockburst prediction in the deep tunnels of hydropower stations based on the use of real-time microseismic (MS) monitoring information and an optimized probabilistic neural network (PNN) model. The input layer is the real-time MS monitoring information in the deep tunnels of the Jinping II hydropower project. Considering that the selected evaluation index should be closely related to micro-fracture activity in the rockburst development process and can reflect the evolution of the rockburst, six MS parameters reflecting the accumulation of total rupture time, strength,

and deformation of the rock mass are selected. Originally, the cumulative number of MS events (N), cumulative MS energy (E), and cumulative MS apparent volume (V) were considered for rockburst prediction in the drilling and blasting tunnel. To account for the temporal evolution factor, three MS parameters on time were added: event rate (n), energy rate (e), and apparent volume rate (v). The proposed method could provide a reference for rockburst prediction in MS monitored deep tunnels of the hydropower project. Zeng et al., (2019) used the rockburst prediction model of the entropy weight grey relational backpropagation (BP) neural network. The model needed to select the evaluation factors according to the engineering practice and establish the sample library. In their study, the indices were selected to describe a tunnel section. The indices included the Russian criterion value (the ratio of maximum tangential stress (σ_θ max) to rock uniaxial compressive strength σ_c), rock brittleness coefficient expressed as the ratio of σ_c to the uniaxial tensile strength of rock (σ_t), the grade of groundwater condition and rock integrity coefficient (K_v value). The rockburst intensity of Qamchiq tunnel was described in four grades: no rockburst (0), slight (1), moderate (2), and severe (3) rockburst. No rockburst means no loosening, breaking of rockburst, or the phenomenon of silent emission.

Zhao et al., (2020) developed a decision tree model to extract rockburst knowledge from microseismic monitoring data. The input parameters were the number of microseismic events, energy, apparent volume, and development time, while the output was the rank of rockburst from no rockburst to violent rockburst. The method was tested on 20 samples and 8 case histories, and the results showed that the decision tree model was reasonable in extracting rockburst features from the microseismic monitoring data. The study concluded that rockburst is a complex dynamic instability phenomenon of rock mass that cannot be predicted or evaluated based solely on rock mechanics.

Zhang et al., (2020a) predicted rockbursts in Jiangbian and Jinping hydropower station water diversion tunnels using weight and extension methods. They evaluated rockburst prediction based on five factors: uniaxial compressive strength, stress coefficient, brittleness coefficient, elastic energy index, and rock mass integrity.

Wojtecki et al., (2021) used a variety of machine learning algorithms, including artificial neural networks, decision trees, random forests, and gradient boosting, to predict the risk of rockbursts in galleries in one of the deep hard coal mines in the Upper Silesian Coal Basin, Poland. They proposed rockburst risk prediction models that use 22 indicators,

divided into four groups: geological (seven indicators), mining (ten indicators), technical/technological (three indicators), and seismic (two indicators).

Ke et al., (2021) used optimized naïve Bayes models for predicting rock-burst failures in underground projects. They used an evolutionary random forest model for identifying significant input parameters. They selected the maximum tangential stress, elastic energy index, and uniaxial tensile stress using feature selection techniques for the optimized naïve Bayes models.

2.11 Summary

Rockburst is a phenomenon of sudden dynamic failure and instability in the rock mass. It often causes injury to workers and results in economic losses for underground excavation, including mining and civil engineering. As mining goes deeper due to the depletion of shallow deposits, the occurrence of rockbursts is expected to increase. Literature reviews have shown that the majority of the mining countries have records of rockburst incidents.

Most studies on predicting rockbursts focus on geotechnical factors like rock properties, stress, and energy. To the best of this Author's knowledge, there are no guidelines for selecting parameters in prediction models. In addition, there is no consensus on a universal rock burst damage classification.

Various methods have been employed to predict rockburst occurrences, including empirical, numerical simulation, monitoring technology, and mathematical or analytical methods. Microseismic monitoring technology is a better approach due to its ability to capture the entire evolution process of the rockmass deformability and instability up to the time of failure. Furthermore, the contour of microseismic event density, magnitude-frequency relation, energy concentration and variation of apparent stress accompanying apparent volume can be used as microseismic criteria to evaluate and predict rockbursts.

The simulation techniques based on numerical modelling are challenged by the poor availability of complete data sets regarding geologic, geometric, and geotechnical data that include post–failure behaviour of conditions of rock masses. Additionally, the lack of reliable model input parameters makes it more challenging to apply this method reliably. Most of the input parameters are derived from laboratory tests, making it even more difficult as this requires a high understanding of rockmass failure behaviour. In addition, the conditions or the behaviour of the rockmass deformability in the laboratory may differ from the field conditions.

The empirical method is promising as it is simple, easy to implement, and can be conveniently used for engineering applications. However, the models have limited validity in some cases, giving rise to doubts concerning their effectiveness since they are often derived from the interpolation of curves and barely have a physical meaning. The empirical approaches are open to improvement because they are based on limited collected data.

The mathematical or intelligent algorithms use ML algorithms and uncertainty theory algorithms and are based on the four models (i.e., linear classification, non-linear classification, classification trees and rule-based, hybrid method and ensemble models) that, with the blossom of AI and big data, intelligent algorithms are increasingly used to predict rockbursts. Compared to empirical, numerical, and experimental methods, the intelligent model has high efficiency and reasonable practicability and can foretell and prevent rockbursts in time. However, it requires high-quality data. Most of the algorithms used either are supervised or unsupervised learning. Indeed, each ML model has its supremacy and drawback, and no model can perform best for every practical engineering based on the "No Free Lunch theorem."

The superiority of the proposed RPTs over previous methods lies in their simplicity and user-friendliness. The tools require little input data, whereas the AI models and the others require many data.

CHAPTER 3: RESEARCH METHODOLOGY

3.1 Introduction

Chapter 3 outlines the research methodology to achieve the objectives stated in Chapter 1. This study aims to identify review the global factors that cause rockbursts, determine the site-specific indicators at Konkola No.1 Shaft, develop predictive tools, and validate them with data from other mines. This chapter covers research philosophy, research type, research strategy, research design, sampling, data collection, analysis techniques, and limitations.

3.2 Research Philosophy

The concept of research philosophy involves theories that explain the reality being studied and how knowledge about it is generated and justified (Natasha, 2020). Essentially, research philosophy refers to a set of beliefs and assumptions about knowledge development (Saunders, 2009). These assumptions are crucial in research because they shape the researcher's understanding of research questions, methods, and interpretation of findings (Crotty, 1988). Hence, assumptions are inherent in every stage of research. Johnson and Clark (2006) emphasize the importance of being aware of the philosophical commitment while selecting a research strategy since it significantly affects the investigation's focus. According to Moon and Blackman (2014), philosophical perspectives are significant because they reveal the assumptions researchers make about their research, leading to choices that apply to the purpose, design, method, and methods of investigation, as well as data analysis and interpretation. They categorise these assumptions into Ontology, Epistemology, and Axiology, which are discussed as research philosophies.

The researcher adopted ontology, epistemology, and axiology as research philosophies in this study. Using ontology helped the researcher understand how studying rockburst phenomena could lead to new knowledge. The study added significant value to the existing academic knowledge base on rockburst prediction by developing tools to predict rockburst potential. This work provides valuable insights for professionals in the industry.

The epistemological stance helped the researcher understand the process of acquiring knowledge. The study began by recognising the rockburst events at Konkola Mine No.1 Shaft as a challenge. Through data analysis and tools development, the researcher gained knowledge that would not have been possible without these rockbursts.

The axiological stance helped the author appreciate the value of the knowledge gained through tool development for predicting rockburst potential. This knowledge will undoubtedly contribute to intellectual knowledge in mining, geology, and civil engineering.

Overall, adopting these three research philosophies helped the researcher understand the rockburst phenomena and its potential impact on the industry.

The Ontology, Epistemology, and Axiology philosophies adopted by the author.

3.2.1 Ontology

The first branch is an ontology, which is concerned with what exists in the world about which humans can acquire knowledge. Ontology helps researchers recognize how certain they can be about the nature and existence of objects they are researching. For instance, what 'truth claims' can a researcher make about reality? Who decides the legitimacy of what is 'real'? How do researchers deal with different and conflicting ideas of reality? Ontology is based on the philosophy that reality is constructed within the human mind, such that no one 'true' reality exists. Instead, the reality is 'relative' according to how individuals experience it at any given time and place (Moon and Blackman, 2014).

3.2.2 Epistemology

The second branch of philosophy known as epistemology deals with questions of knowledge, including what qualifies as valid and legitimate knowledge and how we can convey it to others (Burrell and Morgan, 1979). It encompasses the study of the nature, origin, and limits of human knowledge. The term comes from the Greek words epistēmē ("knowledge") and logos ("reason") and is sometimes referred to as the theory of knowledge. Moon and Blackman (2014) explain that epistemology covers all aspects of how knowledge is acquired, validated, and limited in scope. Researchers rely on epistemology to determine how they approach their work, examining the relationship between subject and object. Objectivist epistemology posits that reality exists independently of individual perception, providing reliability and external validity. In contrast, subjective epistemology suggests that reality is interpreted and shaped by individuals in various symbol and language systems, with people assigning meaning to the world in ways that make sense to them.

3.2.3 Axiology

The third branch of philosophy is axiology that deals with the role of values and ethics in the research process. It focuses on judging the values of various aspects related to research. The term "axiology" is derived from the Greek language and means "value" or "worth". Assessing the role of the researcher's values at all stages of the research process is the main concern of axiology (Saunders et al., 2012). This branch of research philosophy is primarily concerned with determining the aim of the research, whether it is to explain or predict the world, or simply to understand it (Li and Lings, 2008). In other words, axiology highlights the values that a researcher holds while conducting research. This is crucial because values influence the way research is conducted and how research findings are valued.

3.3 Research Paradigms

Alongside the philosophical approaches, also a research paradigm that guides and makes the researcher aware of the existing knowledge and relevant data collection methods. Saunders (2009) presented five major research paradigms in business and management, positivism; critical realism; interpretivism; postmodernism; and pragmatism. Out of these paradigms, the researcher adopted pragmatism.

In this study, the author adopted a pragmatic approach based on several factors, such as the typical knowledge acquisition process, which follows a top-down approach from problem formulation through literature review, data collection, data analysis, and development of tools to predict rockburst potential leading to specific conclusions. Through the pragmatic stance, the author knew the study's objective was to produce practical mining solutions by developing tools to predict rockburst potential. Therefore, the study focused on practical solutions and outcomes with a problem-solving approach that would inform future practices.

The adopted paradigm, pragmatism is briefly discussed.

3.3.1 Pragmatism

Pragmatism states that concepts are only useful if they can be applied to practical actions (Kelemen & Rumens, 2008). This philosophy believes that research should begin with a problem that requires a practical solution to inform future practices.

3.4 Research Type

Dudovskiy (2022) classified research methods into five categories based on various factors, such as the nature and purpose of the study, data collection methods, type of data, research design, and other attributes. The categories include descriptive versus analytical, applied versus fundamental, qualitative versus quantitative, primary versus secondary, and exploratory versus conclusive research.

The author chose to use descriptive research in this study as the goal was to establish facts through data collection and analysis. There was no manipulation of variables or parameters. The author also employed applied research, as the aim was to solve rockburst challenges by developing tools to predict rockburst potential. This study drew verified conclusions through observations, fieldwork, and experimentation.

In this study, both quantitative and qualitative research methods were employed. Quantitative research was used for data collection that involved figures and calculations, such as in Chapter 4, where results were presented in tables, figures, and charts. Qualitative research was also used in Chapters 4 and 5, where geological structures were described rather than quantified. Additionally, rockburst classification was also described using qualitative methods.

Primary data collected included unconfined compressive strength (UCS), unconfined tensile strength (UTS), Rock Quality Designation (RQD), maximum tangential stress calculated based on UCS values, elastic modulus, elastic strain energy (W_{et}) calculated based on elastic modulus and UCS, and principal in situ stress magnitudes based on in situ stress measurements conducted at Konkola Mine No.1 Shaft by Rock Mechanics Technology (RMT) in 2001.

The author used secondary data collection techniques to gather 40 rockburst events from the Konkola microseismic database. For each rockburst event, the author gathered quantitative data on microseismic factors, including local magnitude (M_L), seismic potency (P), seismic energy (E), and the ratios of the S-wave energy (E_S) to the P-wave energy (E_P).

Conclusive research was adopted in this study, as the ultimate aim was to develop tools to predict rockburst potential. Thus, verified conclusions were drawn through observations, fieldwork, and experimentation. Empirical research was also adopted as the study aimed

to develop tools to predict rockburst potential, leading to verified conclusions through observations, fieldwork, and experimentation.

The study employed descriptive and applied research, quantitative and qualitative research methods, and conclusive and empirical research types to develop tools to predict rockburst potential.

3.4.1 Descriptive Versus Analytical Research

In this study, the author adopted descriptive research because the ultimate aim was to establish the facts through data collection and analysis. Furthermore, there was no control over variables or manipulation any of the parameters.

The research type can be divided into two groups: descriptive and analytical. Descriptive research usually involves surveys and studies that aim to identify the facts. In other words, descriptive research mainly deals with the description of the state of affairs as it is at present (Herbst and Coldwell, 2004), and there is no control over variables in descriptive research. In other words, the researcher will not manipulate any of the parameters of interest but will report them as they are.

Analytical research, on the other hand, is fundamentally different in a way that the researcher has to use facts or information already available and analyse these to make a critical evaluation of the material (Herbst and Coldwell, 2004).

3.4.2 Applied vs. Fundamental Research

Research types can be divided into two categories: applied research and fundamental research. Applied research is also referred to as action research, and fundamental research is sometimes called basic or pure research. In applied research, the aim is to find a solution to an immediate problem facing society. Fundamental research is mainly concerned with generalisations and with the formulation of a theory.

3.4.3 Quantitative Versus Qualitative Research

This type of research can be broadly divided into two – quantitative and qualitative categories. An emphasis of this approach is placed on the collection of numerical data and drawing inferences from the data (Kumar, 2008). In simple terms, quantitative research involves figures and calculations in data collection and analysis. In quantitative studies, research findings are presented via tables, graphs, and charts. Qualitative research, on the other hand, is based on words, feelings, emotions, sounds and other non-numerical and

unquantifiable elements. It has been noted, “Information” is considered qualitative in nature if it cannot be analysed using mathematical techniques.

3.4.4 Primary Research versus Secondary Research

Research can be divided into two types: primary and secondary. Primary research involves collecting new data through surveys, interviews, and observation. Secondary research uses existing studies and sources such as books and journals. Primary research also includes analyzing existing data during the literature review stage.

3.4.5 Exploratory Versus Conclusive Research

This type of research is categorised according to research design and can be divided into two groups – exploratory and conclusive. Exploratory studies only aim to explore the research area and they do not attempt to offer final and conclusive answers to research questions. Conclusive studies, on the other hand, aim to provide final and conclusive answers to research questions.

3.4.6 Conceptual Versus Empirical Research

Conceptual research involves exploring abstract ideas or theories, often used by philosophers and thinkers to generate new concepts or reinterpret existing ones. Empirical research, on the other hand, relies on observation and experience, often without considering a systematic approach or theoretical framework. This type of research uses data to draw conclusions that can be verified through observation or experimentation.

3.5 Research Strategy

The research strategy refers to how the research is conducted based on the aims of the study. Several research strategies exist including experiments, case studies, ethnography, grounded theory, action research and phenomenology. Cresswell (2007) presents five approaches: narrative research, phenomenology, grounded theory, ethnography, and case study. Merriam (2009) stated that these approaches have some similarities, they each have a different focus, sample selection, data collection and analysis and write-up.

For this study, a case study approach has been chosen.

3.5.1 Case Study

Case studies have a wide range of applications. They can be used to verify strategic interactions in rationalist scholarship and identify necessary and sufficient conditions. Several scholars have suggested the following uses of case studies:

- They have the potential to challenge established theoretical assumptions by explaining why certain cases do not align with theoretical predictions and specifying the theory's scope conditions (Jason and John, 2014);
- They are helpful when dealing with causal complexity, where there may be equifinality, complex interaction effects, and path dependency (Alexander and Andrew, 2005; John, 2007);
- They may be more appropriate than quantitative methods for empirically verifying strategic interactions in rationalist scholarship (Henry and Martha, 2009); and

- They can identify necessary and sufficient conditions and complex combinations of such conditions (Alexander and Andrew, 2005; John, 2007: Garry and James, 2012).

Overall, case studies can be a valuable tool for gaining in-depth knowledge and insights into specific situations.

Scholars claimed that case studies might also be useful in identifying the scope conditions of a theory: whether variables are sufficient or necessary to bring about an outcome (Alexander and Andrew, 2005; Garry and James, 2012).

The approach for the selection of case studies depends on the research problem at hand. Although a random selection of cases is a valid case selection strategy in Large-N research, numerous scholars claimed it risks generating serious biases in Small-N research (Garry et.al, 1994; Alexander and Andrew, 2005; Bent, 2007; Jason and John, 2014). A random selection of cases may produce unrepresentative cases, as well as uninformative cases (John, 2007).

To resolve the deficiencies in case studies, only cases that have a high-expected information gain should be chosen (Alexander and Andrew, 2005; John, 2014; Jason, 2016). Many scholars claim outlier cases can reveal more information than the potentially representative case (Huayi, 2015; Peter et al., 2016; Jason, 2016).

A common limitation ascribed to case studies is that they do not lend themselves to generalizability (Garry et al., 1994). Owing to the small number of cases, it may be harder to ensure that the chosen cases are representative of the larger population. A common problem in case study research is that of reconciling conflicting interpretations of the same

data (Alexander and Andrew, 2005; John, 2007; Bent, 2014). Another limitation of case study research is that it is hard to estimate the magnitude of causal effects (John, 2007).

3.6 Sampling Strategy

Sampling is a method used by researchers to select a representative subset of items or individuals from a population for observation or experimentation. The choice of sampling technique determines whether inferences can be made about the population or existing theories. There are two types of sampling techniques: probability or random sampling and non-probability or non-random sampling. (Taherdoost, 2016; Sharma, 2017). These techniques are presented in Figure 3.1.

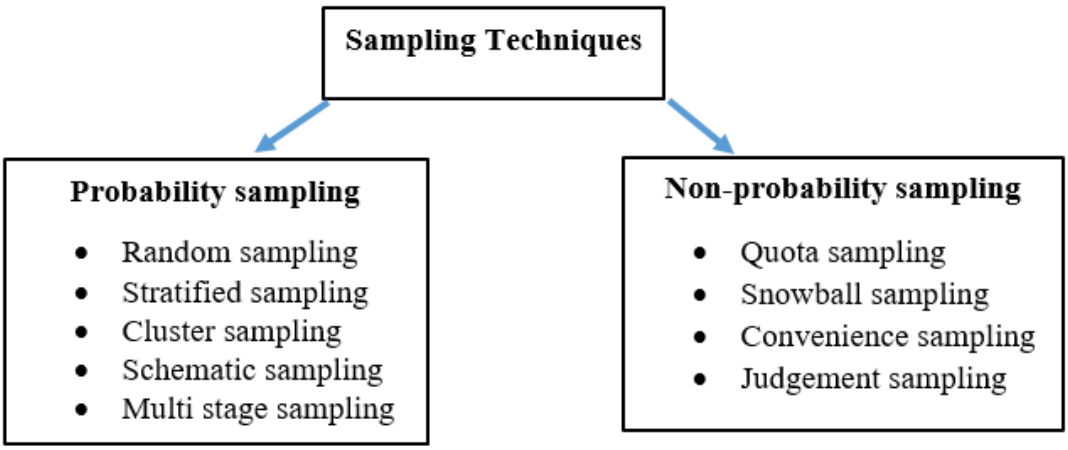

Figure 3.1: Sampling techniques (Taherdoost, 2016)

The author opted for quota sampling based on pre-determined characteristics for the case histories with the most documented rockburst contributing factors. The author chose the convenience sampling technique because of its cost-effectiveness and efficiency. The study specifically focused on rockburst incidents at the Konkola Mine No.1 shaft and global cases with a prior history of rockbursts.

3.6.1 Quota Sampling

This is a non-random sampling technique in which participants are chosen based on pre-determined characteristics so that the total sample will have the same distribution of characteristics as the wider population (Davis, 2005). Quota sampling has inherent strengths and weaknesses. According to Malhotra and Birks (2006), one strength attributable to quota sampling is that sample can be controlled for certain characteristics. The quota sampling has selection bias and no assurance, which is the weakness of this technique. For this study, quota sampling was used to select the case histories that had most and documented rockburst contributing factors.

3.6.2 Convenience Sampling

Convenience sampling is selecting participants because they are often readily and easily available. Typically, convenience sampling tends to be a favoured sampling technique among students as it is inexpensive and an easy option compared to other sampling techniques (Ackoff, 1953). Convenience sampling often helps to overcome many of the limitations associated with research. For example, using friends or family as part of the sample is easier than targeting unknown individuals. Convenient sampling is the least expensive and least time-consuming. However, it has selection bias and the sample is not representative (Malhotra and Birks, 2006).

The author selected this technique because of its cost-effectiveness and efficiency. The study focused on rockburst incidents at the Konkola Mine No.1 Shaft and global rockburst cases with prior rockburst histories.

3.7 Data Collection Methods

To collect data systematically, researchers use various techniques such as observing, interviewing, and surveying (Chaleunvong, 2009). It is important to be systematic in data collection to ensure that the research questions can be answered conclusively. For this study, archival, primary, and secondary data collection techniques were used, which were appropriate for a quantitative case study research strategy.

The primary data collected included unconfined compressive strength (UCS), unconfined tensile strength (UTS), Rock quality designation (RQD), maximum tangential stress calculated based on the UCS values, elastic modulus, elastic strain energy (W_{et}) calculated based on the elastic modulus and UCS and principal in situ stress magnitudes based on the in-situ stress measurements conducted at the Konkola mine No.1 shaft by Rock Mechanics Technology (RMT) in 2001.

These parameters were selected based on three aspects stress, strength and energy criteria.

Using secondary and archival data collection techniques, the author gathered 40 rockburst events from the Konkola microseismic database. For each rockburst event, the authors gathered quantitative data on microseismic factors, including local magnitude (M_L), seismic potency (P), seismic energy (E) and the ratios of the S-wave energy (E_S) to the P-wave energy (E_P).

The researcher adopted archival research, quantitative primary and secondary data techniques.

3.7.1 Archival Research

Archival research involves analysing data that has already been collected by others, even if it has not been analyzed or published. This method is commonly used to understand historical events and the probable conditions that led to phenomena. It is a cost-effective approach since the data already exists and allows for trend analysis over time. This method had limitations, including difficulties accessing data, ethical concerns related to confidentiality, and the possibility of imprecise or incomplete information. Despite its limitations, the author selected the archival method due to its suitability for gathering historical rockburst events and case studies.

3.7.2 Quantitative Primary and Secondary Data Collection

Primary data or raw data is a type of information that is obtained directly from the first-hand source through experiments, surveys, or observations. On the other hand, secondary data collection is used to analyse data from populations that the researcher cannot access first-hand. For example, data for this research was partly collected from the Konkola Mine No.1 Shaft database and through the internet, libraries journals and conference proceedings.

3.8 Research Design

The research design refers to the overall strategy utilised to carry out research. Zach (2020) defines research design as a succinct and logical plan to tackle established research question(s) through data collection, interpretation, analysis, and discussion. In other words, an overall strategy is chosen to integrate the different components of the study coherently and logically in order to effectively address the research problem. The research design used for this study is illustrated in Figure 3.2.

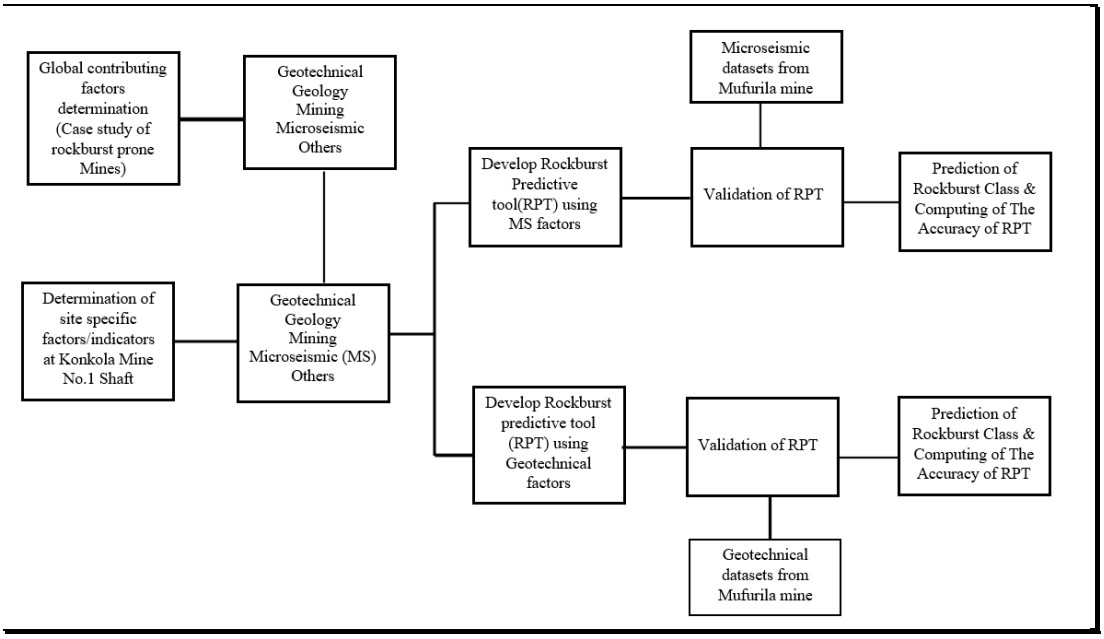

Figure 3.2: Research design flowchart

3.8.1 To review and compile the global factors or conditions that cause rockburst

The author collected 17 rockburst cases from different mines worldwide through a literature survey of conference papers and journals. The mines are presented in Table 3.1.

Table 3.1: Collected 17 rockburst cases from different mines worldwide

Case study No.1	Mine	Location
1	Long Shaft	Australia
2	Lanfranchi	Australia
3	Mount Charlotte	Australia
4	Darlot	Australia
5	Broken Hill	Australia
6	Hongtoushan	China
7	The Ashele	China
8	Dongguashan	China
9	Xincheng	China
10	Bushveld Platinum	South Africa
11	Witwatersrand	South Africa
12	Kolar Gold Fields	India
13	Sunshine	USA
14	Galena	USA
15	Brunswick	USA
16	Lake Shore	USA
17	Nickel Rim South	USA

The brief geology for each of the mines presented in Table 3.1 are described in Appendix A. The researcher selected the mines having experienced the most significant rockburst

activities. Additionally, the mines were selected based on well-documented records of rockburst occurrences and published reports analysing probable causes and mechanisms. The rockburst case histories were analysed using Microsoft Excel to establish the broad range of contributing factors relating to geology, geotechnical, mining and microseismic (MS).

3.8.2 Determination of the site specific rockburst indicators at Konkola Mine No.1 Shaft

Determination of the site-specific rockburst indicators at Konkola Mine No.1 Shaft was achieved using archival and primary data collection techniques to collect quantitative rockburst data. Forty rockburst events from 1995 to 2021 captured by MS system were collected. For each rockburst event, quantitative MS data collected were the location and time of the event, local magnitudes (M_L), logE/J, logP/m^3 and $E_S\_E_P$ ratios. For each rockburst event, the author conducted fieldwork to collect data on geological and geotechnical factors using a geological compass and point load-testing machine respectively as mentioned in Section 3.9. The Leapfrog Geo and Surpac software package was used to visualize the rockburst events in the 3D Models and is discussed in Section 4.3. The collected data were analysed using Microsoft excel to establish the broad range of geotechnical and microseismic factors.

3.8.3 Development of the rockburst predictive tools using rockburst indicators

The development of the rockburst predictive tools (RPTs) followed the essential steps outlined below.

(a) Step one: Collection of data on 40 independent rockburst events

Step one involved the collection of data on 40 independent rockburst events captured by the microseismic (MS) monitoring system at the Konkola Mine No.1 Shaft to establish the significant contributing factors to rockbursts, including geotechnical, microseismic, mining and geological. The Author used primary and secondary data-gathering techniques. The primary data gathering involved laboratory testing of the mechanical properties of the rocks using compression and point loading testing machines, core logging field work and desktop study of these factors. The primary data collected included unconfined compressive strength (UCS), unconfined tensile strength (UTS), Rock quality designation (RQD), maximum tangential stress calculated based on the UCS values, elastic modulus, elastic strain energy (W_{et}) calculated based on the elastic modulus and UCS and principal

in situ stress magnitudes based on the in-situ stress measurements conducted at the Konkola mine No.1 Shaft by Rock Mechanics Technology (RMT) in 2001.

Using secondary and archival data collection techniques, the author collected 40 rockburst events from the Konkola microseismic database. For each rockburst event, the original authors gathered quantitative data on microseismic factors, including local magnitude (M_L), seismic potency (P), seismic energy (E) and the ratios of the S-wave energy (E_S) to the P-wave energy (E_P).

(b) Step Two: Analysis of the collected data

Step two involved the analysis of the collected data to establish a broad range of the contributing factors. The author used statistical tools in Microsoft Excel to analyse the data. 3D modelling software Leapfrog Geo and Surpac were used to analyse and visualise the rockburst events and to estimate hypocentral distances from the stopes, respectively. Step Two established the ranges of the microseismic, geotechnical, geological and mining factors.

(c) Step Three: Examination of the factors to establish the significant factors

Step Three involved the examination of the factors to establish the significant factors to use in the development of the rockburst predictive models. The Author examined the factors and selected the important contributing factors, specifically microseismic and geotechnical factors—the Author chose microseismic factors, including local magnitude (M_L), seismic potency (P), seismic energy (E). The geotechnical aspects selected included unconfined compressive strength (σ_c), rock quality designation (RQD), unconfined tensile strength (σ_t), tangential stress (σ_θ), principal in-situ stress (σ_1) and linear elastic energy (W_{et}).

(d) Step Four: Testing the correlations between the selected factors

Step Four involved testing the correlations between the selected factors for microseismic and geotechnical. The correlations were tested using the determination coefficient, R^2. All the factors had determination coefficients of above 0.5. However, the use of the determination coefficient, R^2 may be subject to certain limitations such as not capable of measuring goodness of fit and predictive error. Further, it does not measure how one variable explains another that could influence the outcomes.

(e) Step Five: Development of the RPTs

Step five involved the development of the RPTs. To develop the RPTs, the author followed Occam's razor principle, which suggests that "simpler models with fewer coefficients are

preferred over complex ones". However, "Things should be made as simple as possible, but no simpler," as Albert Einstein put it.

Essential steps leading to the development of the Microseismic and geotechnical-based rockburst predictive tools followed the following sequential steps:

- Categorising the parameters into four groups and assigning ratings;
- Pre-determined Rockburst classes; and
- Rockburst classification used in the RPTs.

The MS parameters were categorised into four groups with ratings of one to four. The total ratings (TR) were calculated based on the ratings assigned to each factor. Each rockburst event was described using the categories of "no damage", "minor", "moderate", and "strong" (Kaiser et al., 1996; Potvin, 2009).

(f) Step Six: Creating the rockburst prediction tools by writing the code logic in C++

Step Six involved creating the rockburst prediction tools by writing the code logic in C++ to calculate ratings based on the selected parameters for each RPT. For microseismic parameters, the program considered three parameters: Local Magnitude (M_L), Log of seismic potency, log (P/m^3), and logarithmic of seismic energy (log (E/J). Each parameter gets a rating based on specific ranges, indicating the potential class of a rockburst event. For geotechnical parameters, the program considered six parameters: unconfined compressive strength (σ_c), rock quality designation (RQD), unconfined tensile strength (σ_t), tangential stress (σ_θ), principal in-situ stress (σ_1) and linear elastic energy (W_{et}). Each parameter gets a rating based on specific ranges, indicating the potential class of a rockburst event.

(g) Step Seven: Creating the graphical interface with C# Window

Step Seven involved creating the graphical interface with C# Window. The C++ logic code was integrated into a C# Windows Forms application, resulting in a graphical user-friendly interface (GUI). Visual Studio's design tools helped to arrange labels, text boxes, buttons, and a space to show execution time.

Finally, Steps One to Seven resulted in two user-friendly programs, geotechnical-based rockburst (G_RPT) and microseismic-based rockburst predictive tool (MS_RPT) that could be used to predict rockburst classification damage class.

3.8.4 Validation of the rockburst prediction tools

The Author created two rockburst predictive tools (RPT) using the geotechnical and microseismic quantitative data. Following the development of the tools, validation of the RPTs involved testing the performance of the tools on unseen datasets from different mines. In this regard, the Author used microseismic (MS) and geotechnical datasets from the Mufulira mine with a history of rockbursts to verify the performance of the RPTs. The Author chose the mine because it is geographically close to the Konkola Mine No.1 shaft and uses the same MS system provided by the Institute of Mine Seismology (IMS). Furthermore, the geological and geotechnical settings of both Konkola Mine No.1 Shaft and Mufulira Mine are similar, further supporting the selection of the Mufulira Mine for data validation.

Sixteen rockburst events were used for verifying the RPTs. For each rockburst event, the Author collected two data sets. The two datasets, the microseismic and geotechnical, were used as input in the RPTs. The microseismic dataset comprised the local magnitude (M_L), seismic potency (Log/m^3) and seismic energy (LogE/J). The geotechnical dataset consisted of six factors: compressive strength (σ_c), rock quality designation (RQD), unconfined tensile strength (σ_t), maximum tangential strength (σ_θ), principal in-situ stress (σ_θ) and linear elastic energy (W_{et}).

The Author selected accuracy as the metric evaluation index to verify the performance of each RPT. Accuracy is a performance metric that refers to the percentage of correct predictions for the test data. The objective was to estimate the generalisations performance of the predictive performance of tools unseen data. The accuracy is defined as shown in Equation 3.1 (Brownlee, 2021).

$$\text{Accuracy (100\%)} = 1 - \text{Error Rate} \tag{3.1}$$

Where:

$$\text{Error Rate} = \left| \frac{\text{Total number of True predictions} - \text{Total number of actual}}{\text{Total Number of actuals}} \right|$$

3.9 Instruments, Data Analysis Methods and Techniques

This section covers the instruments, data analysis methods, and techniques used to collect study data. The tools and techniques employed in collecting data for research are presented.

3.9.1 Instruments

The following equipment were used to collect the mechanical properties of rock samples:

- A compression testing machine;
- A point load testing machine; and
- A core cutting machine.

Additional tools were also utilised to gather geological data, including a geological compass, measuring tape, and a geological hammer. These pieces of equipment can be found at Konkola Mine No.1 Shaft and Nchanga Soils laboratory, as shown in Figure 3.3.

Figure 3.3: Soils and rock mechanics laboratory at Nchanga Mine of Konkola Copper Mines. The author is standing and pointing to the uniaxial compression-testing machine

3.9.2 Data Analysis Methods/Techniques

Microsoft Excel, Leapfrog Geo, Surpac, and Dips software were used to analyse the data. Microsoft Excel was utilised for data visualisation and statistical analysis, presenting the results through tables, graphs, and charts presented in Chapter 4. Leapfrog Geo and Surpac 3D Modeling software were employed to analyse and visualise rockburst events and estimate hypocentral distances from stopes. Additionally, Dips, a Rocscience stereographic projection program, was used to analyse and present the orientation of

discontinuity-based data from rockburst sites. To create the logic and graphical user interfaces (GUI) for the rockburst prediction tools (RPTS), a C++ program was created. The rockburst prediction results generated by the RPTs are presented as computer printouts in Chapter 5.

3.10 Methodological Limitations

There were only 17 global rockburst case histories and 40 rockburst events at the Konkola Mine No.1 shaft, which limited the research and resulted in a few rockburst controlling factors. A bigger sample size of 40 case histories and 70 rockburst events at the Konkola Mine No.1 Shaft would have highlighted more rockburst controlling factors.

3.10.1 Sample Size Estimations

The assumed sample sizes of 40 and 70 respectively for rockburst case histories and rockburst events were calculated using Equation 3.2 (Kibuacha, 2021).

$$\text{Sample Size} = \frac{(\text{Z-score})^2 \text{ x stdDev x } (1-\text{stdDev})}{(\text{confidence interval})^2} \quad (3.2)$$

Where:

Z- Score = A value that corresponds to a percentage confidence Interval.

StdDev = Standard deviation.

Confidence level = Margin of error with a plus or minus percentage.

For instance, for calculating the sample size of 40 for the rockburst case histories, the following were assumed:

- A Z- score of 1.28 which corresponds to an 80 percent confidence interval;
- A Standard deviation (stdDev) of 0.5; and
- A confidence interval of ± 10 percent.

Similarly, for calculating the sample size of 70 for the rockburst events, the following were assumed:

- A Z- score of 1.96 which corresponds to a 95 percent confidence interval;
- A standard deviation(stdDev) of 0.5; and
- A confidence interval of ± 11.7 percent.

3.11 Ethical Considerations

When conducting research, ethical considerations are a crucial set of principles that guide the entire process. These principles include participation on a voluntary basis, informed consent, anonymity, confidentiality, the potential for harm, and communication of results (Bryman and Bell, 2007). As a researcher, I was mindful of the need to keep Konkola Copper Mines (KCM) and Mopani Copper Mines (MCM) information private and maintain the confidentiality of the data during the data collection phase. Furthermore, the works of others authors were fully acknowledged and listed in the reference section. To address any ethical concerns, I obtained informed consent from KCM and MCM before beginning my research.

3.12 Summary

Chapter 3 explicates the methodology employed to accomplish research objectives. The research philosophies of ontology, epistemology, and axiology were adopted, whereas research paradigms of positivism, critical realism, and pragmatism were selected. The Researcher opted for a case study approach due to the expected highly valuable information it would provide. The non-probability sampling was deemed the most appropriate technique for the study objectives and research questions. Archival, primary, and secondary data collection techniques were used, and Microsoft Excel was utilised for data analysis. Results were presented using graphical tools such as tables, graphs, and charts in Chapter 4. This research had limitations, including the data collection methods, sample size, and a lack of access to previous case studies on rockburst. Finally, ethical considerations for the study were presented, including privacy and confidentiality of data.

CHAPTER 4: DATA COLLECTION, PRESENTATION AND ANALYSIS

4.1 Introduction

Chapter 4 addresses the objectives of the study, including (a) reviewing and compiling the global factors or conditions that cause rockburst, and (b) determination of site-specific rockburst indicators at the Konkola Mine No.1 Shaft. Additionally, a summary of the data analysis and interpretation is provided.

4.2 Rockburst Case Histories from Other Mines and Rockburst Indicators at the Konkola Mine No.1 Shaft

The Author collected 17 rockburst cases from different mines worldwide through a literature survey of conference papers and journals. These mines were selected based on having experienced the most significant rockburst activities. Additionally, the mines were selected based on well-documented records of rockburst occurrences and published reports analysing probable causes and mechanisms. The mines are located in various countries, including Australia, China, South Africa, India, and the USA. Generally, these mines have high quality rocks, which are stiff and brittle. The geology for each of these mines are provided in Appendix A. The locations of these mines are shown in Figure 4.1, while Table 4.1 provides more details on the six underground mines in Australia, four in China, two in South Africa, one in India, and five in the USA.

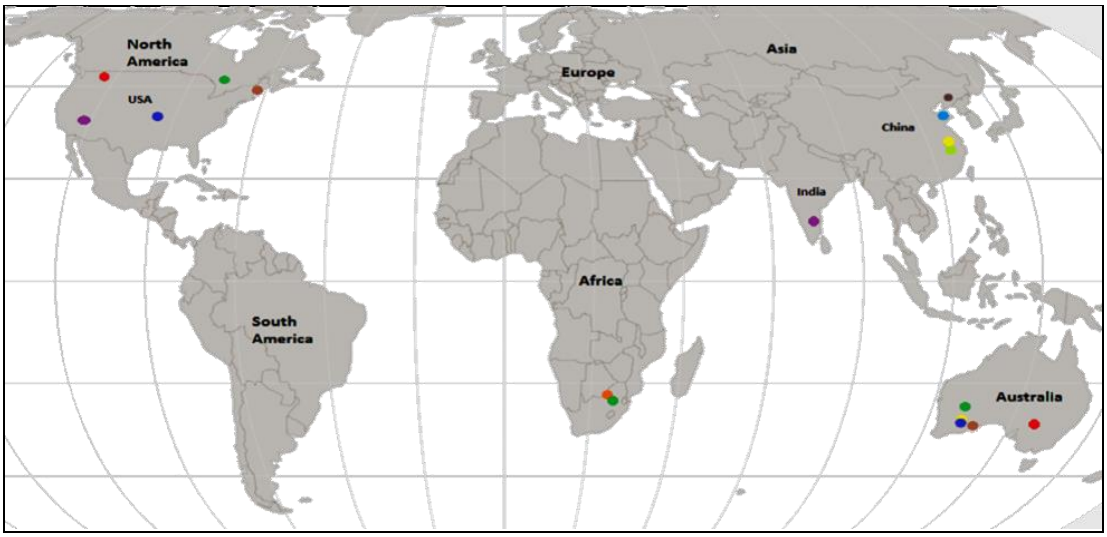

Figure 4.1: World map showing the locations of the burst-prone mines for the present study

Table 4.1: Location of rockburst case studies

Case Study	Mine	Location	*Latitude	*Longitude
1	Long Shaft	Australia	31°10′41″s	121°4′ 40″E
2	Lanfranchi	Australia	31°57′16″S	141°28′43″E
3	Mount Charlotte	Australia	30°44′16″S	121°28′40″E
4	Darlot	Australia	27°53′46″S	121°16′21″E
5	Broken Hill	Australia	31°59′14″S	141°28′01″E
6	Hongtoushan	China	42°01′08″N	124°31′57″E
7	The Ashele	China	48°17′15″N	86°20′16″E
8	Dongguashan	China	30°55′4"N	117°58′4″E
9	Xincheng	China	37°25'51″N	120°8′47″E
10	Bushveld Platinum	South Africa	24°35′40″S	27°24′16″E
11	Witwatersrand	South Africa	26°52′38″S	27°47′57″E
12	Kolar Gold Fields	India	12°56′59″N	78°16′03″E
13	Sunshine	USA	40°30′06″N	116°04′15″W
14	Galena	USA	47°28′39″N	115°58′12″W
15	Brunswick	USA	40°39′45″N	122°38′56″W
16	Lake Shore	USA	32°31′23″N	111°54′09″W
17	Nickel Rim South	USA	46°30′47″N	80°56′44″W

* The coordinate reference frame is the World Geodetic System 1984 (WGS 84)

The rockburst case histories collected for each mine were examined to determine the potential contributing factors to rockbursts. The examination of the cases established five potential classes of data. The classes of data were; microseismic (MS), geological, geotechnical, mining and ground support.

4.2.1 Microseismic Data

MS data on the magnitude, energy release, and rockburst types were extracted from each case study. The data were analysed using Microsoft Excel to determine the probable range of the quantitative seismic parameters.

4.2.1.1 Local Magnitude

A magnitude scale is a means of measuring the size of a seismic event, typically in real-time and using the amplitude of a body wave as a reference. The Local Magnitude (M_L) scale, introduced by Richter in 1935, is the most widely used measure of magnitude and requires no spectral analysis to estimate. This scale characterises mine seismic events

across the globe, except in eastern North America. In the Canadian Shield, the Nuttli (Mn) scale, developed by Nuttli in 1978, is used instead.

Seventeen M_L cases were analysed and presented in Figure 4.2.

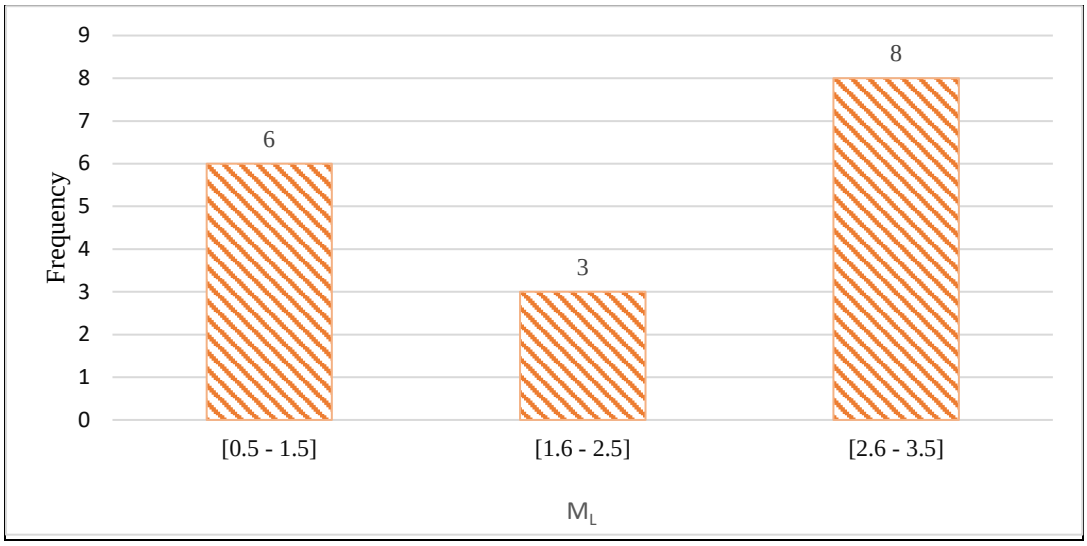

Figure 4.2: Ranges of M_L for the rockburst events for case studies

Figure 4.2 shows that six mines had an M_L from 0.5 to 1.5, three from 1.6 to 2.5, and eight from 2.6 to 3.5. Therefore, the mines affected by rockbursts have a probable M_L range from 0.5 to 3.5.

4.2.1.2 Source Failure Mechanisms (Rockburst Types)

The source failure mechanisms defining the rockburst type for each case study were analysed, as presented in Figure 4.3. The source failure mechanisms were classified as pillar burst, strain burst, and fault slip.

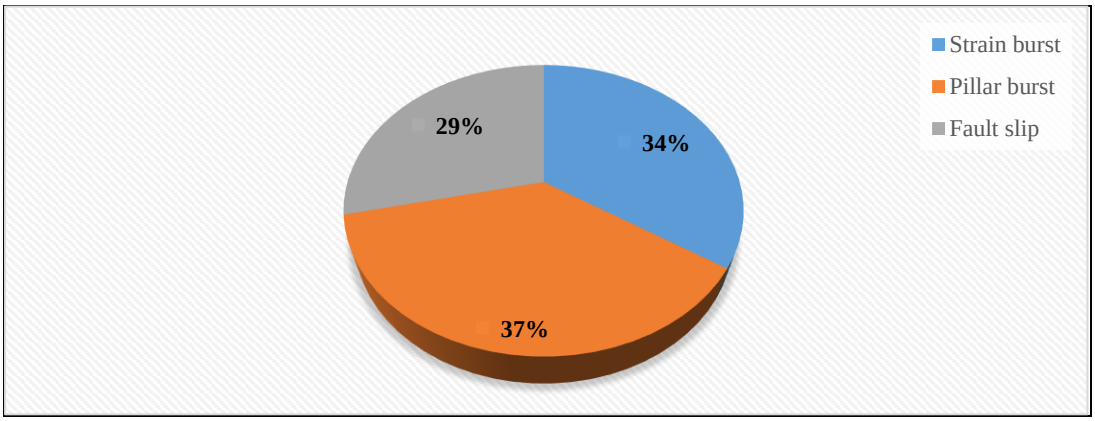

Figure 4.3: Distribution of analysed source failure mechanisms for case studies

Figure 4.3 displays the distribution of source failure mechanisms for rockburst events in case histories. The analysis revealed that pillar bursts accounted for 37 percent of source

failures, strain bursts for 34 percent, and fault slips for 29 percent. This suggests that pillar and strain bursts are more common failure mechanisms linked to the occurrence of rockbursts compared to fault slips.

4.2.2 Geological Data

For each rockburst case study, the following qualitative and quantitative data were extracted:

- The dip of orebodies;
- Lithological units; and
- Significant geological structures.

4.2.2.1 Orebody Orientation

The orientation, specifically the dip of the ore body, is one of the critical factors in mining method selection. Other factors are the size and shape of the ore body, the grade of mineralisation, the strength of the rock materials, and the depths involved. If the dip is greater than 50°, then mining methods using gravity to move the ore can be considered. These methods are open stoping, vertical crater retreat (VCR), shrinkage stoping, and panel stoping. If the dip is less than 25°, the mining methods do not depend on gravity. These methods are cut and fill, room and pillar, and reef mining may be considered. Special mining methods may be required for ore bodies with between 25^0 and 50^0 dips.

The author analysed orebody dips linked to rockbursts in each case study. The orebody dips were identified and presented in Figure 4.4.

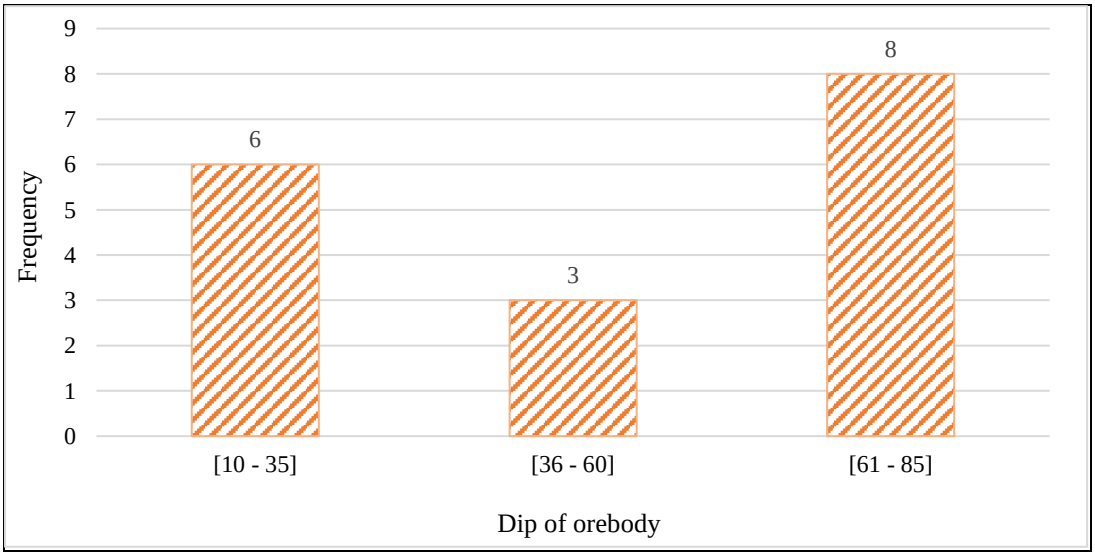

Figure 4.4: Orebody dips linked to rockbursts for the case studies

According to the analysis depicted in Figure 4.4, amongst the 17 case studies reviewed, eight showed an orebody dip from 61^0 to 85^0, while six exhibited a dip ranging from 10^0 to 35^0. The remaining three cases had a dip from 36^0 to 60^0. These findings suggest that mines at a greater risk of rockburst typically have an orebody dip of 61^0 to $85^{0.}$

4.2.2.2 Rock Types

To determine which rock types were most susceptible to rockbursts, an analysis was conducted on the rock types present in each case history. The study categorised the rock types into five groups: igneous, meta-igneous, sedimentary, metasedimentary, and metamorphic. Seventeen cases were examined, and the findings are displayed in Figure 4.5.

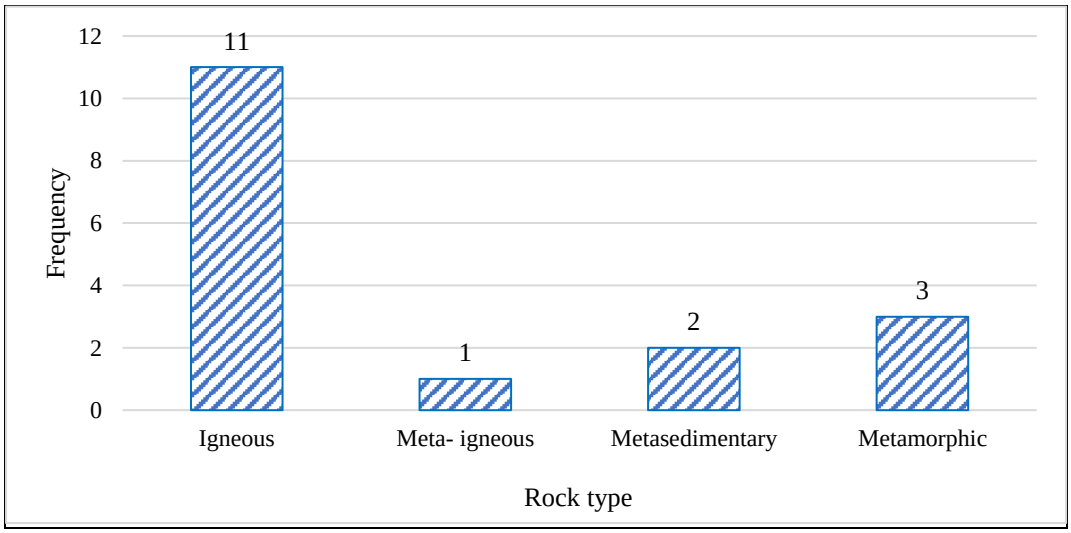

Figure 4.5: Distribution of rock types for case studies

From the analysis of seventeen case studies shown in Figure 4.5, it was observed that 11 cases were associated with igneous rocks, while three cases were related to metamorphic rocks. One and two cases were related to meta-igneous and metasedimentary rocks, respectively. The analysis shows that igneous and metamorphic rocks are more likely to experience rockbursts than other types of rocks. Furthermore, the rock types per location of the rockburst cases were found as shown in Table 4.2.

Table 4.2: Dominant Rock types per location of rockburst cases.

Location	Dominant Rock type
Australia	Igneous
China	Igneous
South Africa	Metasedimentary
India	Metamorphic
USA	Metamorphic and Igneous

4.2.2.3 Geological Structures

For each rockburst case study, qualitative and quantitative data on the significant geological structures were determined, as presented in Figure 4.6. The geological structures were faults, dykes, intrusions, foliations, dense joints, folds, and shear zones.

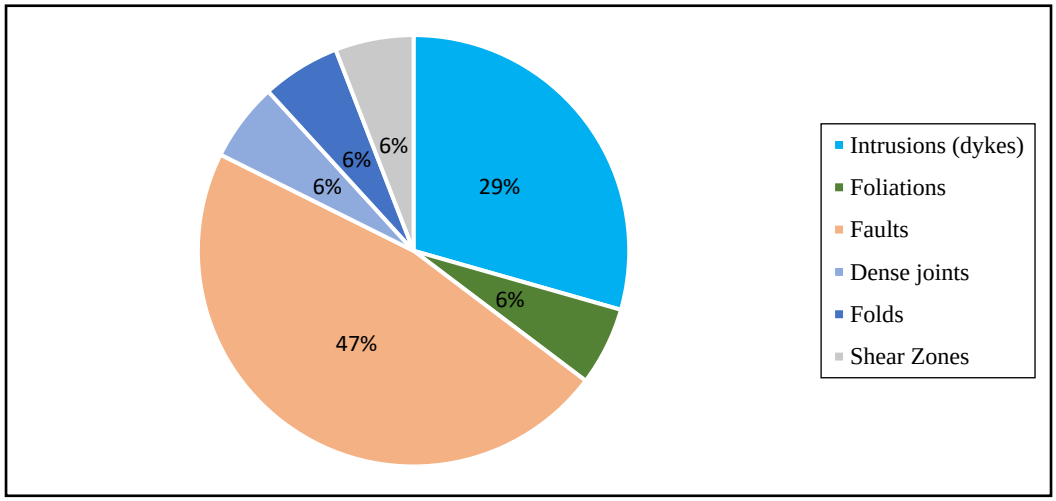

Figure 4.6: Distribution of major geological structures for case studies

Figure 4.6 shows the distribution of major geological structures analysed for the 17 rockburst cases. The geological structures were confined within the rockburst sites. The analysis shows that 47 percent of the geological structures were for faults, 29 percent were for intrusions that included dykes, and six percent each for dense joints, folds, and shear zones. Thus, geological structures, particularly faults and intrusions, are among the most significant rockburst-controlling factors.

4.2.3 Geotechnical Data

Geotechnical data for each rockburst case were analysed to determine the rock mass strength, stress environment, and deformation moduli (Elastic modulus, Poison's ratio) of the rock units.

4.2.3.1 Unconfined Compressive Strength

The uniaxial strength is one of the critical mechanical properties of the rocks, also known as the unconfined compressive strength (UCS), of a rock may be regarded as the highest stress that a rock specimen can carry when unidirectional stress is applied, generally in an axial direction to the ends of a cylindrical specimen(Bell, 2005). The uniaxial compression test is the direct method to obtain the UCS values.

The Author analysed the range of UCS for the case studies. The results are presented in Figure 4.7.

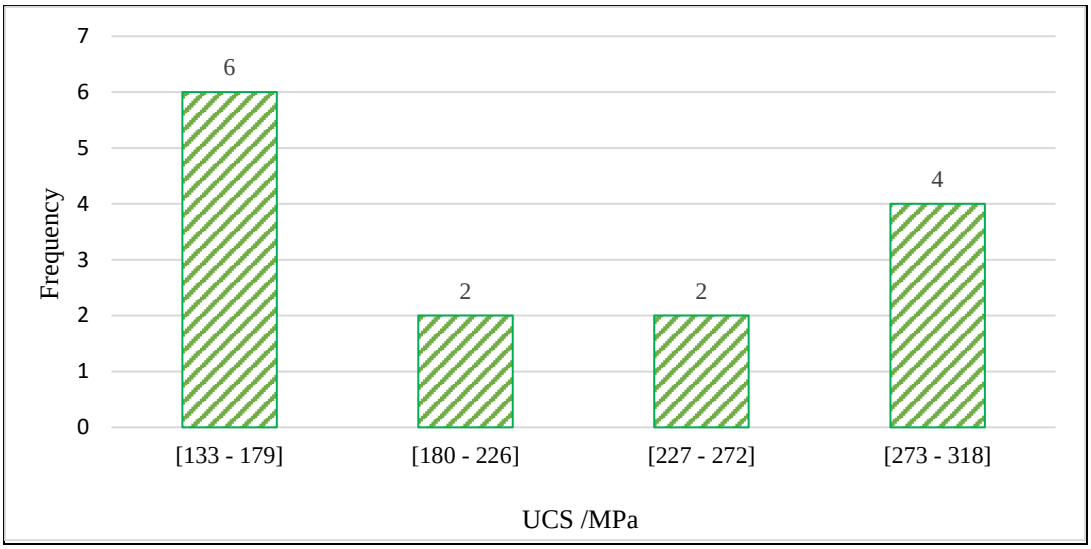

Figure 4.7: Ranges of UCS for the rockburst events for case studies

Based on the 14 case studies reviewed, Figure 4.7 indicates that six cases had an unconfined compressive strength (UCS) of 133 to 179 MPa, while four cases had a UCS of 273 to 318 MPa, two cases had a UCS of 180 to 226 MPa. Additionally, two cases had a UCS of 227 to 272 MPa. These findings suggest that rocks affected by rockbursts typically have a UCS ranging from 133 to 318 MPa.

4.2.3.2 Maximum Tangential Stress

Tangential stress is the critical parameter in the evaluation of rockburst proneness. It has been widely used in many rockburst prediction criteria, as evidenced by the literature on the stress method of rockburst predictions (Turchaninov et al., 1972; Russenes, 1974; Grimstad and Barton, 1993; Wang et al., 1998). Wang et al., (1998) defined the tangential stress criteria as a ratio of the tangential stress around the excavations opening to the UCS of rock. Grimstad and Barton (1993) introduced a criterion for rockburst prediction based on the measured in situ stresses and strength of samples. Rockburst intensity is based on the ratio of the maximum tangential stress to the UCS of rock. Russenes (1974) introduced another empirical method to evaluate rockburst risk. They related tangential stress and the strength of the rock. The method is defined as a ratio of the maximum tangential stress (MTS) surrounding the rock to the UCS of the rock.

Turchaninov et al., (1972) defined the Turchaninov criterion (Turchaninov method) to measure the rockburst intensity. They related the sum of the tangential stress and maximum major principal stress to the UCS of the rock.

The Author analysed the range of MTS for eleven case studies; the results are presented in Figure 4.8.

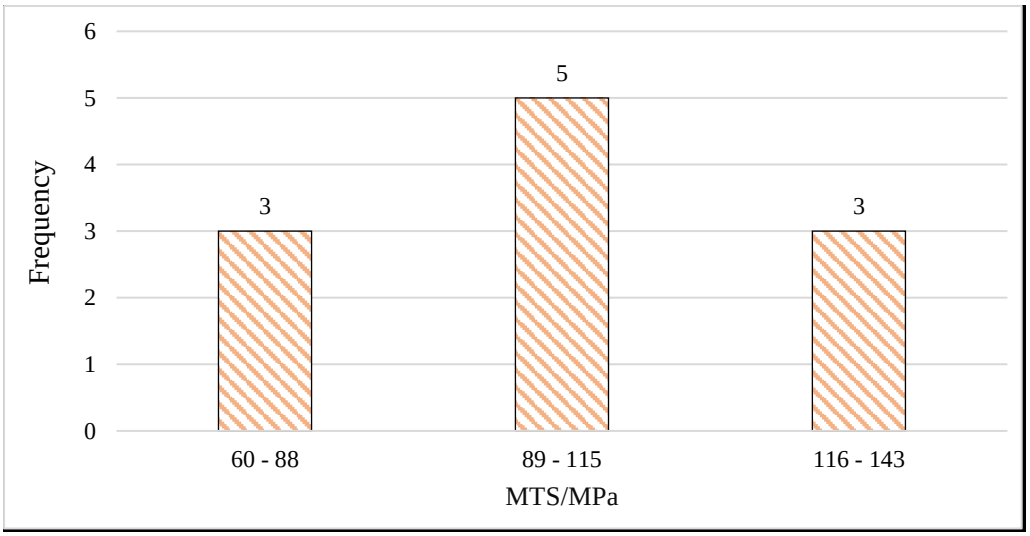

Figure 4.8: Ranges of MTS (MPa) for case studies

Figure 4.8 shows that three cases had maximum tangent stress from 60 to 88 MPa, five had MTS of 89 to 115 and three had MTS between 116 and143 for the 11 out of 17 case histories. Based on this analysis, rockburst typically occurs when maximum tangent stresses range from 60 to 143.

4.2.3.3 Poisson's Ratio

Poisson's ratio measures the deformation of a material in a direction perpendicular to the applied force (Belyadi, 2019). Poisson's ratio is an important mechanical property describing the deformation behaviour of a rock material (Belhaj, 2023). Poisson's ratio (ν) is defined as the ratio of radial to axial strain and is shown in Equation 4.1.

$$\nu = -\frac{\Delta\varepsilon_r}{\Delta\varepsilon_a} \tag{4.1}$$

Where:

$\Delta\varepsilon_r$ = is a change in radial strain, and

$\Delta\varepsilon_a$ = is the change in axial strain.

Poisson's ratio contains a minus sign so that normal materials have a positive ratio (Ebnesajjad, 2015). It ranges between 0.1 and 0.45, is dimensionless, is a crucial measure of a rock's strength, and relates to its closure stress.

The author analysed the range of Poison ratio for nine case studies. The results are presented in Figure 4.9.

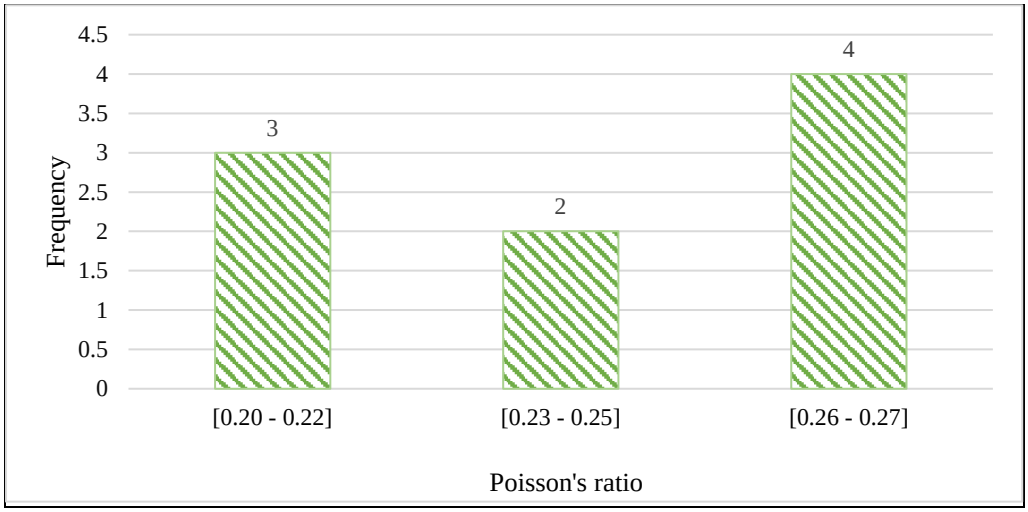

Figure 4.9: Ranges of Poisson's ratios for case studies

Figure 4.9 shows the analysed range of Poisson's ratio from 0.2 to 0.27 for the nine case histories reviewed that had data on poisons ratio. The analysis reveals that rocks prone to rockburst have a Poisson ratio of 0.2 to 0.27.

4.2.3.4 Elastic Modulus

Young's modulus, also known as the elastic modulus (E_m), is an important parameter to describe the stress and strain relationship. E is the ratio of stress to strain given by Equation 4.2 (Hudson and Harrison, 1997).

$$E_m = \frac{\sigma}{\varepsilon} \qquad (4.2)$$

Where:

E_m = Elastic modulus in GPa.

σ = Stress in N/m^2.

ε = Strain.

E_m describes the capacity of rock deformation or the stiffness of a rock. A high E_m rock is less deformable (i.e., stiff). The initial part of the complete stress-strain curve will be steep. A low E_m (soft) rock is more deformable, and the initial part of the complete stress-strain curve will be gentle (Hudson and Harrison, 1997).

E_m is a critical parameter in predicting the ability of a material to withstand pressure and plays a critical role in the design process of rock-related projects. E_m provides insight into

the magnitude and characteristics of the rock mass deformation due to changes in the stress field.

The author analysed the range of E_m for the case studies; the results are presented in Figure 4.10. Out of the 17 case studies, only six mines had elastic modulus data.

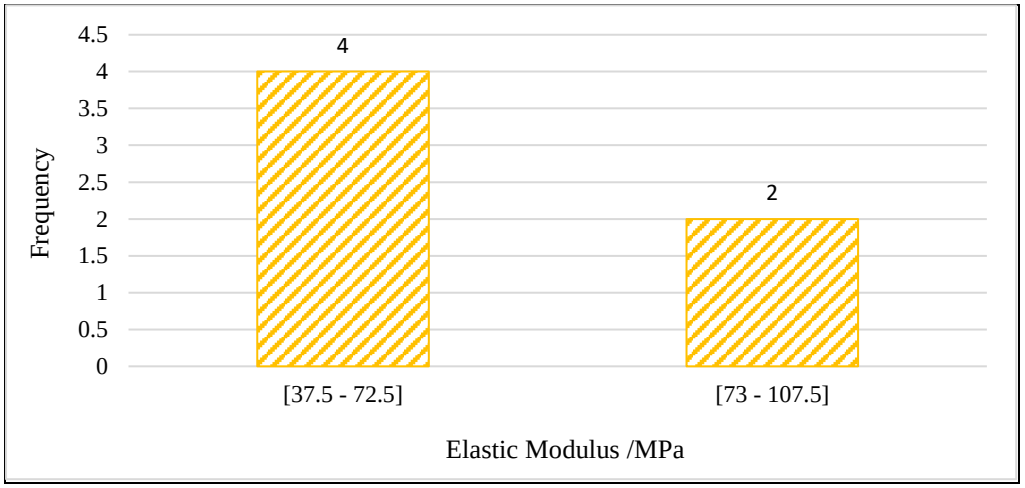

Figure 4.10: Ranges of elastic modulus for case studies

Based on the analysis in Figure 4.10, four had an elastic modulus range of 35.7 to 72.5 GPa, while two had a range of 73.5 to 107.5 GPa. The analysis indicates that rocks that experience rock bursts usually have an elastic modulus range of 37.5 to 107.5 GPa.

4.2.3.5 Unconfined Tensile Strength

The maximum tensile stress that rock material can bear, known as the ultimate strength in tension, defines the unconfined tensile strength of rocks (Hudson and Harrison, 1997). Microcracks present in rock material result in low tensile strength. This makes rock material susceptible to sudden rock failure even under minor strain. Various tests like a direct tensile test, indirect tensile strength, and the Brazilian test are conducted to determine the tensile strength of rock materials. Among them, the Brazilian test is the most commonly used.

The Author analysed the unconfined tensile strength (UTS) range for the case studies presented in Figure 4.11.

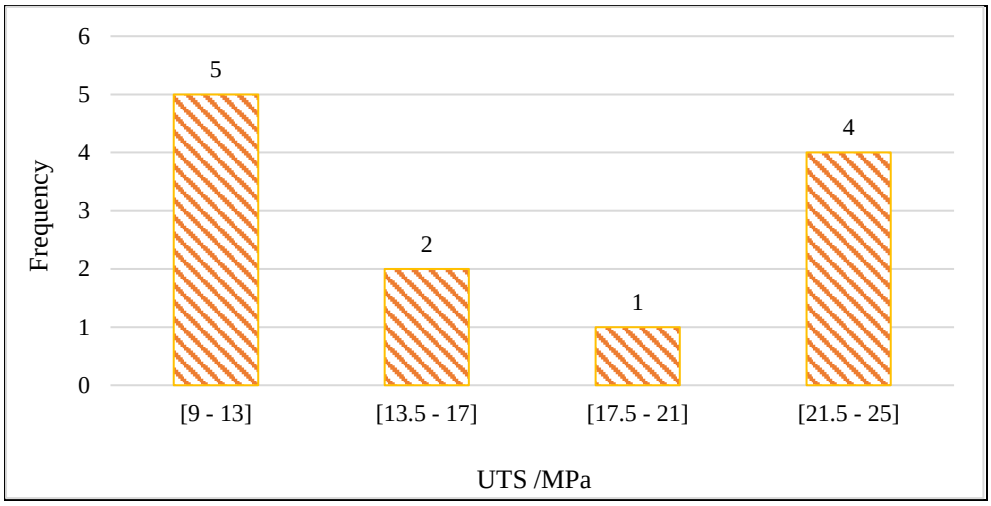

Figure 4.11: Ranges of UTS (MPa) for case studies

Figure 4.11 shows five cases had UTS of 9 to 13 MPa, two with UTS of 13.5 to 17 MPa, one with UTS of 17.5 to 21 MPa and four cases with UTS of 21.5 to 25 MPa. According to the results shown in Figure 4.11, rocks (that were looked at) affected by rockbursts generally have an unconfined tensile strength (UTS) ranging from nine to 25 MPa.

4.2.3.6 Ratio of Major Principal Stress (σ_1) to Minor Principal Stress (σ_3)

The rock in the earth's crust is subjected to an in-situ state of stress, and when an excavation is made in the rock, these stresses are disturbed and re-distributed in the vicinity of the excavation. If the induced stresses become too high and exceed the strength of the rock, fracture occurs. In that case, it can lead to the failure of the adjacent rock near the excavation boundary, which may take the form of gradual closure of the excavation, roof falls and slabbing of sidewalls or, in extreme cases, rockbursts (Hoek and Brown, 1980).

The in-situ stresses are the principal stresses and are customarily denoted by the symbols σ_1, σ_2 and σ_3. By convention, σ_1 is chosen for the largest positive or major principal stress, σ_3 is chosen for the smallest positive or minor principal stress, and σ_2 for the intermediate principal stress.

The Ratios of σ_1 to σ_3 for the case studies were analysed, and are presented in Figure 4.12.

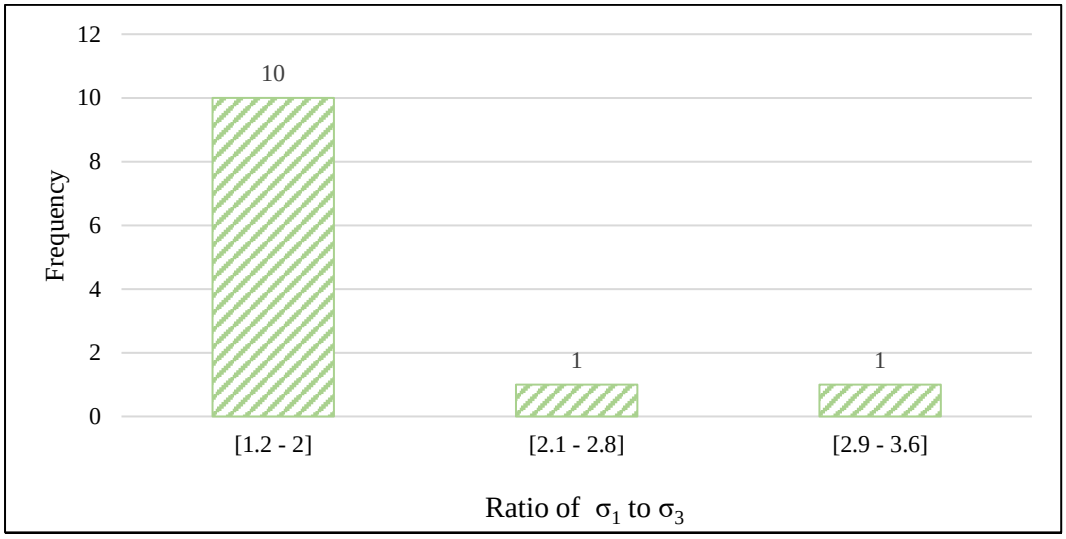

Figure 4.12: Ranges of ratios of σ_1 to σ_3 for case studies

Based on the results presented in Figure 4.12, it can be seen that among the 12 cases, 10 had a ratio of σ_1 to σ_3 ranging from 1.2 to 2. One case had a ratio of 2.1 to 2.8, while the third case had a ratio of 2.9 to 3.6. The results indicate that the ratio of σ_1 to σ_3 for rockburst typically ranged between 1.2 and 3.6 for the cases analysed.

4.2.3.7 Ratio of Unconfined Compressive Strength to Unconfined Tensile Strength

The ratio of unconfined Compressive Strength (UCS) to unconfined Tensile Strength (UTS) determines rock brittleness. This property is a significant index used to determine the intensity of rockburst in underground excavations. The rock brittleness coefficient is a widely used indicator for rockburst liability (Altindag, 2003). Mechanically, brittleness is a reduction in strength resulting from weaker bonds between the rock's grains. Based on experimental results and site investigations, the rock brittleness coefficient is defined as the ratio of UCS to the tensile strength of intact rock (Qiao and Tian, 1998; Chen et al., 2013). It is calculated using Equation 4.3 (Qiao and Tian, 1998).

$$B_i = \frac{\sigma_c}{\sigma_t} \qquad (4.3)$$

Where:

B_i = Rock brittleness coefficient.

σ_c = Uniaxial compressive strength of the rock.

σ_t = Tensile strength of the rock.

The ratios of UCS to UTS for the case studies were analysed, as presented in Figure 4.13.

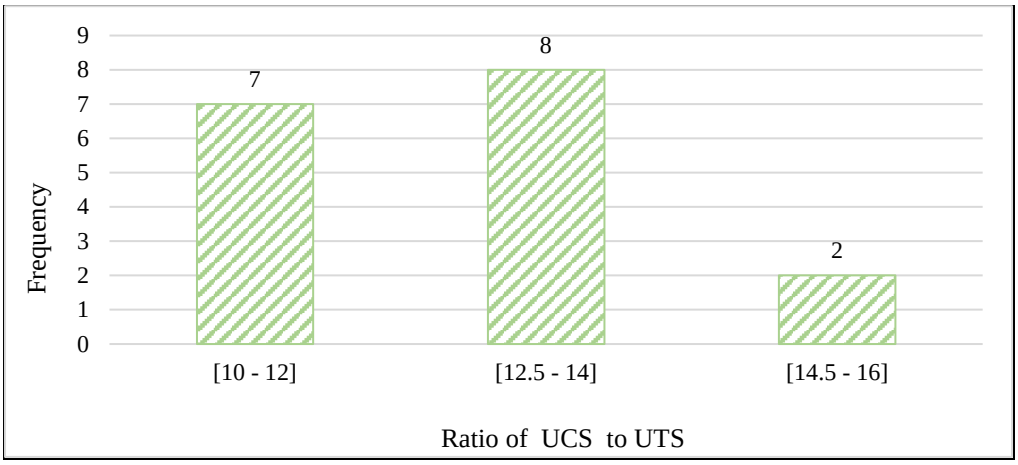

Figure 4.13: UCS (MPa) ratio to UTS (MPa) for case studies

According to the results presented in Figure 4.13, seven case studies had the ratios of unconfined compressive strength to unconfined tensile strength ranging from 10 to 12, eight from 12.5 to 14, and two from 14.5 to 16. This analysis suggests that the majority of cases examined had ratios of unconfined compressive strength to unconfined tensile strength ranging from 10 to 14.

4.2.4 Mining Data

Seventeen case studies were reviewed to determine the mining methods and mining depth in metres below the surface.

4.2.4.1 Mining Methods

The Author analysed the mining methods linked to rockbursts in each case study. Figure 4.14 depicts the distribution of mining methods percentages across all the analysed case studies.

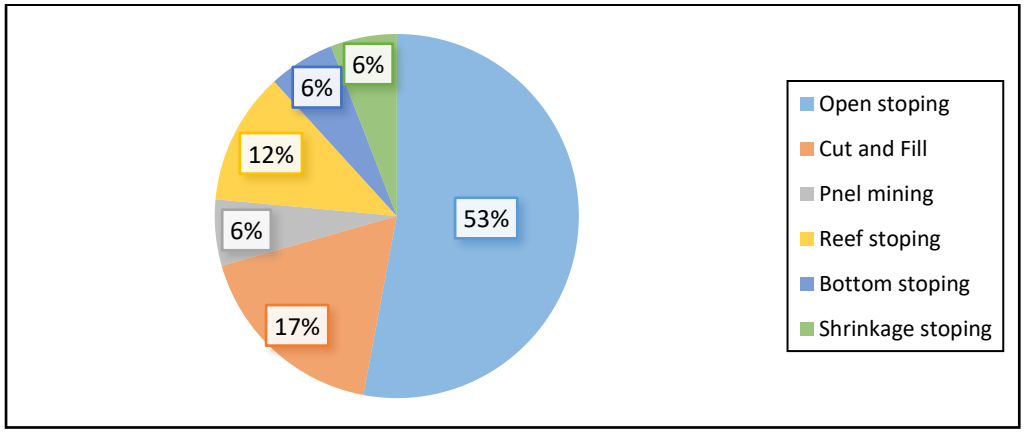

Figure 4.14 Mining methods contributing to rockburst potential for case studies

The potential for rockbursts can vary depending on the mining method used. According to Figure 4.14, open stoping accounts for 53 percent of the mining methods used in current case studies, while cut and fill accounts for 17 percent.

4.2.4.2 Critical Burial Depth for Rockburst Occurrence

In determining the occurrence of rockburst events in mining, a crucial depth below the surface is identified as the threshold depth. The threshold depth, as explained by Zhang et al., (2023), marks the point at which there is an increase in the magnitude and frequency of rockbursts in several mines. This study analysed and illustrated the critical depths for the case histories in Figure 4.15.

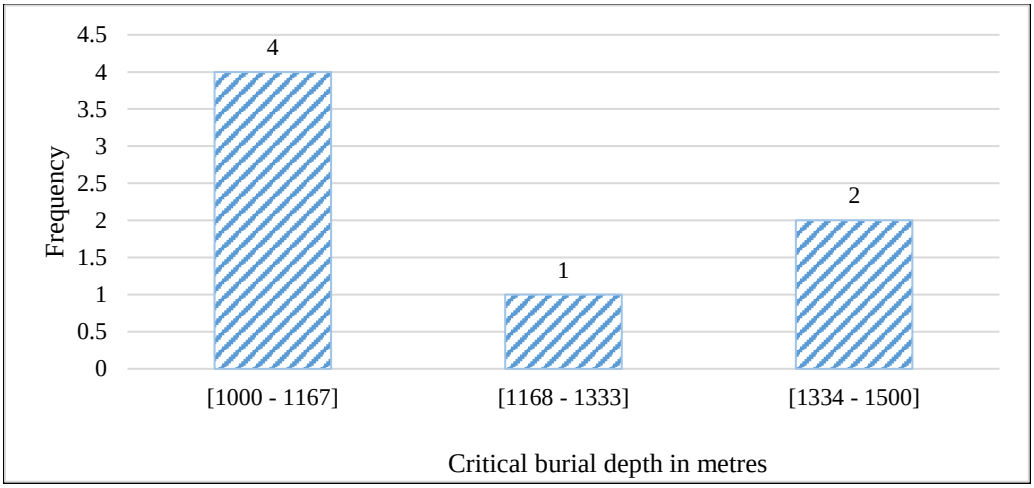

Figure 4.15: Critical depths (m) at which rockburst events were observed

Figure 4.15 shows the analysed threshold depths at which the initial rockburst occurred. Only seven of the seventeen mines examined had sufficient data regarding the critical depth. Four mines had the threshold depth between 1000 m and 1167 m, one mine had a critical depth of 1168 m and 1333 m below the surface, and two mines began experiencing rockbursts when they reached the mining depth of 1334 m and 1500 m. The analysis suggests that mining depths between 1000 m and 1500 m below the surface can be considered threshold depths, as most mines begin experiencing rockbursts at these depths.

4.2.5 Ground Support Data

The Author reviewed ground support and reinforcement measures to mitigate rockbursts for seventeen case histories. The review revealed three categories of support - backfilling of stopes, dynamic and energy-absorbing support, and design optimisation. Design optimisation refers to selecting appropriate mining or excavation methods and sequences,

and by strategically placing developments and other infrastructure (Kaiser and Cai, 2012). The three categories of support are presented in Figure 4.16.

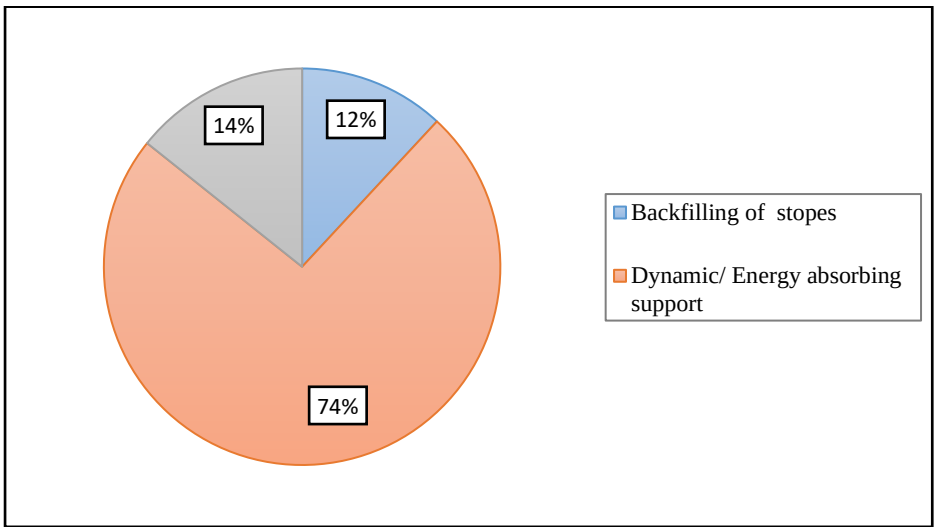

Figure 4.16: Ground support methods to mitigate rockbursts

Figure 4.16 shows that dynamic and energy-absorbing methods account for 74 percent, followed by design optimisation at 14 percent and backfilling support at 12 percent. The analysis shows that dynamic/ energy absorbing ground support methods were the most widely used methods to mitigate rockburst in the cases analysed.

4.3 Determination of the Site-Specific Rockburst Indicators at the Konkola Mine No. 1 Shaft

The Konkola Mine No.1 shaft has experienced several rockburst events since the initiation of mining-induced seismicity in early 1995. A summary of some examples of the rockburst events recorded is presented in Table 4.3.

Table 4.3: Rockburst events and consequences at Konkola Mine No.1 Shaft

Event date	Location	Consequence
01/11/1996	2825 L 502 mS Extraction drive	Production loss and excavation damage
02/06/2000	2900 L 570 mS Footwall haulage	1 fatality, production loss and excavation damage
21/06/2001	3095 L 570 mS draw point crosscut and Footwall haulage	Production loss and excavation damage
15/10/2001	3150 L 312 mN trough drive south	1 fatality, production loss and excavation damage
05/12/2013	960 mL 770 mS trough drive	Personal injuries and production loss
19/06/2014	2900 L 735 mN trough drive	Personal injuries and production loss

According to Mutale's (2004) assessment of seismic hazards at Konkola Mine No.1 Shaft, shakedown events or face bursts were the most common types of seismic activity. These events affected crosscuts more severely and frequently than other excavations. Additionally, rock burst damage was mainly found at the top eastern corner and midway between the roof and floor of the drives, resulting in a "dog ear" shape (Figure 4.17).

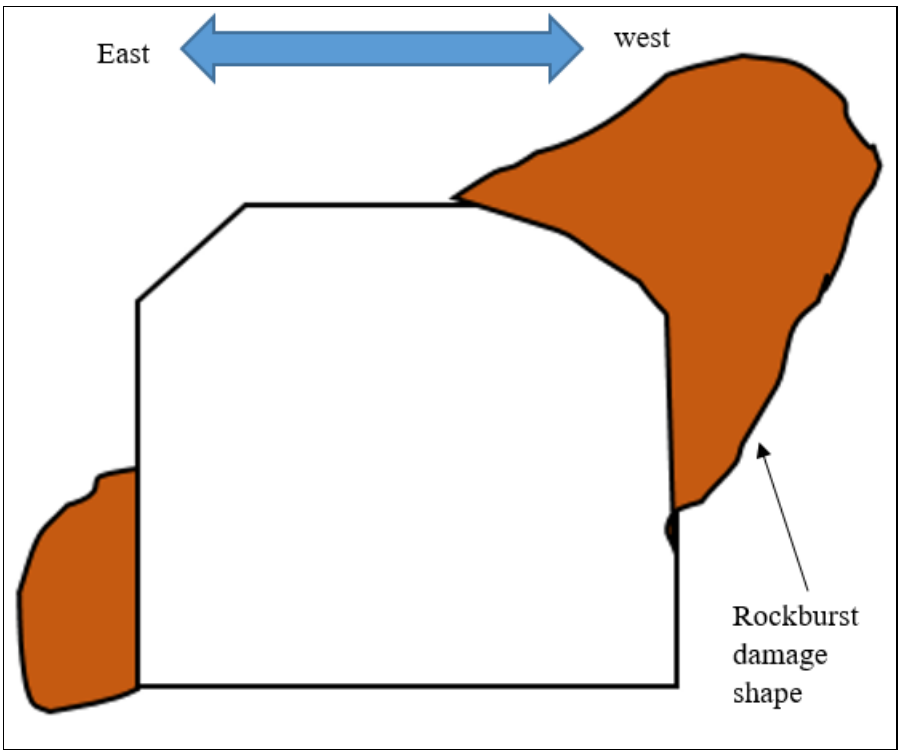

Figure 4.17: A “dog-ear” shape damaged zone after a rockburst in a 4.2 m wide by 4.2 m height crosscut mined in FWSST, FWC and partially in Ore shale (modified after Mutale, 2004)

This shape was due to rock failure in compression by principal stress in a direction sub-perpendicular to the failure zone from the top western side and dipping towards the east. The damage depth was up to 4 m, and minor damage was observed in the western roof and sidewalls. Sometimes, stress-induced fracturing of the ground was noticed in the eastern sidewall, and during severe seismic events, roof bolts were snapped and pulled out. The rock bursts also caused rocks to break around the roof bolts, leaving them protruding, and ripping the wire mesh support (Figure 4.18).

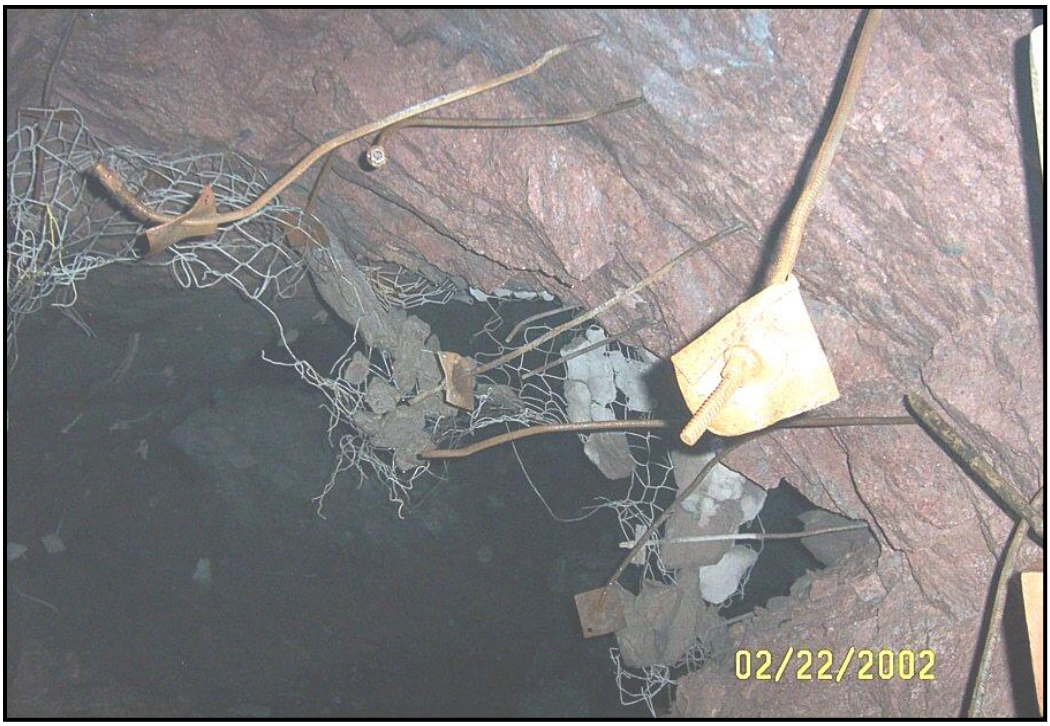

Figure 4:18: 2900L 570 mS Footwall Haulage rockburst event (Mutale, 2004)

Rockbursts severely impacted the excavation, support, production, and safety of workers, resulting in injuries and loss of life. To address these risks, the mine began monitoring microseismic activities in 1995 using the Integrated Seismic System (ISS). The system comprised two triaxial geophones in vertical boreholes - one at the No.1 shaft and the other at the No.3 shaft, approximately 35 – 40 m below the surface. While the system could not identify the precise location of events, it could determine the local Magnitude (M_L) and released energy. In 2002, Konkola replaced the old system with a new mine-wide ISS seismic system consisting of five triaxial geophones, which was operational until March 2007. In 2012, the Institute of Mine Seismology (IMS) developed a new seismic system for the mine, as depicted in Figure 4.19.

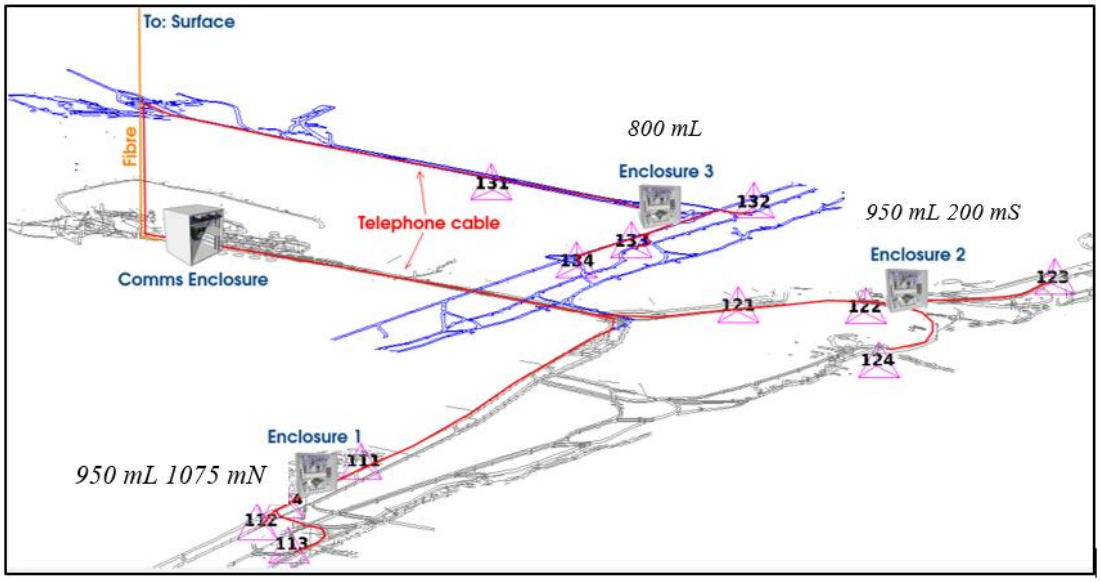

Figure 4.19: Layout of Mine-wide MS at Konkola No.1 Shaft

The system consists of three enclosures, each containing four sensors with two triaxial and two uniaxial 4.5 Hz geophones, resulting in 12 sensors. These sensors are placed in 10 m deep 76 mm diameter boreholes to ensure proper coupling to the solid rock beyond the fracture zone surrounding development tunnels. The 12 sensors are installed on two main levels, 950 mL and 800 mL.

The system uses the latest data acquisition units available from the IMS. The netSP+ (network seismological processor) and netADC (24-bit low noise network analogue to digital converter) use Ethernet technology, enabling communication. The system uses the digital subscriber line (DSL) communications protocol, which extends the network over a single copper pair at distances up to seven kilometers at speeds of up to 5.4 Mbit/sec, enabling communication with the seismic server on the surface. The seismic signals are digitised close to the sensors, so the communications between the seismometers and the central seismic server transmit only digital messages less sensitive to electrical interference. The system stopped functioning from 2013 to 2014 due to flooding that affected the Digital-Subscriber-Line-Access-Multiplexer (DSLAM) at 950mL. The system became operational in late 2015. Since then, the system has continued generating quantitative seismic data, i.e., location and time of the event, event magnitude, energy index, apparent cumulative volume, number of events, the cumulative number of events, etc.

The generated MS parameters were stored in the Konkola Seismological Database (KSD). The KSD comprises the events from 1995 to date.

In this study, the Author collected data on 40 rockbursts from 1995 to 2020, along with their accompanying MS parameters. Additionally, data on geotechnical, geological, and mining factors were collected for each event detected by the seismic system. A thorough analysis of possible indicators of rockbursts was conducted, considering MS, geotechnical, mining, and geological data, to determine site-specific indicators for predicting rockbursts. The significance of each indicator was systematically assessed in relation to the conditions at the Konkola Mine No.1 Shaft.

4.3.1 Microseismic Data

From 1995 to 2021, the Author collected quantitative data on rockburst incidents captured by MS systems, as shown in Figure 4.19. Forty rockburst events were taken from the Konkola seismological database. For each rockburst, the seismic data collected include the event dates, times, local magnitude (M_L), and location in local x, y, and z coordinates. Other data collected include Log E/J, E_S/E_P ratio, and LogP.

4.3.1.1 Rockburst Event Dates History

The author collected data on 40 rockburst events from the Konkola seismological database, specifically the dates on which these events occurred, as captured by MS systems from 1995 to 2021. This data covers nine-year period and includes information on the number of rockbursts. The Author analysed the event dates and corresponding rockburst data. The findings are presented in Figure 4.20.

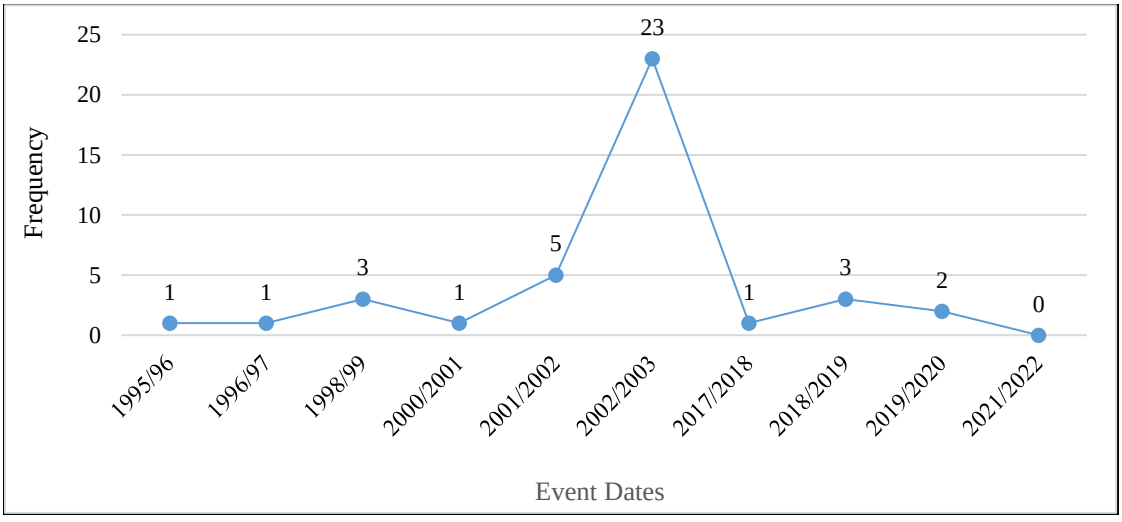

Figure 4.20: Rockburst events from 1995 to 2020

Figure 4.20 shows 40 rockbursts between the financial years (FY) of 1995/96 and 2019/20. The recorded rockburst incidents started at one in 1995/96 and peaked at 23 in the 2002/03 FY. From there, rockbursts gradually decreased, reaching zero in the 2021/22 FY. From

2001/02 to 2002/03, there was a gradual increase in production rates, accompanied by a drastic increase in the rockburst events to 23. From 2002/03 to 2021/22, there was a gradual decrease in both the production rate and the rockburst events.

4.3.1.2 Event Time History and Primary Blasting Schedule

The researcher collected data from the Konkola seismological database on rockburst events between 1995 and 2021, captured by MS systems. The data included the timing of the events and the number of rockbursts that occurred.

At Konkola No.1 Shaft, there were two blasting schedules: one from 05:30 to 6:00 in the morning and another from 17:00 to 18:00. The number of recorded rockbursts during these times was analysed. Additionally, event times and the corresponding number of rockbursts were analysed and presented in Figure 4.21.

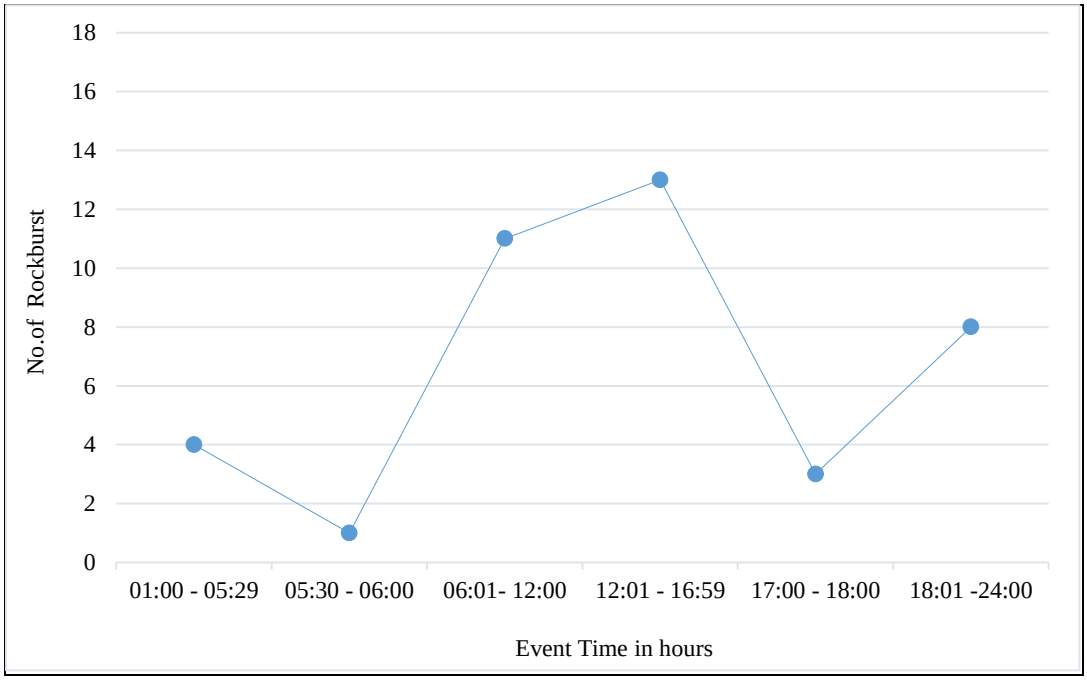

Figure 4.21: Rockburst Event times from 1995 to 2021

As depicted in Figure 4.21, the majority of rockburst incidents were observed during the hours of 06:01 to 16:59 and 18:01 to 24:00. The analysis also reveals a surge in rockburst occurrences immediately following the blasting times, represented by the on the graph. The findings suggest that blasting significantly triggers most rockburst incidents at the Konkola Mine No. 1 Shaft.

4.3.1.3 Local Magnitude

According to Mendecki et al. (1999), magnitude is a relative measure of the strength of a seismic event based on measurements of maximum ground displacement at a given

frequency at multiple seismic sites. A magnitude scale is an attempt to measure the size of a seismic event, ideally in real-time, and for some scales, in terms of the amplitude of part of the body wave that it induces. The proposed magnitude scales are often based on amplitudes recorded over a particular spectral band. The three commonly used magnitude scales are described below. The most commonly cited measure of magnitude is Local Magnitude (M_L) (Richter, 1935). M_L is based on time domain parameters and requires no spectral analysis to estimate the magnitude. Equation 4.4 (Richter, 1935) defines ML.

$$M_L = \text{Log}\,[(A\,(D)\,Kw/K)] - \log A_0\,(D) \qquad (4.4)$$

Where:

M_L = local magnitude.

Kw = the magnification of a Wood-Anderson seismograph at period T.

K = instrument magnification factor.

A (D) = the maximum trace amplitude at distance D.

Log A0 (D) = is a calibration factor.

log A_0 (D) is a calibration factor such that a standard seismograph will have a trace amplitude of 0.001 mm at a distance of 100 km for an $M_L = 0$ event.

The Richter local magnitude scale is used to characterise Mine seismic events worldwide, not just in eastern North America. For mines in the Canadian Shield, the Nuttli (Mn) scale is used (Nuttli, 1978) and expressed by Equation 4. 5.

$$Mn = -0.1 + 1.66 \log D + \log (A\,(D)/K\,T) \qquad (4.5)$$

Where:

D = the epicentral distance to the source, km.

A (D) = half the maximum peak-to-peak amplitude in the S-wave.

K = Instrument magnification factor.

T = Time of ground motion in seconds.

In studies to relate the two magnitude scales, Hasegawa et al., (1989) observed that over the range of primary interest in mine seismicity (M_L = 1.5 to 4.0), for the same event, the Mn scale records magnitudes about 0.3 to 0.6 units greater than the M_L scale.

Moment Magnitude (Hanks and Kanamori, 1979) is based on the seismic moment derived from the spectral density plot parameters and is defined by Equation 4.6 (Hanks and Kanamori, 1979).

$$M = \frac{2}{3} \log M_0 - 6.0 \quad (4.6)$$

Where:

M = the moment magnitude.

M_0 = the seismic moment (Nm).

The moment magnitude is the most commonly used measure of source strength.

It has been found that the various body-wave magnitude scales need to be revised to describe the geomechanical perturbations associated with a seismic event. Mendecki (1993) provides an example of two seismic events of local magnitude M_L = 5.9, with seismic moments Mo, which differs by a factor of 400.

This study collected and analysed 40 rockburst Local Magnitudes based on the Richter scale, as presented in Figure 4.22.

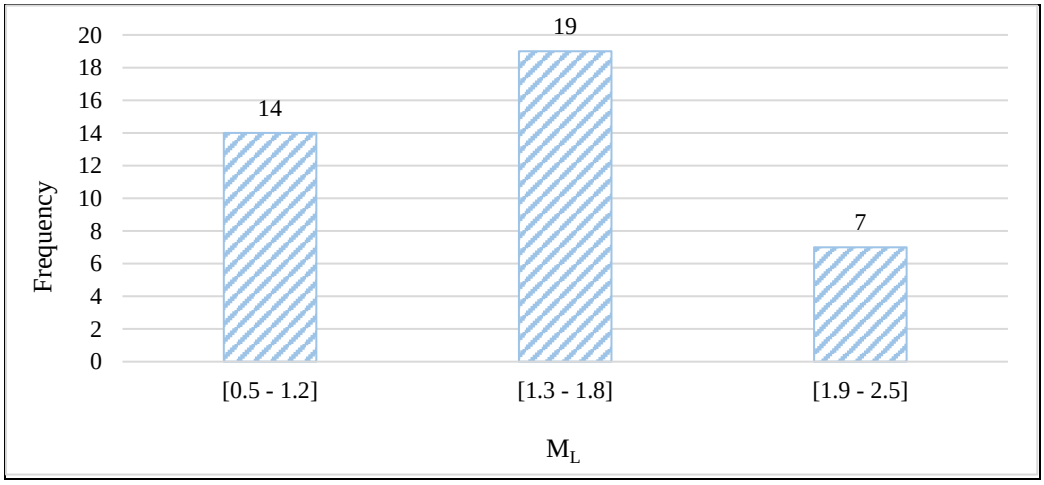

Figure 4.22: M_L and Frequency of rockbursts from 1995 to 2020

As sown on Figure 4.22, there were 40 rockburst events analysed. Among them, 14 events had a local magnitude (M_L) of 0.5 to 1.2, 19 events had an M_L of 1.3 to 1.8, and seven events were in the 1.9 to 2.5 range. The analysis indicates that most rockburst events have an M_L range of 1.2 to 1.8. The analysis suggests that for the rockburst to occur, the M_L should in the range of 0.5 to 2.5.

4.3.1.4 Location of Events in X, Y and Z Coordinates

The M_L data collected were plotted on Konkola Mine No.1 Shaft plans using Leapfrog Geo software to show the high-resolution views of 3D distribution of rockburst events at Konkola Mine No.1 Shaft between 1995 and 2020 (Figure 4.23). The Surpac Mining software was also used to plot the events and surveyed excavations, showing the 3D

distribution along the North, East, and Elevation (Figure 4.23). The rockburst events were contoured to show the event clusters from 1995 to 2020.

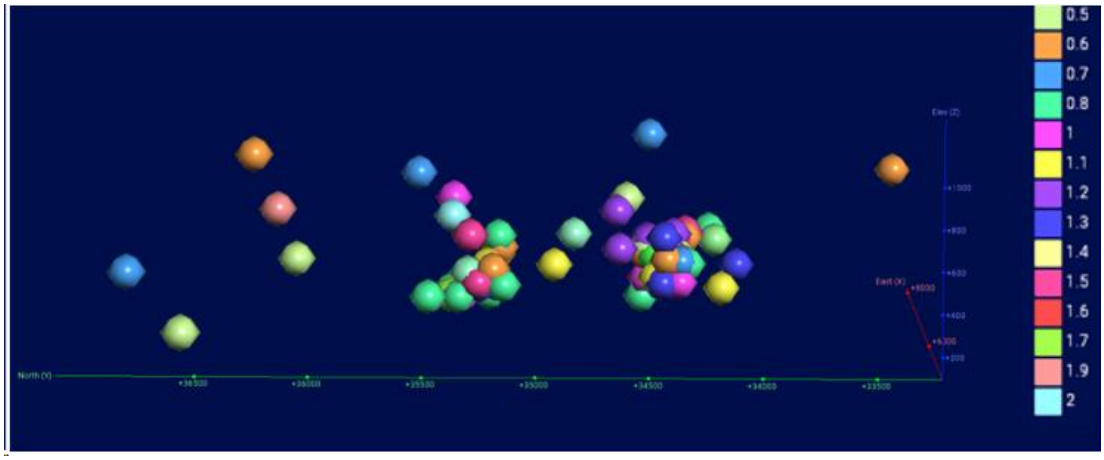

Figure 4.23: 3D Leapfrog Geo plot of the distribution of rockburst events from 1995 to 2020

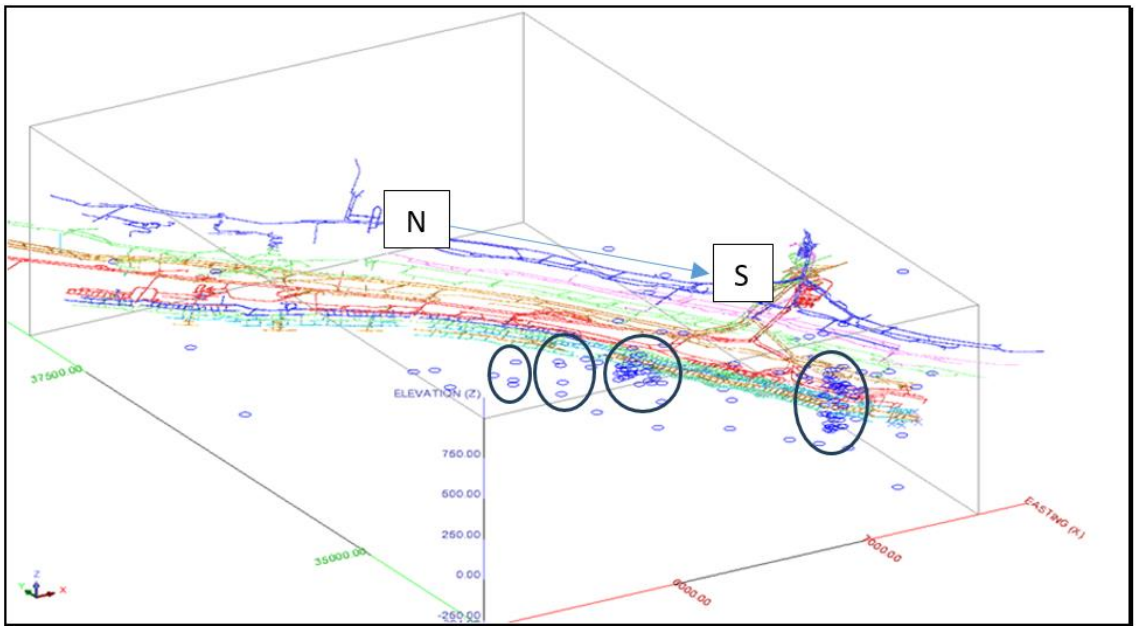

Figure 4.24: Surpac plot showing a 3D model of the seismogenic zone at Konkola No.1 Shaft with the density of rockbursts increasing in the North – south direction along strike. The four circles represent the rockburst clusters

Figures 4.23 and 4.24 show that the zone affected by the rockbursts lies within the range of 34500 mN to 35500 mN along strike, between coordinates 6000 mE and 7000 mE in the east-west direction, between 950m and 200 m above the mean seal level. The area measures 1000 m by 1000 m by 760 m. Leapfrog software was used to analyse the events and determine discernible patterns, as seen in Figure 4.25.

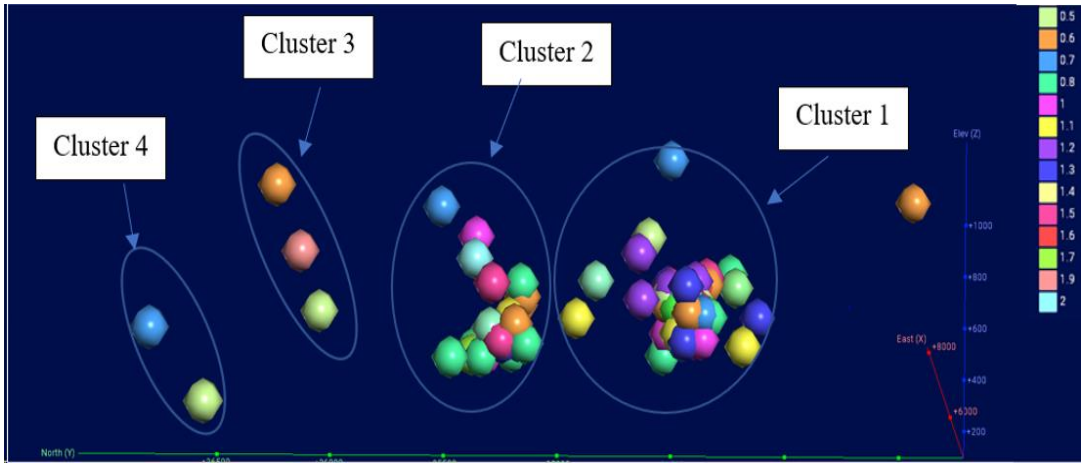

Figure 4.25: Leap Frog plot showing rockburst events Clusters at Konkola No.1 Shaft Mine

Examination of the events depicted in Figure 4.25 revealed that they followed distinct patterns, ultimately forming a cluster (as illustrated in Figure 4.25). These clusters were analysed in Leapfrog Geo software, and their unique characteristics are shown in Table 4.4, including the dip and dip azimuth measured in degrees.

Table 4.4: Orientations of Rockburst event clusters at Konkola Mine No.1 Shaft

Cluster	Dip (0^0)	Dip Azimuth (0^0)
1	55^0	193^0
2	57^0	191^0
3	77^0	192^0
4	47^0	190^0

Table 4.4 shows the characteristics of the four event clusters. The measurements indicate that cluster 1 was sub-vertical dipping at 55^0 and oriented in the SW – NE with an azimuth of 193^0. Cluster 2 was sub-vertical dipping at 57^0 with an azimuth of 191^0 in the SW – NE direction. Cluster 3 was sub-vertical dipping at 47^0 with an azimuth of 190^0 in the SW- NE direction. Cluster 4 was a sub-vertical dipping at 46^0 and the azimuth of 215^0 in the NE – SW direction.

4.3.1.5 Position of the Fault Zone in Relation to the Seismogenic Zone

The Konkola Mine No.1 Shaft has two major and five secondary fault zones. The major fault planes are the Luansobe on the south and the Lubengele to the north. The secondary faults are 2200 mN, 2250 mN, 2300 mN, 2700 mN, 2750 mN and 2800 mN (local coordinates). The Lubengele fault zone consists of faults dipping 79^0 to the south and the Luansobe fault zone with faults dipping 82^0 to the North (Mulenga et al., 1992). Faults have been identified as major regional structures at No.1 Shaft. They occur in groups on

the anticline's southern limb, ranging in width from 40m to 60m. The dip averages 75^0 - 85^0 to the north and trends in the east-west direction. The fault zones are characterised by extensive fracturing and leaching, resulting in weak ground with low friction strength. The rockburst events and fault planes were plotted using Leapfrog software to show the locality of the planes with the seismogenic zone, as shown in Figure 4.26.

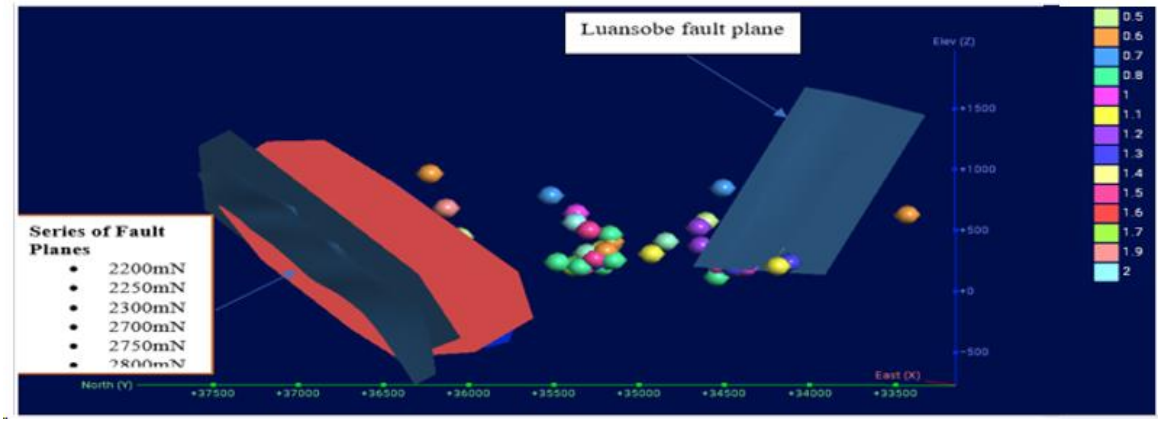

Figure 4.26: Leapfrog Geo plot showing the positions of fault planes with the seismogenic zone at Konkola Mine No.1 Shaft. The coloured balls represent the magnitudes of rockbursts

Figure 4.26 shows that one (1) major fault zone, the Luansobe on the south and the secondary fault zones bound the zone affected by the rockbursts to the north.

4.3.1.6 Seismic Potency (P/m^3)

A single dislocation source's seismic potency, denoted as P, is calculated by multiplying the average slip and the source area according to Equation 4.7 (Mendecki, 2013a).

$$P = uA \qquad (4.7).$$

Where:

P = Seismic potency.

u = average slip.

A = Source area.

In the case of a complex source, the potency is determined by multiplying the source strain and the source volume, which is given by Equation 4.8 according to Mendecki (2013a).

$$P = \Delta\sigma/\mu\ V \qquad (4.8)$$

Where:

$\Delta\sigma$	=	averaged stress drop.
μ	=	rigidity of the rock mass surrounding the source.
V	=	volume of the displaced rock.

The seismic potency is a measurable attribute found in the low-frequency range of the displacement spectrum. Correcting and estimating seismic energy is easier, making it a less uncertain parameter. Seismic potency is the second-best option for hard rock mines for seismic hazard assessment in mines (Mendecki, 2013b).

Forty seismic potencies for the rockburst events captured by the MS monitoring system were collected and analysed, as presented in Figure 4.27.

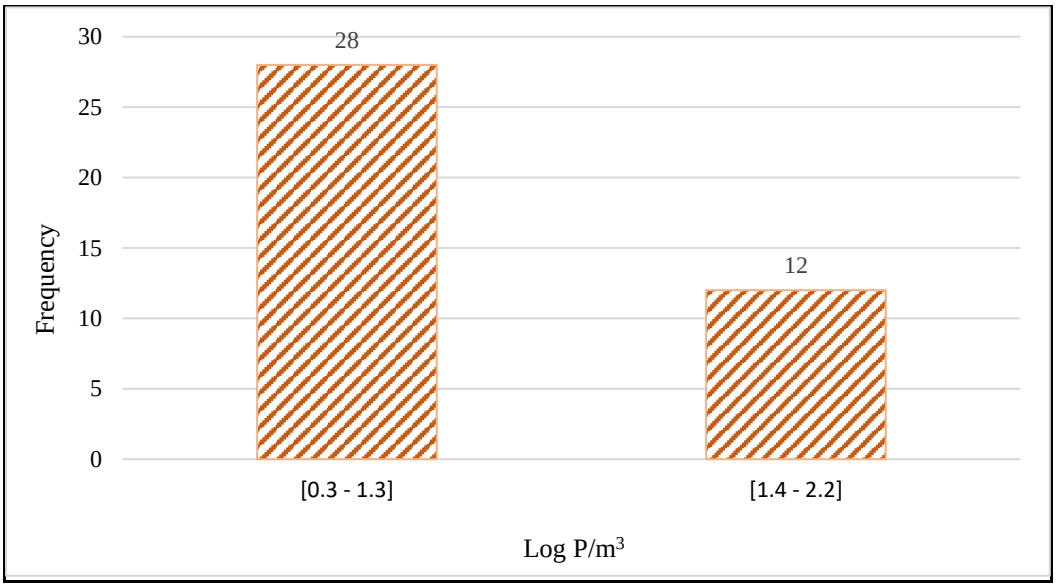

Figure 4.27 shows that 28 rockburst events had Log (P/m^3) in the range of 0.3 to 1.3 and 12 events had Log (P/m^3) in the range of 1.4 to 2.2. The analysis shows that the Log (P/m^3) for the rockburst events analysed for Konkola Mine No.1 Shaft ranged from 0.3 to 2.2.

4.3.1.7 Seismic Energy (E/J)

The radiated seismic energy, E, is the most appropriate measure of the strength of a seismic source since it controls the high-frequency radiation and drives the strong ground motion. (Mendecki, 2013a).

Forty Logarithmic values of seismic Energy (E/J) for the rockburst events captured by the MS monitoring system were collected and analysed, as presented in Figure 4.28.

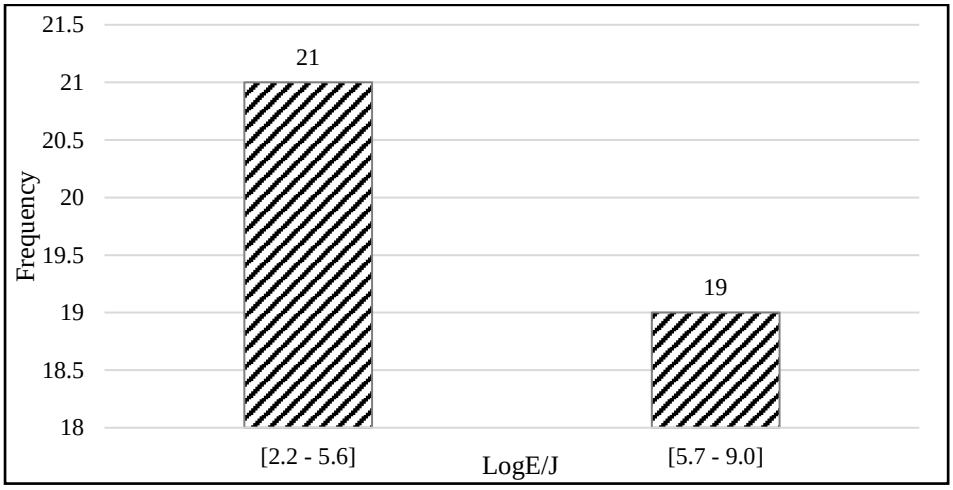

Figure 4.28: Distribution of Log (E/J) for the rockburst events from 1995 to 2020

The analysis shown in Figure 4.28 indicates that 21 rockburst events had Log (E/J) in the range of 2.2 to 5.6. Nineteen rockburst events had Log (E/J) in the range of 5.7 to 9. The results show that for the rockburst event to occur, the log (E/J) should be in the range of 2.2 to 9.0.

4.3.1.8 Ratio of E_S to E_P data

The ratio of P-wave energy to S-wave energy is an important indicator of the source mechanism of a seismic event. The ratio depends on the source mechanism; for an explosive source (blast), it is lower, and for a fault slip, it is higher (Mendecki, 2013a). The Es/Ep ratios to define the source failure mechanisms for each rockburst event were collected for this study. Fifty ratios for the rockburst events were collected and analysed. The analysis results are presented in Figure 4.29.

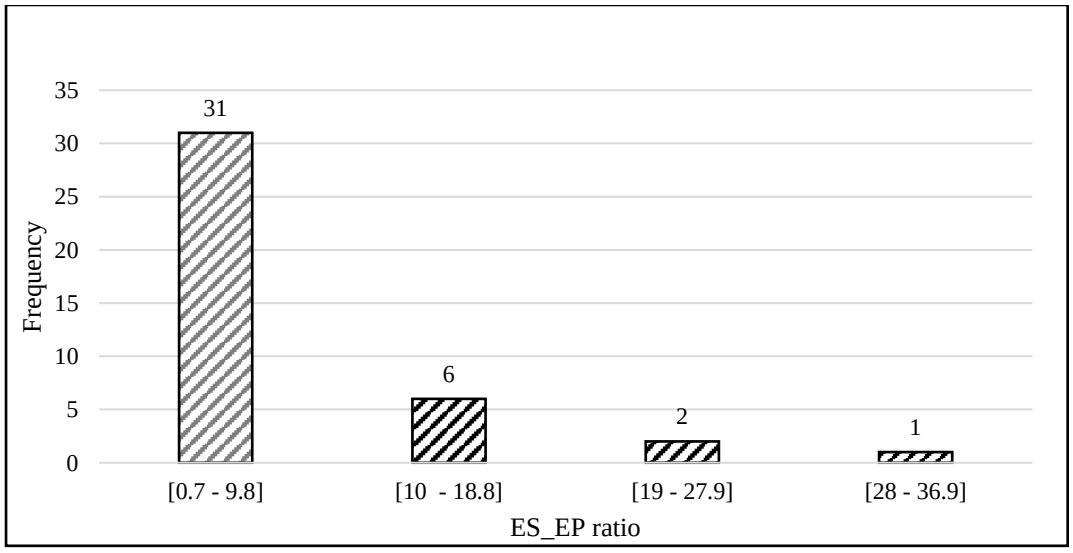

Figure 4.29: Ranges of Es/E_P ratios for Konkola Mine No.1 Shaft from 1995 to 2020

Figure 4.29 shows the E_S/E_P ratios for Konkola Mine No.1 Shaft from 1995 to 2020 for the 40 rockburst events. Thirty - one rockbursts had the E_S/E_P ratios from 0.7 to 9.8; six had the ratios in the range of 10 to 18.8, two events had the ratios in the range of 19 to 27.9 and one event had the ratios in the range of 28 to 36.9. The analysis reveals that the E_S/E_P ratios for the rockburst event were the range of 0.7 to 36.9.

4.3.1.9 Distances of Rockburst Events from Stopes (Ore shale)

In Seismology, a hypocenter is a position where the strain energy stored in the rock is first released, marking where the rock or fault begins rupturing. This occurs directly beneath the epicentre, at a distance known as the hypocentral or focal depth (UGS, 2010). Oxford English dictionary defines the epicentre, or epicentrum in seismology, as the point on the Earth's surface directly above a hypocenter or focus, where an earthquake or an underground explosion originates.

For this study, the author focused on measuring the hypocentral distances from the ore shale/ stopes. These measurements were based on rockburst events plotted on sections and plans for each elevation.

The rockbursts were plotted on the dip section using Surpac mining software. The hypocentral distances of the rockburst events were measured on three levels i.e. 500 m, 450 m and 310 m above the mean sea level. The estimated hypocentral distances are presented in Figure 4.30.

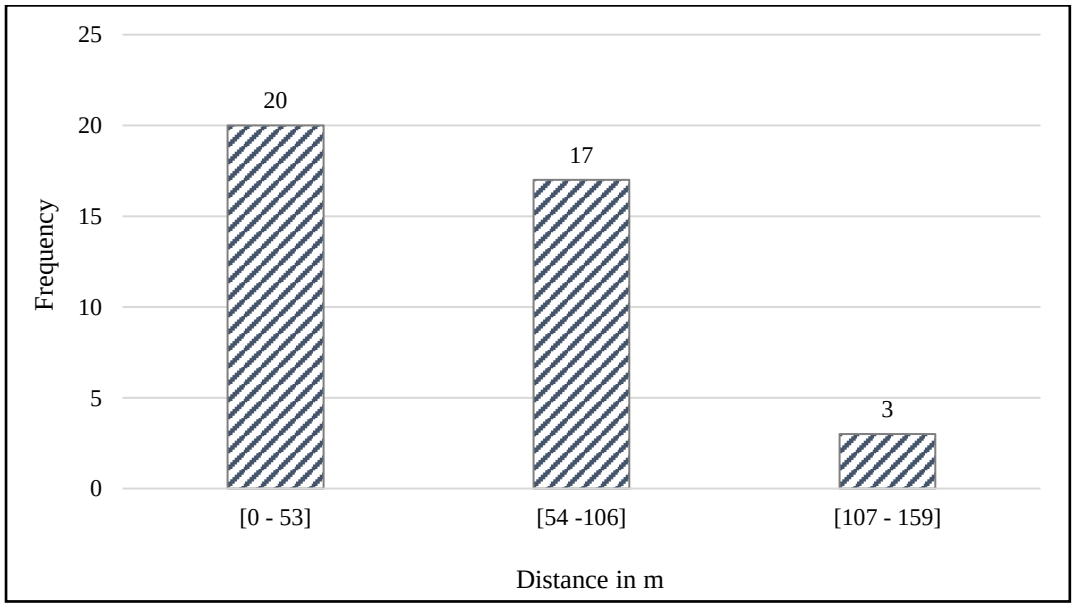

Figure 4.30: Hypocentral horizontal distances of rockburst events from stopes to the footwall side

Figure 4.30 shows the analysed hypocentral distances in meters to the stopes. Out of the 40 measured hypocentral distances for each event, 20 were between zero (0) and 53 m, 17 were between 54 m and 106 m, and the remaining three were between 107 m and 159 m. This analysis shows that the hypocentral distances at Konkola Mine No.1 Shaft were between 0 and 159 m from the stopes, with excavations within 53 m most affected by rockburst events. On the other hand, excavations such as declines and haulages located beyond 159 m from the stope face were least affected, as the number of rockburst events decreased linearly with increased hypocentral distances from the stope faces.

4.3.2 Geological Data

The Author collected qualitative and quantitative data on the lithological units, significant geological structures and orientation of orebody (dips) for the areas affected by rockbursts. The data were presented as follows:

- Rock types, and
- Geological structures

4.3.2.1 Rock Types Affected by Rockburst Events

At the Konkola No. 1 Shaft, sedimentary deposits consist of six different rock types from the hangingwall quartzite (HWQ) to the Footwall. The HWQ lies beneath the Hangingwall Aquifer (HWA) and immediately above the Ore Shale (OS), which is divided into five ore horizons (A, B, C, D, and E) and has a variable thickness of 5 to 20 m. The lowest geological unit of the orebody is Unit A, which varies in thickness from 0.5 to 1.2 m and is finely bedded, frequently weathered to brown micaceous clay, and the weakest geological unit of the orebody. The HWQ rockmass and the Footwall Sandstone (FWSST) bound the ore shale. It is thinly bedded and laminated, making it prone to bedding separation due to the tensile zone. The footwall formations (FW) underlie the ore shale and consist of various rock types, including Footwall Conglomerate (FWC), Footwall Sandstone (FWSS), Porous Conglomerate (PC), Argillaceous Sandstone (AGSS), Footwall Quartzite (FWQ), Pebble Conglomerate (PBC), and Boulder Conglomerate (BC), with the basement gneisses and schist formations underlying all these.

To determine the locations and types of rockburst events, the Author plotted the events on the dip section using Surpac mining software (Figure 4.31).

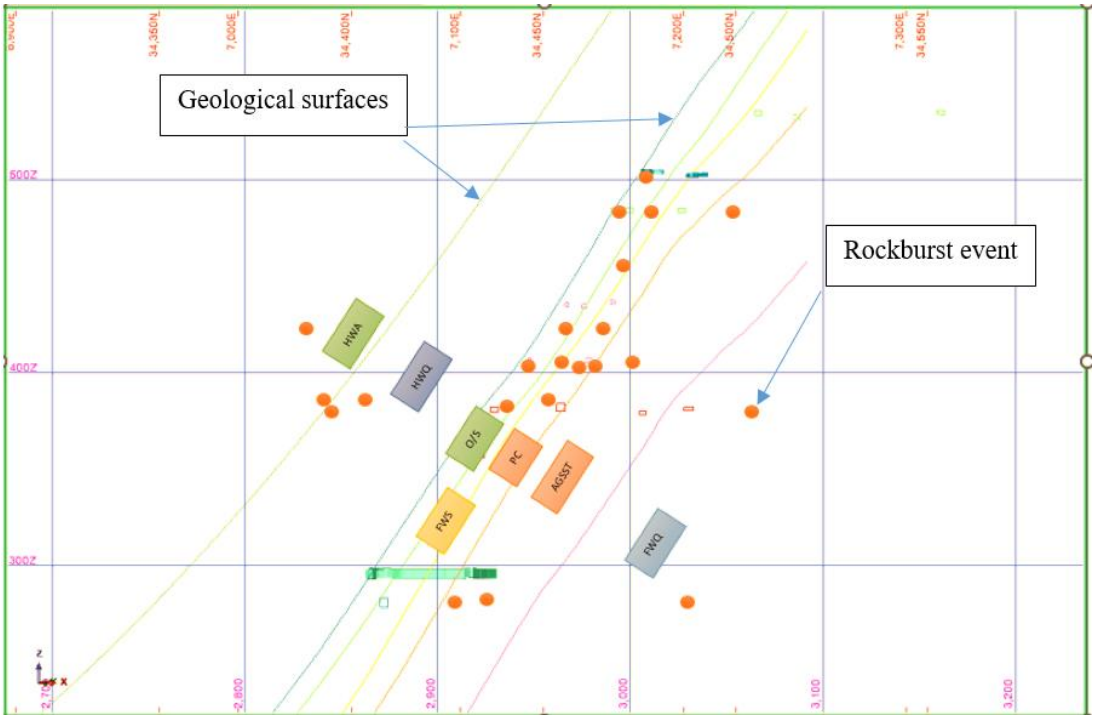

Figure 4.31: Dip section showing rock types affected by rockburst events (the events are the dotted circles and the rock types are represented by the geological surfaces)

Leapfrog Geo 3D geological modelling software owned by Sequeent Ltd was used to plot the events and geological surfaces (Figures 4.32 to 4.36).

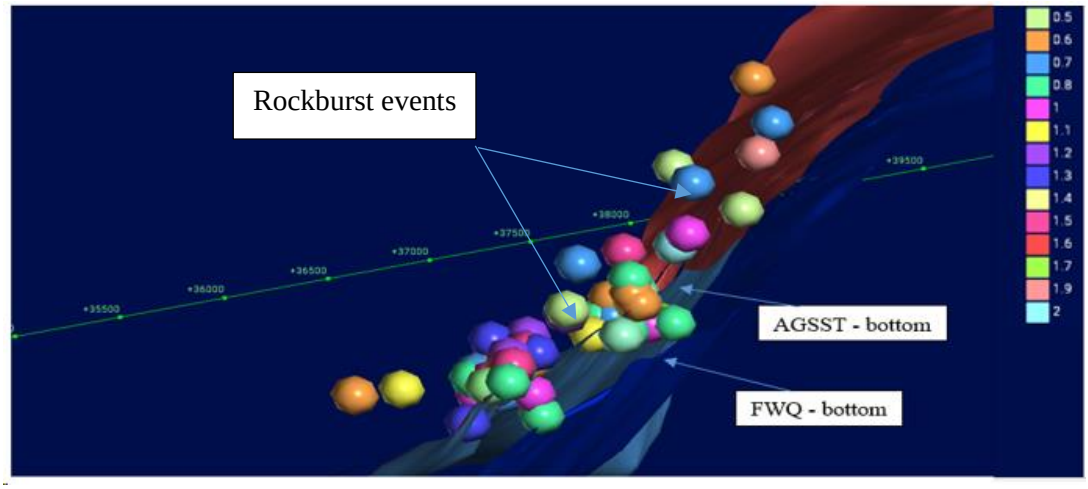

Figure 4.32: Leapfrog Geo plot showing the distribution of rockbursts in the FWQ rock unit bounded by AGSST and FWQ. (Rockbursts represented by the coloured balls)

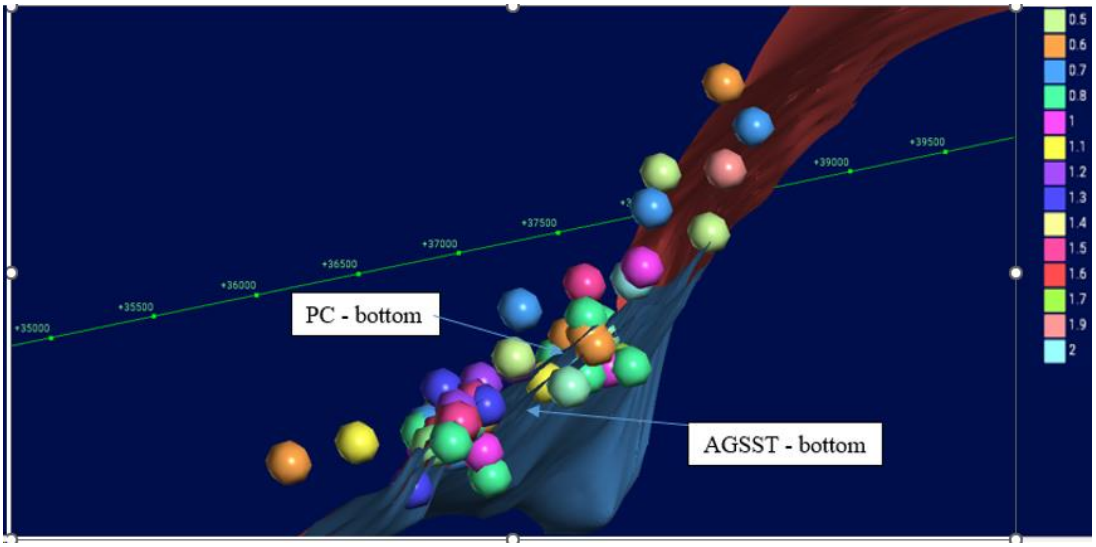

Figure 4.33: Leapfrog Geo showing the distribution of rockbursts in the PC rock unit

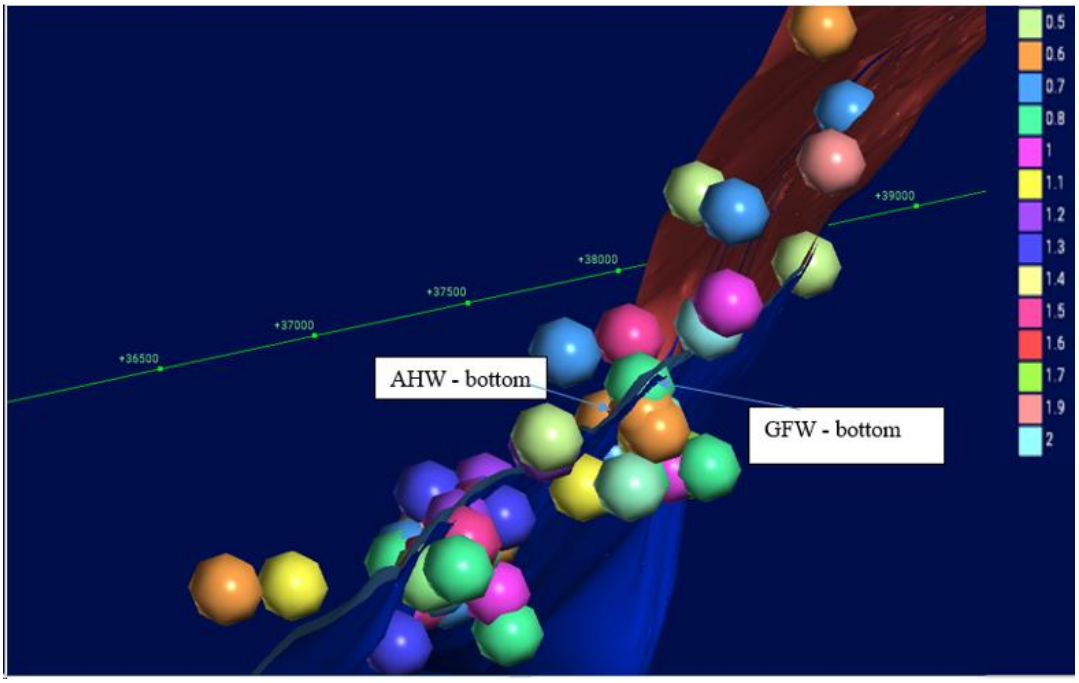

Figure 4.34: Leapfrog Geo plot showing the distribution of rockbursts in Ore shale rock unit bounded by AHW and GFW

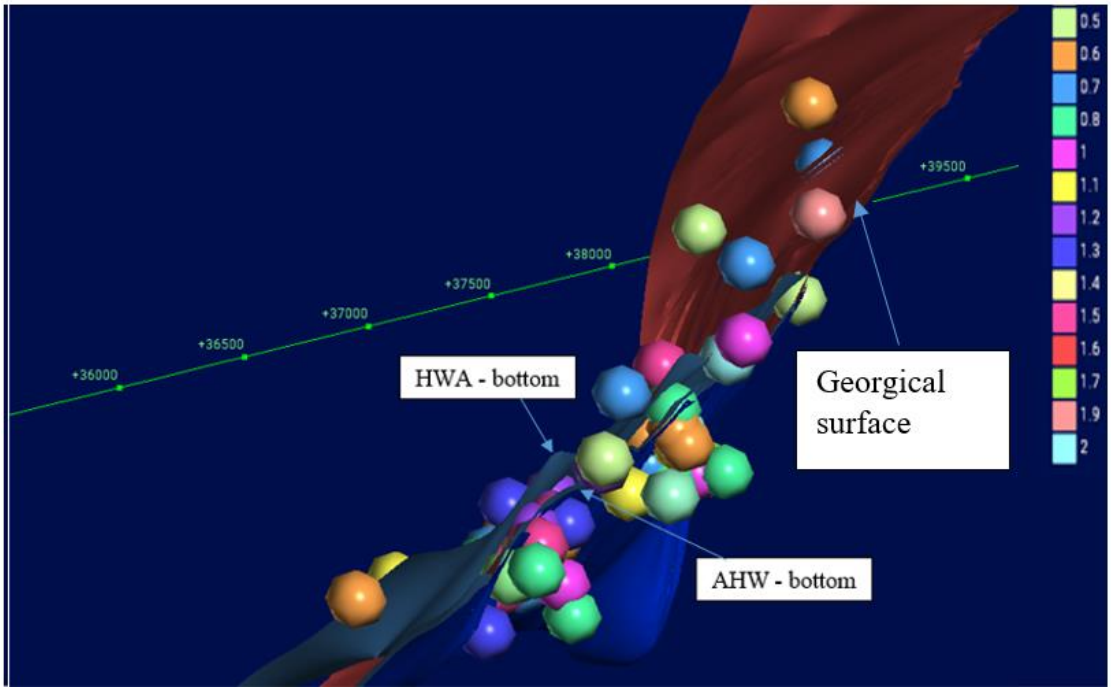

Figure 4.35: Leapfrog Geo plot showing the distribution of rockbursts in HWQ rock unit bounded by HWA and AHW. The colours of the balls represent the magnitudes of the rockbursts ranging from 0.5 to 2.0

The resulting plots were then used to determine the percentage distribution of rockburst events, as shown in Figure 4.36.

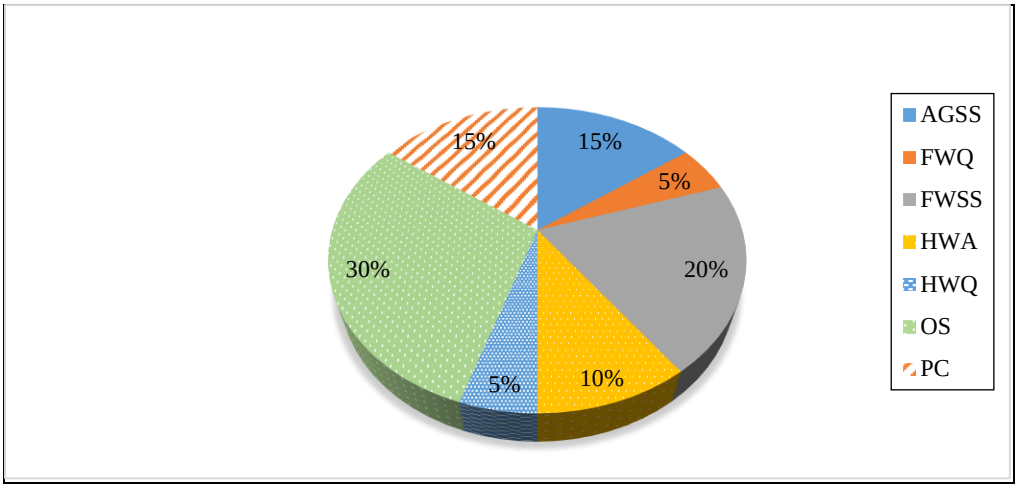

Figure 4.36: Rock types affected by rockbursts at Konkola No.1 Shaft Mine

Based on the data presented in Figures 4.32 to 4.35, it is evident that out of 14 rock types, the rocks most impacted by rockburst were FWQ, AGSST, PC, FWS, OS, HWQ, and HWA. Furthermore, Figure 4.36 highlights that OS accounted for 30 percent of all rockburst events, 20 percent for FWSS, AGSS and PC each accounted for 15 percent, 10

percent for HWA. FWQ and HWQ each accounted for 5 percent. The results show that OS rock unit was the most affected while AGSS and HWQ were least affected.

4.3.2.2 Geological Structures within the Areas Affected by Rockburst

The Author used a geological compass to spot-map major discontinuity planes on mining levels (2825 L, 2900 L, 3095 L, and 3150 L) affected by rockbursts. However, mapping could not be conducted where rockbursts occurred due to inaccessibility caused by falls of ground and inadequate ventilation. Instead, nine mapping sites near the affected areas were chosen, including trough drives, draw point crosscuts, and extraction drives (Figure 4.37).

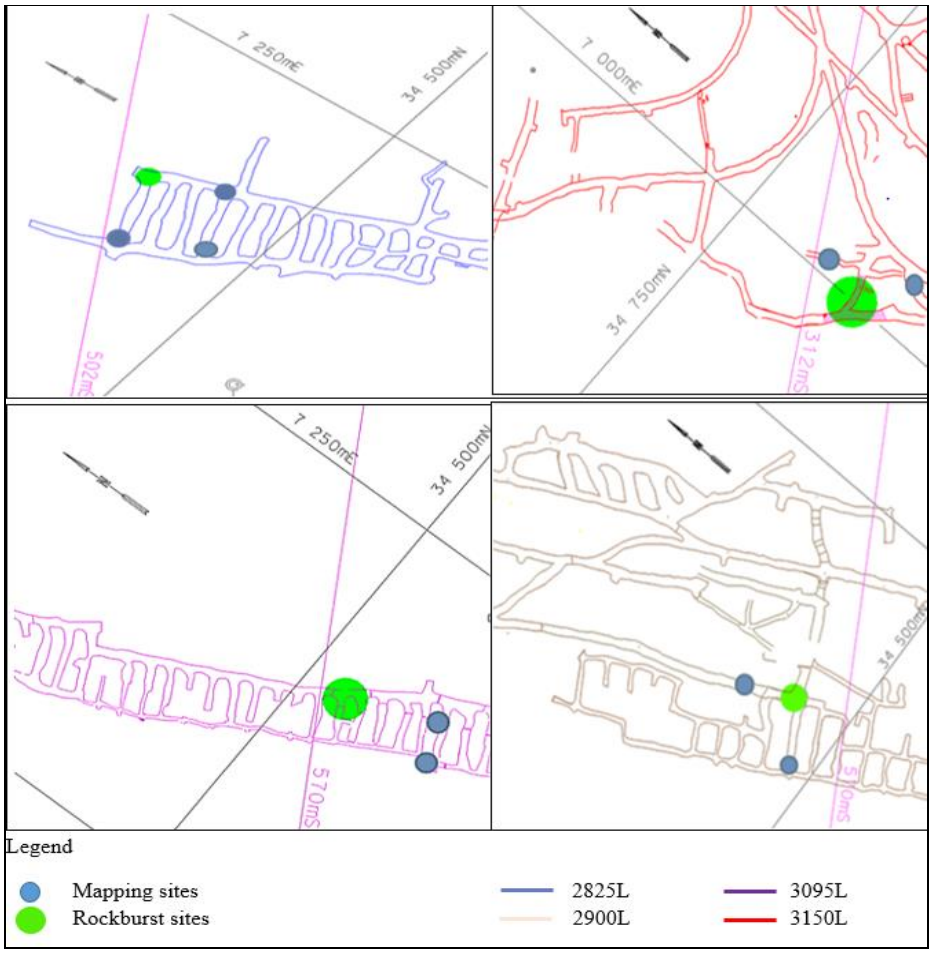

Figure 4.37: Locations of mapping sites for discontinuity measurements

The representative discontinuity planes for these sites were drawn on the lower hemispherical of an equal-angle projection, as displayed in Figure 4.38.

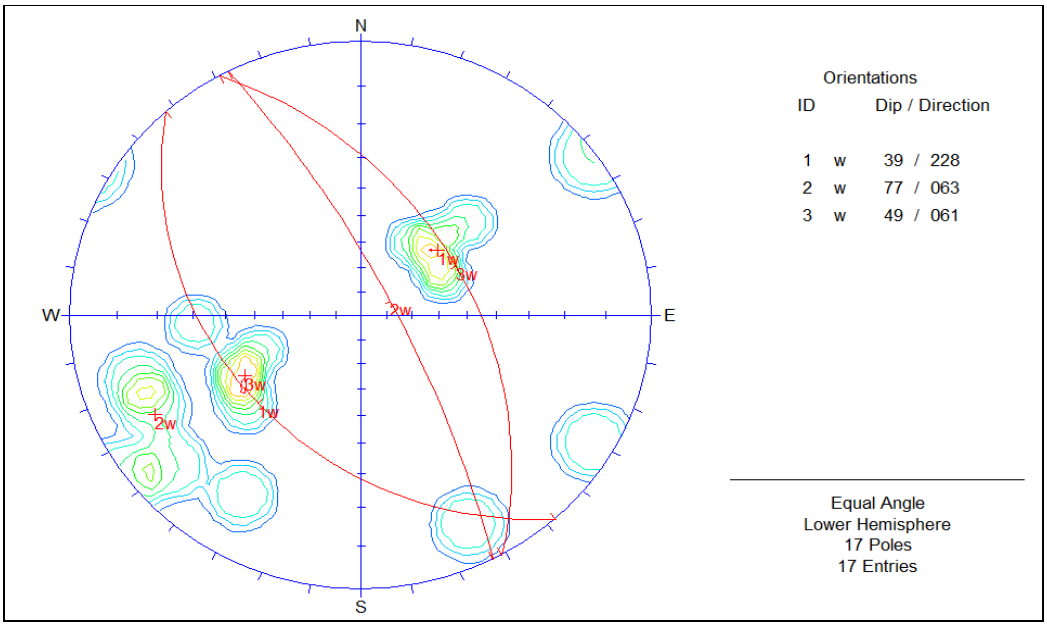

Figure 4.38: Plot of major discontinuity planes on lower hemispherical of an equal angle projection

The plot shown in Figure 4.38 shows there are three discontinuity sets in the areas that were affected by the rockburst. The discontinuity planes were identified as bedding planes with a dip and dip direction of $38^0/228^0$ and two joint sets with dip/dip directions of $77^0/063^0$ and $49^0/061^0$.

4.3.3 Geotechnical Data

The geotechnical data collected at the Konkola Mine No.1 Shaft was obtained through sampling and testing various lithological units. The data collected on the in-situ principal stress magnitudes were based on the measurements conducted by Rock Mechanics Technology Limited (RMTL) in 2001 to determine the principal stresses at the Mine (Walker, 2001; Carvill, 2001).

Informed by the review conducted in Chapter 3, the geotechnical data collected for each rockburst case was analysed to determine: rock quality designation (RQD), unconfined compressive strength (UCS), unconfined tensile strength (UTS), Elastic modulus (EM), and Poisson's ratio. The ratio of UCS to UTS was also calculated, along with the maximum tangential stress (MTS), using empirical methods. The in-situ stress data collected were also analysed.

4.3.3.1 RQD Data

The Rock Quality Designation Index (RQD) was developed by Deere (Deere et al., 1967) to provide a quantitative estimate of rock mass quality from drill core logs. RQD is defined

as the percentage of intact core pieces longer than 100 mm in the total length of the core drilled. The percentages of RQD were obtained using Equation 4.9 (Deere, 1989).

$$\text{RQD} = \frac{\Sigma \text{Core pieces} > 10\text{cm}}{\text{Total length of core run}} \text{ x } 100 \quad (4.9)$$

Where:

RQD = Rock Quality designation in percentage (percentage).

The Author determined the RQD values in this study through core logging of the four (4) boreholes (Table 4.5). The boreholes logged and sampled for rock testing were drilled explicitly for exploration. These boreholes were ideal for the study because of their locations, where rockbursts occurred.

Table 4.5: Drilled boreholes in rockburst sites

Borehole ID	**X (mN)**	**Y (mE)**	**Z (m)**	**Inclination (0^0)**	**Azimuth (0^0)**
KLB 135	6292	35133	1299	90	000
KLB 25	6996	34998	1310	90	000
BV 1496	6770.781	35026.31	318.168	3	225
BV 1171	7338.227	34208.149	461.285	0	240

The KLB 135 and KLB 25 were drilled from the surface, with depths of 1506 m and 823 respectively. Figure 4.39 displays the locations of the four boreholes, including the BV 1496 and BV 1171, drilled from underground.

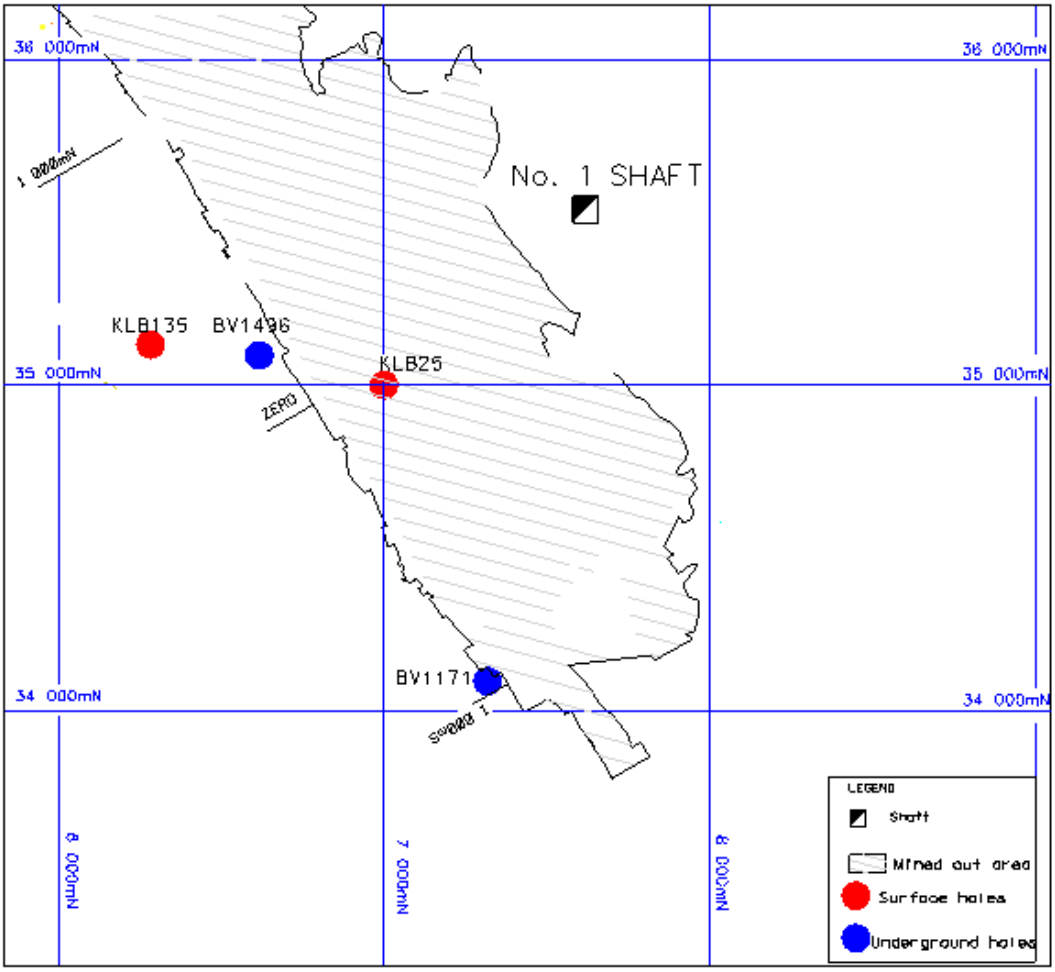

Figure 4.39: Plan of the surface and underground boreholes logged and sampled for rock testing

The author logged and collected core samples from each unit of the four boreholes for testing using point load and compression machines. The aim was to cover all rock units in the study area adequately. Table 4.6 displays the four boreholes and the intersecting rock units.

Table 4.6: Four boreholes and the intersecting rock units

Borehole ID	Rock Unit intersected
KLB 135	HWA, HWQ, OSU, unit A, FWSST, PC, AGSST, FWQ
KLB 25	HWA, HWQ, OSU, unit A, FWSST, PC, AGSST, FWQ
BV 1496	PC, FWSST, Unit A, OSU, HWQ
BV 1171	PC, FWSST, OSU. HWQ, HWA

Figures 4.40 and 4.41 display some boreholes where the researcher collected core samples for testing after logging them.

Figure 4.40: Logged BV 1171 for RQD determinations

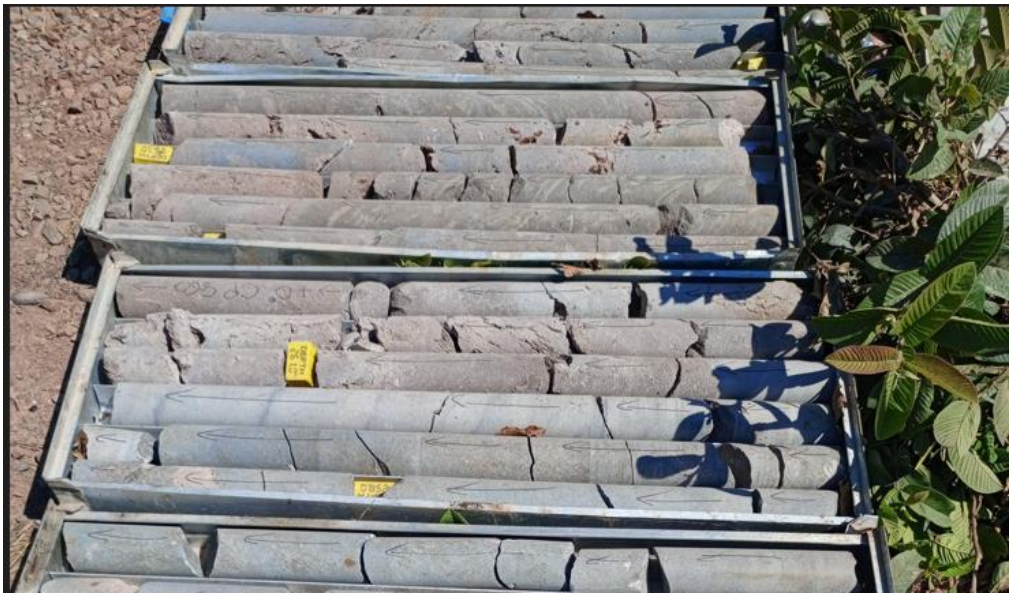

Figure 4.41: Logged BV1496 for RQD determinations

RQD for the rock samples were obtained using Equation 4.7. The determined RQD in percentages are presented in Figure 4.42.

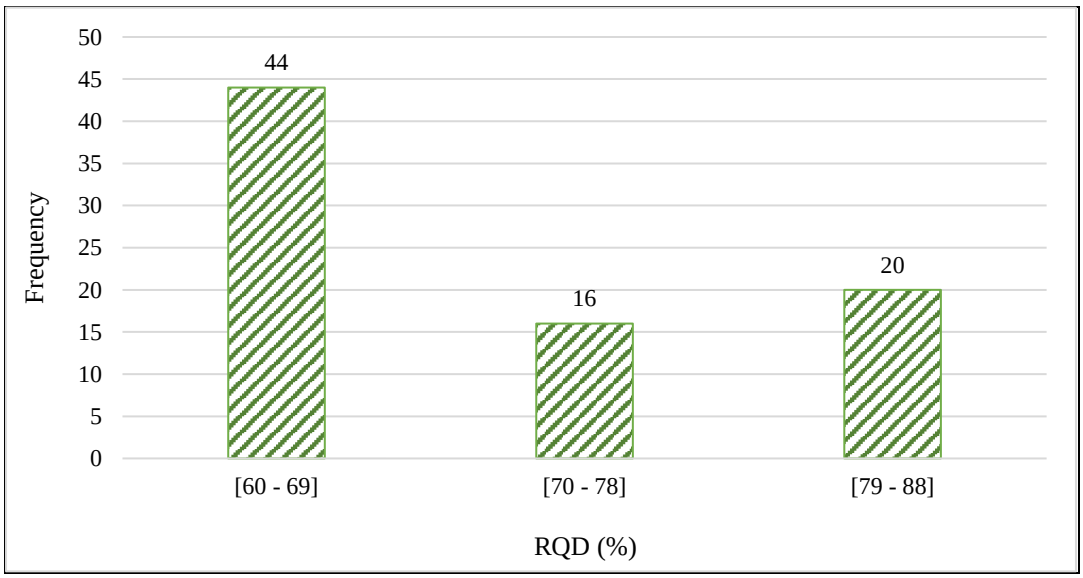

Figure 4.42: Ranges of RQD (percentage) for the rock samples at Konkola Mine No.1 Shaft

Figure 4.42 shows the RQD (percentage) for the core samples. Of the 80 samples logged, 44 had the RQD in the 60 to 69 percent; 16 had RQD in the 70 to 78 percent and 20 samples in the 79 to 88 percent. This analysis implies that the rocks affected by rockbursts at Konkola Mine No.1 Shaft have an RQD of 60 to 88 percent.

4.3.3.2 Unconfined Compressive Strength Data

The Uniaxial compressive strength (UCS) of rock, or compressive strength, is the maximum compressive stress of the rock specimen before failure under uniaxial compression loading. It is a relatively intuitive factor in evaluating the possibility of rockburst. The greater the UCS of rock, the greater the accumulated elastic strain energy, and the more likely the rockburst occurrence. Therefore, the UCS of rock is taken as an evaluation index of rockburst intensity.

The Author tested 60 rock core samples to determine their UCS values. Among the 60 samples, 20 were tested using a compression testing machine (Figure 4.43), while the remaining 40 were tested using a point load testing machine (Figurer 4.44). The compression testing machine was used to test the NX 50 mm core samples, while the point load testing machine was used for the irregular samples.

Figure 4.43: Point load testing machine used for determining the UCS for core samples

Figure 4.44: Compressive testing machine used for determining the UCS for core samples

The values of the UCS of the rock core samples determined using the point load test machine were calculated using Equation 4.10 as:

$$UCS = 22\ (I_s50) \qquad (4.10)$$

Where:

UCS = Uniaxial compressive strength of the rock in MPa.

22 = Correlated factor, a function of core diameter.

I_s50 = Corrected point load strength index for the standard core size of 50mm.

Figure 4.45 displays the UCS (MPa) values of the core samples that were tested.

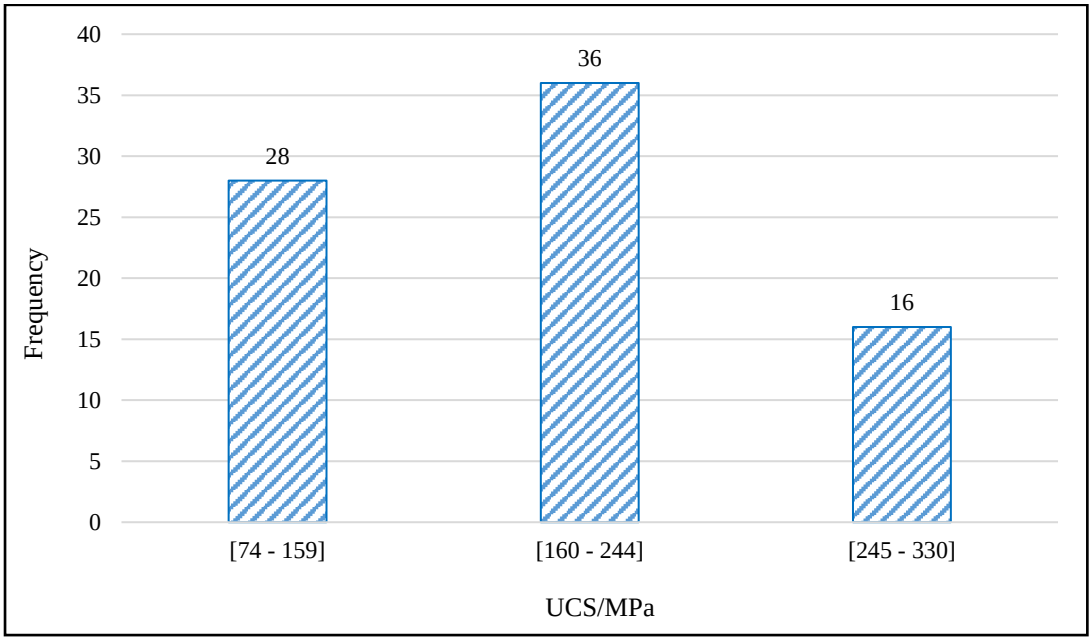

Figure 4.45: Ranges of UCS (MPa) for the rock samples at Konkola mine No.1 Shaft

Figure 4:45 shows the UCS (MPa) for the core samples that were tested. Out of the 80 rock samples tested, 28 samples had the UCS in the 74 to 159 MPa, 36 had UCS in the 160 to 244 MPa and 16 samples were in the range of 245 to 330 MPa. This analysis implies that the rocks affected by rockbursts at Konkola Mine No.1 Shaft have a UCS of 74 to 330 MPa.

4.3.3.3 Unconfined Compressive Strength Data for 'A' unit

The ore shale has a variable thickness of 5 – 20 m with a dip of about 55^0 and is divided into five (5) ore horizons (A, B, C, D and E). 'A unit' is the lowest geological unit of the orebody with a variable thickness of 0.5 -1.2m, which increases with steepening of the dip.

It is finely bedded and frequently weathered to brown micaceous clay and is the weakest geological unit of the orebody.

In section 4.3.3.1, the logging of the boreholes revealed the presence of a strong ‘A’ unit. Figure 4.46 depicts the position of ‘A’ unit in relation to Orebody and FGW.

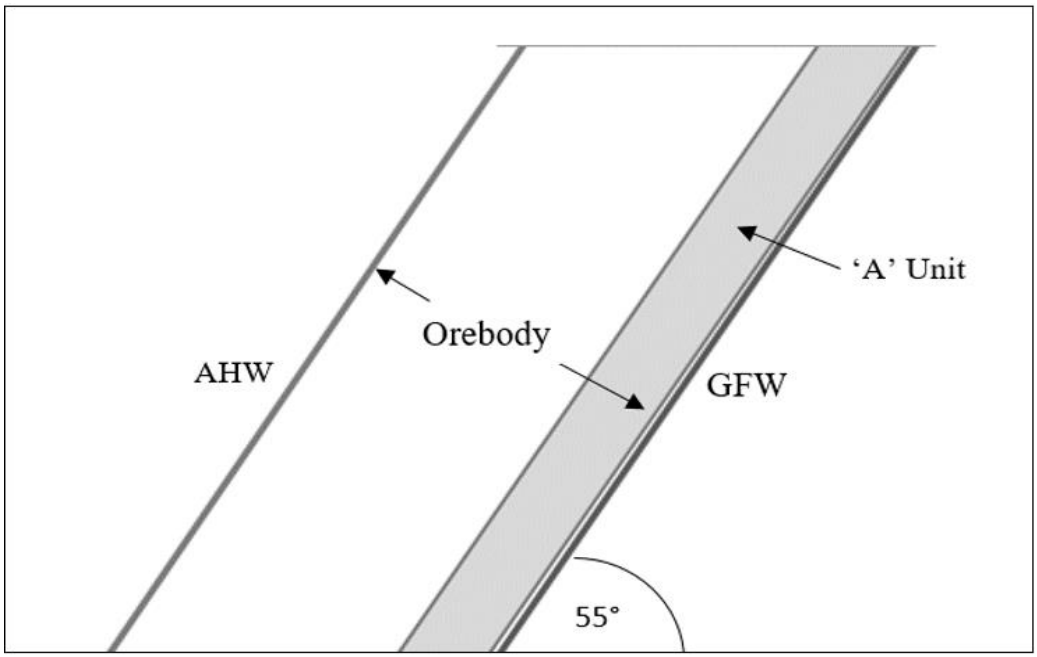

Figure 4.46: Position of ‘A’ unit in relation to Orebody and FGW

Twenty regular samples were tested using a point load-testing machine to determine the UCS of ‘A unit’. The analysis results are presented in Figure 4.47.

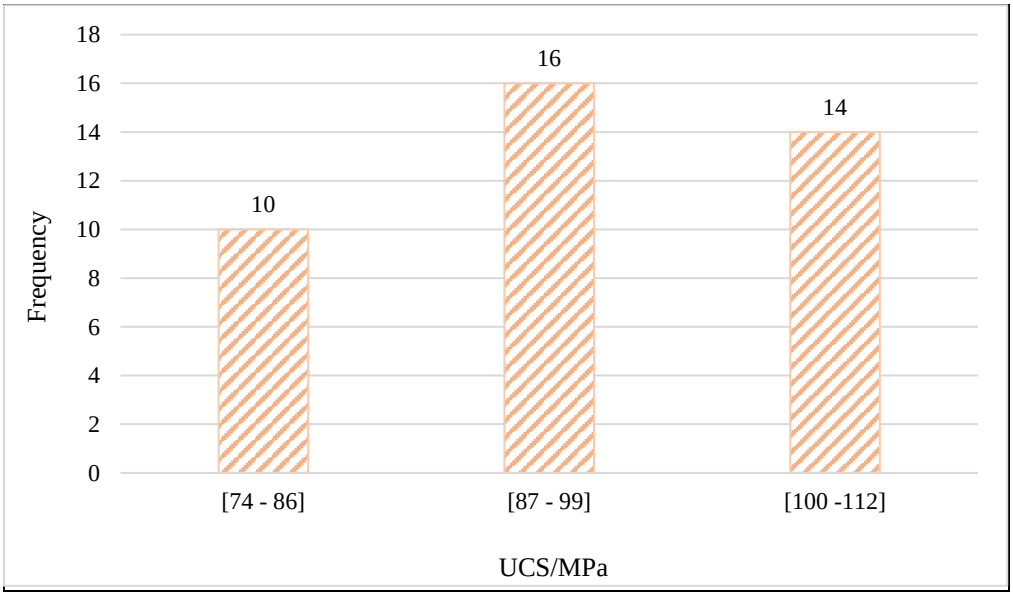

Figure 4.47: Ranges of UCS/MPa data for Unit A at Konkola Mine No.1 Shaft

Figure 4.47 shows the UCS (MPa) for the core samples retrieved from unit A. Ten samples had a UCS in the range of 74 to 86 MPa, 16 were in the range of 87 to 99 MPa, and 14 were in the range of 100 to 112 MPa. This analysis shows that the UCS of the unit A affected by rockbursts at Konkola Mine No.1 Shaft has a UCS of 74 to 112 MPa.

4.3.3.4 Unconfined Tensile Strength Data

The strength of rock under tension, known as unconfined tensile strength (UTS), plays a crucial role in assessing the likelihood of rockbursts. This parameter has been utilised in various rockburst prediction criteria, as evidenced by research on the stress method of rockburst predictions (Altindag, 2003; Qiao and Tian, 1998; Chen et al., 2013). UTS is also important in determining the rock brittleness coefficient, which is the ratio of UCS to the confined tensile strength of intact rock (Qiao and Tian, 1998; Chen et al., 2013).

The unconfined tensile strength (UTS) of rock is defined as the pulling force required to rupture a rock sample, divided by the sample's cross-sectional area. The UTS of rock is minimal and can be estimated as 0.1 times the compressive strength (Bernt and Looyeh, 2019).

The intact rock samples' UTS were determined using a relation shown by Equation 4.11:

$$UTS = 0.1\ UCS\ (MPa) \qquad (4.11)$$

Where:

UTS = Unconfined Tensile stress (MPa).

UCS = Unconfined Compressive Stress (MPa).

The analysis results are presented in Figure 4.48.

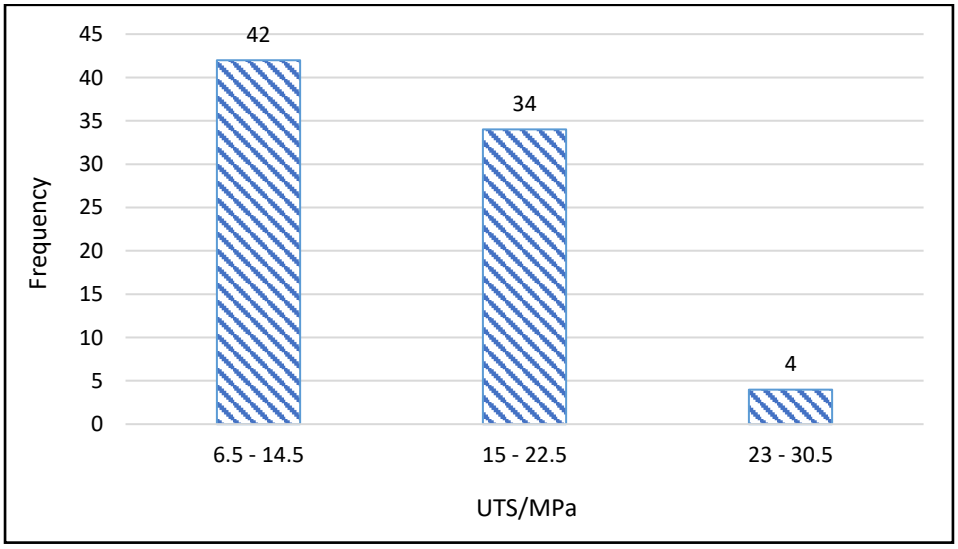

Figure 4.48: Ranges of UTS (MPa) for Konkola Mine No.1 Shaft

Figure 4.48 shows the estimated UTS (MPa) for the core samples close. Out of the 80 rock samples measured, 42 samples had the UTS in the 6.5 to 14 MPa range; 34 had UTS in the 15 to 22.5 MPa range, and four had the UTS in the 23 to 30.5 MPa range.

4.3.3.5 Maximum Tangential Stress Data

Peng et al., (2023), in their investigations of the characteristics of ground pressure disaster and rockburst proneness in deep gold mining, found that when the Maximum Tangential Stress (MTS) of the tunnel were about 0.4 and 0.55 times UCS of rock, the tunnel might suffer spalling. Peng et al., (2021), in their field investigation and analysis of rockburst and spalling in a deep hard-rock Mine, found that when the maximum tangential stress was between 0.4 and 0.6 times the uniaxial compressive strength of surrounding rock, surrounding rock was prone to local spalling.

From these empirical estimations, the Author assumed an MTS of 0.5 times the uniaxial compressive strength of surrounding rock for rockburst potential or proneness as given by Equation 4.12 as:

$$MTS = 0.5\sigma_c \qquad (4.12)$$

Where:

MTS = Maximum Tangential Stress (MPa).

σ_c = unconfined compressive stress (MPa).

MTS values for the 70 rock core samples were calculated using Equation 4.12 and the results are presented in Figure 4.49.

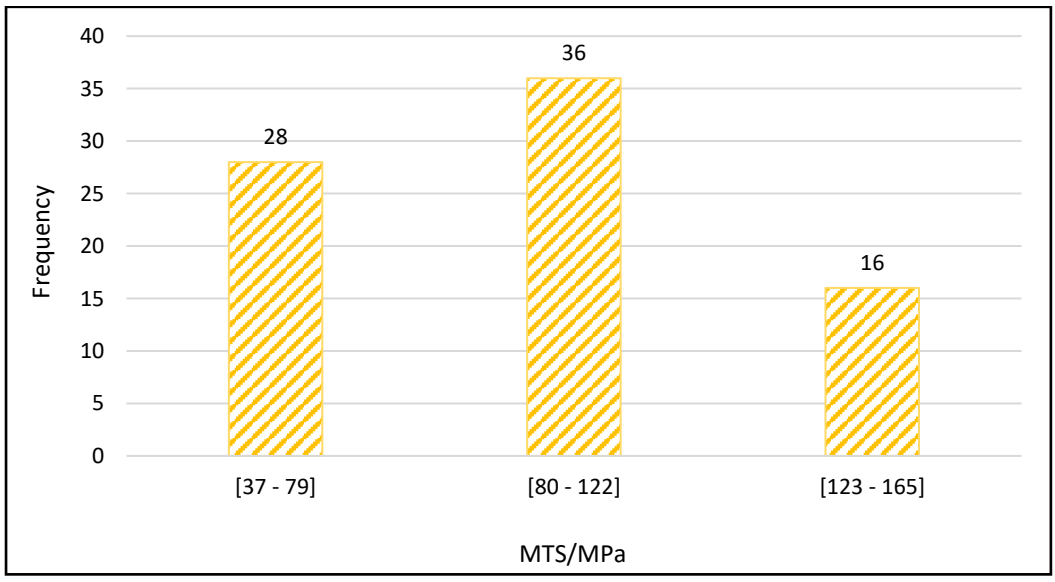

Figure 4.49: Ranges of MTS (MPa) for case studies

Out of 70 samples, 28 had an MTS between 37 and 79.6 MPa, 36 had MTS in the range of 80 to 122 MPa and 16 had were in the range of 123 to 165 MPa. This suggests that the MTS of rocks affected by rockbursts at the Konkola mine ranges from 37 to 165 MPa.

4.3.3.6 Elastic Modulus Data

The Elastic modulus (E_m) is one of the most important mechanical properties of the rocks. It measures the stiffness of an elastic material, defined as the ratio of stress to strain (Ma et al., 2016). Rocks with low E tend to be ductile, and rocks with high E tend to be brittle. In most research (Hudson and Harrison, 1997), the elastic property is best studied through the complete stress-strain curve for a rock sample being compressed in one direction, i.e., uniaxial compression in uniaxial compression (Figure 4.50).

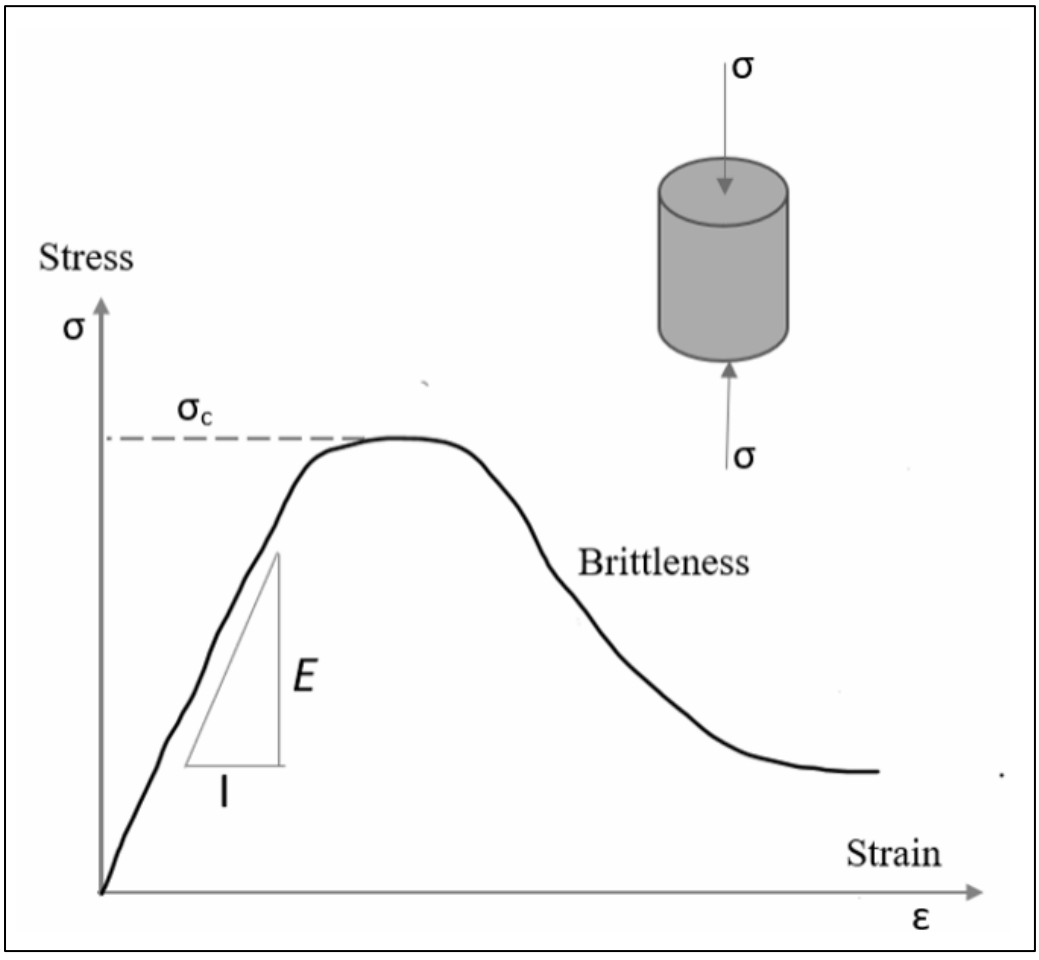

Figure 4.50: Complete stress-strain curve illustrating the stiffness (or modulus, E), strength, $\sigma_{c,}$ and brittleness (after Hudson and Harrison, 1997)

The elastic modulus can be expressed as the Tangent modulus (TM) or the secant modulus (SM), depending on where the stress-strain gradient is taken from. The TM is typically calculated at 50 percent of the peak strength, while the SM can be taken from any point on the stress-strain curve. The initial part of the stress-strain curve will be steep in stiff materials, while in soft materials, it will be more gradual (Hudson and Harrison, 1997). Different methods have been used in the literature to relate the deformation modulus with RMR (rockmass rating) or Geological strength index, GSI (E.g. Bieniawski, 1978; Serafim and Pereira, 1983; Hoek and Brown,1997), with Q (e.g. Barton et al.,1980; Barton, 2002), and with unconfined compressive strength (e.g. Rowe and Armitage,1984; Palmström and Singh, 2001).

The method developed by Palmström and Singh (2001) related deformation modulus with unconfined compressive strength and is given by Equation 4.13 as:

$$E_m = 0.2\sigma_c \qquad (4.13)$$

Where:

E_m = Deformation modulus in GPa.

σ_c = unconfined compressive strength in MPa.

For this study, Equation 4.13 was used to estimate the deformation moduli for the rock types at the Konkola Mine No.1 Shaft because of its simplicity, and requiring only a single parameter, i.e., unconfined compressive strength. The estimated values of the deformation moduli are presented in Figure 4.51.

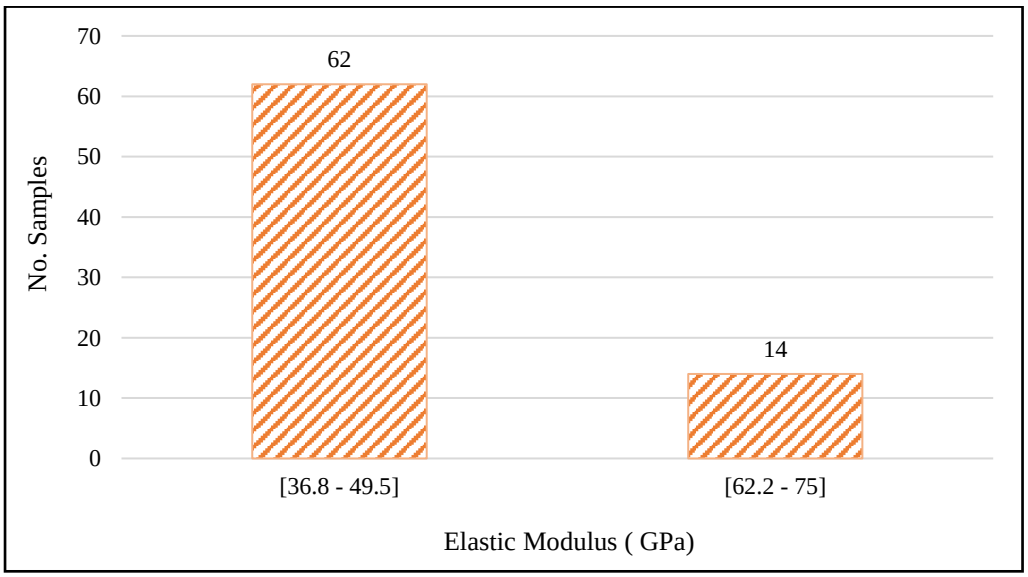

Figure 4.51: Ranges of E_M (GPa) for Konkola Mine No.1 Shaft

The results showed that out of the 76 samples, 62 had E_m between 36.8 to 49.5 GPa, while 14 had E_m between 62.2 to 75 GPa. This analysis suggests that the rocks prone to rockbursts at Konkola Mine No.1 Shaft have an E_m range of 36.8 to 75 GPa.

4.3.3.7 Linear Elastic energy

The Wang and Park (2001) introduced the linear elastic energy (W_{et}), which is defined as the linear elastic energy stored in the rock specimen before the rock failure point. It is one of the indicators for predicting the rockburst intensity and is expressed in Equation 4.14 as:

$$W_{et} = \frac{\sigma_c^2}{2E_u} \tag{4.14}$$

Where:

W_{et} = the linear elastic energy.
σ_c = the UCS of intact rock (MPa).
E_u = the elastic modulus.

For this study, the W_{et} were calculated using the Equation 4.14 that takes into account the UCS and E of the intact rock. The logs of W_{et}/Jm^{-3}) were calculated for 80 samples from the areas impacted by the rockburst. Figure 4.52 shows the calculated values of log (W_{et} / Jm^{-3}).

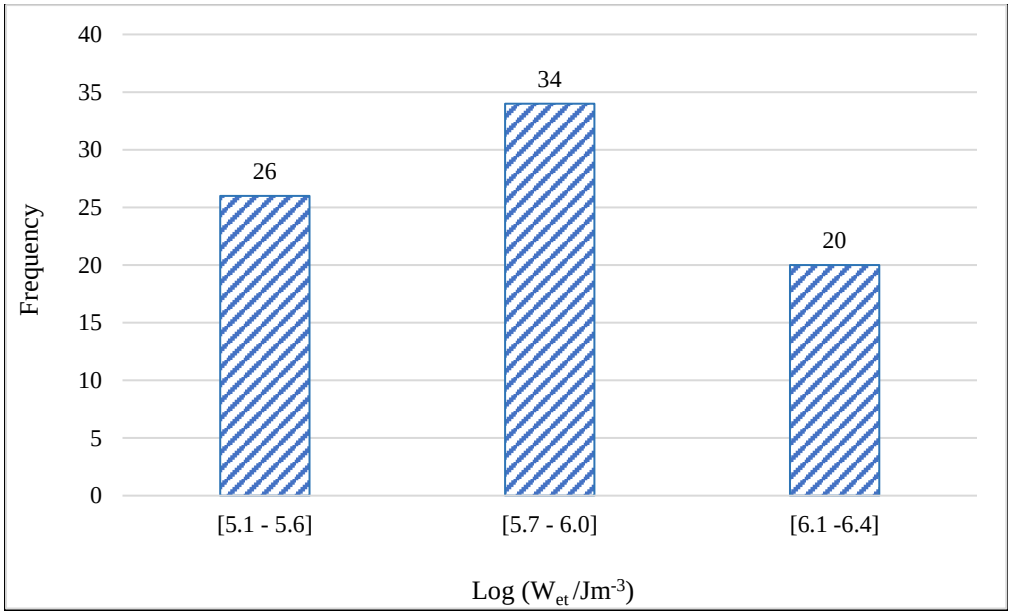

Figure 4.52: Ranges of values of log (W_{et}/Jm^{-3}) for cases for Konkola Mine No.1 Shaft

Figure 4.52 shows that out of the 80 samples, 26 had log (W_{et}/Jm^{-3}) between 5.1 and 5.6, 34 had log (W_{et}/Jm^{-3}) between 5.7 and 6.0 and 20 had log (W_{et}/Jm^{-3}) between 6.1 and 6.4. This analysis suggests that the rocks prone to rockbursts at Konkola Mine No.1 Shaft have a log (W_{et}/Jm^{-3}) range of 5.1 to 6.4.

4.3.3.8 In-Situ Stress Data

Rock Mechanics Technology (RMT) Limited carried out the in-situ stress measurements at Konkola Mine in 2001 (Walker, 2001; Carvill, 2001) in 2001 using the Commonwealth Scientific and Industrial Research Organisation (CSIRO) Hollow inclusion stress cell based on an overcoring technique. The measurements were carried out to determine the three–dimensional (3D) state of the entire stress regime. Three sites were chosen around the limbs of the fold (Figure 4.53) as follows:

- Test Site 1 - No. 3 Shaft, 590 mL level SPR development on 725 mN Section line;
- Test Site 2 - No. 3 Shaft, 590 mL level old PPCF development on 2160 mW Section Line; and
- Test Site 3 - No. 1 Shaft, 950 mL 2700 mN dewatering crosscut.

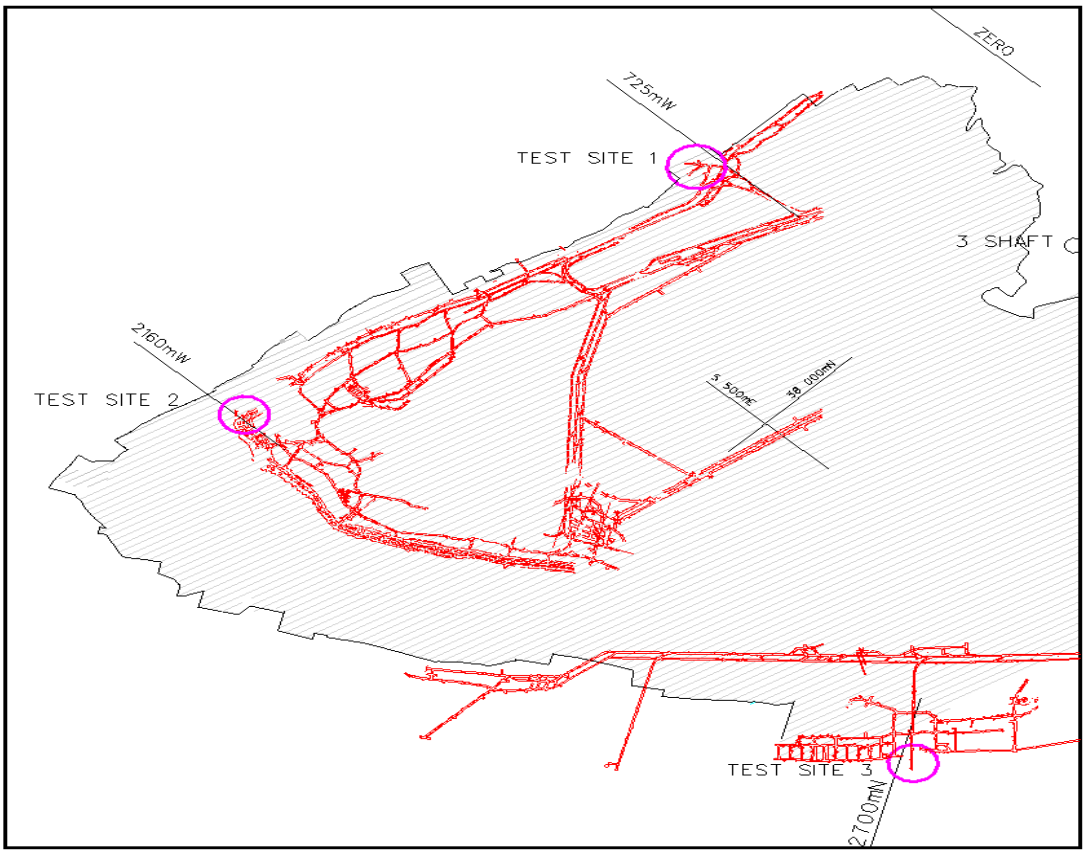

Figure 4.53: Stress measurement sites at Konkola Mine where pink circles representing the test sites

The selected sites were located at a considerable distance from active mining operations, ensuring the accuracy of measurements for in-situ conditions rather than induced stresses. The measurements were carried out in the HWQ rock unit, due to its homogeneous and solid composition, unlike Ore Shale, which is fissile and anisotropic.

For this study, the calculated in-situ stresses were based on Test Site 3, which was close to the study area. The directions of principal stresses concerning the bedding plane (the primary structural feature in all the rock types) were plotted on the equal area net (Figure 4.54).

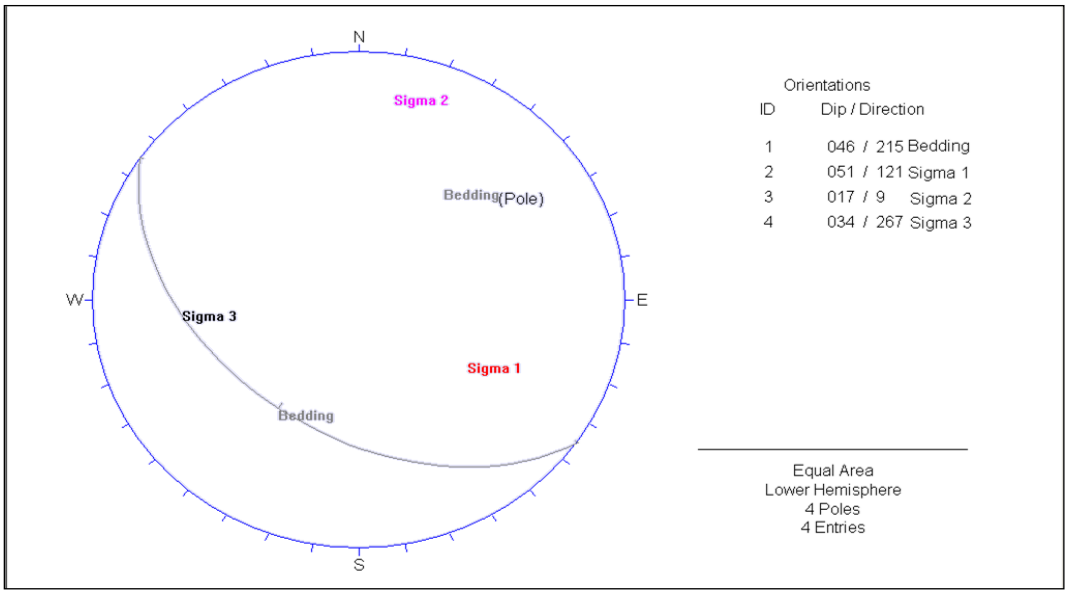

Figure 4.54: Plot of lower hemispherical showing orientation of principal Stresses in relation to the bedding plane at Konkola Mine No. 1 Shaft at 950mL/2700mN

Figure 4. 54 indicates the following:

- The major principal stress was sub-vertical dipping at 51^0 and oriented in the NW – SE with an azimuth of 121^0;
- The intermediate principal stress was sub-horizontal dipping at 17^0 with an azimuth of 009^0 in the NE – SW direction;
- The minor principal stress was sub-vertical dipping at 34^0 with an azimuth of 267^0 in the SW- NE direction; and
- The dominant geological structure was a bedding plane with a sub-vertical dipping at 46^0 and an azimuth of 215^0 in the NE – SW direction.

The transformations of the measured principal stresses into vertical and horizontal stresses carried out by RMT in 2001 indicated that the principal stresses increase with depth and follow relations expressed by Equations 4.15 to 4.17 (RMT, 2001) as:

$$\sigma_v = 0.0263h + 4.0 \quad (4.15)$$

$$\sigma_H = 0.85\ \sigma_v \quad (4.16)$$

$$\sigma_h = 0.60\ \sigma_v \quad (4.17)$$

Where:

σ_v = major principal vertical stress in MPa.

σ_H = intermediate principal horizontal stress in MPa.

σ_h = minor principal horizontal stress in MPa.

h = depth in meters.

The σ_v, σ_H, and σ_h in - situ stress fields were calculated for each rock burst event location using Equations 4.15. 4.16 and 4.17. The calculated results are presented in Figures 4.55, 4.56, and 4.57.

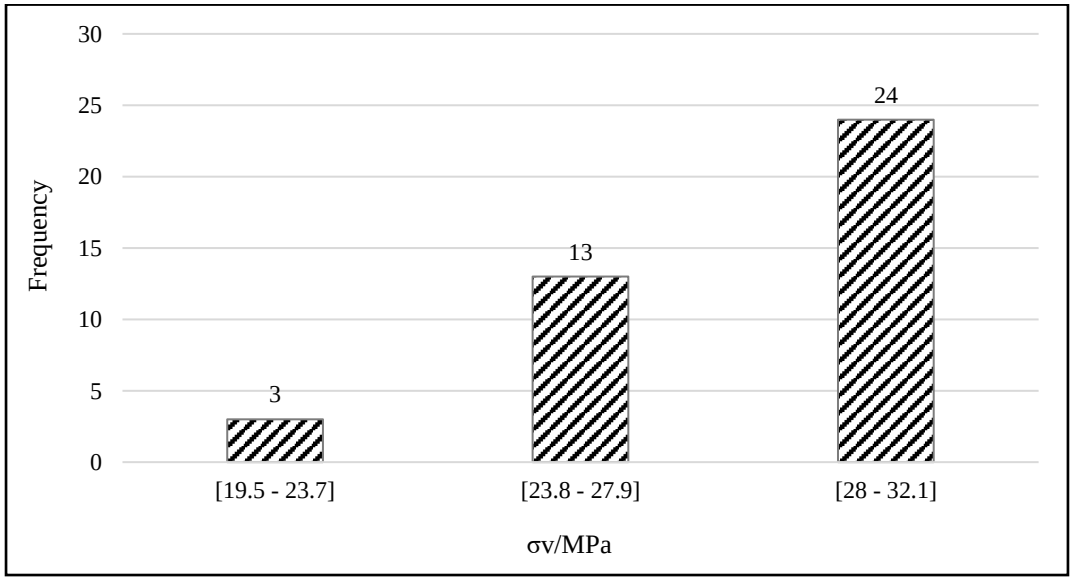

Figure 4.55: σ_v in (MPa) analysed for each rockburst site

Figure 4.54 shows that for 40 rockburst sites, three sites had σ_v in the range of 19.5 to 23.7 MPa, 13 sites were in the range of 23.8 to 27.9 MPa and 24 had σ_v between 28 and 32.1MPa. The analysis revealed that the σ_V for sites affected by rockburst ranged from 19.5 to 32.1 MPa.

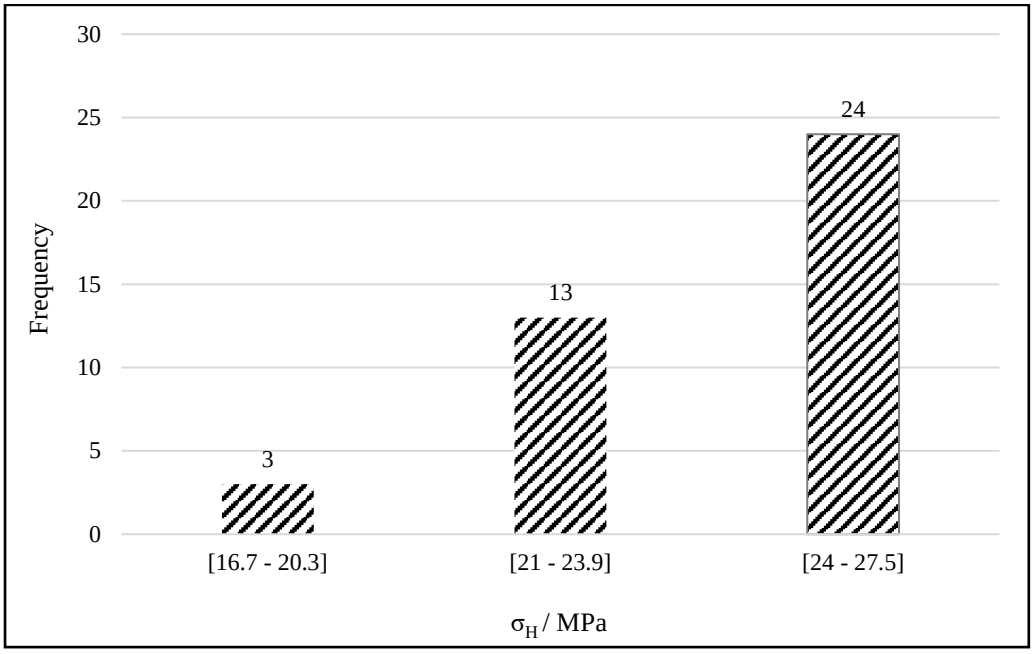

Figure 4.56: σ_H/ MPa analysed for each rockburst site

Figure 4.56 shows that for 40 rockburst sites, three sites had σ_H in the range of 16.7 to 20.3 MPa, 13 sites were in the range of 21 to 23.9 MPa and 24 sites were in the range of 24 to 27.5 MPa. The analysis revealed that the σ_H for sites affected by rockburst ranged from 16.7 to 27.5 MPa.

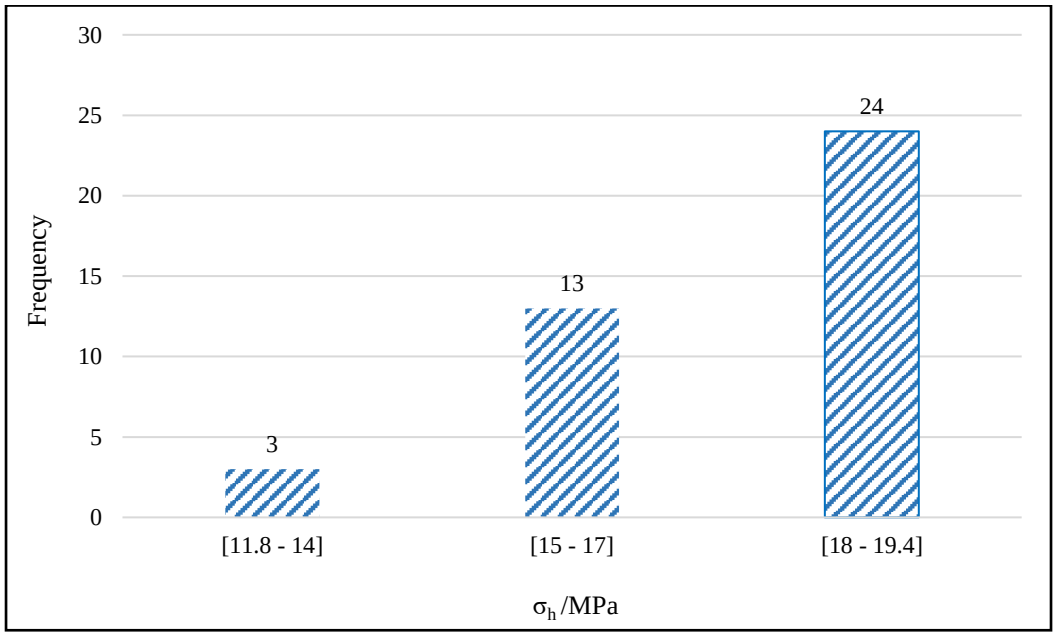

Figure 4.57: σ_h /MPa analysed for each rockburst site

Figure 4.57 shows that for 40 rockburst sites, three sites had σ_h in the range of 11.8 to 14 MPa, 13 sites were in the range of 15 to 17 MPa and 24 sites were in the range of 18 to

19.4 MPa. The analysis revealed that the σ_h for sites affected by rockburst ranged from 11.8 to 19.4 MPa.

4.3.3.9 Ground Support Data

The author collected data on ground support installed and the number of rockburst events in the affected area. Table 4.8 displays the descriptions of the support types installed in the area before the rockburst events, and Figure 4.57 shows the analysis results.

Table 4.7: Ground support types

Rock Type	Support Elements
S0	No support
S1	Rockbolts only
S2	Rockbolts and wiremesh
S3	Rockbolts, wiremesh and tendon straps
S4	Rockbolts, wiremesh, tendon straps and cablebolts
S5	Splitsets, weldmesh and cablebolts

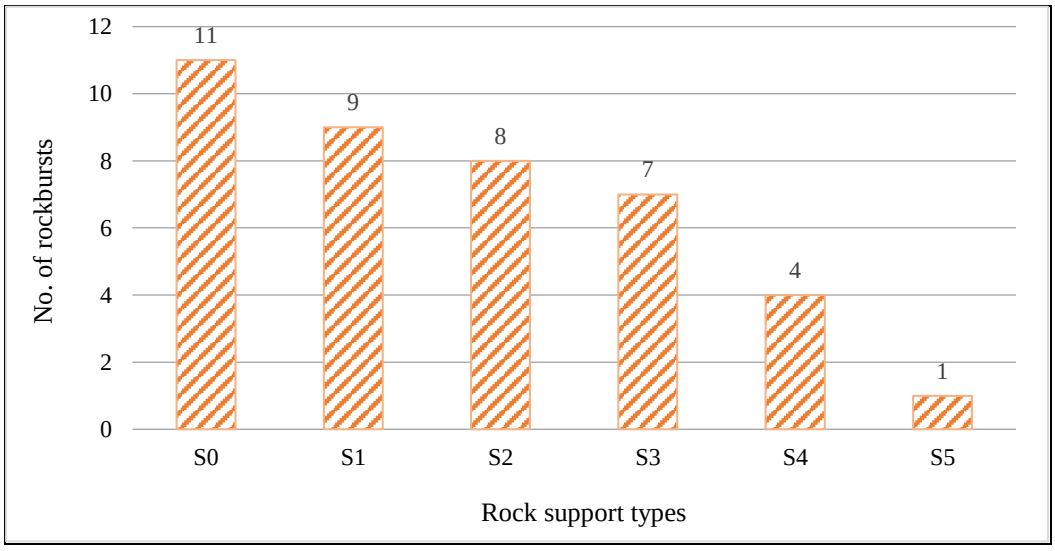

Figure 4.58: Distribution of ground support analysed in the areas affected by rockbursts

According to Figure 4.58, 11 rockburst events occurred in the areas with no support installed, nine events occurred in the areas supported only with rockbolts, eight events in the areas supported with rockbolts and wiremesh, seven events occurred in the areas supported with rockbolts, wiremesh and tendon straps, four events occurred in the areas supported with rockbolts, wiremesh, tendon straps and cablebolts and one event occurred in the areas supported with splitsets, weld mesh and cablebolts. The analysis results reveals

that the areas with no support experienced the most rockburst events (11), while the least affected areas were those supported with splitsets, weld mesh, and cablebolts with only one event.

4.3.4 Mining Data

The mining data collected on the areas where the rockburst occurred were as follows;

- Mining method employed; and
- Production rates.

4.3.4.1 Mining Methods

At Konkola Mine No.1 Shaft, the orebody thickness and dip vary between 4.0m to 15m and 50º to 70º, respectively. The mining method (Figure 4.59) used at Konkola Mine No.1 Shaft is predominantly open stoping (SLOS).

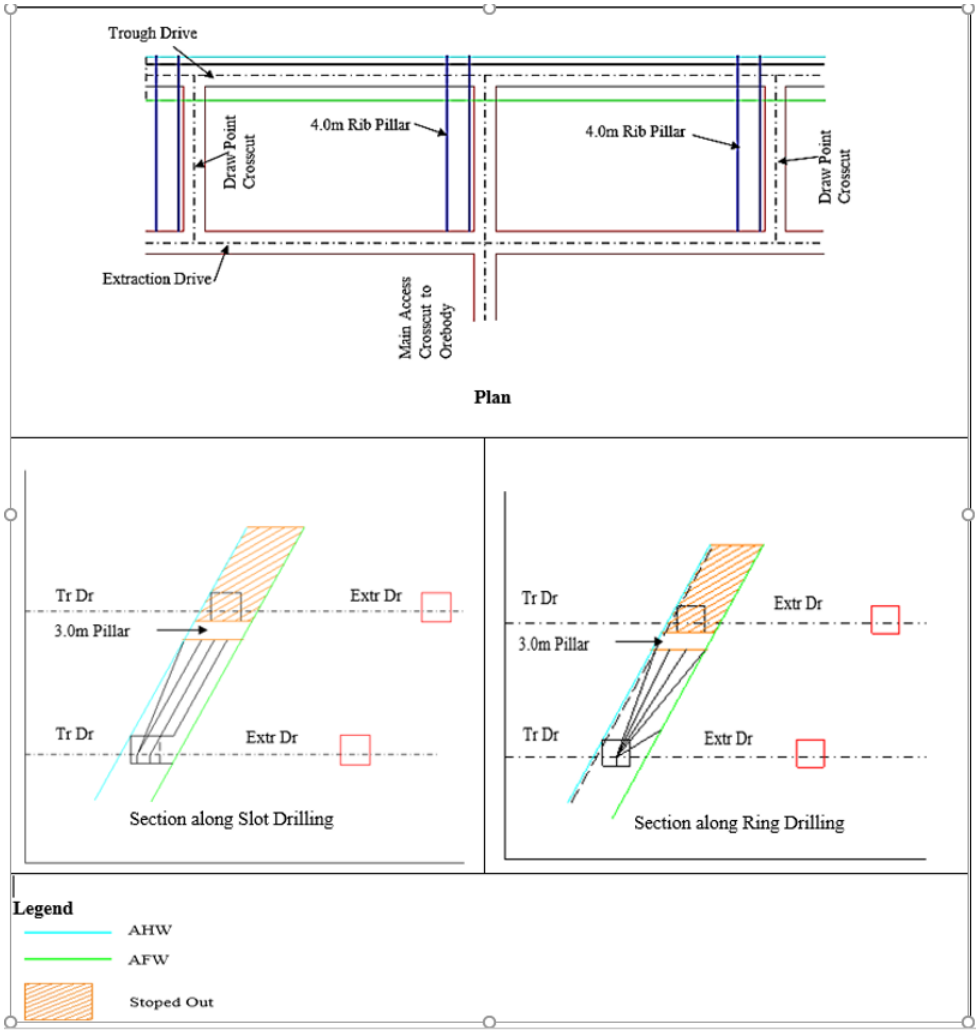

Figure 4.59: Layout of the SLOS at Konkola No.1 Shaft

The stopes are developed by mining two horizontal drives, one in ore and the other in waste, connected by the draw point crosscuts on the extraction level. This defines the stope geometry of 60 m along strike, the back length of 20 m, and nine (9) -12 m in width. Each stope is designed with one draw point on the extraction level. The cut-out raise is mined along the rib pillar on the footwall side up to the crown pillar position. The exposure crosscut is mined in the pillar positions on both levels. Each stope is designed with a rib pillar of 6 m and a crush pillar of 3 m. The designed stope rings are drilled using a mechanised solo machine. The ore is broken by drilling and blasting from the trough drives. At least three stopes are fully developed before blasting. A stope can start in either the north or south. To achieve this, a 45^0- echelon line must be maintained while developing. In this method, production starts by enlarging the slot raise in the ore body. The stope rings are then blasted into the slot, and ore gravitates to the bottom of the stope. The ore is pulled from the stope until waste contamination, which is assessed through visual inspections of the draw points, becomes unacceptable.

4.3.4.2 Production Rates versus the Number of Recorded Rockbursts

Production rates represent the number of ore produced annually. The objective of collecting data on rockburst events and yearly production was to identify any correlation between them. The production rates were collected from 1995 to 2021, along with the number of rockburst events that occurred during the same period, as shown in Figure 4.60

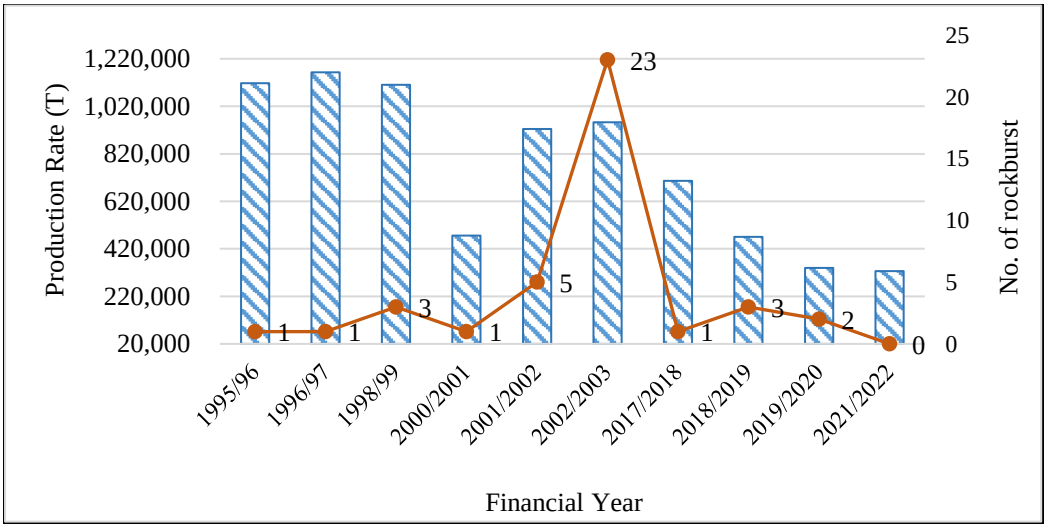

Figure 4.60: Number of rockburst recorded yearly from 1995/96 to 2021/2022 at Konkola Mine No.1 Shaft

Figure 4.60 shows that the Mine's production rate was consistent at around 1 million tonnes per year from 1996/97 to 1998/99. However, during this period, there was an increase in

rockburst events, from one in 1995/96 to three in 1998/99. In 200/01 year, the production rate drastically reduced to about 500,000 tonnes, with a corresponding decrease in rockburst events from three to one. From 2001/02 to 2002/03, there was a gradual increase in production rates, accompanied by a drastic increase in the rockburst events to 23. From 2002/03 to 2021/22, there was a gradual decrease in both the production rate and the rockburst events. The correlation between production rates and rockburst events is evident, with increased production leading to a higher occurrence of rockbursts.

4.4 Summary

This chapter discusses the first two objectives of the study. The first objective was to review rockburst case studies from different mines to identify the factors that could contribute to rockbursts. The second objective was to establish site-specific indicators at Konkola Mine No.1 Shaft that could be applied to predict the occurrence of rockbursts. After analysing the case studies, four potential contributing categories were identified: microseismic (MS), geological, geotechnical, and mining. Table 4.8 presents the probable and frequent ranges for each of these classes.

Table 4.8: Global quantitative rockburst contributing factors for the case studies

Class	Factor	Range	Most frequent range
Microseismic	M_L	0.5 - 3.5	2.6 - 3.5
Geological	Orebody inclination (0^0)	10 - 85	61 - 85
Geotechnical	UCS/MPa	133 - 318	133 - 179
	UTS/MPa	9 - 25	9 - 13
	E/GPa	37.5 - 107.7	37.5 - 72.5
	MTS/MPa	60 - 143	89 - 114
	UCS/UTS	10 - 16	12.5 - 14
	ν	0.2 - 0.27	0.26 - 0.27
	σ_1: σ_3	1.2 - 3.6	1.2 - 2
Mining	Threshold Depth below surface (m)	1000 - 1500	1000 - 1167

The study also established that the open stoping in Australian mines and cut and fill mining methods in China and the USA were predominantly associated with a higher rockburst potential than reef mining (South Africa), bottom stoping, and shrinkage (Canada). The research also established that geological structures, particularly faults, dykes, intrusions, foliations, dense joints, folds, and shear zones, were among the most significant rockburst-controlling factors.

The Author analysed rockburst data at the Konkola Mine No.1 Shaft to identify rockburst indicators. The study identified four potential indicators: MS, geotechnical, and mining. Table 4.9 summarises the likely ranges for these indicators.

Table 4.9: Quantitative rockburst contributing factors at Konkola Mine No.1 Shaft

Class	Factor	Range	Most frequent range
MS	M_L	0.5 - 2.5	1.3 - 1.8
	Log(E/J)	2.2 - 9.0	2.2 - 5.6
	E_S/E_P	0.7 - 36.9	0.7 - 9.8
	$Log(P/m^3)$	0.3 - 2.2	0.3 -1.3
	Distance(m) from the stope	0 - 159	0 - 53
Geotechnical	RQD /%	60 - 88	60 - 69
	UCS /MPa	74 - 330	160 - 244
	UTS /MPa	6.5 - 30.5	6.5 -14.5
	E_m /GPa	36.8 - 75	36.8 - 49.5
	MTS /MPa	37- 165	80 - 122.4
	Log (W_{et} (Jm^{-3})	5.1 - 6.4	5.6 - 6.0
	σ_v /MPa	19.5 - 32.1	28 - 32.1
	σ_H /MPa	16.7 - 27.5	24 - 27.5
	σ_h /MPa	11.8 - 19.4	18 - 19.4
Mining	Threshold Depth (m) below the surface	950	
Geology	Orebody dip (0^0)	50 - 70	55
	Number of Joint sets	2	

The analysis further revealed that rockburst events at Konkola were localised to a specific area and were observed in four distinct groups or clusters. They were limited to the Luansobe fault zone on the southern boundary and secondary fault zones on the northern boundary. The most commonly affected rock type was OS, accounting for 30% of total rockburst events. The study identified a correlation between rate of production and the occurrence of rockburst events. A lower production rate resulted in fewer rockburst incidents, while a higher production rate led to more rockburst incidents.

Chapter 5 will explore developing and validating tools that utilise the analysed geotechnical and microseismic factors to predict the potential of rockburst occurrence, and specifically the rockburst damage class.

CHAPTER 5: DEVELOPMENT AND VALIDATION OF ROCKBURST PREDICTIVE TOOLS

5.1 Introduction

In this chapter, development and validation of the rockburst prediction tools using geotechnical and microseismic data is presented. The aim was to create two user-friendly tools that could be utilised by field engineers, even with limited data. Relevant geotechnical and microseismic parameters were selected, tested for correlations, categorised, and assigned ratings. A C++ computer program was developed for each tool, which predicts the rockburst damage class by comparing ratings to pre-determined classes. To validate the effectiveness of the tools, two datasets from Mufulira Mine were used.

The Mufulira Mine is located on the Copperbelt region of Zambia about 10 km south of the border with Democratic Republic of Congo (DRC) and approximately 59 km east of Konkola Mine. It lies on the north - eastern side of the Kafue Anticline approximately 1250 m above sea level.

Finally, the guidelines for obtaining the RPTs input parameters are also provided.

5.2 Rockburst Predictive Tools

The rockburst predictive tools (RPTs) using geotechnical and microseismic data were developed as follows:

- Selection of the suitable contributing factors;
- Testing correlation among MS factors;
- Categorizing the parameters into four groups and assigning ratings for each category;
- Evaluation of pre-determined rockburst classes;
- Establishment of the rockburst classification used in the prediction tools;
- Creating the RPTs;
- Validation of the RPTs using external data from Mufulira Mine, and
- Computation of the prediction accuracy for each RPT.

These essential steps are shown in the flow chart presented in Figure 5.1.

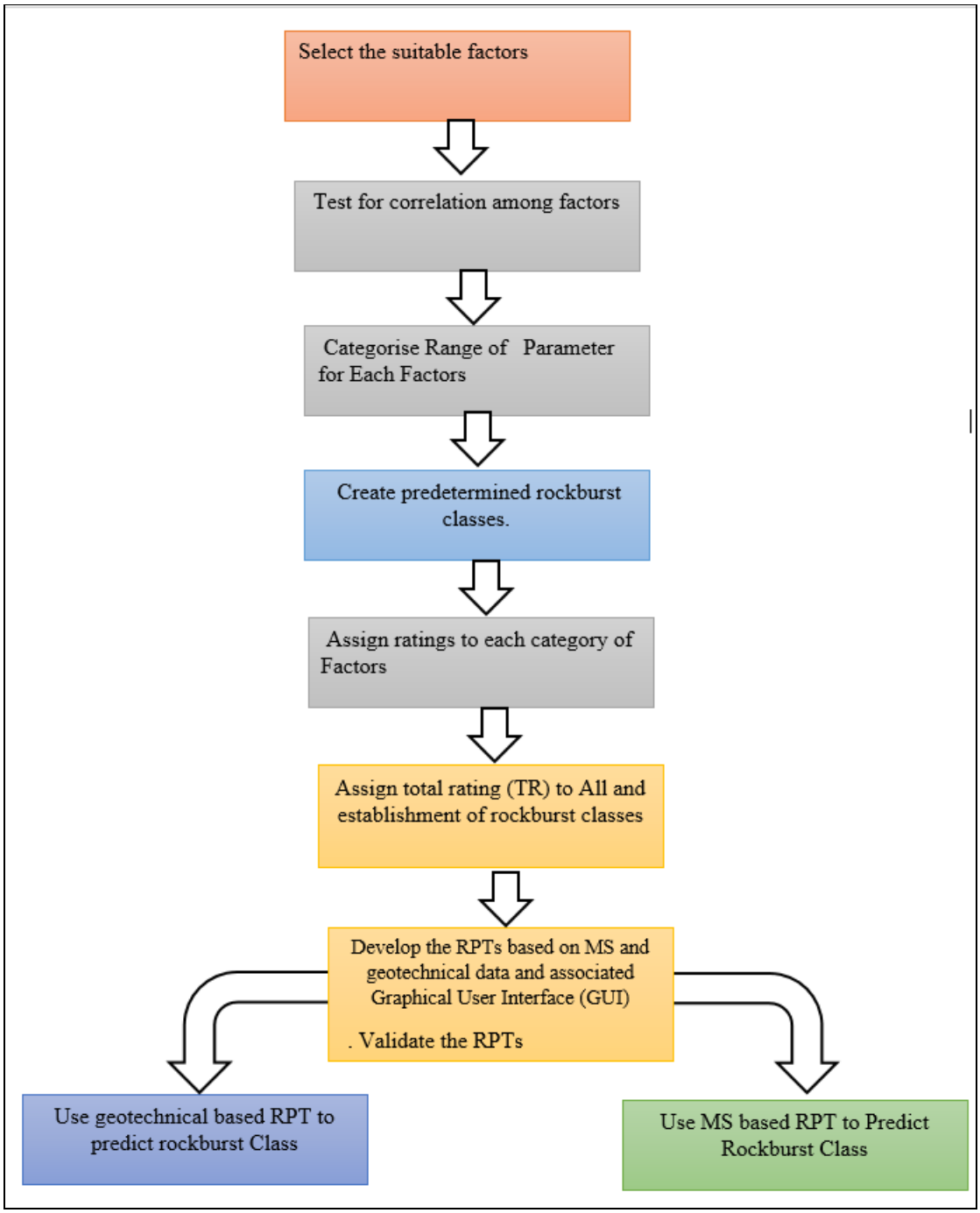

Figure 5.1: Steps in rockburst predictive tools (RPTs)

5.2.1 Selection of the Suitable Contributing Factors

The study conducted by the Author analysed different microseismic and geotechnical factors that contribute to rockburst. This research established the most common ranges for these factors.

5.2.1.1 Microseismic Factors

The Author identified five contributing microseismic (MS) factors that significantly impact rockburst in Chapter 4. These factors are presented in Table 5.1 and include the

local magnitude (M_L), seismic energy (logE/J), seismic potency (logP), E_S_E_P energy ratios, and hypocentral distance (measured in metres) from the stope.

Table 5.1: MS factors

Factor	Range	Most frequent range
M_L	0.5 - 2.2	1.3 -1.8
Log(E/J)	2.2 - 9.0	2.2 - 5.6
E_S/E_P	0.7 - 36.9	0.7 - 9.8
Log($P/m^{3)}$	0.3 - 2.2	0.3 - 1.3
Hypocentral distance (m) from the stope	0 - 159	0 - 53

Three significant factors, M_L, log (E/J), and log (P/m^3), were selected and analysed to develop a predictive tool. Statistical parameters including mean, standard deviation (Stdev), minimum (min), and maximum (max) values were established and shown in Table 5.2.

Table 5.2: Statistical parameters of microseismic factors

Parameter	Mean	Stdev	Min	Max
M_L	1.4	0.5	0.5	2.5
Log(P/m^3)	1.1	0.5	0.3	2.2
Log(E/J)	5.9	1.4	2.2	9.0

Table 5.2 shows that the standard deviation, a measure of how dispersed the data is in relation to the mean, indicated that the parameters in the data sets were clustered around the means.

5.3 Testing Correlation among MS Factors

Figures 5.2 to 5.4 display the correlation curves plotted for various factors including Seismic Energy (Log E/J), Seismic Potency (Log P/m^3) and Local Magnitude (M_L).

5.3.1 Relationship between logP and logE

Rockbursts can be caused by the amount of energy that is radiated, according to Spottiswoode and McGarr (1975). The log (E/J) value, a significant parameter, can determine the probability of a rockburst occurrence. When combined with other indicators, this parameter can accurately predict the likelihood of a rockburst event.

To compare log (E/J) values against logP, the values of logP and logE from 40 rockburst events were analyzed. The values of logE ranged from 1.4 to 9.0 and were plotted against the values of logP, ranging from 0.3 to 2.2. Figure 5.2 shows a moderate correlation between these values, with a determination coefficient of $R^2 = 0.53$. The correlation is indicated using Equation 5.1.

$$LogE = 2.32 \, Log \, (P) + 3.26 \quad (5.1)$$

Where:

LogE = Logarithmic of seismic energy in J.

LogP = Logarithmic of Seismic potency in J/m^3.

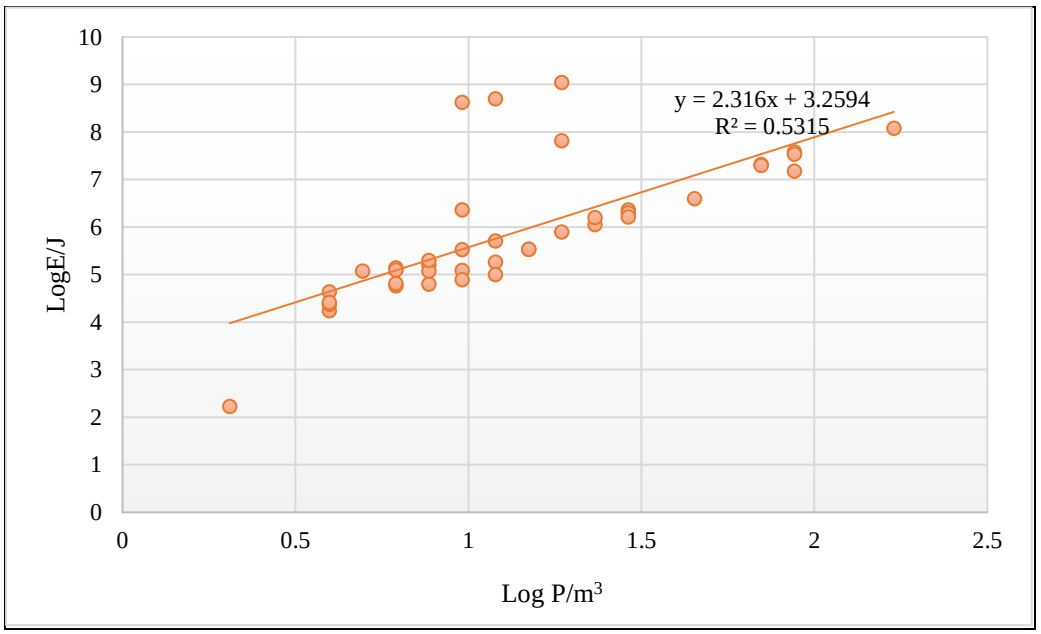

Figure 5.2: Correlation curve for logE and logP

5.3.2 Relationship between logP and M_L

Seismic potency is a measure of rock mass deformation during a seismic event at its source (King, 1978; Ben-Menahem and Singh, 1981). According to Drover and Villaescusa (2019), seismic potency may measure rock mass damage during any violent instability driven by the quasi-static mining-induced stress.

Seismic potency is a precursor to rockburst, which occurs when the rock mass undergoes inelastic deformation. Co-seismic inelastic deformation at the source is a significant factor in rockbursts. Studies by Ortlepp and Stacey in 1994 suggest that rockbursts related to seismic events can occur at a broad range of magnitudes, typically ranging from undetectable to 5 on the Richter scale. An analysis of 40 rockburst events at the Konkola Mine No.1 Shaft revealed that most of these events fell within the scale range of 1.2 to 1.8. The study suggests that the magnitude should be between 0.5 and 2.5 for a rockburst to occur. Additionally, it was found that an event with a magnitude below 0.5 did not result in a rockburst. This correlation between local magnitude and rockburst occurrence

indicates that M_L can be used as an important indicator of potential rockbursts. It helps predict the likelihood of such an event occurring.

To compare the values of Log P with M_L, the values of logP and M_L were obtained from the 40 rockburst events. The values of logP, ranging from 0.3 to 2.2, were plotted with the values of M_L, which ranged from 0.5 to 2.5, as shown in Figure 5.3. Figure 5.3 shows an almost perfect correlation with a determination coefficient of $R^2 = 0.94$. The correlation is given by Equation 5.2 as follows:

$$LogP = 0.90M_L - 0.12 \quad (5.2)$$

Where:

LogP = Logarithmic of seismic potency in J/m^3.

M_L = Dimensionless local magnitude of seismic event.

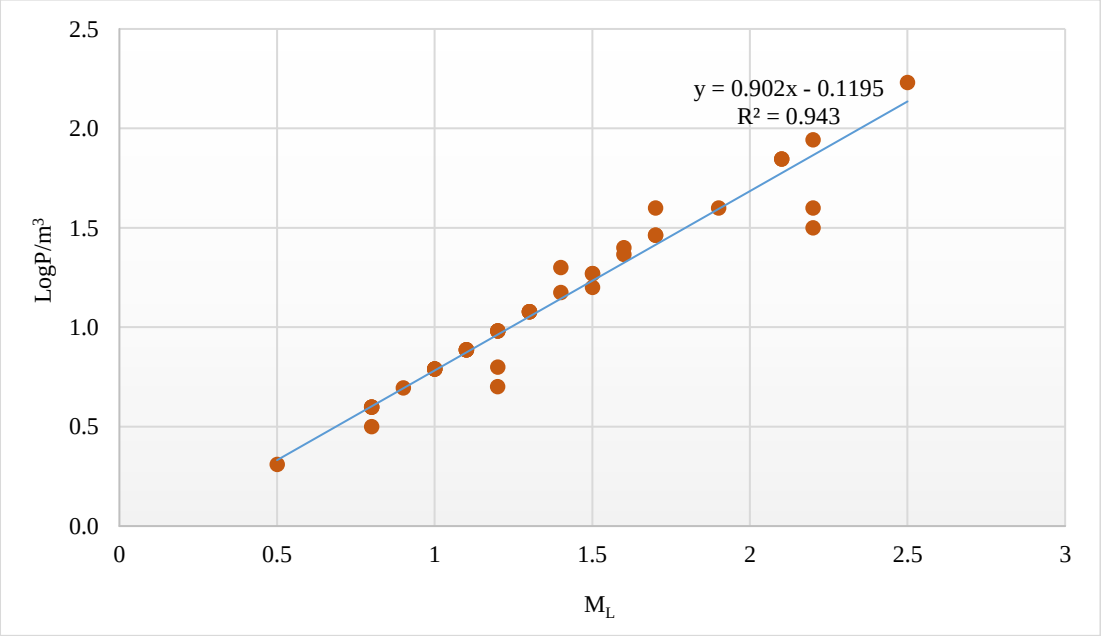

Figure 5.3: Correlation curve for M_L and LogP

5.3.3 Relationship between M_L and logE

The study plotted the values of M_L (magnitude) and LogE (energy) obtained from analysing 40 rockburst events to establish a relationship between them. The range of M_L values, which varied from 0.5 to 2.5, was plotted against the range of logE values, which varied from 2.2 to 9.0, as shown in Figure 5.4. The graph shows a moderate correlation with a determination coefficient of $R^2 = 0.53$. The correlation is indicated using Equation 5.3.

$$M_L = 0.239\log E - 0.041 \quad (5.3)$$

Where:

M_L = Dimensionless local magnitude of seismic event.

LogE = Logarithmic of seismic energy in J.

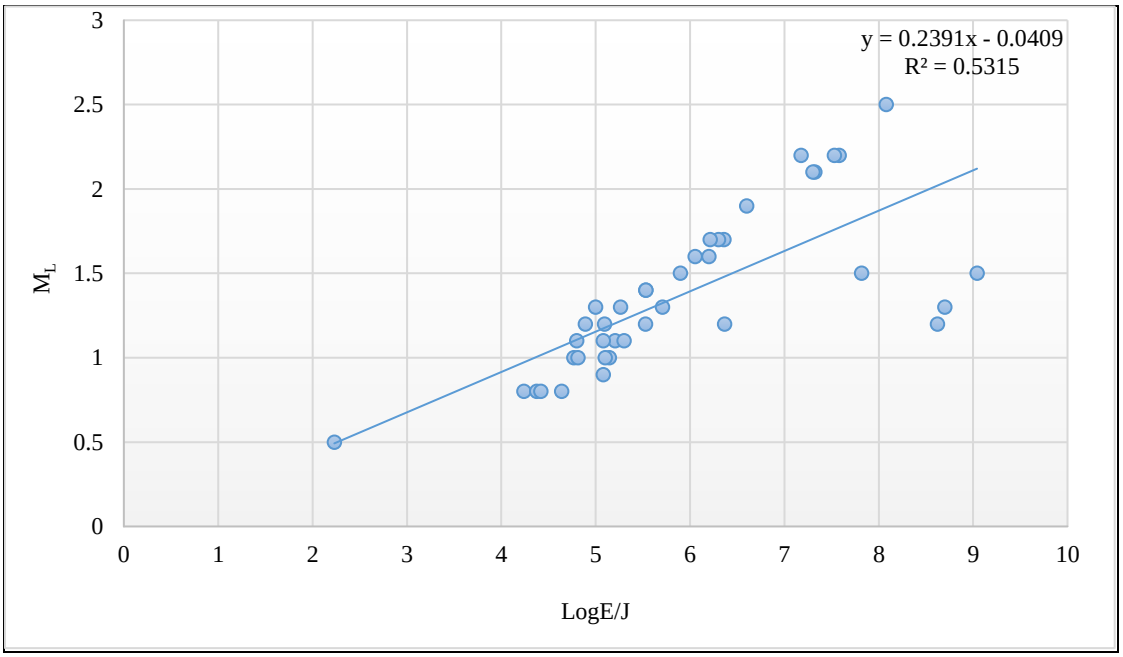

Figure 5.4: Correlation curve for M_L and Log E

These curves provided a visual representation of the relationship between these factors. The R^2 for all the curves were above 0.5 implying that the parameters were correlated and could be used for the development for the RPT.

5.4 Essential steps leading to development of MS_RPT

The steps leading to the development of the Microseismic based rockburst predictive tool followed the following sequential steps as follows:

- Categorising the parameters into four groups and assigning ratings;
- Pre-determined Rockburst classes; and
- Rockburst classification used in the MS_RPT.

5.4.1 Categorising the parameters into four groups and assigning ratings

The MS parameters were categorised into four groups with assigned ratings as presented in Tables 5.3 to 5.6.

Table 5.3: Rating (R1) for M_L

M_L	R1
$M_L < 0.5$	1
$0.5 \leq M_L < 1.5$	2
$1.5 \leq M_L < 2.5$	3
$M_L \geq 2.5$	4

Table 5.4: Rating (R2) for Seismic Potency ($LogP/m^3$).

$Log(P/m^3)$	R2
$Log(P/m^3) < 0.6$	1
$0.6 \leq Log(P/m^3) < 1.4$	2
$1.4 \leq Log(P/m^3) < 2.2$	3
$Log(P/m^3) \geq 2.2$	4

Table 5.5: Rating (R3) for Seismic Energy (Log (E/J)

Log (E/J)	R3
Log (E/J) < 2.2	1
2.2 ≤ Log (E/J) < 5.6	2
5.6≤ Log (E/J) < 9.0	3
Log (E/J) ≥ 9.0	4

5.4.2 Pre-determined Rockburst classes

The total ratings (TR) were calculated based on the ratings assigned to each factor with the minimum TR of three. The rockburst classification based on TR is shown in Table 5.6.

Table 5.6: Rockburst class prediction based on total rating (TR)

TR	Rockburst Classification
TR = 3	No damage
4 ≤ TR <7	Minor
7 ≤ TR < 10	Moderate
10 ≤ TR < 13	Strong
TR ≥ 13	Severe

5.4.3 Rockburst classification used in the MS_RPTS

Each rockburst event was described using the categories of no damage, minor, moderate, and strong (Kaiser et al., 1996; Potvin, 2009 ;). The rockburst damage classes are presented in Table 5.7.

Table 5.7: Rockburst Damage Classification (Kaiser et al., 1996; Potvin, 2009)

Rockburst class	Failure characteristics
Minor	- Support system is loaded, loose in mesh, plate deformed, shotcrete cracked - Rock spitting, spalling or shallow slabbing - A shallow skin of fractured or loose rock, generally less than 0.25 thick - Moderate new mesh bagging with a few broken wires. - Minor mesh bagging for a standard support system. If rock ejection is the mechanism involved - Minor falls of ground may occur, although the thickness (weight) of rock would be small enough that a standard support system should be capable of retaining this material in place - The weight of the rock in the failing ground is less than m^2
Moderate	- Some broken bolts, mesh bulged, shotcrete fractured - The rock is heavily fractured and may have displaced violently - Mesh will be bagged at its capacity and is often torn or pulled over rock bolt plates - Many holding elements will have failed but the volume of broken rock is limited such that drifts are still accessible - Shotcrete would be heavily fractured - Generally characterized by fractured or loosened rock of 0.25 m to 0.75 m in thickness
Strong/Major	- Major damage to support system, retention capacity severely compromised - Wide scale Fall of ground that may render it impassable due to substantial amounts of displaced rock - Most ground support components would be broken or damaged and shotcrete or other retaining elements would have lost their functionality, permitting unraveling of broken rock between holding elements. - Deep fracturing or the presence of damaged rock to a depth of more than 0.75 m around the opening
Extra strong/ Severe	- Complete failure of support and almost complete closure of the all drift or drive - Seismic energy release in excess of 10^9 Joules - Local magnitude of greater than 2.5

5.5 Creating a Seismic Based Rockburst Prediction Tool

The MS_RPT is a program that helps predict rockburst events using seismic parameters. It combines C++ logic code for calculations with a user-friendly interface designed in C#

Windows Forms. The development of a MS_RPT followed the following steps as outlined in the flowchart (Figure 5.5):

- Calculating Seismic Parameters in C++;
- Creating the Interface with C# Windows Forms;
- Designing the User Interface;
- Handling Errors and Validation;
- Measuring Execution Time;
- Bringing It All Together, and
- Validation with external data.

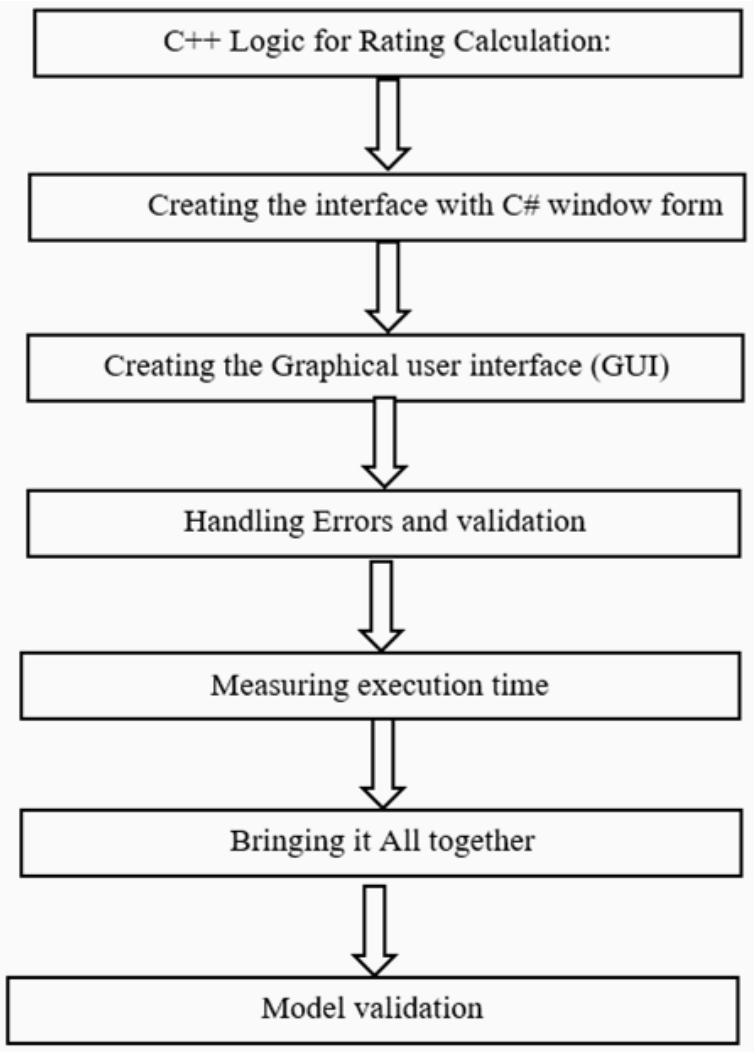

Figure 5.5: Creating a MS_RPT

5.5.1 Calculating Seismic Parameters in C++

The first step was writing the code logic in C++ (Appendix B1) to calculate ratings based on seismic parameters. The program considers three parameters; Local Magnitude (M_L), Log of Seismic Potency, log (P/m^3), and Log of Seismic Energy (log (E/J). Each parameter gets a rating based on specific ranges, indicating the potential class of a rockburst event. The MS_RPT combines C++ and C# to create an easy-to-use application.

5.5.2 Creating the Graphical Interface with C# Window

The C++ logic code (Appendix B2) was integrated into a C# Windows Forms application, resulting in a graphical user-friendly interface (GUI). Visual Studio's design tools helped to arrange labels, text boxes, buttons, and a space to show execution time. The user-friendly GUI, as shown in Figure 5.6, was carefully designed.

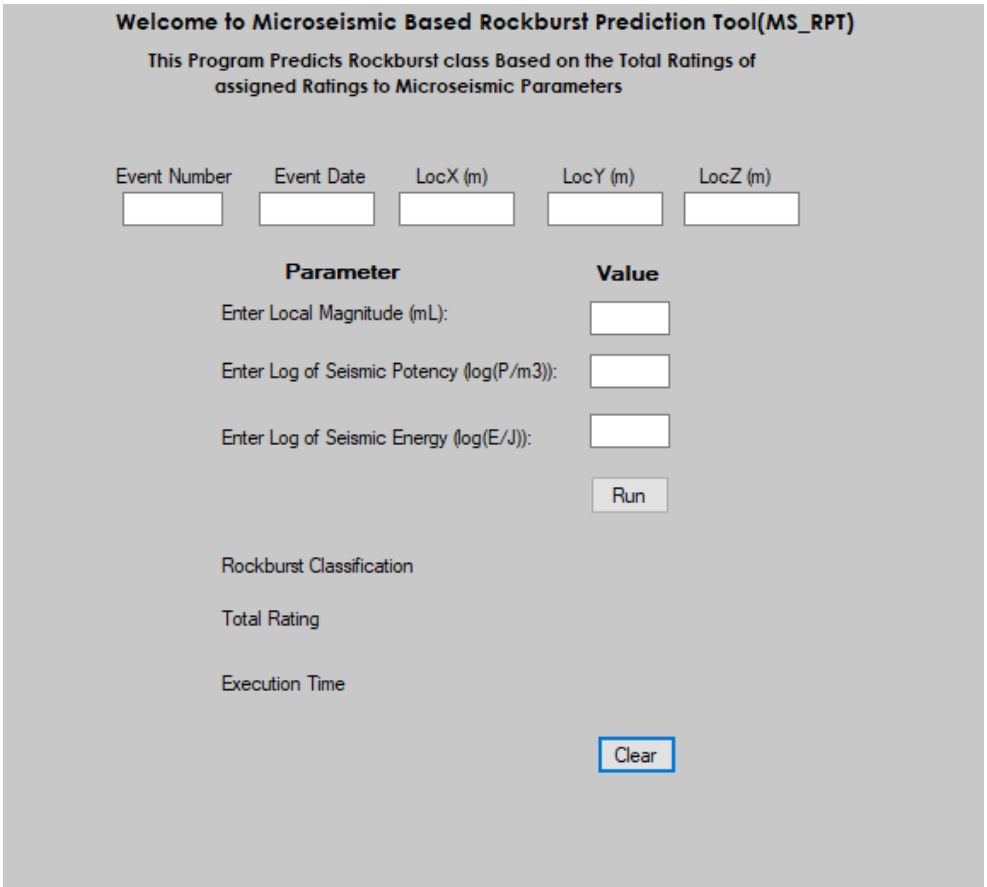

Figure 5.6: Screenshot of GUI for the MS_ RPT

The user inputs the three seismic parameters of an event 1: M_L = 2.4, logP = 1.7 and logE = 7.8, representing local magnitude, seismic potency and seismic energy, respectively. A "Run" button starts the prediction process, and a "Clear" button resets the input fields. The GUI displays the prediction results, as shown in Figure 5.7.

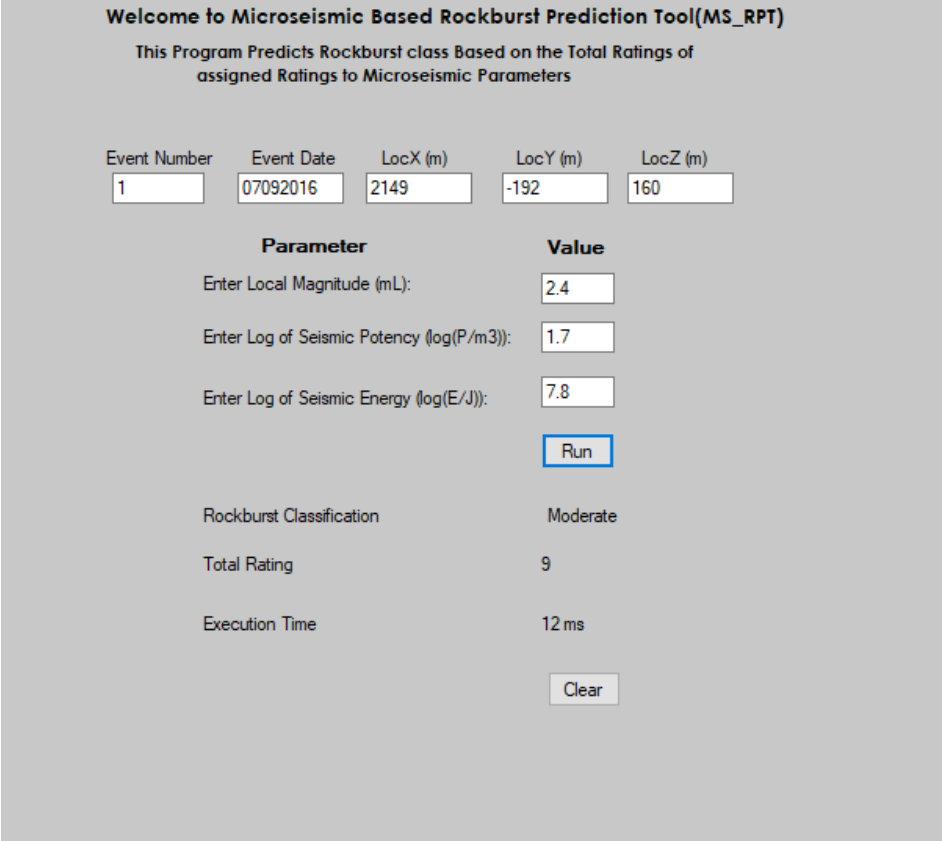

Figure 5.7: Rockburst damage classification results predicted using MS_RPT

5.5.3 Handling Errors and Validation

To ensure accurate predictions, the program checks user input for valid numbers. If there is an error, a message informs the user about it.

5.5.4 Measuring Execution Time

The Stopwatch class from System Diagnostics is used to measure the time it takes for predictions. This time is shown in milliseconds on the interface (Figure 5.7), helping users understand how fast the program works.

5.5.5 Bringing It All Together and Testing

The C++ logic was integrated into the C# program. The method was created to calculate ratings for each parameter, which are then combined to provide a prediction. The result is displayed along with the execution time.

5.5.6 Validation of the Seismic Predictive Rockburst Tool

The MS_RPT was validated using 16 sets of MS data from the Mufulira Mine with a history of rockbursts. The mine was chosen because it is geographically close to the Konkola Mine No.1 Shaft and uses the same MS system provided by the Institute of Mine

Seismology (IMS). The details of the rockburst events included Event No., Event Date, Event Time, LocX (m), LocY (m), and LocZ (m) as shown in Table 5.8.

Table 5.8: Details of rockburst events used for validation of the MS_RPT

Event No.	Event Date	Event Time	LocX (m)	LocY (m)	LocZ (m)
1	7-Oct-16	0:34	2149	-192	160
2	7-Oct-16	1:05	2200	-245	144
3	30-Aug-16	14:06	2269	-348	164
4	10-Sep-16	16:54	3050	-654	-49
5	10-Sep-16	16:54	3050	-654	-49
6	19-Sep-16	6:48	3378	-464	-51
7	19-Sep-16	10:53	3063	-569	4
8	13-Nov-16	19:33	3112	-418	-31
9	14-Nov-16	19:19	3104	-581	-36
10	28-Jan-17	3:50	2761	-676	-595
11	12-Jul-17	8:43	1496	-243	98
12	16-Jan-18	17:07	3270	-903	-715
13	25-Oct-19	5:20	2661	-312	-532
14	27-Oct-20	4:54	3085	-539	-279
15	21-Nov-22	0:51	3129	-511	-379
16	21-Nov-22	1:01	3051	-514	-169

Table 5.9 presents the MS factors including M_L, Log (E/J) and log (P/m^3) used to validate the G_RPT.

Table 5.9: Microseismic data used for validation of the MS_ RPT

Event	M_L	Log(P/m^3)	Log(E/J)
1	2.4	1.7	7.8
2	1.7	1.2	6.5
3	1.4	0.9	6.0
4	1.4	0.9	6.0
5	1.4	0.9	6.0
6	2.2	1.5	7.4
7	1.4	0.9	6.0
8	1.3	0.9	5.8
9	1.7	1.2	6.5
10	1.6	1.1	6.3
11	2.2	1.5	7.4
12	2.8	2.0	8.5
13	1.2	0.8	5.6
14	2.1	1.5	7.2
15	1.9	1.5	6.9
16	1.5	1.3	5.8

The MS_RPT was used to rank the datasets to predict the class of the rockburst. The ranking was based on the sum of the ratings for each microseismic factor. The total ratings

(TR) were then compared to the pre-determined rockburst class to predict the rockburst class are shown in Table 5.10.

Table 5.10: Microseismic data used for validation of the MS_ RPT

Event	M_L	Log(P/m^3)	Log(E/J)	Prediction Class
1	2.4	1.7	7.8	Moderate
2	1.7	1.2	6.5	Moderate
3	1.4	0.9	6.0	Moderate
4	1.4	0.9	6.0	Moderate
5	1.4	0.9	6.0	Moderate
6	2.2	1.5	7.4	Moderate
7	1.4	0.9	6.0	Moderate
8	1.3	0.9	5.8	Moderate
9	1.7	1.2	6.5	Moderate
10	1.6	1.1	6.3	Moderate
11	2.2	1.5	7.4	Moderate
12	2.8	2.0	8.5	Strong
13	1.2	0.8	5.6	Moderate
14	2.1	1.5	7.2	Moderate
15	1.9	1.5	6.9	Moderate
16	1.5	1.3	5.8	Moderate

Table 5.10 shows that the MS_RPT predicted one strong and 15 moderate rockburst instances respectively. The rockburst classes predicted were compared to 16 actual classes determined by geotechnical engineers at the Mufulira Mine (Table 5.11).

Table 5.11: Validation results for the MS_ RPT

Event	M_L	Log(P/m^3)	Log(E/J)	Prediction Class	Actual
1	2.4	1.7	7.8	Moderate	Strong
2	1.7	1.2	6.5	Moderate	Moderate
3	1.4	0.9	6.0	Moderate	Moderate
4	1.4	0.9	6.0	Moderate	Moderate
5	1.4	0.9	6.0	Moderate	Moderate
6	2.2	1.5	7.4	Moderate	Moderate
7	1.4	0.9	6.0	Moderate	Moderate
8	1.3	0.9	5.8	Moderate	Moderate
9	1.7	1.2	6.5	Moderate	Moderate
10	1.6	1.1	6.3	Moderate	Moderate
11	2.2	1.5	7.4	Moderate	Moderate
12	2.8	2.0	8.5	Strong	Strong
13	1.2	0.8	5.6	Moderate	Moderate
14	2.1	1.5	7.2	Moderate	Moderate
15	1.9	1.5	6.9	Moderate	Moderate
16	1.5	1.3	5.8	Moderate	Moderate

Table 5.11 shows that the MS_RPT accurately predicted 15 true rockburst damage classes and one (1) incorrect out of 16 events. The prediction accuracy was calculated using Equation 5.4.

$$\text{Accuracy (100\%)} = 1 - \text{Error Rate} \quad (5.4)$$

Where:

$$\text{Error Rate} = \left| \frac{\text{Total number of True predictions} - \text{Total number of actual}}{\text{Total Number of actuals}} \right|$$

The total number of the actual rockburst damage classes were 16 and the total number of the rockburst class predicted as true class were 15. The accuracy for the MS_ RPT was calculated as 94 percent.

5.6 Development of the Geotechnical - Based Predictive Tool

5.6.1 Geotechnical Factors used in the Tool

Six geotechnical factors were established as contributing factors to rockburst. The factors are shown in Table 5.12. The factors were unconfined compressive strength (σ_c), rock quality designation (RQD), unconfined tensile strength (σ_t), tangential stress (σ_{θ}), principal in-situ stress (σ_1) and linear elastic energy (W_{et}).

Table 5.12: Geotechnical Factors

Factor	Range	Most frequent range
RQD /%	60 - 88	60 - 69
σ_c /MPa	74 - 330	160 - 244
σ_t /MPa	6.5 - 30.5	6.5 - 14.5
σ_{θ} /MPa	37 - 165	80 - 122.3
σ_1 /MPa	19.5 - 32.1	28 - 32.1
Log (W_{et} /Jm^{-3})	5.1 - 6.4	5.6 - 6.0

Table 5.12 shows the factors that were selected to develop geotechnical based-based rockburst predictive tool (G_RPT). The factors were deemed pertinent to forecasting the rockburst potential. Subsequently, a thorough analysis of the factors was conducted to determine various statistical parameters, including but not limited to the mean, standard deviation (Stdev), as well as the minimum (min) and maximum (max) values. The statistical parameters generated from this analysis are shown in Table 5.13.

Table 5.13: Statistical parameters for the Geotechnical factors

Parameter	RQD (%)	σ_c (MPa)	σ_t (MPa)	σ_θ (MPa)	Log (W_{et} (Jm^{-3})	σ_1 (MPa)
Mean	70	176	13.8	87.8	5.7	27.8
STDEV	11	77	6.0	38.3	0.4	2.7
Min	60	74	6.5	37.0	5.1	19.5
Max	88	315	30.5	157.5	6.4	32.1

Based on Table 5.13, the calculated standard deviation, which indicates the degree of dispersion of the data from the mean, implies that the parameters in the datasets were closely clustered around their respective means.

5.6.2 Testing Correlation among Geotechnical Factors

The correlation curves were plotted for the unconfined compressive strength (σ_c), rock quality designation (RQD), unconfined tensile strength (σ_t), tangential stress ($\sigma_{\theta)}$ linear elastic energy (W_{et}) and major principal vertical stress (σ_1).

5.6.2.1 Relationship between σ_c and RQD

The rock's uniaxial compressive strength (UCS) is the rock specimen's maximum compressive stress before failure under uniaxial compression loading. According to Zhang et al., (2020), the UCS is a relatively intuitive factor in evaluating the possibility of rockburst. Nussbaumer (2000) analysed the mechanical properties of 16 different rocks from research conducted in South Africa by Hill and Denkhaus (1961), specifically examining the values obtained from the "relative violence of rupture" test. He found a strong linear correlation ($r^2 = 0.89$) between the UCS and the likelihood of burst-prone existence. Rocks with high UCS are prone to violent bursting.

The RQD refers to the percentage of core pieces that are longer than 100 mm and remain intact in the drilled core's overall length. The index is useful in predicting rockbursts (Tang, 2000). It reflects the rock's ability to store energy and its integration, which also indicates the tendency of rockbursts (Cai, 2016). A higher RQD value indicates stronger rock integration and a greater likelihood of rockbursts.

The author plotted the values of RQD in percentage and UCS (σ_c) obtained from analysing 40 rockburst events to establish a relationship between them. The range of RQD values, which varied from 60 to 80 percent, was plotted against the range of σ_c values, which varied from 74 to 315 MPa, as shown in Figure 5.8. The graph shows a good correlation with a determination coefficient of $R^2 = 0.77$. The correlation is shown in Equation 5.5.

$$\sigma_c = 6.23\ RQD - 262 \quad (5.5)$$

Where:

σ_c = Rocks compressive strength in MPa.

RQD = Rock Quality Designation in percentage (percentage).

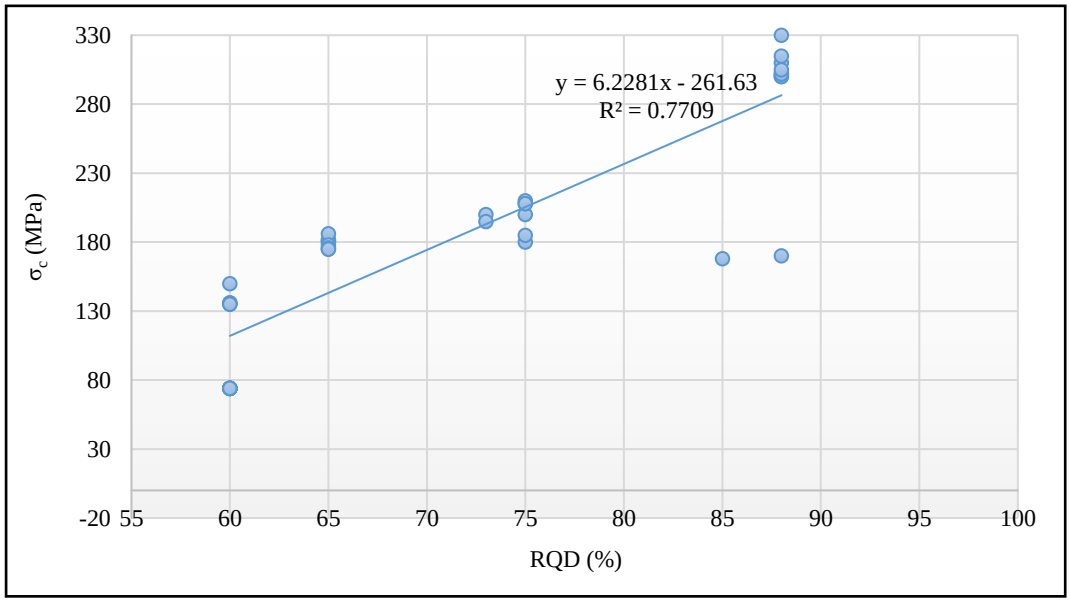

Figure 5.8: Correlation curve for RQD and σ_c

5.6.2.2 Relationship between σ_t and σ_c

The strength of rock under tension, known as unconfined tensile strength (UTS), plays a crucial role in assessing the likelihood of rockbursts. This parameter has been utilised in various rockburst prediction criteria, as evidenced by research on the stress method of rockburst predictions (Qiao and Tian, 1998; Altindag, 2003; Chen et al., 2013). UTS is also important in determining the rock brittleness coefficient, which is the ratio of UCS to the confined tensile strength of intact rock (Qiao and Tian, 1998).

The researcher plotted the values of σ_t and σc obtained from analysing 40 rockburst events to establish a relationship between them. The range of σ_t values, which varied from 6.5 to 30, was plotted against the range of σ_c values, which varied from 74 to 315 MPa, as shown in Figure 5.9. The graph shows a good correlation with a determination coefficient of R^2 = 0.72. The correlation is shown in Equation 5.6.

$$\sigma_t = 0.08\ \sigma_c + 1.1 \quad (5.6)$$

Where:

σ_c = Rock's compressive strength in MPa.

σ_t = Rock's unconfined tensile strength in MPa.

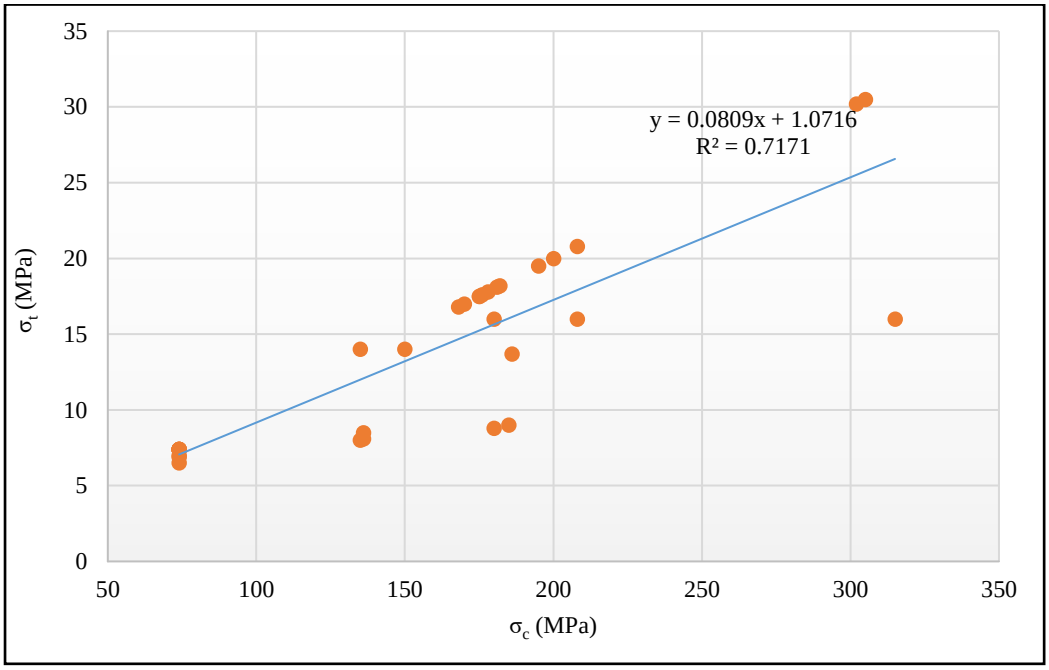

Figure 5.9: Correlation curve for σ_t and σ_c

5.6.2.3 Relationship between elastic strain energy and maximum tangential stress

Peng et al., (2023), in their investigations of the characteristics of ground pressure disaster and rockburst proneness in deep gold mining, found that when the maximum tangential stress (MTS) of the tunnel were about 0.4 and 0.55 times UCS of rock, the tunnel might suffer spalling. Peng et al., (2021), in their field investigation and analysis of rockburst and spalling in a deep hard-rock Mine, found that when the maximum tangential stress was between 0.4 and 0.6 times the uniaxial compressive strength of surrounding rock, surrounding rock was prone to local spalling.

As discussed in Section 2.6.2.1, Wang and Park (2001) introduced the linear elastic energy (W_{et}), which is defined as the linear elastic energy stored in the rock specimen before the rock failure point. It is one of the indicators for predicting the rockburst intensity

The Author plotted the values of σ_θ and W_{et} obtained from analysing 40 rockburst events to establish a relationship between them. The range of σ_θ values, which varied from 37 to 157 MPa, was plotted against the range of Log (W_{et}/Jm^{-3}) values, which varied from 5.1 to 6.4, as shown in Figure 5.10. The graph shows almost a perfect correlation with a determination coefficient of $R^2 = 0.96$ as shown in Equation 5.7.

$$LogW_{et} = 0.01\ \sigma_\theta + 4.85 \quad (5.7)$$

Where:

$LogW_{et}$ = Logarithmic of the linear elastic energy in J/m^3).

σ_θ = Maximum tangential stress in MPa.

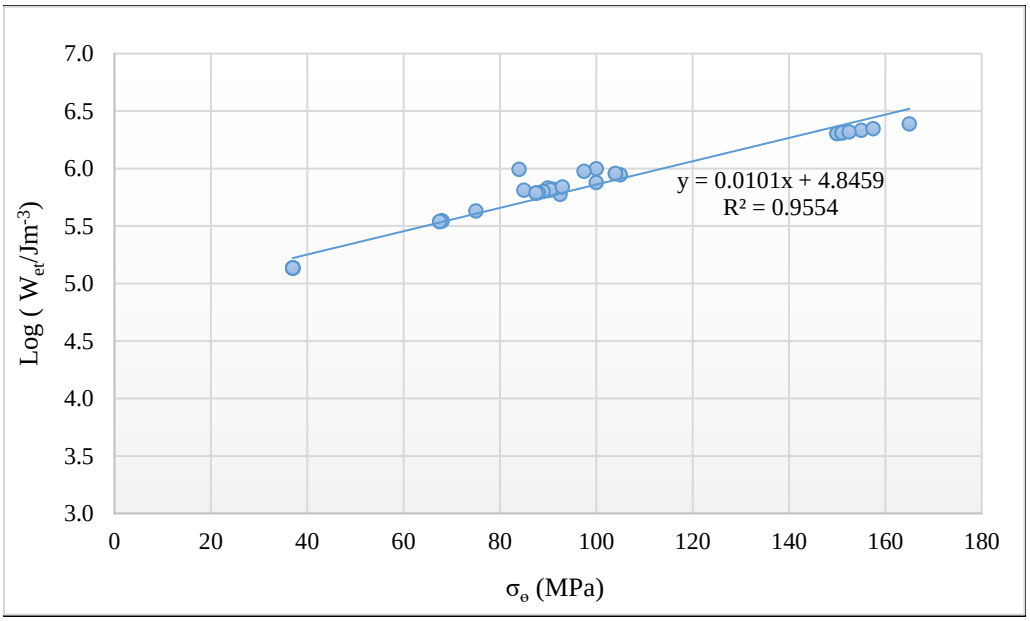

Figure 5.10: Correlation curve for W_{et} and σ_θ

5.6.3 Relationship between σ_1 and other factors

The analysis of the principal stress field (σ_v) in areas affected by rockburst at Konkola Mine No.1 Shaft varied between 19 and 32 MPa. When the principal stress field exceeds the compressive strength of the rock mass next to the excavation boundary, it is expected to fail. The major principal stress is a significant factor that affects the incidence of rockbursts. As the stress increases, it directly impacts the mechanical properties of the rock such as RQD, UCS, tangential stress, unconfined tensile strength, and elastic strain energy. Stress values were plotted against the values of RQD, UCS, tangential stress, unconfined tensile strength, and elastic strain energy in order to analyse the correlation between the major principal stress and these properties.

5.6.3.1 Relationship between σ_1 and σ_c

The Author plotted the values of σ_1 and σ_c obtained from analysing 40 rockburst events to establish a relationship between them. The range of σ_1 values, which varied from 26 to 31 MPa, was plotted against the range of σ_c values, which varied from 74 to 195 MPa, as shown in Figure 5.11. The graph shows a fair correlation with a determination coefficient of $R^2 = 0.54$. The correlation is shown in Equation 5.8.

$$\sigma_c = 15\ \sigma_1 - 274 \quad (5.8)$$

Where:

σ_c = Rock's compressive strength in MPa.

σ_1 = Principal Major Stress in MPa.

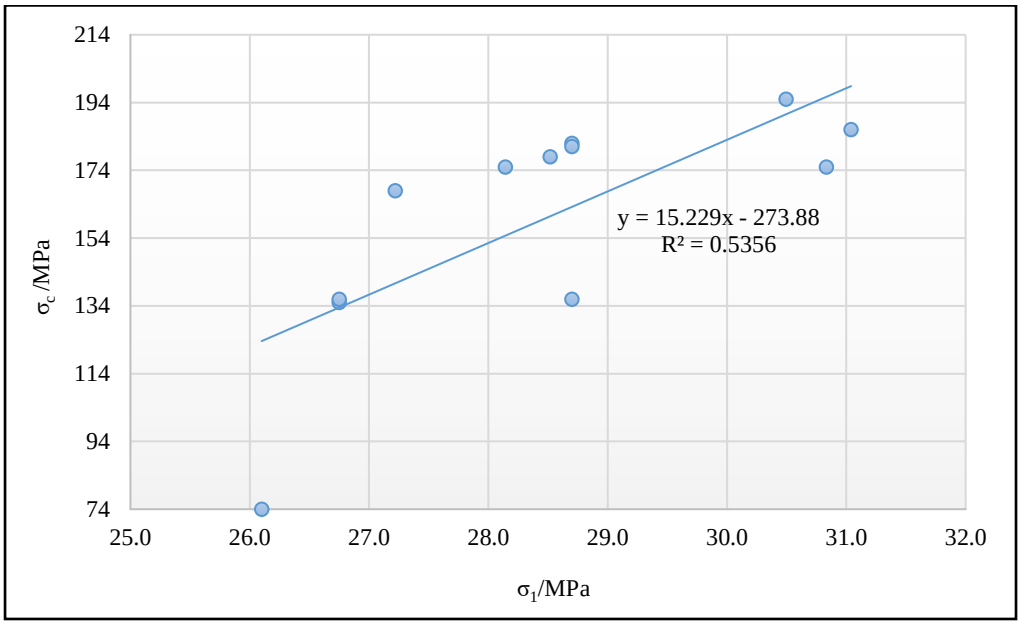

Figure 5.11: Correlation curve for σ_1 and σ_c

5.6.3.2 Relationship between σ_1 and RQD

The Author plotted the values of σ_1 (MPa) and RQD in percentage obtained from analysing 40 rockburst events to establish a relationship between them. The range of σ_1 values, which varied from 26 to 31 MPa, was plotted against the range of RQD values, which varied from 60 to 88 percent, as shown in Figure 5.12. The graph shows a fair correlation with a determination coefficient of $R^2 = 0.51$. The correlation is shown in Equation 5.9:

$$RQD = 2.03\ \sigma_1 - 17.8 \quad (5.9)$$

Where:

RQD = Rock Quality Designation in percentage (percentage).

σ_1 = Principal Major Stress in MPa.

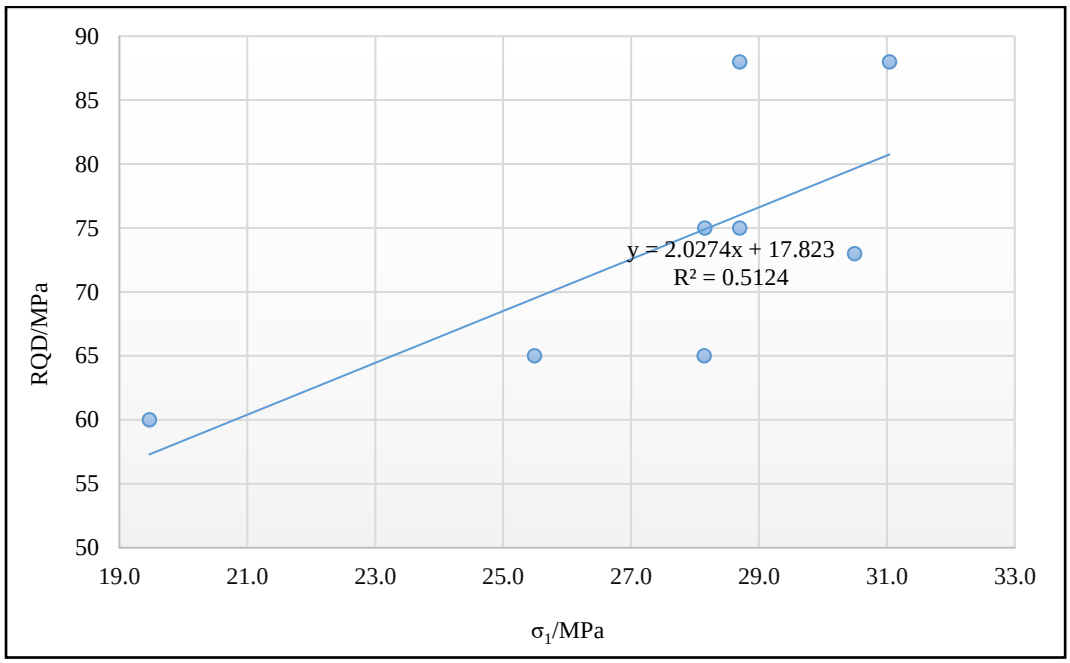

Figure 5.12: Correlation curve for σ_1 and RQD

5.6.3.3 Relationship between σ_1 and σ_θ

The range of σ_1 values, which varied from 26 to 31 MPa, was plotted against the range of σ_θ values, which varied from 68 to 98 MPa, as shown in Figure 5.13. The graph shows a fair correlation with a determination coefficient of $R^2 = 0.58$. The correlation is shown in Equation 5.10:

$$\sigma_\theta = 2.61\ \sigma_1 + 10.9 \qquad (5.10)$$

Where:

σ_θ = Maximum tangential stress in MPa.

σ_1 = Principal Major Stress in MPa.

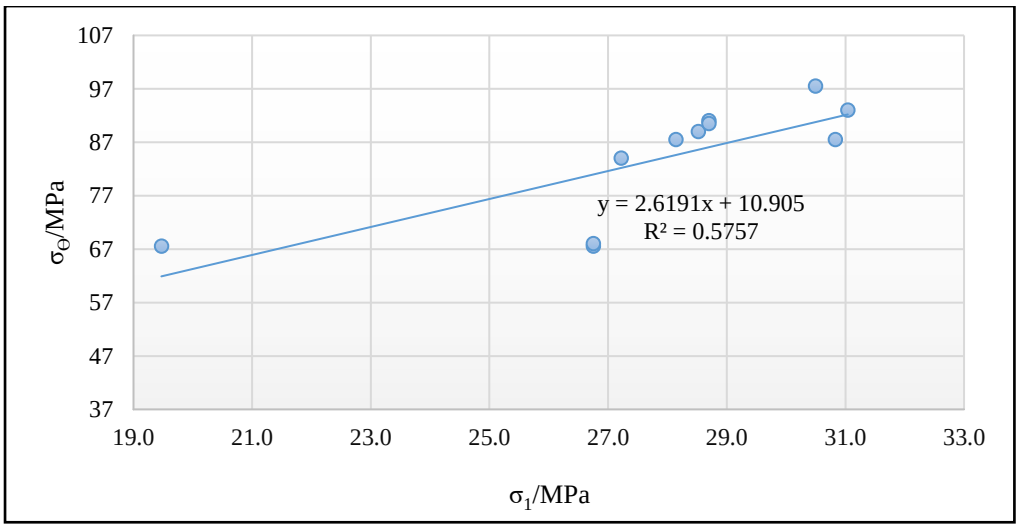

Figure 5.13: Correlation curve for σ_1 and σ_θ

5.6.3.4 Relationship between σ_1 and σ_t

The Author plotted the values of σ_1 (MPa) and σ_θ, obtained from analysing 40 rockburst events to establish a relationship between them. The range of σ_1 values, which varied from 25.5 to 31 MPa, was plotted against the range of σ_t, values, which varied from 16 to 30 MPa, as shown in Figure 5.14. The graph shows a fair correlation with a determination coefficient of $R^2 = 0.60$. The correlation is shown in Equation 5.11:

$$\sigma_t = 1.91\ \sigma_1 + 35.4 \qquad (5.11)$$

Where:

σ_t = Rocks unconfined tensile strength in MPa.

σ_1 = Principal Major Stress in MPa.

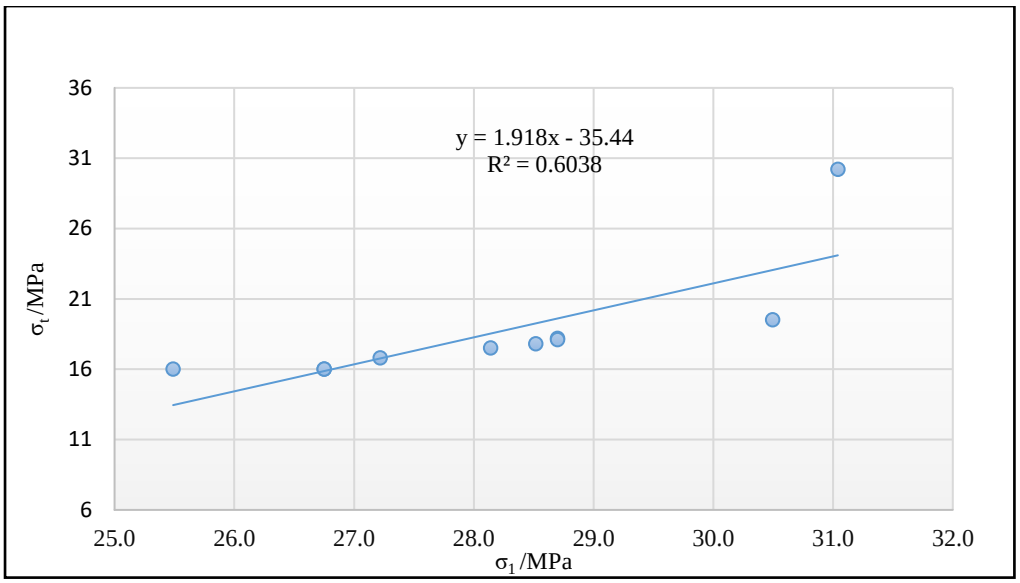

Figure 5.14: Correlation curve for σ_1 and σ_t

5.6.3.5 Relationship between σ_1 and W_{et}

The Author plotted the values of σ_1 (MPa) and W_{et}, obtained from analysing 40 rockburst events to establish a relationship between them. The range of σ_1 values, which varied from 26 to 32 MPa, was plotted against the range of log (W_{et}/Jm^{-3}), values, which varied from 5.1 to 6.8 MPa, as shown in Figure 5.15. The graph shows a fair correlation with a determination coefficient of $R^2 = 0.58$. The correlation is shown in Equation 5.12:

$$\text{Log Wet} = 0.17\ \sigma_1 + 1.1 \qquad (5.12)$$

Where:

σ_θ = Maximum Tangential Stress in MPa.

σ_1 = Principal Major Stress in MPa.

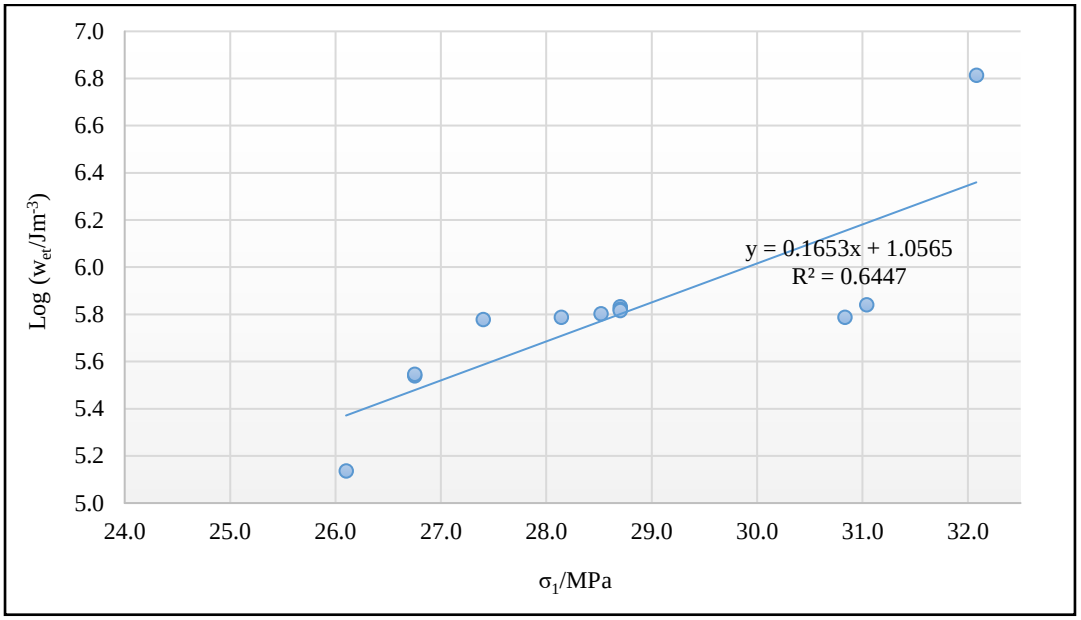

Figure 5.15: Correlation curve for log W_{et} and σ_1

Figures 5.8 to 5.15 display the correlation curves plotted for various factors including unconfined compressive strength (σ_c), rock quality designation (RQD), unconfined tensile strength (σ_t), tangential stress (σ_θ), linear elastic energy (W_{et}) and principal in-situ stress (σ_1) These curves provide a visual representation of the relationship between these factors. The determination coefficients of R^2 for all the curves were above 0.5 implying that the parameters were correlated and could be used for the development for the RPT.

5.7 Essential steps leading to development of G_RPT

The steps leading to the development of the Geotechnical based rockburst predictive tool (G_RPT) followed the following three sequential steps:

- Categorising the parameters into four groups and assigning ratings;
- Assigning pre-determined Rockburst classes; and
- Implementing rockburst classification used in the G_RPT.

5.7.1 Categorising the parameters into four groups and assigning ratings for each category

The geotechnical factors were categorised into four groups with assigned ratings as presented in Tables 5.14 to 5.19. The groups were based on the ranges of factors in Tables 5.12 and 5.13. The ranges were the most common at Konkola Mine No.1 Shaft for the rockbursts. Table 5.14 indicates that the ranges above 74 MPa have a high potential for rockbursts and vice versa.

Table 5.14: Rating (R1) for Compressive Stress, σ_c (MPa)

σ_c (MPa)	R1
$\sigma_c < 74$	1
$74 \leq \sigma_c < 202$	2
$2002 \leq \sigma_c < 330$	3
$\sigma_c \geq 330$	4

Table 5.15: Rating (R2) for Rock quality designation, RQD (%)

RQD (%)	R2
RQD < 60	1
60 ≤ RQD < 74	2
74 ≤ RQD < 88	3
88 ≤ RQD ≤ 100	4

Table 5.16: Rating (R3) for Tensile strength, σt (MPa)

σ_t (MPa)	R3
$\sigma_t < 6.5$	1
$6.5 \leq \sigma_t < 18.5$	2
$18.5 \leq \sigma_t < 30.5$	3
$\sigma_t \geq 30.5$	4

Table 5.17: Rating (R4) for Tangential stress, σ_θ (MPa)

σ_θ (MPa)	R4
$\sigma_\theta < 37$	1
$37 \leq \sigma_\theta < 101$	2
$101 \leq \sigma_\theta < 165$	3
$\sigma_\theta \geq 165$	4

Table 5.18: Rating (R5) for Principal in – situ Stress, σ_c (MPa)

σ_1 (MPa)	R5
$\sigma_1 < 19$	1
$19 \leq \sigma_1 < 26$	2
$26 \leq \sigma_1 < 32$	3
$\sigma_1 \geq 32$	4

Table 5.19: Rating (R6) for Linear Elastic Energy, W_{et} (J/m^3)

Wet (J/m^3)	**R6**
Log (W_{et}) < 5.1	1
5.1 ≤ Log (W_{et}) < 5.9	2
5.9 ≤ Log (W_{et}) < 6.4	3
Log (W_{et}) ≥ 6.4	4

5.7.2 Pre-determined Rockburst classes

The total ratings (TR) were calculated based on the ratings assigned to each factor with the minimum TR of six. Six was the minimum sum of adding the lowest values of R values (R1 + R2 + R3 + R4 + R5 + R6) from Tables 5.14 and 5.19. The rockburst classification based on TR is shown in Table 5.20.

Table 5.20: Rockburst class prediction based on total rating (TR)

TR	**Rockburst Classification**
TR = 6	No damage
6 ≤ TR < 15	Minor
15 ≤ TR ≤ 20	Moderate
20 ≤ TR < 24	Strong
TR ≥ 24	Extra strong

5.7.3 Rockburst classification used in the G_RPTS

Each rockburst event was described using the categories of no damage, minor, moderate, and strong (Kaiser et al., 1996; Potvin, 2009). The rockburst damage classes are presented in Table 5.12.

Table 5.21: Rockburst Damage Classification (Kaiser et al., 1996; Potvin, 2009)

Rockburst class	Failure characteristics
Minor	- Support system is loaded, loose in mesh, plate deformed, shotcrete cracked - Rock spitting, spalling or shallow slabbing - a shallow skin of fractured or loose rock, generally less than 0.25 thick - Moderate new mesh bagging with a few broken wires. - Minor mesh bagging for a standard support system. If rock ejection is the mechanism involved - Minor falls of ground may occur, although the thickness (weight) of rock would be small enough that a standard support system should be capable of retaining this material in place - The weight of the rock in the failing ground is less than m^2
Moderate	- Some broken bolts, mesh bulged, shotcrete fractured - The rock is heavily fractured and may have displaced violently - Mesh will be bagged at its capacity and is often torn or pulled over rock bolt plates - Many holding elements will have failed but the volume of broken rock is limited such that drifts are still accessible - Shotcrete would be heavily fractured - Generally characterized by fractured or loosened rock of 0.25 m to 0.75 m in thickness
Strong/Major	- Major damage to support system, retention capacity severely compromised. - Wide scale Fall of ground that may render it impassable due to substantial amounts of displaced rock - Most ground support components would be broken, or damaged and shotcrete or other retaining elements would have lost their functionality, permitting unraveling of broken rock between holding elements - deep fracturing or the presence of damaged rock to a depth of more than 0.75 m around the opening
Extra strong/ Severe	- Complete failure of support and almost complete closure of the all drift or drive - Seismic energy release in excess of 10^9 Joules - Local magnitude of greater than 2.5

5.7.4 Creating a Geotechnical Based Rockburst Prediction Tool

The G_RPT is a computer software application developed to predict the potential occurrence of rockburst events based on assigned ratings to geotechnical parameters. The

application combines C++ logic for rating calculations with a C# Windows Forms graphical user interface to provide an intuitive and user-friendly experience. The development of a G_RPT followed the steps as outlined in the flowchart (Figure 5.16):

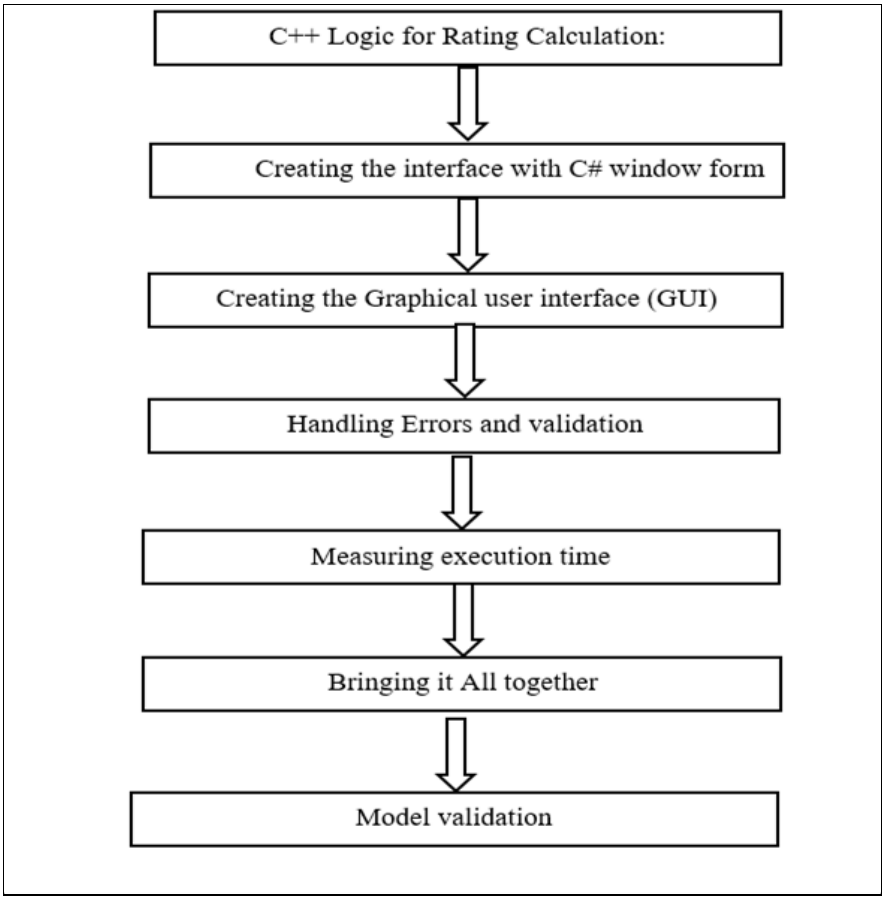

Figure 5.16: Creating a G_RPT

5.7.4.1 C++ Logic for Rating Calculation

The first step involved writing the code rating calculation logic in C++ (refer to Appendix C1). The logic considers six geotechnical parameters: Rock Quality Designation (RQD), unconfined compressive strength (UCS), unconfined tensile strength (UTS), maximum tangential stress (MTS), log of linear elastic energy (W_{et}), and in-situ maximum principal stress (σ_1). Each parameter is assigned a rating based on predefined ranges. The program calculates total ratings to make predictions about the class of rockburst events.

5.7.4.2 Integration with C# Windows Forms

The C++ logic was integrated with a C# Windows Forms application to create a user-friendly graphical interface. Visual Studio was utilised to design the interface, which includes various elements such as labels, text boxes, and buttons.

5.7.4.3 Graphical User Interface Design

Visual Studio's designer was used to create a user-friendly interface. Labels guided users and text boxes allowed input. A "Run" button initiated the prediction process, and an additional label displayed the execution time of the prediction.

5.7.4.4 Creating the Graphical Interface with C# Window

The C++ logic code in Appendix C2 was integrated into a C# Windows Forms application using Visual Studio's design tools, resulting in a user-friendly GUI with labels, text boxes, buttons, and an execution time display (Figure 5.17).

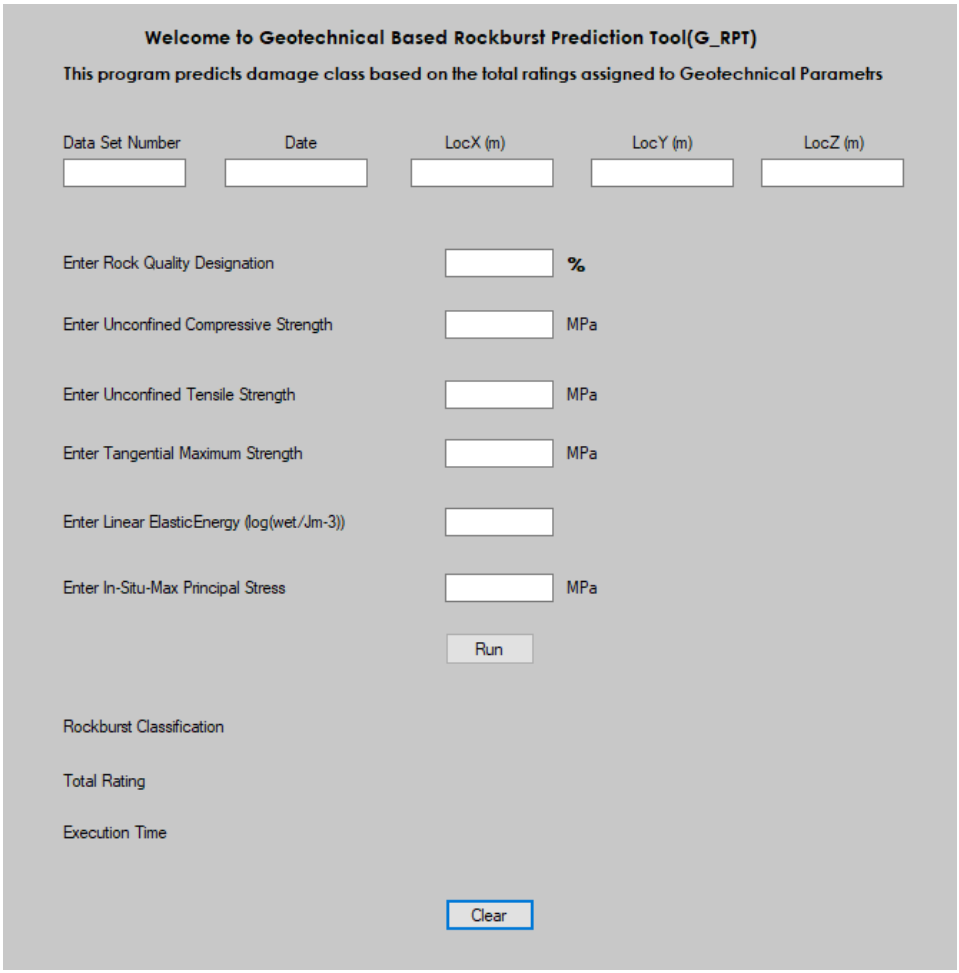

Figure 5.17: GUI for the Geotechnical based RPT

The user inputs the details of a rockburst event that include dataset number, date and location. The user then inputs the six geotechnical parameters for the event 1: rock quality designation (RQD) = 80 percent, unconfined compressive strength (UCS) = 270 MPa, unconfined tensile strength (UTS) = 26 MPa, maximum tangential stress = 162 MPa, log (elastic linear energy) = 6.4 and principal in-situ maximum stress = 38 MPa. After entering the information, the user can start the prediction process by clicking the "Run" button and

the prediction results are presented in the GUI (Figure 5.18). A "Clear" button resets the input fields so the user can input another dataset.

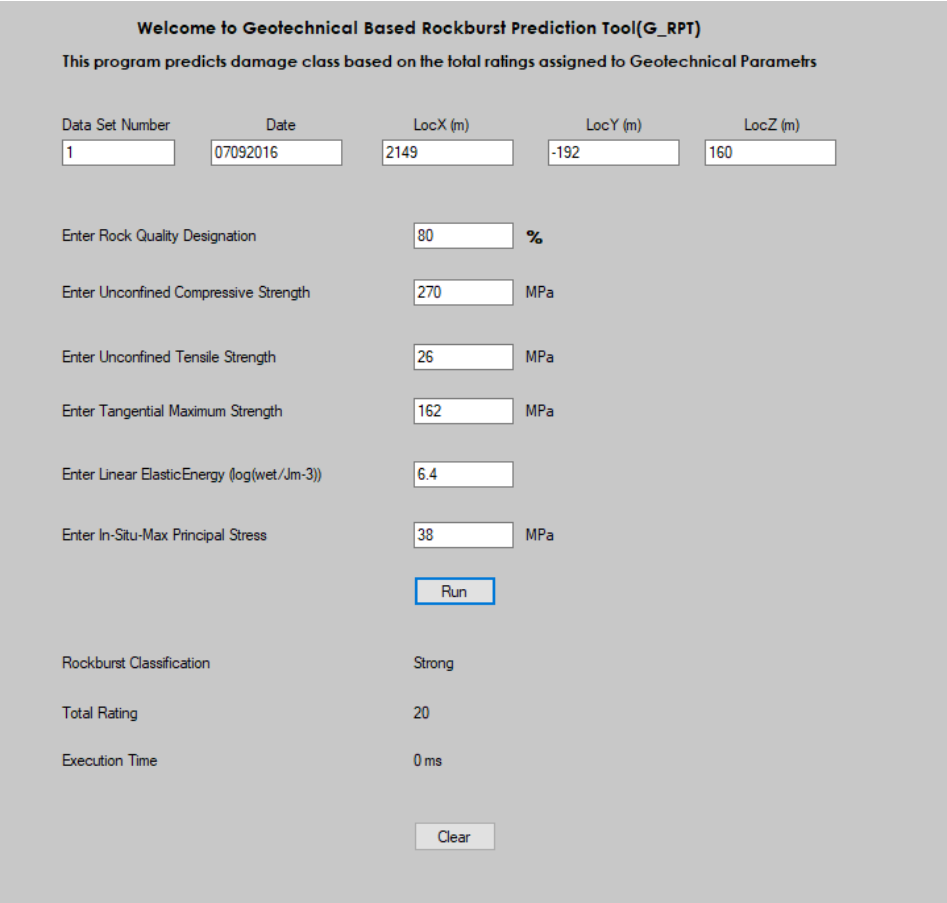

Figure 5:18: Rockburst damage classification results predicted using G_RPT

5.7.4.5 Error Handling and Validation

The user inputs were validated to ensure that only valid numeric values were entered. If invalid input were detected, a message box would display, indicating an error.

5.7.4.6 Execution Time Measurement

The Stopwatch class from the System Diagnostics namespace was used to measure the execution time of the prediction process. The execution time was then displayed in milliseconds on the interface.

5.7.4.7 Final Integration and Testing

The C++ rating calculation logic was integrated into the C# program by creating methods to calculate ratings for each parameter. The ratings were then summed to calculate the total rating. Predictions were made based on the total rating, and the result was displayed on the GUI.

5.7.4.8 Addition of a Clear Button

As an enhancement to the user experience, a "Clear" button was implemented. This button, when clicked, resets all input text boxes to an empty state, allowing users to input the next set of entries without manual deletion.

5.7.4.9 Validation of the Geotechnical based Predictive Rockburst Tool

To validate G_RPT, the author used 16 sets of geotechnical data from rockburst events at Mufulira Mine, chosen due to its proximity and similar geotechnical and geological characteristics to the Konkola Mine No.1 Shaft.

The details of the rockburst events included Event No., Event Date, Event Time, LocX (m), LocY (m), and LocZ (m) as shown in Table 5.22. Table 5.23 presents the geotechnical factors including RQD, σ_c, σ_t, σ_θ, Wet and σ_1 that were used to validate the G_RPT.

Table 5.22: Details of rockburst events used for validation of the G_RPT

Event No.	Event Date	Event Time	LocX (m)	LocY (m)	LocZ (m)
1	7-Oct-16	0:34	2149	-192	160
2	7-Oct-16	1:05	2200	-245	144
3	30-Aug-16	14:06	2269	-348	164
4	10-Sep-16	16:54	3050	-654	-49
5	10-Sep-16	16:54	3050	-654	-49
6	19-Sep-16	6:48	3378	-464	-51
7	19-Sep-16	10:53	3063	-569	4
8	13-Nov-16	19:33	3112	-418	-31
9	14-Nov-16	19:19	3104	-581	-36
10	28-Jan-17	3:50	2761	-676	-595
11	12-Jul-17	8:43	1496	-243	98
12	16-Jan-18	17:07	3270	-903	-715
13	25-Oct-19	5:20	2661	-312	-532
14	27-Oct-20	4:54	3085	-539	-279
15	21-Nov-22	0:51	3129	-511	-379
16	21-Nov-22	1:01	3051	-514	-169

Table 5.23: Geotechnical data used for validation of the G_RPT

Instance	RQD (%)	σ_c (MPa)	σ_t (MPa)	σ_Θ (MPa)	W_{et} (J/m3)	σ_1 (MPa)
1	80	270	26	162	6.4	38.0
2	80	250	24	150	6.3	38.4
3	80	250	23	150	6.3	32.6
4	80	283	24	170	6.4	38.4
5	80	247	24	148	6.3	38.4
6	80	267	25	160	6.3	38.4
7	80	247	24	148	6.3	38.4
8	80	263	25	158	6.3	38.9
9	80	252	24	151	6.3	38.4
10	80	255	25	153	6.3	38.9
11	80	260	25	156	6.3	38.9
12	80	256	24	154	6.3	38.9
13	80	247	23	148	6.3	39.3
14	80	268	24	161	6.3	39.8
15	80	267	25	160	6.3	40.2
16	80	251	25	151	6.3	40.2

The ranking was based on the sum of the ratings for each geotechnical parameter. The total ratings (TR) were then compared to the pre-determined rockburst class to predict the rockburst class, shown in Table 5.24.

Table 5.24: Geotechnical data used for validation and prediction of the rockburst class in G_RPT

Event	RQD (%)	σ_c (MPa)	σ_t (MPa)	σ_Θ (MPa)	W_{et} (J/m^3)	σ_1 (MPa)	Predicted Class
1	80	270	26	162	6.4	38.0	Strong
2	80	250	24	150	6.3	38.4	Moderate
3	80	250	23	150	6.3	32.6	Moderate
4	80	283	24	170	6.4	38.4	Strong
5	80	247	24	148	6.3	38.4	Moderate
6	80	267	25	160	6.3	38.4	Moderate
7	80	247	24	148	6.3	38.4	Moderate
8	80	263	25	158	6.3	38.9	Moderate
9	80	252	24	151	6.3	38.4	Moderate
10	80	255	25	153	6.3	38.9	Moderate
11	80	260	25	156	6.3	38.9	Moderate
12	80	256	24	154	6.3	38.9	Strong
13	80	247	23	148	6.3	39.3	Moderate
14	80	268	24	161	6.3	39.8	Moderate
15	80	267	25	160	6.3	40.2	Moderate
16	80	251	25	151	6.3	40.2	Moderate

Table 5.24 shows that the G_RPT predicted two strong and 13 rockburst instances respectively. The rockburst classes predicted were compared to the actual classes determined by geotechnical engineers at the Mufulira Mine. The actual rockburst classes for the 16 rockburst events are shown in Table 5.25.

Table 5.25: Validation results FOR the G_RPT

Event	RQD (%)	σ_c (MPa)	σ_t (MPa)	σ_Θ (MPa)	W_{et} (J/m^3)	σ_1 (MPa)	Predicted class	Actual
1	80	270	26	162	6.4	38.0	Strong	Strong
2	80	250	24	150	6.3	38.4	Moderate	Moderate
3	80	250	23	150	6.3	32.6	Moderate	Moderate
4	80	283	24	170	6.4	38.4	Strong	Moderate
5	80	247	24	148	6.3	38.4	Moderate	Moderate
6	80	267	25	160	6.3	38.4	Moderate	Moderate
7	80	247	24	148	6.3	38.4	Moderate	Moderate
8	80	263	25	158	6.3	38.9	Moderate	Moderate
9	80	252	24	151	6.3	38.4	Moderate	Moderate
10	80	255	25	153	6.3	38.9	Moderate	Moderate
11	80	260	25	156	6.3	38.9	Moderate	Moderate
12	80	256	24	154	6.3	38.9	Moderate	Strong
13	80	247	23	148	6.3	39.3	Moderate	Moderate
14	80	268	24	161	6.3	39.8	Moderate	Moderate
15	80	267	25	160	6.3	40.2	Moderate	Moderate
16	80	251	25	151	6.3	40.2	Moderate	Moderate

Table 5.25 shows that the G_RPT predicted 14 correct and two (2) incorrect rockburst damage classes respectively.

Given the predictions of the rockburst classes, the usefulness of the tool was verified using the prediction accuracy as an evaluation index. The accuracy was computed using Equation 5.13:

$$\text{Accuracy (100\%)} = 1 - \text{Error Rate} \tag{5.13}$$

Where:

$$\text{Error Rate} = \left| \frac{\text{Total number of True predictions} - \text{Total number of actual}}{\text{Total Number of actuals}} \right|$$

The number of actual rockburst events was 16, with 14 correctly predicted. Equation 5.2 were used to calculate 87.5 percent accuracy for the G_RPT.

5.8 Guidelines for obtaining the RPTs input parameters

The following information outlines several important G_RPT and MS_RPT input parameters, including location, date, their units of measure and the methods for obtaining them:

- The dataset number, location, and date show the dataset's identification number, where it was collected, and when it was measured.
- Rock quality designation (RQD) is measured in percentage. This parameter can be obtained through core logging or using empirical formulae;
- Uniaxial compressive strength (UCS) is measured in megapascals (MPa), this parameter can be obtained through rock core testing using either compressive or point load testing machines;
- Uniaxial tensile strength (UTS) measured in MPa); this parameter can be obtained through rock core testing using the Brazilian test index or estimated from UCS using the empirical formula cited in this thesis;
- Maximum tangential stress (MTS), measured in MPa, can be obtained through numerical modelling or the formula proposed by (Kirsch,1898) or estimated from UCS using the empirical formula cited in this thesis;
- Elastic strain energy or energy density (W_{et}) measured in joules per cubic meter (J/m^3). The input parameter in the G_RPT is logarithmic of $W_{et.}$ This parameter can be obtained through laboratory testing or estimated from UCS using the empirical formula cited in this thesis;
- Principal in situ major principal stress (σ_1) measured in MPa. This parameter can be obtained through in - situ stress measurements of the stress regime at a mine site or otherwise; and
- Microseismic monitoring systems provide measurements of seismic potency (P) in cubic metres (m^3), seismic energy (E) in Joules (J), and local magnitude (M_L). The input values in the MS_RPT are the magnitude of local magnitudes and the logarithmic values of E and P.

5.9 Summary

In this chapter, a method is presented for creating two rockburst predictive tools i.e., G_RPT and MS_RPT. The G_RPT utilise geotechnical and microseismic data respectively. When creating the tools, the aim was to make these tools easily accessible to field engineers, even with limited data. The development process involved selecting

relevant MS and geotechnical parameters, testing for correlations using R^2 Coefficient, categorising the parameters into three groups, and assigning ratings for each category.

The R^2 method may be subject to certain limitations such as not capable of measuring goodness of fit and predictive error. Further, it does not measure how one variable explains another that could influence the outcomes. Thus, it is advisable to perform sensitivity analysis to ascertain the critical parameters.

Next, the ratings for each parameter in a dataset were combined to determine the rockburst class based on the predetermined rockburst classes. The author developed a C++ computer program for each rockburst predictive tool. Using this program, engineers can predict rockbursts by comparing ratings to pre-determined classes.

The tools were validated using two datasets - geotechnical and MS from the Mufulira Mine, which has a history of rockbursts. The Mufulira Mine was chosen because it is geographically close to the Konkola Mine No.1 Shaft and uses the same MS system provided by the Institute of Mine Seismology (IMS). Additionally, both mines' geological and geotechnical settings are similar, further supporting the selection of the Mufulira Mine for data validation.

CHAPTER 6: RESULTS AND DISCUSSION

6.1 Introduction

In the previous chapter, the Author analysed the data from the case studies and Konkola Mine No.1 Shaft to identify the primary factors responsible for the rockburst. The significant contributing factors were established. This chapter will explore these factors in-depth, covering geological, geotechnical, microseismic, and mining aspects. The appropriate parameters or indices to use in the model development will be selected. Finally, a discussion summary will be presented to conclude the chapter.

6.2 Geological Factors

The geological factors that will be discussed include orebody dip, RQD, rock types affected by rockburst events, and geological structures within the areas affected by rockburst.

6.2.1 Orebody Dip

Amongst the seventeen case studies reviewed, eight showed an orebody dip from 61 to 85^0, while six exhibited a dip ranging from 10^0 to 35^0. The remaining three mines had a dip from 36^0 to 60^0. The case studies revealed that the orebody dip ranged from 61^0 to 85^0. Similarly, the analysis indicated that the orebody dip at Konkola Mine No.1 Shaft ranged from 50^0 to 70^0. The findings suggest that mines at a greater risk of rockburst typically have an orebody dip of 50^0 to 85^0, which aligns with Hoek and Brown (1980). They noted that when mining in an inclined orebody (without a specific dip attached to the orebody), the stress field acting upon the excavations and pillars between them is no longer parallel to and normal to the excavation boundaries. This inclination of the stress field may lead to significant stress due to stress superposition, causing instability in the excavation, resulting in a higher induced stress magnitude than the strength of the rock at an excavation boundary, leading to rockmass brittle failure.

6.2.2 RQD

The RQD refers to the percentage of core pieces that are longer than 100 mm and remain intact in the drilled core's overall length. The index is useful in predicting rockbursts (Tang, 2000). It reflects the rock's ability to store energy and its integration, which also indicates the tendency of rockbursts (Cai, 2016). A higher RQD value indicates stronger rock integration and a greater likelihood of rockbursts. According to Wang and Park (2001), the probability of rockbursts increases as the RQD index increases. For the

Konkola Mine No.1 Shaft, the RQD of the rocks affected by rockbursts ranged from 60 to 88 percent. Tajduś et al., (1997) suggested an RQD of 50 to 75 percent indicated a moderate risk of violent rupture. Therefore, the RQD is considered a significant indicator of rockbursts.

6.2.3 Rock Types Affected by Rockburst Events

The analysis of 17 case studies showed that 11 cases were associated with igneous rocks, while three cases were related to metamorphic rocks. One and two cases were related to meta-igneous and metasedimentary rocks, respectively. The finding indicates that igneous and metamorphic rocks are more likely to experience rockbursts than other types of rocks. Obert and Duvall (1967) also confirmed this finding in their investigations, stating that igneous and metamorphic rocks are more prone to rockburst potential than other types. According to Jaeger et al., (2007), rock lithology significantly contributes to determining the rockburst potential because the mechanical behaviour of rocks or rock masses primarily depends on their basic composition structure. Furthermore, factors such as mineral composition, grain size and angularity, grain packing patterns and the nature of cementing materials between grains all influence how fracture initiates and propagates (Brady and Brown, 2005). In general, igneous, and metamorphic rocks have a higher potential for a rock burst than sedimentary rocks.

The Author analysed the rock units impacted by the rockbursts; the study's findings showed that the rock types affected by rockburst were FWQ, AGSST, PC, FWS, OS, HWQ, and HWA. The results highlighted that OS accounted for 30 percent of all rockburst events, FWSS for 20 percent, AGSS and PC each for 15 percent, and FWQ and HWQ each for 5 percent. These findings imply that most rockbursts occur in the ore shale, a sedimentary rock unit during the development and stoping phases. The stress migrates to nearby rock units via the pillars to the abutments and the 'A' unit. Because the 'A' unit is competent, the stresses can be transferred to the nearby lithological units. The rock units were less affected, i.e., FWQ and HWQ, far away from the ore shale or stopping. Thus, a rockburst will probably occur in excavations mined close to the ore shale or stopes. However, the rockburst events are associated with some rock units.

6.2.4 Geological Structures within the Areas Affected by Rockburst

The distribution of major geological structures was analysed for the 17 rockburst cases. The analysis showed that 47 percent of the geological structures were for faults, 29 percent were for intrusions that included dykes, and six percent each for dense joints,

folds, and shear zones. Thus, geological structures, particularly faults and intrusions, are among the most significant rockburst-controlling factors. Geological structures significantly influence rockburst occurrence, and deep excavations in mining are more prone to rockburst when they approach any structural plane (Morissette et al., 2014; Haile, 1999; Durrheim et al., 1998a; Hedley, 1992). Stresses are usually concentrated near geological structures. When the excavation approaches the structure, the stresses overcome the normal stress, causing an unclamping of the structural plane, resulting in an enormous amount of energy released due to the shear slip along the structure plane. Dykes form potential seepage paths and zones of low stiffness and shear strength where movements are concentrated (Brady and Brown, 2005). Because of their high stiffnesses, unweathered dyke rocks can develop high stresses and so be susceptible to stress-induced failure or, as in the deep-level gold Mines of South Africa, be associated with rockburst conditions.

The Author used a geological compass to spot-map major discontinuity planes on mining levels (2825L, 2900L, 3095L, and 3150L) affected by rockbursts. Mapping was impossible at the actual rockburst sites due to ground falls and poor ventilation. Nine sites were chosen near the affected areas, including Trough Drives, Draw Point Crosscuts, and Extraction Drives; the lower hemispherical of an equal-angle projection showed three discontinuity sets. The bedding plane had a dip/dip direction of $38^0/228^0$, and two joint sets had dip/dip directions of $77^0/063^0$ and $49^0/061^0$. Geological structures show weak zones or planes of weakness along which the rockmass slips and fails, and their failure mechanism is often structurally controlled in a low-stress setting. The intact rocks may fracture in a high-stress environment, and the failure mechanism is stress driven. This finding implies that the geological structures are among the contributing factors to rockbursts. However, in a strict sense, the geological structures may not be one of the rockburst indicators. The role of the rock fracture in the rock bursting process is to facilitate the dissipation of the total potential energy, which comprises the seismic energy input to the burst rock and the potential strain energy stored in the rock before bursting (Li et al., 2022).

The rockburst events and fault planes for the Konkola Mine were plotted using Leapfrog 3d modelling software to show the positions of the planes for the rockburst event's locality. The analysis established that the zone affected by the rockbursts is bounded by one major fault zone, the Luansobe on the south and the secondary fault zones to the

north. The findings indicate that the rockburst events are enveloped between the fault zones. The area is linked to high stress because of the tectonic forces involved in this region. There were no rockburst events beyond the extremes of the fault zones.

To some extent, the fault zones act as the stress release valves and because the material composing the faults is leached and weak with low friction strength; the zones are low stress and, therefore, no accumulation of strain energy that can cause rockburst events. However, the fault planes, once activated, can cause the release of substantial energy. This finding implies that fault zones are among the factors contributing to the rockburst potential.

6.3 Geotechnical Factors

The geotechnical factors that will be discussed include Poisson's ratio, the ratio of σ_1 to σ_3 unconfined compressive strength, unconfined compressive strength data for unit a, unconfined tensile strength results, the ratio of unconfined compressive stress to unconfined tensile strength, maximum tangential stress, Elastic modulus, and in situ principal stress magnitudes.

6.3.1 Poisson's Ratio

The analysis of the case histories revealed that rocks prone to rockburst have a Poisson ratio of 0.22 to 0.27. This finding is consistent with Belyadi's (2019) study of rock mechanical properties and in-stresses, which found that rocks with a low Poisson ratio, between 0.1 and 0.25, are more susceptible to easy fracturing. A high Poisson ratio, between 0.35 between 0.45, shows that rocks are more difficult to crack. Nussbaumer (2000), in his comprehensive review of rockbursts, analysed the mechanical properties of 16 different rocks from research in South Africa by Hill and Denkhaus (1961) and the values obtained for the "relative violence of rupture" test. He found no evidence to suggest a correlation between Poisson's ratio and the "relative violence of rupture."

6.3.2 Ratio of σ_1 to σ_3 results

The author examined the ratios between the principal stress (σ_1) and the minor principal stress (σ_3) for the 17 cases. Out of those 17, 10 had a ratio between 1.2 and 2. One case had a ratio of 2 to 2.8, while the third case had a ratio of 2.8 to 3.6. The analysis revealed that the typical ratio of σ_1 to σ_3 in rockburst falls within the range of 1.2 to 3.6. This finding highlights the importance of higher values of ratios of σ_1 to σ_3 as a predictor of rockburst potential.

6.3.3 Unconfined Compressive Strength Results

Based on the 14 case studies reviewed, six cases had an unconfined compressive strength (UCS) of 133 to 179 MPa, while four cases had a UCS of 272 to 318 MPa. Four cases had a UCS of 179 to 272 MPa. These findings suggest that rocks affected by rockbursts typically have a UCS of at least 133 MPa. Obert and Duvall's (1967) research further supports this, as they found that rocks affected by rockbursts have a UCS between 100 to 400 MPa. In a comprehensive review of rockbursts, Nussbaumer (2000) analysed the mechanical properties of 16 different rocks from research conducted in South Africa by Hill and Denkhaus (1961), specifically examining the values obtained from the "relative violence of rupture" test. He found a strong linear correlation ($R^2 = 0.89$) between the UCS and the likelihood of burst-prone existence. Rocks with high UCS are prone to violent bursting.

The analysis of the UCS for the NX 50 mm rock core samples showed that the rocks affected by rockbursts at the Konkola Mine No.1 Shaft had a UCS of 74 to 330 MPa. The finding agrees partially with previous studies, which show that a UCS of the rocks must be above 133 MPa for the rockburst to occur. For example, investigations by Obert and Duvall (1967) suggested that rocks usually have UCS of 100 MPa to 400 MPa. Nussbaumer (2000) comprehensively reviewed rockbursts and analysed the mechanical properties of 16 different rocks from research in South Africa by Hill and Denkhaus (1961), finding a strong linear relationship ($R^2 = 0.89$) between UCS and the likelihood of being burst-prone. Rocks with high UCS are extremely prone to bursting and will do so violently. This finding highlights the importance of UCS as a predictor of rockburst potential.

6.3.4 Unconfined Compressive Strength Results for Unit A

Konkola Mine No.1 Shaft contains five layers of ore shale; each designated as A, B, C, D, and E, with varying thicknesses. The lowest and weakest layer is Unit A, which has a thickness between 0.5 and 1.2 m that can increase with the steepening of the dip. This layer is finely bedded and often weathered to brown micaceous clay. The logging data from deep surface boreholes indicate that the unit has a medium to high strength, with a measured UCS between 74 and 112 MPa. While most areas of the mine have weak and unconsolidated Unit A that act as a "stress relief valve," there are exceptions. Specifically, between 34500 mN and 3600 mN, Unit A becomes stronger, allowing for transferring stresses from the hanging wall to the footwall via ore pillars and remnants.

Seismicity is expected to be more common as the mine develops deeper, particularly in this area.

Although Unit A contributes to the potential rockburst by the transferring stresses from the hanging wall to the footwall via ore pillars and remnants.

6.3.5 Unconfined Tensile Strength Results

The strength of rock under tension, known as unconfined tensile strength (UTS), plays a crucial role in assessing the likelihood of rockbursts. This parameter has been utilised in various rockburst prediction criteria, as evidenced by research on the stress method of rockburst predictions (Qiao and Tian, 1998; Altindag, 2003; Chen et al., 2013). UTS is also important in determining the rock brittleness coefficient, which is the ratio of UCS to the confined tensile strength of intact rock (Qiao and Tian, 1998).

Rock's unconfined tensile strength (UTS) is the pulling force required to rupture a rock sample, divided by the sample's cross-sectional area. The UTS of rock is minimal and is 0.1 times the compressive strength (Bernt and Looyeh, 2019). The UTS were estimated for the rock core samples. The analysis of the UTS revealed that the rocks affected by rockbursts at the Konkola Mine No.1 Shaft had a UTS of 6.5 to 30.5 MPa.

6.3.6 Ratio of UCS to UTS Results

Seventeen cases were analysed for UCS/UTS ratios. Thirteen instances had the ratio of UCS to UTS between seven and 14, four cases had a ratio of 10 to 12 and one had a ratio of 14 to 16. This analysis suggests that the ratio of UCS to UTS for rockburst occurrence ranges from 10 to 16, which supports previous research on the topic. The rock brittleness coefficient, the ratio of UCS to the tensile strength of intact rock, is often used to show rockburst susceptibility. Studies by Qiao and Tian (1998), Altindag (2003), and Chen et al., (2013) have shown that this factor significantly contributes to rockburst. Rockburst intensity is described by the brittleness coefficient (BI). A BI of 40 or greater indicates no rockburst, 26.7 to 40 is weak, 14.5 to 26.7 is moderate, and below 14.5 is strong (Wang and Park, 2001). Chen et al., (2013) suggest that commonly used BI values range between 10 and 30.

6.3.7 Maximum Tangential Stress Results

The values of the maximum tangential stress (MTS) were calculated for the rock core samples. The study found that the MTS for the rock core samples impacted by rockbursts at the Konkola Mine No.1 Shaft ranged from 37 to 165 MPa. While the MTS evaluated

for the case studies ranged from 60 to 168 MPa. The findings indicated that rockburst typically occurs when maximum tangent stresses range from 60 to 168 MPa.

The tangential stress is important for assessing the rockburst potential because the rock mass's failure around the excavation's periphery depends on the tangent stress's magnitude. The tangential stress is elevated in the contour of the rock opening after excavation; the rock then fails when the tangential stress exceeds the strength of the rock (Li et al., 2022).

Kirsch (1898) used the closed-form solutions for stress and displacement distributions around the circular opening in a biaxial stress field. The surface was traction free; the only non-zero stress component was the circumferential component. The maximum and minimum boundary stresses occurred in the excavation's sidewall ($\theta = 0$) and crown ($\theta = \pi/2$). The maximum Tangential stress was three times the far field stress component.

The tangential stress is one of the critical parameters that can assess rockburst potential. This study considers the tangential stress a rockburst indicator.

6.3.8 Elastic Modulus Results

The Elastic modulus (E_m) is a mechanical rock property which measures the stiffness of an elastic material, defined as the ratio of stress to strain (Ma et al., 2016). Rocks with low E_m tend to be ductile, and rocks with high E_m tend to be brittle. In most research (Hudson and Harrison, 1997), the elastic property is best studied through the complete stress-strain curve for a rock sample being compressed in one direction, i.e., in uniaxial compression.

After analysing 17 case studies, it was discovered that six had an E_m range of 35.7 to 72.5 GPa, and two had a range of 72.5 to 107.5 GPa. These findings indicate that rocks prone to rock bursts typically have an elastic modulus range of 37.5 to 107.5 GPa, which is in line with the research conducted by Obert and Duvall in 1967. Their study suggested that rocks affected by rockburst generally have an elastic modulus range of 40 to 90 GPa.

The E_m for the rock core samples was calculated, and the results showed that out of the 76 values, 62 fell between 36.8 to 49.5 GPa, while 14 had E_m between 62.2 to 75 GPa. This analysis suggests that the rocks prone to rockbursts at Konkola Mine No.1 Shaft have an E_m range of 36.8 to 75 GPa. These findings align with Obert and Duvall's (1967) research, which found that rockbursts occur when the rock's elasticity modulus falls between 40 and 90 GPa. E_m value is one significant factor contributing to the potential

for rockburst. When this value is combined with UCS, it creates an index that can be used to calculate the strain energy. This energy level is useful in evaluating the likelihood of a rockburst potential.

6.3.9 In-Situ Principal Stress Magnitudes Results

The study found that the principal stress field (σ_V) for areas affected by rockburst at Konkola Mine No.1 Shaft were in a range of 19.5 to 32.1 MPa, while the intermediate principal stress (σ_H) range of 16.7 to 27.5 MPa, and the minor principal stress(σ_h) were between 11.8 and 19.4 MPa. The directional orientations of the σ_V were found at $51^0/121^0$ in the NW–SE direction, the σ_H was at $17^0/009^0$ in the NE-SW direction, and the σ_h was identified at $34^0/267^0$ in the SW–NE direction.

The Trough and Extraction drives run in a SE-NW direction, parallel to the main stress and perpendicular to the intermediate and minor stresses. When the minor principal stress surpasses the rock's tensile strength surrounding the drives, the adjacent rock in the excavation boundary is expected to fail. The Draw point crosscuts are perpendicular to the principal stress and aligned with the intermediate and minor stresses. The rock adjacent to the excavation boundary in the crosscuts is expected to fail when the principal stress field exceeds the compressive strength of the rock mass surrounding the crosscut.

6.3.10 Linear Elastic Energy Results

Based on the analysis, the logarithmic values of W_{et}/Jm^{-3} ranged from 5.1 to 6.4. The log (W_{et} /Jm^{-3}) values calculated indicate that rocks prone to rockbursts at Konkola Mine No.1 Shaft have a log (W_{et} /Jm^{-3}) range of 5.1 to 6.4. This is consistent with the finding by Wang and Park, (2001) that log (W_{et} /Jm^{-3}) should be greater than 4.7 for rockburst to occur, with a log (W_{et}/Jm^{-3}) of greater than 5.1 indicating severe rockburst. Therefore, W_{et} is considered as one of the significant factors for predicting rockburst intensity.

6.4 Microseismic Factor

The microseismic factors that will be discussed include events dates, events times, and the number of rockbursts, local magnitude (M_L), and zone affected by the rockbursts, seismic potency (P/m^3), seismic energy (E/J) and E_S_E_P ratios.

6.4.1 Events Times and the Number of Rockbursts

The author collected data on rockburst events at Konkola Mine No. 1 Shaft between 1995 and 2020 from the Konkola seismological database for this study. The data included the time of the events and the number of rockbursts that occurred. The mine had two blasting

schedules: one from 5:30 am to 6:00 am and another from 5:00 pm to 6:00 pm. The Author analysed the event times and the corresponding number of rockbursts and found that most rockburst incidents occurred between 6:01 am to 4:59 pm and 6:01 pm to midnight. The analysis also revealed a significant increase in rockburst occurrences immediately following the blasting times. The study found that blasting triggers most rockburst incidents at the mine. Blasting releases high energy due to gas pressure, increasing the likelihood of a rockburst. As a precaution, it is important to avoid entering burst-prone areas immediately after a blast and follow the re-entry period strictly, as areas may still be active, and rockburst risks may be high. Overall, blasting and event times are not reliable indicators of rockbursts. Blasting adds energy in form of seismic pulse to the already highly stressed rock mass, increasing the potential for rockburst incidents.

6.4.2 Local Magnitude (M_L)

The local magnitude (M_L) ranges on the Richter scale were analysed for 17 mines with rockbursts. The analysis revealed that six mines had an M_L from 0.5 to 1.5, 3 from 1.6 to 2.5, and 8 from 2.6 to 3.5. Therefore, the mines affected by rockbursts have a probable M_L range from 0.5 to 3.5. This finding aligns with Ortlepp and Stacey's (1994) investigations, which suggest that rockbursts related to seismic events, can occur at a broad range of M_L, typically from undetectable to five.

This study analysed the M_L based on the Richter scale of 40 rockburst events at Konkola Mine No.1 Shaft. The study found that most of these events fell within the scale range of 0.5 to 2.5 with the most frequent range being between 1.3 and 1.8. The analysis suggests that for the rockburst to occur, the M_L should in the range of 0.5 to 2.5. This correlation between local magnitude and the occurrence of rockburst events suggests that M_L can be considered a significant indicator of potential rockbursts. It can predict the likelihood of such an event occurring.

6.4.3 Seismic Potency (P/m^3)

Seismic potency measures the rock mass deformation during a seismic event at the source (King, 1978; Ben-Menahem and Singh, 1981). According to Drover and Villaescusa (2019), seismic potency may measure rock mass damage during any violent instability driven by the quasi-static mining-induced stress. Seismic potency is a precursor to rockburst, where the rock mass must undergo inelastic deformation. For the Konkola Mine No.1 Shaft, research has shown that a log (P/m^3) range of 0.3 to 2.2 is necessary

for a rockburst event. This finding shows that seismic potency is a significant factor for rockburst because of the co-seismic inelastic deformation at the source.

6.4.4 Seismic Energy (E/J)

The Author analysed 40 rockburst events and found that the Log (E/J) value ranged from 2.2 to 9.0 for each event. This study showed that for a rockburst to occur, a sufficient amount of radiated energy must be released, typically ranging from 10^2 to 10^9 Joules. This study's findings match Chen et al., (2013), and Spottiswoode and McGarr (1975), who found that radiated energy is essential in rockburst occurrence and intensity. Log (E/J) is another important parameter used to evaluate the potential for rockburst. When combined with other indicators, Log (E/J) can predict the likelihood of a rockburst event.

6.4.5 E_S_E_P ratios

An analysis of rockburst events for 17 case histories showed that 37 percent of these events were due to pillar bursts, 34 percent were due to strain bursts, and only two percent were due to fault slips. This indicates that pillar and strain bursts are more common source failure mechanisms of rockbursts than fault slips. Pillar failure is caused by the high stress that pillars are subjected to from mining activities such as drilling and blasting in underground mining (Hedley, 1992). This stress weakens the pillars and causes them to fail. Strain bursts are also caused by high stress on the rock mass. The source failure mechanism was not found to be a contributing factor in this study.

The analysed E_S_E_P ratios for Konkola Mine No.1 Shaft from 1995 to 2020 for the 40 rockburst events showed that 31 rockbursts had the E_S_E_P ratios from 0.7 to 9.8, six had the ratios in the range of 9.8 to 18.8, two events had the ratios in the range of 18.8 to 27.9 and one event had the ratios in the range of 27.9 to 36.9. The analysis reveals that the E_S_E_P ratios for the rockburst event were the range of 0.7 to 36.9.

Results showed that 78 percent of the ratios were below ten, while 22 percent were above ten. These findings were consistent with earlier studies conducted at mines in Germany and Canada (Gibowicz and Kijko, 1994; Urbancic and Young, 1993). The ratios combined tensile and shear failure mechanisms typically found in Mines. When the E_S_E_P ratio is less than ten, volumetric deformation occurs, and when it is greater than 10, pure shear occurs (Hudyma & Potvin, 2010; Boatwright and Fletcher, 1984). The Konkola Mine No.1 Shaft has tensile and pure shear mechanisms, supported by the M_L ranging from 0.5 to 2.2 and indicating strain bursting, buckling, and face crush, per Ortlepp and Stacey's (1994) research findings. Brake and Hedley (2003) state that strain

bursts are common in rockburst-prone mines during drilling. They occur when the rock ahead of the advancing face or heading cannot adjust to an immediate stress increase caused by the blast, resulting in small-scale failures along a geological structure such as a joint. Although E_S_E_P ratios can aid in understanding failure mechanisms, they cannot predict the potential for rockburst.

6.4.6 Zone Affected by the Rockbursts

Rockburst events were plotted on mine plans using Leapfrog Geo software. The Author plotted the events and surveyed excavations using Surpac mining software. The area affected by rockbursts was between 34500 mN and 35500 mN, 6000 mE and 7000 mE east - west, and 760 m to 0 m above sea level. Further zone analysis showed that the events had a discernible pattern defining the clusters. Rockburst events do not occur chaotically but follow a specific pattern. Thus, understanding and interpreting the pattern can aid in forecasting the rockburst potential. This discovery is important because it highlights the need for caution when mining in this area.

6.5 Mining Factor

The mining factors discussed include production rate, mining method, threshold burial depth and the horizontal hypocentral distances from the ore shale/ stopes to the footwall excavations and ground support.

6.5.1 Production Rate

Figure 4.61 shows that the Mine's production rate was consistent at around 1 million tonnes from 1996/97 to 1998/99. However, during this period, there was an increase in rockburst events, from one in 1995/96 to three in 1998/99. In 200/01 year, the production rate drastically reduced to about 500,000 tonnes, with a corresponding decrease in rockburst events from three to one. From 2001/02 to 2002/03, there was a gradual increase in production rates, accompanied by a drastic increase in the rockburst events to 23. From 2002/03 to 2021/22, there was a gradual decrease in both the production rate and the rockburst events. The correlation between production rates and rockburst events is evident, with increased production leading to a higher occurrence of rockbursts.

Lenhardt (1992) also found a linear relationship between production and the number of events ($M_L > 0$) at the Carbon Leader reef, East Driefontein Mine, Witwatersrand. The correlation was attributed to the amount of mining representing the stress change that ultimately leads to instability.

6.5.2 Mining Method

The potential for rockbursts can vary depending on the mining method used. For the 17 case studies, the analysis showed that open stoping accounted for 53 percent of the mining methods, while cut and fill accounted for 17 percent. Based on the analysis results, the open stoping and cut and Fill mining methods are more likely to have a higher risk of rockbursts than other mining methods, such as panel mining, reef mining, bottom stopping, and shrinkage methods.

The open stoping mining method has been dominant at Konkola Mine No.1 Shaft from 1995 to 2020, with large voids created due to the stopes needing to be backfilled. This mining method has specific characteristics, including leaving stopes unfilled with backfill or waste rocks and allowing rib and crown pillars with low safety factors to crush on their own, following ore extraction. As a result, there is a significant risk of stress concentration and migration towards unmined or solid areas nearby. Stress concentration and migration are the main reasons for rockbursts in the literature review, attributed to the unfilled voids/gobs (Tian and Yao, 2009; Liu and Feng, 2018).

6.5.3 Threshold burial depth

Out of the 17 examined Mines, only seven had sufficient data on the burial depth for the initial rockburst. Four mines reached the threshold depth between 1000 m and 1167 m. One mine reached a critical depth of 1168 m and 1333 m below the surface, and two mines began experiencing rockbursts when they reached a mining depth of 1334 m and 1500 m. The analysis suggests that mining depths between 1000 m and 1300 m below the surface are considered threshold depths since most mines start experiencing rockbursts at these depths due to increase in the induced stresses. These findings are consistent with other studies that indicate the probability of rockbursts increases as the mine's depth increases. Peng et al. (2021) found that rockburst and spalling in a deep hard rock mine began at 745 m, and rockburst and large-area collapses began at a depth of 980 m. However, some mines have reported rockbursts occurring at a burial depth approximately 500 m below the surface, such as the Zhazixi Antimony Mine in China (Ma et al., 2018). Investigations by Ma et al., 2018 showed that the rockburst in the transport roadway occurred when mining depth was −115 m level where the surrounding rocks were relatively intact sandstone and slate with many endogenetic cracks. The initial stress equilibrium state of surrounding rock was disturbed after excavation. Furthermore, the tangential stress increased sharply, and the radial stress decreased, and

tensile cracks extension was accelerated on the surface of roadway, resulting in multilayer lamellar spalling at the spandrel.

The Erdaogou gold Mine in China also recorded rockbursts at a depth of 400 m due to the large gobs created by the open stope method. As the underground mining advances to greater depths, i.e., greater than 900 m, the stresses in the rock mass increase. Consequently, induced seismicity usually increases with the potential to result in a rockburst. These findings thereby confirm that that rockburst activity is influenced by factors other than just depth below the surface. Burial depth is a contributing factor towards rockburst occurrence since the stresses in the rock mass increase as underground mining advances to greater depths, resulting in induced seismicity and potential for rockburst.

For Konkola Mine No.1 Shaft, the critical burial depth was found at 950 m below surface.

6.5.4 Hypocentral Distances from the Ore Shale/ Stopes to the footwall side

This study measured the distance between the ore shale/stopes and the location of rockburst events. The analysis revealed that at the Konkola Mine No.1 Shaft, the hypocentral distances ranged from zero to 159 m from the stopes. The excavations within 53 m from the stopes were most affected by rockburst events, while excavations beyond 159 m from the stope face were the least affected. This finding strongly suggests that rockbursts at the mine are caused by stress redistribution and migration to nearby areas, strongly linked to stoping. Most of the event hypocenters were observed to fall within the zone where the changes in stress were substantial due to mining in the vicinity. The risk of rockbursts is higher in excavations close to the stope faces.

6.5.5 Ground support and Rockburst

The Author reviewed ground support and reinforcement measures to mitigate rockbursts for 17 case histories. The review revealed three categories of support - backfilling of stopes, dynamic and energy-absorbing support, and design optimisation. The analysis showed that dynamic and energy-absorbing methods accounted for 21 percent of the ground support, followed by design optimisation at 14 percent and backfilling support at 12 percent. The analysis demonstrated that the dynamic/ energy absorbing ground support methods are most effective and widely used methods to mitigate rockburst.

The Author collected data on ground support installed and the number of rockburst events in the affected area at Konkola Mine No.1 Shaft. The analysis showed that eleven

rockburst events occurred in the areas with no support installed, nine events occurred in the areas supported only with Rockbolts, eight events in the areas supported with Rockbolts and wiremesh, seven events occurred in the areas supported with Rockbolts, wiremesh and tendon straps, four events occurred in the areas supported with Rockbolts, wiremesh, Tendon straps and cablebolts and one event occurred in the areas supported with splitsets, weld mesh and cablebolts.

The study found that areas without support had the most rockburst events (11), while those with split sets, weld mesh, and cablebolts only had one event. This suggests that areas with no support are more prone to rockbursts, and the absence of support in burst-prone areas could increase the potential for rockbursts.

6.6 Development and Validation of Rockburst Predictive Tools

Two predictive tools for rockburst (RPTs) were developed, one based on the MS system and the other on geotechnical factors. The geotechnical aspects included RQD in percentage, σ_θ (MPa), σ_c (MPa), σ_t (MPa), log (W_{et}/Jm^{-3}) and σ_1 (MPa). The MS factors were the M_L, the log (P/m^3), and log (E/J).

Two datasets from the Mufulira Mine were utilised to verify the RPTs. The RPTs were evaluated on 16 cases from each dataset, and the study found that the MS data-based RPT had a prediction accuracy of 94 percent, while the geotechnical factor-based RPT had an accuracy of 87.5 percent. RPTs can reasonably predict rockbursts.

The selection of input parameters for the RPTs was left to the Author's discretion, given the lack of universal guidelines in this regard. Regression analysis was employed in Excel to identify and test the correlations among the parameters. It was found that the correlations among the factors had the determination coefficients, R^2 of greater 0.5. However, this method may be subject to certain limitations that could influence the outcomes. Thus, it is advisable to perform sensitivity analysis to ascertain the critical parameters. The RPTs were verified using only 16 rockburst events from Mufulira Mine, which could have affected the accuracy and validation of the RPTs. Therefore, more MS and geotechnical data should be tested to enhance the accuracy of RPTs.

The establishment of a standardised classification system for rockbursts is of utmost importance due to the likelihood of varying methods of assessment employed by different researchers. The categories utilised in RPTs may diverge among mines, potentially

affecting the efficiency and reliability of the RPTs. Thus, it is imperative that researchers reach a consensus on a universal classification system.

The graphical user interfaces (GUIs) had some limitations, including inability to import all the parameters at once. Hence, each set of parameters was computed per run. However, the computing time or speed was found to be fast with the results being obtained in milliseconds.

6.7 Summary

The discussion has highlighted that multiple contributing factors must combine for a rockburst to occur. Therefore, a rockburst is a complex phenomenon requiring multiple factors. This means that no single factor can predict the potential for a rockburst. Four factors were identified as controlling rockburst: geotechnical, geology, microseismicity, and mining.

There is no consensus on the critical parameters needed for predicting rockburst potential; previous studies cite the utilization of different factors.

The current study explored the development of rockburst prediction tools (RPTs) based on specifically geotechnical and MS factors. Geotechnical factors include Elastic modulus, tangential stress, compressive stress, tensile strength, and principal stress, while MS factors include local magnitude, seismic potency, and energy release. Two predictive tools were developed, one based on MS and the other on geotechnical factors. The study found that the MS data-based RPT had a 94 percent prediction accuracy, while the geotechnical factor-based RPT had an 87.5 percent accuracy. The GUIs had some limitations of not able to import all the parameters at once. Hence, each set of parameters was computed per run. However, the computing time or speed was found to be fast with the results being obtained in milliseconds.

CHAPTER 7: CONCLUSIONS AND RECOMMENDATIONS

7.1 Introduction

Chapter 7 provides a summary of the research study's findings, including its conclusion, limitations and recommendations for future research. Additionally, the chapter highlights the significant contributions of the study to the field of Mining engineering.

7.2 Conclusions

The current research aimed to develop tools for predicting the potential for rockburst using MS and geotechnical data. The specific objectives of this study were to:

- To review and compile the global factors or conditions that cause rockburst;
- To determine the site-specific rockburst indicators at Konkola Mine No. 1 Shaft;
- To develop the tools that can be used to predict rockburst potential based on the determined rockburst indicators; and
- To validate the predictive tools on rockburst data from other mines.

The study conducted by the author involved analysing case studies of rockburst incidents in other mines. The study identified four potential contributing factors to rockburst: microseismicity (MS), geological properties, geotechnical factors, and mining methods. According to the study, mining methods such as open stoping and cut and fill were found to have a higher likelihood of causing rockburst than methods like panel mining, reef mining, bottom stoping, and shrinkage methods. Additionally, the study highlighted that geological structures like faults, dykes, intrusions, foliations, dense joints, folds, and shear zones play a significant role in rockburst incidents. The study also found that mines with an orebody dip of 61^0 to 85^0 are at a higher risk of experiencing rockbursts. The study also revealed that most rockbursts occurred in mines at a threshold depth of between 1000 m and 1300 m, with pillar and strain bursts being more common than fault slips.

The study classified potential contributing factors of rockburst at the Konkola Mine No.1 shaft as MS, geotechnical, geology and mining. The geotechnical indicators were unconfined compressive strength (σ_c), rock quality designation (RQD), unconfined tensile strength (σ_t), tangential stress (σ_θ), principal in-situ stress (σ_1), and linear elastic energy (W_{et}). The microseismic (MS) factors included the local magnitude (M_L), seismic energy (logE/J), seismic potency (logP), E_S_E_P energy ratios, and epicentral distance (measured in meters) from the stope.

After analysing the event times and the number of rockbursts, the study found a significant increase in rockburst occurrences immediately following blasting times. The study found that blasting is the main trigger for rockburst incidents at the Konkola Mine No.1 Shaft.

Most areas of the mine have weak and unconsolidated rock Unit A, which acts as a "stress relief valve." However, between 34500 mN and 3600 mN, Unit A becomes stronger, allowing for transferring stresses from the hanging wall to the footwall via ore pillars and remnants. As the Mine develops deeper, microseismicity, and particularly rockburst, is expected to be more common, especially between 34500 mN and 3600 mN.

The analysis of the hypocentral distances from the stope towards the footwall side revealed that at Konkola Mine No.1 Shaft, the hypocentral distances ranged from zero to 53 m from the stopes. Excavations within 53 m from the stopes were most affected by rockburst events, while excavations beyond 148 m from the stope face were the least affected. This finding suggests that rockbursts at the Mine are caused by stress redistribution and migration to nearby areas, strongly linked to stoping.

Using Surpac and Leapfrog Geo 3D modelling software packages, the study also found that the rockburst events at the Mine were localised to a specific area and occurred in four distinct groups or clusters. The clusters were confined to the Luansobe fault zone on the southern boundary and secondary fault zones on the northern boundary. Rockburst patterns were confined by fault zones in the south and north, and certain rock types, such as AGSST, PC, FWS, and OS, were more susceptible to rockbursts. The study identified a correlation between production rate and rockburst occurrence. A lower production rate of 500,000 tonnes resulted in fewer rockburst incidents, while a higher production rate of 1 million tonnes led to more rockburst.

Predicting rockbursts can be challenging since they involve multiple contributing factors, making them a complex occurrence that cannot be predicted with just one factor. The Author developed two predictive tools for rockburst (RPTs), involving multiple contributing factors, one based on the MS system and the other on geotechnical factors. The geotechnical aspects included RQD (in percentage), σ_θ (MPa), σ_c (MPa), σ_t (MPa), Log (W_{et}/Jm^{-3}) and σ_1 (MPa). The MS significant factors were the M_L, the Log (P/m^3), and Log (E/J).

The Author utilised two datasets from the Mufulira Mine with a history of rockbursts to verify the RPTs. The Mine was chosen because it is geographically close to the Konkola Mine and uses the same MS system provided by the IMS. Additionally, both Mines' geological and geotechnical settings are similar, further supporting the selection of the Mufulira Mine for data validation.

The RPTs were evaluated on 16 cases from each dataset, and it was found that the MS data-based RPT had a prediction accuracy of 94 percent. In contrast, the geotechnical factor-based RPT had an accuracy of 87.5 percent. Based on the prediction accuracies of 87.5 percent and 94 percent for geotechnical factor-based RPT and the MS data-based RPT, respectively, the proposed RPTs show promise for reasonable predicting of rockbursts.

This research has successfully achieved its objectives by comprehensively examining the key factors that contribute to rockbursts, particularly those associated with geotechnical and microseismic activity. Furthermore, the study has proposed RPTs that can lead to the reasonable prediction of rockbursts.

7.3 Limitations of the Research

The selection of input parameters for the RPTs was left to the Author's discretion, given the lack of universal guidelines in this regard. Regression analysis was employed in Excel to identify the parameter with $R^2 \geq 0.5$. However, this method may be subject to certain limitations such as not capable of measuring goodness of fit and predictive error. Further, it does not measure how one variable explains another that could influence the outcomes. Thus, it is advisable to perform sensitivity analysis to ascertain the critical parameters. The RPTs were verified using only 16 rockburst events, which could have affected the accuracy and validation of the RPTs. Therefore, additional MS and geotechnical data should be investigated to enhance the accuracy of RPTs in future studies.

The establishment of a standardised classification system for rockbursts is of utmost importance due to the likelihood of varying methods of assessment employed by different researchers. The categories utilised in RPTs may diverge among mines, potentially affecting the efficiency and reliability of the RPTs.

7.4 Recommendations for Future Work

The study conducted an extensive analysis and identified particular issues and limitations that require attention for future work. The recommended actions are as follows:

- Delve into more detailed studies to explain why the southern part of the Konkola Mine No.1 Shaft is susceptible to rockbursts;
- Establish the causes of the observed mining induced seismicity below the current operating level (1040 mL) in the southern portion of the Konkola Mine No.1 Shaft;
- Conduct sensitivity analysis to determine the critical parameters for RPTs that will help to identify the most important factors that influence the occurrence of rockbursts;
- Gather more MS and Geotechnical data from other mines with rockburst case histories to validate the RPTs; and
- Establish a universal classification system for rockbursts that will provide a consistent and standardised approach to identifying and classifying different types of rockbursts for the RPTs.

7.5 Research Contributions

A thorough review of the key factors contributing to rockbursts, particularly those associated with geotechnical and microseismic activity, has been obtained through this research. This knowledge and improved understanding hold immense significance for mining, geotechnical, and civil engineering professionals.

The study has yielded the two RPTs that can reasonably predict the likelihood of rockbursts. This development is paramount in bolstering safety measures in mining operations by implementing customised protocols that mitigate the risk of rockbursts while concurrently improving the overall efficacy and operational safety of mining activities.

The research has contributed significant value to the existing academic knowledge base on rockburst prediction using geotechnical and microseismic data, thus providing a wealth of insights and benefits for fellow professionals in the industry.

REFERENCES

Ackoff, R. L., 1953. The Design of Social Research, Chicago, University of Chicago Press.

Afraei, S.K., K. Shahriar and S. H. Madani. 2018. "Statistical assessment of rock burst potential and contributions of considered predictor variables in the task," Tunnelling and Underground Space Technology, vol. 72, pp. 250–271.

Aki, K., 1966. "Generation and propagation of G waves from the Niigata earthquake of June 16, 1964". Part 2: Estimation of earthquake moment, released energy, and stress strain drop from the G-wave spectrum, Bulletin Earthquake Research Institute Tokyo University, 44, 73–88.

Alexander, G. L. and B. Andrew, 2005. Case Studies and Theory Development in the Social Sciences. MIT Press. ISBN 978-0-262-30307-1. OCLC 944521872.

Altindag, R., 2003. "Correlation of specific energy with rock brittleness concepts on rock cutting." J South Afr Inst Min Metall; 103(3): P.163–171.

Amoussou. A and Wu, Li. 2011. "Fuzzy Inference Systems-based Approaches in Geotechnical Engineering-a Review". Electronic Journal of Geotechnical Engineering. 16. 1543-1558.

Askaripour, M., A. Saeidi, A. Rouleau and P.M. Langevin. 2022. 'Rockburst in underground excavations: A review of mechanism, classification, and prediction methods,' Underground Space, Volume 7, Issue 4, Pages 577-607, ISSN 2467-9674,

Bajpai, N., 2011. Business Research Methods. Pearson Education India. Publisher, Pearson Education India; ISBN, 9332511756, 9789332511750; Length, 792 pages.

Baltz, R., and A. Hucke. 2008. "Rockburst prevention in the German coal industry". In S. S. Peng, Ch Mark, G. Finfinger, S. Tadolini, A. W. Khair, & K. Heasley, (Eds.). Proceedings of the 27th International Conference on Ground Control in Mining, July 29–31, 2008 (pp. 46–50). Morgantown, VA: Dept. of Mining Engineering, College of Engineering and Mineral Resources, West Virginia University.

Barton, N., 2002. "Some New Q value correlations to assist in site characterisation and tunnel design". International Journal of Rock Mechanics and Mining Sciences, 39 (2002), pp. 185-21.

Barton, N., F. Løset, R, Lien and J. Lunde.1980. "Application of the Q-system in design decisions". In Subsurface space, (ed. M. Bergman) 2, 553-561.

Belhaj, H, A., 2023. Chapter 4 - Formation evaluation of tight unconventional reservoirs, Tight Oil Reservoirs: Characterization, Modeling, and Field Development, volume 1 in unconventional Reservoir Engineering Series.

Bell, F.G., 2005. Engineering Geology | Rock Properties and Their Assessment, in Encyclopedia of Geology, reference book. (Ed, Richard C. Sellery, Robin. M and Ian R. Plimer,)

Belyadi, H., E. Fathi and F. Belyadi, 2019. Chapter Thirteen - Rock mechanical properties and in situ stresses. in Hydraulic Fracturing in Unconventional Reservoirs (Second Edition). Editor(s): Hoss Belyadi, Ebrahim Fathi, Fatemeh Belyadi. Gulf Professional Publishing, 2019, Pages 215-231, ISBN 9780128176658,

Ben-Menahem, A. and S.J. Singh, 2012. Seismic waves and sources. Springer Science & Business Media.

Bent, F., 2007. Five Misunderstandings about Case-Study Research Inquiry. In Seale, Clive; Silverman, David; Gobo, Giampietro; Gubrium, Jaber F. (eds.). Qualitative Research Practice: Concise Paperback Edition. Qualitative Inquiry. Vol. 12. Thousand Oaks, CA: SAGE Publications. p. 390.

Bent, F., 2014. Five Misunderstandings about Case-Study Research" (PDF), Case Studies, SAGE Publications Ltd, pp. III33,

Bernt, S. and L. Reza, 2019. Rock Strength and Rock Failure, in Petroleum Rock Mechanics (Second Edition).

Bieniawski, Z.T., 1978. “Determining rock mass deformability: experience from case histories”. International Journal of Rock Mechanics and Mining Sciences & Geomechanics Abstracts, Volume 15, Issue 5, 1978, Pages 237-247, ISSN 0148-9062

Blake, W and D. F. G. Hedley, 2009. “Rockbursts case studies from north American hard-rock mines”. Soc. Min. Metal. Explor. Littleton Colo.

Blake, W. and D.G. Hedley. 2003. “Rockbursts: Case studies from North American hard-rock mines”. Littleton, CO: Society for Mining, Metallurgy, and Exploration, Inc. p. 121.

Boatwright, J. and J.B Fletcher.1984. “The Partition of Radiated Energy between P and S Waves”. Bulletin of the Seismological Society of America Vol. 74, No.2. 361–376. 10.1785/BSSA0740020361.

Brady, B.H. G. and E.T. Brown, 2006. Rock Mechanics for Underground Mining. Springer Science eBook.

Brauner, G., 1994. Rockburst in Coal mines and Their Prevention. Taylor & Francis Group. (1st Edition), Balkema, Netherlands.

Bromley, D. B., 1986. The case-study method in psychology and related disciplines. Chichester: Wiley. ISBN 0-471-90853-3. OCLC 12235475.

Brownlee, J., 2021. Failure of classification accuracy for imbalanced class distributions. Retrieved from https://machinelearningmastery.com/failure-of-accuracy-for-imbalanced-class-distributions/ 10 October 2023.

Bryman, A. and E. Bell, 2007. Business Research Methods. 2nd edition. Oxford University Press.

Burkov, A., 2019. The hundred-page machine learning book. ISBN-10. 1999579518; ISBN-13. 978-1999579517; Edition. Hard Cover ed. Publisher. Andriy Burkov.

Burrell, G. and G. Morgan, 1979. Sociological Paradigms and Organisational Analysis. London: Heinemann.

Cai, M and P.K. Kaiser. 2018. “Rockburst Support Reference Book Volume I: Rockburst phenomenon and support characteristics.” MIRARCO – Mining Innovation, Laurentian University, Sudbury, Ontario, Canada

Cai, M., 2008. “Influence of stress path on tunnel excavation response - numerical tool selection and modeling strategy”. Tunnelling and Underground Space Technology 23(6): 618-628.

Cai, M., 2016. “Prediction and prevention of rockburst in metal mines – A case study of Sanshandao gold Mine.” Journal of Rock Mechanics and Geotechnical Engineering. 25: 1–32.

Cai, M, P.K. Kaiser and C.D. Martin. 2001. “Quantification of rock mass damage in underground excavations from microseismic event monitoring”. Int J Rock Mech Min Sci. 38(8):1135–1145

Carvill, P., 2001. In - situ Stress measurements site location report For Konkola Mine.

Chaleunvong, K., 2009. Data collection techniques. GFMER - WHO - UNFPA - LAO PDR.

Chen, B.R., X. T. Feng, Q. P. Li, R. Z. Luo and S.J. Li. 2013. “Rock burst intensity classification based on the radiated energy with damage intensity at Jinping II hydropower station, China”. Mechanics and Rock Engineering, 48(1), 289–303.

Chen, D., L. Gray and M.R. Hudyma. 2005. “Understanding Mine Seismicity—A Way to Reduce Mining Hazards at Barrick’s Darlot Gold Mine”. In Y Potvin & M Hudyma (eds), RaSiM6: Proceedings of the Sixth International Symposium on Rockburst and Seismicity in Mines Proceedings, Australian Centre for Geomechanics, Perth, pp. 269–274.

Chen, Y., J. Zhang, B. Xu, L. Zhang and W. Li. 2021. “Rockburst Precursors and the Dynamic Failure Mechanism of the Deep Tunnel: A Review”. Energies, 14, 7548.

Colson, C. M., 1950. Rockburst. Master thesis. Missouri S & T University.

Cook, N. G. W., E. Hoek, J.P.G. Pretorius, W.D. Ortlepp and M.D.G. Salamon. 1966. “Rock mechanics applied to the study of rockbursts”. J. S. Afr. Inst. Min. Metall., 66(10): 436–528.

Cook, N.G., 1965. “A note on rockburst considered as a problem of stability.” J. South Afr. Int. Min. Metallurgy

Cook, N.G.W., 1976. “Seismicity associated with mining.” Eng. Geol., 10 (2–4) (1976), pp. 99-122.

Creswell, J. W., 2007. Qualitative Inquiry and Research Design: Choosing among Five Approaches (2nd ed.). Thousand Oaks, CA: Sage Publications. 4 Pages.

Crotty, M., 1998. The Foundations of Social Research. London: Sage Publications. London Thousand Oaks New Delhi, 10 Pages.

Dai, F., B. Li, N. Xu, Y. Fan, C. Zhang. 2016. “Deformation forecasting and stability analysis of large-scale underground powerhouse caverns from microseismic monitoring”. Int. J. Rock Mech. Min. Sci., 86, 269–281

Dai, F., B.Lit., N. Xu, Y. Zhu and P. Xiao. 2015. “Stability Evaluation on Surrounding Rocks of Underground Powerhouse Based on Microseismic Monitoring”. Shock Vib. 937181.

Davis, D., 2005. Business Research for Decision Making, Australia, Thomson South-Western.

Deere, D.U., 1989. Rock quality designation (RQD) after 20 years. U.S. Army Corps Engrs Contract Report GL-89-1. Vicksburg, MS: Waterways Experimental Station.

Deere, D.U., A.J. Hendron, F. D. Patton and E.J. Cording.1967. “Design of surface and near-surface construction in rock”. In Failure and breakage of rock, proc. 8th U.S. symp. Rock Mech., (ed. C. Fairhurst), 237-302. New York: Soc. Min. Engrs, Am. Inst. Min. Metall. Petrolm Engrs.

Deng, J., 2014. 'The induced mechanism of pillar rockbursts in deep hard rock mines, in M Hudyma & Y Potvin (eds), Deep Mining 2014: Proceedings of the Seventh International Conference on Deep and High-Stress Mining, Australian Centre for Geomechanics, Perth, pp. 689–697.

Dong, L., J. Wesseloo, Y. Potvin and X.Li. 2016. “Discrimination of Mine seismic events and blasts using the fisher classifier, naive Bayesian classifier and logistic regression”. Rock Mech Rock Eng; 49(1):183–211. Mechanics, 42(8): 2225–2238.

Dongqiao, L., 2018. “Rockburst mechanism research and its control. International Journal of Mining Science and Technology”. 28. 10.1016/j.ijmst.2018.09.002.

Dou, L.M., Z.I. Mu, Z. I. Li, et al. 2014. ‘Research progress of monitoring, forecasting, and prevention of rockburst in underground coal mining in China.’ Int J Coal Sci Technol 1, 278–288 (2014). https://doi.org/10.1007/s40789-014-0044-z

Drover, C. and E. Villaescusa. 2019. “A comparison of seismic response to conventional and face destress blasting during deep tunnel development”, Journal of Rock Mechanics and Geotechnical Engineering, Volume 11, Issue 5, 2019, Pages 965-978, ISSN 1674-7755.

Dudovskiy. J., 2022. The Ultimate Guide to Writing a Dissertation in Business Studies: A Step-by-Step Assistance (6th edition) FT/Prentice Hall.

Durrheim, R., M. Roberts, A. Haile, T. Hagan, A. Jager, M. Handley, S. Spottiswoode and W. Ortlepp. 1998a. “Factors influencing the severity of rockburst damage in South African gold mines.” J.-S. Afr. Inst. Min. Metall.

Durrheim, R.J., A. Haile, M.K.C. Roberts, J.K. Schweitzer, S.M. Spottiswoode and J.W. Klokow. 1998. “Violent failure of a remnant in a Deep South African Gold Mine”. Tectonophysics, 289, 105–116. Engineering Geology, vol. 137-138, no. 7, pp. 85– 96.

Durrheim, R.J., Spottiswoode, S.M., Roberts, M.K.C., A.J., and Brink, A.van Z. 2005. “Comparative Seismology of The Witwatersrand Basin and Bushveld Complex and emerging technologies to manage the risk of rockbursting.” The Journal of the South African Institute of Mining and Metallurgy

Ebnesajjad, S., 2015. “18 - Properties of Tetrafluoroethylene Homopolymers”, Editor(s): Hadi A. Belhaj, In Unconventional Reservoir Engineering Series, Tight Oil Reservoirs, Gulf Professional Publishing, Volume 1, 2023, Pages 35-83, ISBN 9780128202692, Editor(s): Richard C. Selley, L. Robin M. Cocks, Ian R. Plimer, Encyclopedia of Geology. Editor(s): Sina Ebnesajjad, Fluoroplastics (Second Edition), William Andrew Publishing.

Farhadian, H., 2021. “A new empirical chart for rockburst analysis in tunnelling: Tunnel rockburst classification (TRC)”, International Journal of Mining Science and Technology, Volume 31, Issue 4, 2021, Pages 603-610, ISSN 2095.

Feagin, J.R., A. M. Orum and G. Sjoberg, 1991. A Case for the case study. Chapel Hill: University of North Carolina Press. ISBN 0-8078-1973-5. OCLC 22909879.

Feng, G., G. Xia, B. Chen, Y. Xiao and R. Zhou. 2019a. “A Method for Rockburst Prediction in the Deep Tunnels of Hydropower Stations Based on the Monitored Microseismicity and an Optimized Probabilistic Neural Network Model”. Sustainability. 2019; 1(11):3212.

Garry, K, K.O. Robert and V. Sidney.1994). “Designing Social Inquiry. Scientific Inference in Qualitative Research”. Princeton University Press, 1994.Jack, L (2014), "Case Studies: Types, Designs, and Logics of Inference", Case Studies, SAGE Publications Ltd, pp. II113, doi:10.4135/9781473915480.n26, ISBN 978-1-4462-7448-4

Gary, G. and M. James, 2012. A Tale of Two Cultures. Princeton University Press. pp. 221–227. doi:10.23943/Princeton/9780691149707.001.0001. ISBN 978-0-691-14970-7.

Gay, N. C. and W.D. Ortlepp, 1979. “Anatomy of a mining-induced fault zone. Bull”. Geol. Soc. Am., 90: 47–58.

Gibowicz, S, J., H.P. Harjes and M. Schaefer, 1990. “Source parameters of seismic events at Heinrich Robert Mine”, Ruhr Basin, Federal Republic of Germany: evidence for non-double-couple events. Bull. Seism. Soc. Am., 80(1): 88–109.

Gibowicz, S. J. and A. Kijko, 1994. Introduction to Mining Seismology. Academic Press: London. Institute of Mining and Metallurgy, London, pp. 37–52.

Gibowicz, S. J., 1990. “The mechanism of seismic events induced by mining – a review”. Rockbursts and Seismicity in Mines, Proc. 2nd Int. Symp. on Rockbursts and Seismicity in Mines, Minneapolis (ed.C. Fairhurst), 3–27. A. A. Balkema: Rotterdam.

Gibowicz, S. J., 2009. “Seismicity induced by mining: Recent research. Advances in Geophysics”, 51, 1–53.

Gibowicz, S.J. and S. Lasocki, 2001. “Seismicity induced by mining: Ten years later”. In: Dmowska, R. and Saltzman, B., Eds., Advances in Geophysics, Academic Press, Academic Press, 39-181.

Goundar, S., 2012. Chapter 3 – Research Methodology and Research Method. Retrieved from https://www.researchgate.net/publication/333015026.

Grimstad, E. and N. Barton, 1993. “Updating of the Q-System for NMT. Proceedings of the International Symposium on Sprayed Concrete”, Fagernes, 22-26 October 1993, 46-66.

Haile, A.T. A., 1999. Mechanistic Evaluation and Design of Tunnel Support Systems for Deep Level South African mines. Ph.D. Dissertation, University of Natal, Durban, South Africa.

Hanks, T. C. and H. Kanamori, 1979. A moment amplitude scale. J. Geophys. Res., 84: pp. 2348–50.

Hans-Gerd, R., 2017. "The theory contribution of case study research designs". Business Research. 10 (2): 281–305. doi:10.1007/s40685-017-0045-z. ISSN 2198-2627.

Hasegawa, H. S., R. J. Wetmiller and D.J. Gendzwill, 1989. “Induced seismicity in mines in Canada – an overview”. Pure Appl. Geophys., 129(3–4): 423–53.

Hawkes, I., 1966. Stresses in rock, A.A Balkema, 179 pages.

He, H., L.R. Sousa, T. Miranda and G. Zhu, 2015. “Rockburst laboratory tests database— application of data mining techniques”, Engineering Geology, 185 (5), pp. 116-130

He, S., J. Lai, Y., Zhong, K., Wang, W., Xu, L., Wang, T., Liu, and C. Zhang.2021. “Damage behaviors, prediction methods and prevention methods of rockburst in 13 deep traffic tunnels in China. Engineering Failure Analysis”. 121 (2021) 105178.

Hedley, D. G. F., 1992. “Rockburst Handbook for Ontario Hardrock mines”. Energy, Mine and Resources, Ottawa, Canada. Special. Report SP92-1E. CANMET, Energy, Mines and Resources Canada. 305 p.

Henry, F and F. Martha. 2009. "Ontology, methodology, and causation in the American school of international political economy". Review of International Political Economy. 16 (1): 58–71. doi:10.1080/09692290802524075. ISSN 0969-2290. S2CID 145230528.

Herbst, F. and D. Coldwell, 2004. Business Research, Juta and Co Ltd, p.15.

Hill, F.G. and H.G. Denkhaus .1961. "Rock Mechanics Research in South Africa, with Special Reference to Rock Bursts and Strata Movement in Deep Level Gold Mines"; Trans. Seventh Commonwealth Min. and Met. Cong. S. Africa

Hoek, E. and E.T. Brown, 1980. Underground Excavations in Rock. Inst. Min. 537 Metall, London.

Hoek, E. and E.T. Brown. 1997. “Practical estimates of rock mass strength”. International Journal of Rock Mechanics and Mining Sciences, 34 (1997), pp. 1165.

Huang, M.Q., J. Nini and Q. Zhang. 2021. “BIM, machine learning and computer vision techniques in underground construction: Current status and future perspectives”. Tunnelling and Underground Space Technology (2020): 103677.

Huayi, H., 2015. Development of New Methods to Support Systemic Incident Analysis (PDF) (Doctoral dissertation). London: Queen Mary University.

Hudson, J.A. and J.P. Harrison, 1997. Rock Engineering Mechanics- An Introduction to the Principles. Elsevier, Oxford.

Hudyma, M and Y.H. Potvin .2010. “An engineering approach to seismic risk management in hard rock Mines”, Rock Mechanics and Rock Engineering, vol. 43, pp. 891-906. Hutchinson, DJ & Diederichs, MS 1996, Cable bolting in Underground Mines, BiTech Publishers Ltd, Richmond.

Jaeger, J.C., N.G.W. Cook, R. Zimmerman, 2007. Fundamentals of rock mechanics. Rock Mechanics and Rock Engineering, vol. 51, no. 2, pp. 375–389.

Jason, B., 2019. Master machine learning algorithms edition V1.14. Ebook. Computers. 163 pages.

Jason, S. and G. John, 2014. Case Selection Techniques in Case Study Research: A Menu of Qualitative and Quantitative Options", Political Research Quarterly, doi:10.4135/9781473915480.n31, ISBN 978-1-4462-7448-4

Jason, S., 2016. Case Selection after Regression. Multi-Method Social Science: Combining Qualitative and Quantitative Tools, Cambridge University Press, pp. 75–106, doi:10.1017/cbo9781316160831.004, ISBN 978-1-107-09771-1, retrieved 2021-02-11

Javed, A., Z. Mu, S. Bacha, G. Liu, J. Yang, N. M. Shahani, S. A. Mairaj-haider, Faisal and M.A. arif .2019. “A Review on Rockburst Phenomenon-Theories, Mechanism Forecasting and Classification”. International Journal of Science and Business, 3(4), 1-16.

Jenkins, F.M., T.J. Williams and C. J. Wideman. 1990. “Rock burst mechanism studies at the Lucky Friday Mine. Proceedings of the 31st U.S. Symposium on Rock Mechanics”. WV University, Rotterdam: Balkema. p. 955–962.

Jia, Y., Q. Lu and Y. Shang, 2013. “Rockburst prediction using particle swarm optimization algorithm and general regression neural network”. Chin J Rock Mech Eng; 32(2):343–8.

John, G., 2007. Case Study Research: Principles and Practices. Cambridge University Press. pp. 43, 49. ISBN 978-0-521-85928-8.

Johnson, P. and M. Clark, 2006 ‘Editors’ introduction: Mapping the terrain: An overview of business and management research methodologies’, in P. Johnson and M. Clark (eds) Business and Management Research Methodologies. London: Sage, pp. xxv–iv.

Kaiser, P.K. and M. Cai . 2012. “Design of rock support system under rockburst condition”. J. Rock. Mech. Geotech. 2012, 4, 215–227

Kaiser, P.K., 1996. Canadian Rockburst Support Handbook. Geomechanics Research Centre, Sudbury.

Kaiser, P.K., and M. Cai, 2018. Rockburst support reference book. Volume I: Rockburst Phenomenon and Support Characteristics. Mirarco – Mining Innovation, Laurentian University, Sudbury, Ontario, Canada

Kaiser, P.K., D. D. Tannant and D.R. McCreath, 1996. Canadian Rockburst Support Handbook. Geomechanics Research Centre, Laurentian University, Sudbury, Ontario, pp. 314.

Kaiser, P.K., S, Yazici, and S. Maloney. 2001. “Mining-Induced Stress Change and Consequences of Stress Path on Excavation Stability-A Case Study.” Int J Rock Mech Min Sci 38(2): 167-180.

Katunansa S., 2021. Life of Mine plan for Konkola Mine, Internal Report, unpublished

Ke, B., M. Khandelwal, P. Asteris, A. Skentou, A. Mamou and A.D. Jahed. 2021. “Rock-Burst Occurrence Prediction Based on Optimized Naïve Bayes Models.” IEEE Access. 9. 91347-91360. 10.1109/ACCESS.2021.3089205.

Kelemen, M. and N. Rumens, 2008. An Introduction to Critical Management Research. London: Sage

Keneti, A and B.A. Sainsbury, 2018. “Review of published rockburst events and their contributing factors”. Eng. Geol., 246, 361–373.

Kidybinski A., 1981. “Bursting liability indices of coal. International journal of rock mechanics and mining sciences & Geomechanics abstracts”, vol. 18, no. 4. Pergamon. p. 295–304.

Kibuacha, F., 2021. How to determine sample size for a research study. Retrieved from https://www.geopoll.com/blog/sample-size-research/ 17/11/2023

King, G. C. P., 1978. Geological faults, fractures, creep and strain, Philosophical Transactions of the Royal Society of London. Series A, Mathematical and Physical Sciences, 288(1350), 197–212.

Kirsch, E.G., 1898. “Die Theorie der Elastizität und die Bedürfnisse der Festigkeitslehre”. Zeitschrift des Vereines deutscher Ingenieure, 42, 797–807.

KMRL., 2019. Structural features associated with the Konkola ore deposit. Internal report, unpublished.

Kumar, C.R., 2008. Research Methodology. Publisher, APH Publishing Corporation, ISBN, 8131304191, 9788131304198. Length, 152 pages.

Lai, X, C. Jia, F. Cui, J. Chen, Y. Zhu, Y. Feng and Y. Gaa. 2022. “Microseismic energy distribution and impact risk analysis of complex heterogeneous spatial evolution of extra-thick layered strata”. Research square.

Lee, N. and I. Lings, 2008. Doing Business Research: A Guide to Theory and Practice” SAGE.

Lenhardt, W.A., 1992. “Seismicity associated with deep-level mining at Western deep-Levels Limited.” Journal of South African Inst Min Metall 92 113-120.

Leveille, P., M. Sepehri and D.B Apel. 2017. “Rock bursting potential of kimberlite: A case study of Diavik diamond Mine”. Rock Mechanics and Rock Engineering, 50(12), 3223–3231.

Li, C.C., T. Zhao, Y. Zhang and W. Wan.2022. “A study on the energy sources and the role of the surrounding rock mass in strain burst”, International Journal of Rock Mechanics and Mining Sciences, Volume 154, 105114, ISSN 1365-1609,

Li, D., Z. Liu, D. J. Armaghani et al. 2022. “Novel ensemble intelligence methodologies for rockburst assessment in complex and variable environments”. Sci Rep 12:1–23

Li, T. C., M.L. Ma, M. Zhu and G. Chen. 2022. ‘Geomechanical types and mechanical analyses of rockbursts” Engineering Geology, 222 (2017), pp. 72-83.

Li, X., E. Wang, Li. Z, Z. Liu, D. Song and L. Qiu. 2016. “Rock Burst Monitoring by Integrated Microseismic and Electromagnetic Radiation Methods”. Rock Mech Rock Eng 49:4393–4406. DOI 10.1007/s00603-016-1037-6

Li, X., H. Mao, B. Li and N. Xu. 2021. “Dynamic early warning of rockburst using microseismic multi-parameters based on Bayesian network Engineering Science and Technology”, an International Journal 24 715-27.

Li, X., Z. Li and E. Wang, et al. 2017. “Microseismic Signal Spectra, Energy Characteristics, and Fractal Features Prior to Rockburst”: A Case Study from the Qianqiu Coal Mine, China. Journal of Earthquake Engineering, 2017, 21(6):891–911

Li, Y and C. Zhou. 2021. “Rockburst Inducement Mechanism and Its Prediction Based on Microseismic Monitoring”. Hindawi Geofluids Volume 2021, Article ID 4028872, 9 pages.

Li, Y.S., 1985. “Rockburst mechanism and its preliminary application”. J China Inst Min Technol 3, 42–48 (in Chinese).

Lingga, B. A and D.B. Apel. 2018. “Shear properties of cemented rock fills. Journal of Rock Mechanics and Geotechnical Engineering”, 1–10.

Liu, J., H. Shi, R. Wang, Y. Si, D. Wei and Y. Wang. 2021. “Quantitative Risk Assessment for Deep Tunnel Failure Based on Normal Cloud Model: A Case Study at the Ashele Copper Mine, China”. Appl. Sci. 2021, 11, 5208.

Liu, J.P. and X.T. Feng. 2018. “Case Histories of Rockbursts at Metal Mine”. Sub-chapter 3.1 Rockbursts in Metal Mines in China.

Liu, X. and E. Wan. 2018. “Study on characteristics of EMR signals induced from fracture of rock samples and their application in rockburst prediction in a copper Mine”. J. Geophys. Eng 15:909–920.

Liu, Z., Shao, J. W. Xu and Y. Meng. 2013. “Prediction of rock burst classification using the technique of cloud models with attribution weight. Nat Hazards”. 68. 1-20. 10.1007/s11069-013-0635-9.

Lu, C.P, Y. Liu, N. Zhang, T. Zhao and H. Wang. 2018. “In- situ and experimental investigation of rockburst precursor and prevention induced by fault slip.” International Journal of Rock Mechanics and Mining Sciences, 108 (2018), pp. 86-95.

Luo X, King A, Ross J. 2000. Microseismic monitoring at Southern Colliery for understanding roof-fracturing mechanisms. Brisbane.

Ma, C.S., W.Z. Chen, X.J. Tan, H.M. Tian, J.P. Yang and J.X. Yu. 2018. “Novel rockburst criterion based on the TBM tunnel construction of the Neelum-Jhelum (NJ) hydroelectric project in Pakistan”. Tunnelling and Underground Space Technology, 81 (2018), pp. 391-402

Ma, K., C.A. Tang, Z.H. Liang, Z.H. J. Wu, N. W. Xu and D.Y. Zhuang. 2016. “Stability analysis of the surrounding rock of underground water-sealed oil

storage caverns based on microseismic monitoring during construction". Chin. J. Rock Mech. Eng, 35, 1353–1365.

Ma TH, Tang CA, Tang LX, Zhang WD, Wang L. 2015. Rockburst characteristics and microseismic monitoring of deep-buried tunnels for Jinping II Hydropower Station. Tunnelling Underground Space Technol. 49:345–368.

Ma, Y., C. Liu, F. Wu and X. Li. 2018. "Rockburst Characteristics and Mechanisms during Steeply Inclined Thin Veins Mining: A Case Study in Zhazixi Antimony Mine", China. Shock and Vibration, vol. 2018, Article ID 3786047, 16 pages, 2018.

Ma, Y.Z. and J. R. Garzon. 2016. Glossary for Unconventional Oil and Gas Resource Evaluation and Development in Unconventional Oil and Gas Resources Handbook.

Ma, T.H., Tang, CA. Liu., F. Zhang., SC, and ZQ. Feng. 2021. Microseismic monitoring, analysis and early warning of rockburst, Geomatics, Natural Hazards and Risk, 12:1, 2956-2983, DOI: 10.1080/19475705.2021.1968961

Mahesh, B.,2019. "Machine Learning Algorithms - A Review", International Journal of Science and Research (IJSR) ISSN: 2319-7064, Research Gate Impact Factor (2018): 0.28 | SJIF (2018): 7.426 DOI: 10.21275/ART20203995.

Maleki, H., 1981. Coal Mine Ground Control. PhD Dissertation, Colorado School of Mines.

Maleki, H., 1992. "In Situ Pillar Strength and Failure Mechanisms for U.S. Coal Seams, in Workshop on Coal Pillar Mechanics and Design, comp". U.S. Bur. Mines IC 9315, 1992, pp. 73–77.

Maleki, H., 2015. "Cavability, the Least Known Engineering Factor Influencing Mine Designs in Secondary Extraction Systems", in: American Rock Mechanics Association, 2015, pp. 15–144.

Malhotra, N.K. and D. Birks, 2006. Marketing Research: An Applied Approach. 3rd Edition, Prentice Hall, Upper Saddle River.

Manyika, J., 2019. Ore resources and reserves at Konkola Mine. Internal report, unpublished

McGarr, A., D. Simpson and L. Seeber. 2000. "Case histories of induced and triggered Mechanics and Rock Engineering", vol. 49, No. 1, pp. 343–369.

Mendecki A.J., 1996. Seismic Monitoring in Mines, Chapman and Hall Press, London.

Mendecki, A. J., 1993. "Real-time quantitative seismology in Mines. Proc. 3rd Int. Symp. Rockbursts and Seismicity in Mines", Kingston (ed. R. P. Young), 287–95. A. A. Balkema: Rotterdam.

Mendecki, A., 2013a. Mine Seismology: Glossary of Selected Terms. 10.13140/2.1.1182.7846.

Mendecki, A., 2013a. Mine Seismology: Glossary of Selected Terms. 10.13140/2.1.1182.7846.

Mendecki, A., 2013b. Frequency Range, logE, log P, and Magnitude.

Mendecki, A., G. Van Aswegen and P. Mountfort, 1999. A Guide to Routine Seismic Monitoring in Mines.

Mendecki, A.J and G. van Aswegen .2001. “Seismic monitoring in Mines: selected terms and definitions”. In Proceedings of Rockbursts and Seismicity in Mines – RaSiM 5, Johannesburg, September 2001. ed. G. van Aswegen et al, 563-570. Johannesburg: South African Institute of Mining and Metallurgy.

Mendecki, A.J., 1997. Seismic Monitoring in Mines, Chapman & Hall, London.

Mendecki, M.A., 1999. A Guide to Routine Seismic Monitoring in Mines. Creda Communications, Cape Town.

Mendecki, M.J., R. Pakosz and Ł. Wojtecki. 2021. “Spatiotemporal analysis of elastic and inelastic deformations in roof-rocks from seismological observations”. International Journal of Mining Science and Technology, 2021, 31,241–251.

Merriam, S. B., 2009. Qualitative research: A guide to design and implementation. San Francisco, CA: Jossey-Bass.

Michael, B., 2009. The Extended Case Method: Four Countries, Four Decades, Four Great Transformations, and One Theoretical Tradition. Berkeley: University of California Press. ISBN 978-0-520-94338-4.

Milev, A.M. and S.M. Spottiswoode. 2002. “Effect of the rock properties on mining-induced seismicity around the Ventersdorp contact roof, Witwatersrand Basin, South Africa”. Pure Appl Geophys. 2002(159):165–177.

Minney, D., G. Kotze and G.van Aswegen.1997. “Seismic Monitoring of the Caving Process above a Retreating Longwall at New Denmark Colliery, South Africa”. In Proceedings of Rockbursts and Seismicity in Mines, Krakow, (ed. S. Gibowicz and S. Lasocki), pp. 125-130.

Misich, I., and A. Lang, 2001. “Examples of rockburst damage in Western Australia”. Proceedings of the 5th international Symposium, South African Institute of Mining & Metallurgy, 59–68.

Moon, K. and D. Blackman, 2014. A Guide to Understanding Social Science Research for Natural Scientists. Conservation Biology, 28: 1167-1177

Morissette, P., J. Hadjigeorgiou, A. Punkkinen and D. Chinnasane. 2014. “The influence of change in mining and ground support practice on the frequency and severity of rockbursts”. In Proceedings of the Seventh International Seminar on Deep and High-Stress Mining, Australian Centre for Geomechanics, Perth, Australia, 16–18 September 2014; pp. 165–177.

Mulenga, S., R. Fernandez- Rubio, A. Leon and J. Baquero. 1992. “Estimation of quantitative Water inflow from different water sources in Konkola Mine”, Mine water and the environment, 11(4), pp.1-22.

Mutale, A., 2004. “Assessment of Seismic Risk at Konkola Mine – No. 1 Shaft”. South. African National Institute of Rock Engineering, South Africa. 126 pages.

Natasha, M., 2020. Research philosophies and why they matter. 10.4337/9781788975636.00018.

Nussbaumer, M.M., 2000. A Comprehensive Review on Rock Burst, MSc, Department of Civil and Environmental Engineering, the Massachusetts Institute of Technology

Nuttli, O. W., 1978. Nomenclature and Terminology for Seismology. Association of Earth Science Editors: Tulsa, Oklahoma.

Obert, L. and W.I. Duvall, 1967. “Rock Mechanics and the Design of Structures in Rock.” Wiley, 1967. The University of Michigan, 0471652350, 9780471652359. 650 pages.

Ortlepp, W. D. and T.R. Stacey. 1994. “Rockburst mechanisms in tunnels and shafts. Tunnelling and Underground Space Technology”, 9(1), 59-65.

Ortlepp, W. D., 1978. “The mechanism of a rockburst”. Proc. 19th U. S. Symp. Rock Mech., Reno, 476–83. University of Nevada: Reno

Ortlepp, W. D., 1997. “Rock Fracture and Rockbursts - An Illustrative Study”, Monograph Series M9, 126 pp., South African Institute of Mining and Metallurgy.

Ortlepp, W., 1998. “Factors influencing the severity of rockburst damage in South African gold mines”. J.-S. Afr. Inst. Min. Metall.

Ortlepp, W.D and T.R. Stacey. 1994. “Rockburst mechanisms in tunnels and shafts.” Tunnelling and Underground Space Technology, 9 (1), pp. 59-65.

Palmström, A. and R. Singh. 2001. “The deformation modulus of rock masses-comparisons between in situ tests and indirect estimates”. Tunnelling and Underground Space Technology, 16 (2001), pp. 115-131.

Peng, X. H. Liu, and G. Zhao. 2023. “Characteristics of Ground Pressure Disaster and Rockburst Proneness in Deep Gold Mine. Lithosphere”. 2022. 10.2113/2023/9329667.

Peng, X., G. Zhao and H. Liu. 2021. “Field investigation and analysis of rockburst and spalling in a deep hard-rock mine". 10.21203/rs.3.rs-197278/v1.

Peter, U., W. Patrick and B. Graham. 2016. “Accident investigation in the wild. – A small-scale, field-based evaluation of the STAMP method for accident analysis". Safety Science. 82: 129–43. DOI: 10.1016/j.ssci.2015.08.014.

Petukhov, I.M. and A.M. Linkov. 1979. “The theory of post-failure deformations and the problem of stability in rock mechanics.” Int J Rock Mech Min Sci Geomech Abstr 16(2):57–76.

Phipps, D., B. Simser, G. Swan and R.M. Engineer. 2013. “Rockburst Case Histories: 1985, 1990, 2001 & 2013.” CAMIRO Mining Division for the Deep Mining Research Consortium: Sudbury, ON, Canada.

Potvin, Y 2009, ‘Strategies and tactics to control seismic risks in mines’, The Journal of The Southern African Institute of Mining and Metallurgy, vol. 109, pp. 177–186.

Potvin, Y., M. Hudyma and R.J. Jewell. 2000. “Rockburst and seismic activity in underground Australian Mines- an introduction to a new research project”. ISRM

Pu, Y., D. Apel and H. Xu. 2018b. “A principal component analysis/fuzzy comprehensive evaluation for rockburst potential in Kimberlite”. Pure Appl Geophys; 175 (6):2141–51.

Pu, Y., D.B. Apel, B. Lingga. 2018a. “Rockburst prediction in kimberlite using decision tree with incomplete data”, Journal of Sustainable Mining 17 Pg158–165

Qian, Y., F. Sun, Y. Zhang and L. Huo. 2014. “Metallogenic and Metamorphic Age of the Hongtoushan Copper–Zinc Massive Sulfide Deposit, Liaoning Province, China”. Resource Geology.

Qian, Y., S. Fengyue, Y.F. Zhang and L. Huo. 2014a. “Use of Microseismic Monitoring Data as an Aid to Rock Mechanics Decision Making and Mine Design Verification”. Simser, Jalbout, Deredin and Butler.

Qiang, S., P. Yi-Shan, L. Yi-Jie. 2005. “The typical cases and analysis of rockburst in China. Coal Mining Technology”, 10(2), 13–17 (in Chinese).

Qiao, C. and Z. Tian. 1998. “Possibility of rockburst occurrence in Dongguashan copper deposit”. Chinese Journal of Rock Mechanics and Engineering, 1998.

Raschka, R., 2018. “Model Evaluation, Model Selection, and Algorithm Selection in Machine Learning.” eBook.

Richter, C. F., 1935. “An instrumental earthquake magnitude scale”. Bull. Seism. Soc. Am., 25: 1–32.

Ross.T.A., W.R. Stanley, Jason.Q, and C.E. Bechtel. 2018.” Independent Technical Report Site 4 Xincheng Gold Mine Shandong Province, China”. Appendix III Competent Person’s Report- AA1 Report Site 4.

Rowe, R. K. and H.H. Armitage, 1984. The Design of Piles Socketed into Weak Rock. Faculty of Engineering Science, the University of Western Ontario, London, Ont., Research Report GEOT-11-84.

Russenes, B. F., 1974. “Analysis of rock spalling for tunnels in steep valley sides”. M.Sc. thesis, Norwegian Institute of Technology, Trondheim, Norway, 247 (in Norwegian).

Ryder, J. A., 1987. “Excess shear stress (ESS): an engineering criterion for assessing unstable slip and associated rockburst hazards”. Proc. 6th Congr., Int. Soc. Rock Mech., Montreal (eds G. Herget and S. Vongpaisal), 2: 1211–15, A.A. Balkema: Rotterdam.

Ryder, J. A., 1988. “Excess shear stress in the assessment of geologically hazardous situations”. J. S. Afr. Inst. Mining Metall., 88(1), 27–39.

Sainsbury, B.N. and K. Nurses. 2019. “Impact of intact rock properties on proneness to rockbursting,” Bulletin of Engineering Geology and the Environment.1-8.

Sakala. B., 1996. History of Konkola Mine, Zambia Consolidated Copper Mines Limited. Internal Report, Unpublished.

Salamon, M. D. G., 1984. “Energy considerations in rock mechanics: Fundamental results”. J. S. Afr. Inst. Mining Metall., 84(8), 233–246.

Saunders, M., P. Lewis and A. Thornhill. 2012. “Research Methods for Business Students”. 6th edition, Pearson Education Limited

Saunders, M.N.K., 2009. “Understanding research philosophies and approaches”. (Accessed from https://www.researchgate.net/publication/309102603_Understanding_research_philosophies_and_approaches).

Scriven, M. (1967). "The methodology of evaluation". In Stake, R. E. (ed.). Curriculum evaluation. Chicago: Rand McNally. American Educational Research Association (monograph series on evaluation, no. 1

Seawright, J. and G. John. 2014. Case Selection Techniques in Case Study Research: A Menu of Qualitative and Quantitative Options", Political Research Quarterly, doi:10.4135/9781473915480.n31, ISBN 978-1-4462-7448-4.

Senfaute G, Chambon C, Bigarre P, Guise Y, Josien JP. 1997. “Spatial distribution of mining tremors and the relationship to rockburst hazard”. Pure Appl Geophys. 150(3-4):451–459

Serafim, J. L. and J.P Pereira. 1983. “Considerations of the geomechanics classification of Bieniawski”. In Proc. Int. Symp. Eng. Geol. Underground Constr., Vol. 1, Lisbon, pp. I133-1142.

Shang, X., X. Li, K. Peng, Z. Wang and L. Weng. 2017. “Application of FSWT-SVD model in the feature extraction of rock mass microseismic signals”. J Vib Shock; 36 (14):52–60.

Sharma, A and P. Mishra. 2020. “State-of-the-Art in Performance Metrics and Future Directions for Data Science Algorithms”. Journal of scientific research. 64. 221-238. 10.37398/JSR.2020.640232.

Sharma, G., 2017. “Pros and cons of different sampling techniques”. International Journal of Applied Research 2017; 3(7): 749-752

Shen B, King A, Guo H. 2008. Displacement, stress and seismicity in roadway roofs during mining -induced failure. Int J Rock Mech Min Sci. 45(5):672–688.

Simser, B.P., V. Falmagne, D. Gaudreau, and T. MacDonald. 2003. “Seismic Response to Mining at the Brunswick Mine”. CIM AGM, Montreal. 12 pages.

Simser, B. and A.T.Butler, 2016. Ground Support Practice at Glencore's Nickel Rim South Mine – with a link to seismic monitoring data. : Retrieved from https://www.researchgate.net/publication/308401444. 10/10/2023.

Sleefe, E. and Gerard, et al. 1995. "The Use of Broadband Microseisms for Hydraulic-Fracture Mapping." Spe Formation Evaluation, https://doi.org/10.2118/26485-pa.

Snelling, P.E., L. Godin and S.D. McKinnon. 2016. “The role of geologic structure and stress in triggering remote seismicity in Creighton Mine”, Sudbury, Canada. Int. J. Rock Mech. Min. Sci. 2013, 58, 166–179. Volume 8, Issue 2, April 2016, Pages 204-21.

Spottiswoode, S. M., 1984. “Source mechanisms of mine tremors at Blyvooruitzicht Gold Mine. Rockbursts and Seismicity in Mines.” (Eds N. C. Gay and E. H. Wainwright), 29–38. S. Afr. Inst. Min. Metall.: Johannesburg.

Spottiswoode, S. M., and A. McGarr.1975. “Source parameters of tremors in a deep-level gold Mine”, Bull. Seismol. Soc. Am., pp. 65, 93 – 112

Spottiswoode, S.M., 1989. “Perspectives on seismic and rockburst research in the South African gold mining industry: 1983-1987”, Pure and Applied Geophysics, vol. 129, no. 3- 4, pp. 673-80.

Su, G.S., Y. J. Shi, X. T. Feng, J. Jiang, J. Zhang and Q. Jiang. 2018. “True-triaxial experimental study of the evolutionary features of the acoustic emissions and sounds of rockburst process,” February 2018Rock Mechanics and Rock Engineering 51(2). DOI: 10.1007/s00603-017-1344-6.

Sun, J., L.G. Wang, H. Zhang and Y. T. Shen. 2009. “Application of fuzzy neural network in predicting the risk of rockburst”. Procedia Earth Planet Sci; 1(1):536–43.

Taherdoost, H., 2016. “Sampling Methods in Research Methodology; How to Choose a Sampling Technique for Research”. International Journal of Academic Research in Management (IJARM), Vol. 5, No. 2, 2016, Page: 18-27, ISSN: 2296-1747

Tajduś A., J. Flisiak and M. Ca. 1997. Estimation of rockburst hazard basing on 3D stress field analysis. Rockburst & Seismicity in Mines (edited by Lasocki).

Tan, Y. A., 1992. “Rockbursting characteristics and structural effects of rock mass”. International Journal of Rock Mechanics and Mining Sciences & Geomechanics Abstracts, 29(6), 402–403Sci. Chin, 35(8), 981–990.

Tan.L. and K. Xia. (2009). “Prevention and Control of Rockbursts in Dongguashan Copper Mine. OCKENG09: Proceedings of the 3rd CANUS Rock Mechanics Symposium, Toronto, and May 2009” (Ed: M. Diederichs and G. Grasselli)

Tang, B. Y., 2000. Rock burst control using distress blasting. Ph.D. thesis. McGill University, Montreal, Canada.

Tang. CA, J-M. Wang, J-J. Zhang. 2010. “Preliminary engineering application of microseismic monitoring technique to rockburst prediction in tunneling of Jinping II project”. J Rock Mech Geotech Eng. 2(3):193–208.

Tao, Z. Y., 1988. Support design of tunnels subjected to rock bursting. Rock mechanical power plants, Romana, ed., Balkema, Rotterdam, Netherlands, 407–411.

Torremans, K., P. Muchez, M. Stuntubin and O. Sikazwe. 2012. “Structural control and ore distribution at the Konkola copper- Cobalt deposit, Zambia”, Journal of African Earth Sciences, 79, pp.10-13.

Tsioptsias, N., A.A. Tako and S. Robinson. 2016. “Model validation and testing in simulation: a literature review”. Mine. Sub-chapter 3.1 Rockburst in Metals mines in China.

Turchaninov, I. A., et al. 1972. “State of stress in the upper part of the Earth’s crust based on direct measurements in Mines and on tectonophysical and seismological studies”. Phys. Earth Planet. Inter., 6(4), 229–234.

Turchaninov, I.A and G.A Markov. 1981. Conditions of changing of extra-hard rock into weak rock under the influence of tectonic stresses of massifs. Proc. Int. Sympos. Weak Rock, Tokyo, 21 (1981), pp. 555-559

UGS, 2010."Earthquake Glossary - hypocenter". United States Geological Survey (UGS) (Accessed from the original on 15 March 2010.)

Urbancic, T.I. and R.P. Young, 1993. Space–time variations in source parameters of mining-induced seismic events with M-0. Bull. Seismol. Soc. Am. 83, 378–397

Van Aswegen, G and A. G. Butler.1993. “Applications of quantitative seismology in South African gold Mines, in Proceedings of the 3rd International Symposium on Rockbursts and Seismicity in Mines”, Kingston, Ontario, Canada, edited by R. P. Young, pp. 261–266, Balkema, Rotterdam, ISBN 90 5410320 5.

Walker, G., 2001. In-situ Stress measurement at Konkola Mine.

Wang, J., D.B. Apel, Y. Pu, R. Hall, C. Wei and M. Sepehri. 2021. “Numerical modeling for rockbursts: A state-of-the-art review”. J. Rock Mech. Geotech. Eng. 2021, 13, 457–478. – 9.

Wang, J.A. and H. Park. 2001. “Comprehensive prediction of rockburst based on analysis of strain energy in rocks”. Tunn Undergr Space Technol; 16(1): P.49–57.

Wang, Y. H., W.D. Li and Q.G. Li. 1998. “Method of fuzzy comprehensive evaluations for rockburst prediction”. Chinese Journal of Rock Mechanics and Engineering, 15, 493-501.

Wen, Z., X. Wang, Y. Tan, H. Zhang, W. Huang and Q. Li. 2016. “A Study of Rockburst Hazard Evaluation Method in Coal Mine”. Shock and Vibration, 16: 1–9.

Wiles, T. D., 2002. “Loading system stiffness—A parameter to evaluate rockburst potential.” Proc., 1st Int. Seminar on Deep and High Stress

Wiles, T. D., 2005. “Rockburst prediction using numerical modelling: Realistic limits for failure prediction accuracy”. Proc., 6th Int. Symp. on Rockbursts and Seismicity in Mines (RaSiM 6), Australian Centre for Geomechanics, Perth, Australia

Wojtecki, L., S. Iwaszenko, D.B. Apel and T. Cichy. 2021. “An Attempt to Use Machine Learning Algorithms to Estimate the Rockburst Hazard in Underground Excavations of Hard Coal Mine”. Article in Energies · DOI: 10.3390/en14216928

Wolpert, D.H., 1996. “The lack of a priori distinctions between learning algorithms. Neural computation”, 8(7), 1341-1390.

Wu, J., X. Zhang, L. Yu, et al., 2022a. “Rockburst mechanism of rock mass with structural planes in underground chamber excavation”. Eng Fail Anal 139: 106501.

Wu, M., Y. Ye, Q. Wang and N. Hu, 2022b. ‘Development of rockburst research: A comprehensive review’ Applied Sciences, 12 (3), p. 974

Wyss, M and J. N. Brune. 1968. “Seismic moment, stress and source dimensions for earthquakes in the California-Nevada region”, Journal of Geophysical Research, 73, 4681–4694.

Xianghui, T, Z., Li, D and Song, et al. 2020. “Study on microseismic precursors and early warning methods of rockbursts in a working face”. Chinese Journal of Rock Mechanics and Engineering, 39(12):2471–2482.

Xiao, Y. X., X.T. Feng, J. Hudson, B.R. Chen, G. Feng and J. P. Liu. 2016.” ISRM Suggested Method for In Situ Microseismic Monitoring of the Fracturing Process in Rock Masses”. Rock Mechanics and Rock Engineering. 49. 10.1007/s00603-015-0859-y.

Xiao YX, Feng XT, Li SJ, Feng GL, Yu Y. 2016. Rock mass failure mechanisms during the evolution of rockbursts in tunnels. Int J Rock Mech Min Sci. 83:174–181

Xiao. P, Zhao. G, Liu H. 2021. Field Investigation and Analysis Of Rockburst And Spalling In A Deep Hard Rock Mine. Unpublished.

Xu, N., T. Li, F. Dai, B. Li, Y. Zhu and D. Yang. 2015. “Microseismic monitoring and stability evaluation for the large-scale underground caverns at the Houziyan hydropower station in Southwest China”. Eng. Geol., 188, 48–67.

Xu. S, X. Yang. F. Zhang and J. Liu. 2022. “Application of a Microseismic Method of Rockburst Risk Assessment under Blasting Mining in Ashele Copper Mine. Shock and Vibration”. Volume 2022, Article ID 5377528, 13 pages. https://doi.org/10.1155/2022/5377528

Yang, J.P, W.Z. Chen and W.S. Zhao. 2017. “Geohazards of tunnel excavation in interbedded layers under high in situ stress Engineering Geology,” 230, pp. 11-22.

Yıldırım, E., A. Gülbag, G. Horasan and E. Dogan.2011. “Discrimination of quarry blasts and earthquakes in the vicinity of Istanbul using soft computing techniques”. Comput Geosci; 37(9):1209–17.

Yin, R. K., 2003. Case study research, design and methods, Newbury Park, CA, SAGE.

Yin, X., Q. Liu, X. Huang and Y. Pan. 2021. “Real-time prediction of rockburst intensity using an integrated CNN-Adam-BO algorithm based on microseismic data and its engineering application”. Tunnelling and Underground Space Technology 117 104133.

Yoon, J. S., 1994. Tunnel Engineering, 160–162.

Zach, C., 2022. “Research Guides: Organizing Academic Research Papers: Types of Research Designs. "(https://library.sacredheart.edu/c.php?g=29803&p=185902). Accessed September 17, 2022.

Zhang, C., H. Zhou and J.P. Feng. 2011. “An Index for Estimating the Stability of Brittle Surrounding Rock Mass” FAI and its Engineering Application. Rock Mechanics and Rock Engineering. 44. 401-414.

Zhang, C., I. Canbulat, B. Hebblewhite and C.R. Ward. 2017. “Assessing Coal Burst Phenomena in Mining and Insights into Directions for Future Research”. Int. J. Coal Geology. 179, 28–44. doi: 10.1016/j.coal.2017.05.011.

Zhang, C.Q., Y.U. Jin, J. Chen, J. Lu and H. Zhou. 2016. “Evaluation method for potential rockburst in underground engineering”. Rock Soil Mech37 (s1):341–349 (in Chinese) He, M., Fuqiang, R.

Zhang, L., X. Zhang, J. Wu, D. Zhao and H. Fu. 2020a. “Rockburst prediction model based on comprehensive weight and extension methods and its engineering application”. Bulletin of Engineering Geology and the Environment. 79. 10.1007/s10064-020-01861-4.

Zhang, S.C., T.H. Ma, C.A. Tang, P. Jia Y. C. Wang. 2020b. “Microseismic Monitoring and Experimental Study on Mechanism of Delayed Rockburst in Deep-Buried Tunnels”. Rock Mech. Rock Eng., 53, 2771–2788.

Zhang, J., D. Li and Y. Wang. 2020c. “Predicting tunnel squeezing using a hybrid classifier ensemble with incomplete data.” Bulletin of Engineering Geology and the Environment 79 3245-56.

Zhang, M.T., 1987. “Instability theory and mathematical model for coal/rock bursts”. Chin J Rock Mech Eng 6(3):197–204 (in Chinese).

Zhang, Z.X., F. Gong and E. Kozlovskaya, 2023. “Characteristic Impedance and Its Applications to Rock and Mining Engineering”. Rock Mech Rock Eng 56, 3139–3158.

Zhao, H., B. Chen and C. Zhu. 2020. “Decision Tree Model for Rockburst Prediction Based on Microseismic Monitoring”, Hindawi, Advances in Civil Engineering Volume 2021, Article ID 8818052, 14 pages.

Zhao, Z. and L. Gross. 2017. “Using supervised machine learning to distinguish microseismic from noise events”. Paper presented at the 2017 SEG international exposition and annual meeting, 2017.

Zheng, Y., H. Zhong, Y. Fang, W. Zhang, K. Liu and J. Fang. 2019. “Rockburst Prediction Model Based on Entropy Weight Integrated with Grey Relational BP Neural Network”. Advances in Civil Engineering. 2019. 1-8.

Zhou J, Li X and X. Shi 2012. “Long-term prediction model of rockburst in underground openings using heuristic algorithms and support vector machines”. Saf Sci; 50(4):629–44.

Zhou, H., C.Q. Zhang, and X. T. Feng. 2011. “An index for estimating the stability of brittle surrounding rock mass: FAI and its engineering application”. Rock Mech. Rock Eng., 44(4), 401–414.

Zhou, J., Li, X and H. Mitri. 2016. “Classification of Rockburst in Underground Projects: Comparison of Ten Supervised Learning Methods”. Journal of Computing in Civil Engineering. 30. 04016003. 10.1061/(ASCE)CP.1943-5487.0000553.

Zhou, J., X.Li and H.S. Mitri. 2018. “Evaluation method of rockburst: State-of-the-art literature review”. Tunn. Undergr. Space Technol. 81, 632–659.

Zhou, J., X.Li and X. Shi. 2012. “Long-term prediction model of rockburst in underground openings using heuristic algorithms and support vector machines”. Saf Sci; 50(4):629–44.

Zhou, Y and T. Wan. 2017. “PNN-based Rockburst Prediction Model and Its Applications”. Earth Sciences Research Journal, 21(3). 141 -146.

Zhu W.C, Z. H. Li, L. Zhu, and C. A. Tang. 2010. “Numerical simulation on rockburst of underground opening triggered by dynamic disturbance,” Tunnelling and Underground Space Technology, vol. 25, no. 5, pp. 587–599.

APPENDICES

Appendix A: Geology for the Selected Mines with Rockburst Case Histories

No.	Mine/Location	Geology	Authors
1	Long Shaft mine – Australia	Tabular and steep orebody dipping at about 75° ; Footwall(meta-basalt); Hangingwall (basalt, antigorite, talc, magnesite/chlorite ultramafic); Orebody (massive sulphide), presence of dykes(felsic porphyry).	Keneti and Sainsbury, 2018
2	Lanfranchi – Australia	Tabular and shallow dipping orebodies dipping approximately 30°; Footwall (meta-basalt); Hangingwall (talc, magnesite ultramafic); Orebody (massive sulphide).	Keneti and Sainsbury, 2018
3	Mount Charlotte mine – Australia	Steeply dipping orebodies at about 70° hosted in a block stiff and strong dolerite; two major reverse faults bound the orebody.	Keneti and Sainsbury, 2018
4	Darlot Mine – Australia	Shallow westernly dipping gold associated quartz vein mineralization bounded between mineralized footwall and hangingwall faults. several intersecting major structures across the orebody; The mineralization is hosted within a magnetic dolerite unit, which is part of a 400m thick dolerite sill intruded within a moderate easterly dipping sequence of basalts and pyroclastic sediments reverse faults (45° dip, N-S strike).	Keneti and Sainsbury, 2018; Chen et al., 2005
5	Broken Hill Mine – Australia	Lead zinc mineralisations in a shear bound and hosted in a deformed and altered meta- sedimentary sequence; Geological structures. Orebody dips between 36 and 45°.	Keneti and Sainsbury, 2018
6	Hongtoushan copper mine – China	Extremely complicated geological condition, structural planes. The Hongtoushan Cu–Zn deposit contains three types of orebodies: layered, layer-like, and lenticular. The main orebodies are generally in conformable contact with the surrounding rocks, although they are intensely deformed; the host rocks of these orebodies have foliations that are roughly parallel to lithological boundaries and dip towards the SE at 60°–80°.	Liu and Feng, 2018;
7	The Ashele Copper Mine – China	Volcanogenic massive sulphide (VMS) of Cu- Zn deposit; Orebody is between 20 and 45m thick, dipping at 70-80° Chalcopyrite is the orebody. The orebody is bounded by the base tuff and roof basalt	Liu and Feng, 2018; Xu et al., 2022

8	Dongguashan Copper Mine - China	Average dip of the orebody is 20°; average thickness of the orebody is 40m; maximum thickness of the orebody is 85m; orebody is mainly composed of Cupriferous Skarn, with marble and siltstone forming the roof and quartz diorite forming the floor; there are few large faults and dense joints in the orebody.	Tan and Xia, 2009; Liu and Feng ,2018
9	Xincheng Gold Mine – China	The ore body is mainly pyrite sericite; surrounding rock is mainly sericitized granodiorite; average inclination of ore body is about 30°.	Xiao et al., 2009; Ross et al., 2018
10	Bushveld Platinum Mines – South Africa	Complex layered intrusions, thin reefs of gentle dip	Wilson Blake and Hedley, 2003
11	Witwatersrand Gold Mines- South Africa	Predominantly detrital sedimentary rocks interspersed sporadically with Auriferous and uraniferous quartz pebble conglomerate	Durrheim et.al, 2005;
12	Kolar Gold Fields - India	Highly metamorphosed hornblende schists, fine grained, dense, and compact; Schists are folded, faulted, and intruded by dolerite, porphyry dykes, and pegmatite intrusions; Schists are generally hard, homogeneous, highly crystalline, and brittle	Wilson Blake and Hedley, 2003
13	Sunshine Mine - USA	Host rocks for the mineralization is hosted in the St. Regis and Revett formations of the Precambrian Belt Series; siderite quartz veins contain tetrahedrite-rich ore shoots; Mineralization is best developed in the folded north limb of the Big Creek anticline, which is intersected by a number of north-west and east-striking faults.	Wilson Blake and Hedley, 2003
14	Galena Mine - USA	The deep silver veins (dipping about 65°) of the Galena Mine occur along a shear zone between two major faults; veins are oriented normal to the shear zone, which strikes some N50° to 60°W and is parallel to the direction of maximum principal stress; the harder Revett quartzite.	Wilson Blake and Hedley, 2003
15	Brunswick Mine - Canada	Massive sulfide orebody with some parallel lenses dipping some 75° to the; metamorphosed volcanic sequence of sediments and tuffs; hanging wall and footwall rocks are much softer and weaker than the massive sulfide ore; presence of intrusive porphyry dyke	Wilson Blake and Hedley, 2003
16	Lake Shore mine - Canada	Narrow gold-bearing quartz veins are associated with a fault system designated as the Main Break, or Kirkland Lake Fault. Orebody dip of 8°. The orebody follows the hanging wall side of a diabase dike.	Wilson Blake and Hedley, 2003
17	Nickel Rim South Mine - Canada	A mixture of hard igneous host rocks with both nickel rich and copper rich semi-massive to massive sulphides as ore zones. Steeply dipping ore zones of 70° complex system of faulting and variable geology, but generally high-quality rock.	Simser et al., 2015

Appendix B.1: C++ code for MS_RPT

```
#include <iostream>
using namespace std;
//Welcome to Microseismic Based Rockburst Prediction Tool (MS_RPT)
//This Program Predicts Rockburst class Based on the Total Ratings of assigned Ratings to Microseismic Parameters

//VARIABLE DECLARATION
double magnitude, potency, energy, prediction;
double Ratingmagnitude, Ratingpotency, Ratingenergy, Ratingprediction;

//MAIN PROGRAM

int main(){

   cout<< "Enter Magnitude(mL)"<< endl;
   cin>> magnitude;

   cout<< "Enter Seismic potency(log(P/m3))"<< endl;
   cin>> potency;

   cout<< "Enter Seismic Energy(log(logE))"<< endl;
   cin>> energy;

   //MAGNITUDE
   if(magnitude<0.5){

      Ratingmagnitude=1;

            } else if(magnitude>=0.5 && magnitude<1.5){
              Ratingmagnitude=2;
                                    }
                    else if(magnitude>=1.5 && magnitude<2.5){
                    Ratingmagnitude=3;
                                          }
                            else if(magnitude>=2.5){
                            Ratingmagnitude=4;
                                          }
 //POTENCY
 if(potency<0.6){

      Ratingpotency=1;

            } else if(potency>=0.6 && potency<1.4){
              Ratingpotency=2;
                                    }
                    else if(potency>=1.4 && potency<2.2){
                    Ratingpotency=3;
                                          }
                            else if(potency>=2.2){
```

```
                                    Ratingpotency=4;
                                    }
  //ENERGY
    if(energy<2.2){
      Ratingenergy=1;
                } else if(energy>=2.2 && energy<5.6) {
                 Ratingpotency=2;
                                        }
                            else if(energy>=5.6 && energy<9){
                           Ratingenergy=3;
                                                }
                                    else if(energy>=9){
                                    Ratingenergy=4;
                                    }
//RESULT
 prediction = Ratingmagnitude+Ratingpotency+Ratingenergy;

if(prediction<3){

      cout << "Rockburst prediction is None/green: " << prediction << endl;
                } else if(prediction==3){
                 cout << "Rockburst prediction is No damage: " << prediction << endl;
                                        }
                            else if(prediction>=4 && prediction<7){
                            cout << "Rockburst prediction is minor: " << prediction << endl;
                                                }
                                    else if(prediction>=7 && prediction<10){
                                    cout << "Rockburst prediction is Moderate: " <<
prediction << endl;
                                    }
                                          else if(prediction>=10 && prediction<13){
                                    cout << "Rockburst prediction is Strong: " <<
prediction << endl;
                                                                        }

                                       else if(prediction>=13){
                                       cout << "Rockburst prediction is Extra Strong: "
<< prediction << endl;
                                                                          }
   return 0;
}
```

Appendix B.2: GUI Code for MS_RPT

```
using System;

using System.Diagnostics;
using System.Windows.Forms;

namespace RockburstPredictionApp
{
   public partial class Form1 : Form
   {
      public Form1()
      {
         InitializeComponent();
      }

      private void buttonCalculate_Click(object sender, EventArgs e)
      {

      }

      private void buttonCalculate_Click_1(object sender, EventArgs e)
      {
         Stopwatch stopwatch = new Stopwatch();
         stopwatch.Start();

         if (!Double.TryParse(textBoxMagnitude.Text, out double magnitude) ||
               !Double.TryParse(textBoxPotency.Text, out double potency) ||
               !Double.TryParse(textBoxEnergy.Text, out double energy))
         {
            MessageBox.Show("Invalid input. Please enter valid numeric values.", "Input
Error", MessageBoxButtons.OK, MessageBoxIcon.Error);
            return;
         }

         double Ratingmagnitude, Ratingpotency, Ratingenergy, prediction;

         // Rating calculations for magnitude, potency, and energy
         if (magnitude < 0.5)
         {
            Ratingmagnitude = 1;
         }
         else if (magnitude >= 0.5 && magnitude < 1.5)
         {
            Ratingmagnitude = 2;
         }
         else if (magnitude >= 1.5 && magnitude < 2.5)
         {
            Ratingmagnitude = 3;
         }
         else
```

```
{
   Ratingmagnitude = 4;
}

if (potency < 0.6)
{
   Ratingpotency = 1;
}
else if (potency >= 0.6 && potency < 1.4)
{
   Ratingpotency = 2;
}
else if (potency >= 1.4 && potency < 2.2)
{
   Ratingpotency = 3;
}
else
{
   Ratingpotency = 4;
}

if (energy < 2.2)
{
   Ratingenergy = 1;
}
else if (energy >= 2.2 && energy < 5.6)
{
   Ratingenergy = 2;
}
else if (energy >= 5.6 && energy < 9)
{
   Ratingenergy = 3;
}
else
{
   Ratingenergy = 4;
}

prediction = Ratingmagnitude + Ratingpotency + Ratingenergy;

string predictionText;
if (prediction < 3)
{
   predictionText = "" + prediction;
}
else if (prediction == 3)
{
   predictionText = "No damage ";
}
else if (prediction >= 4 && prediction < 7)
{
```

```
        predictionText = "Minor";
    }
    else if (prediction >= 7 && prediction < 10)
    {
        predictionText = "Moderate ";
    }
    else if (prediction >= 10 && prediction < 13)
    {
        predictionText = "Strong ";
    }
    else
    {
        predictionText = "Extra Strong " + prediction;
    }

    double predictionText2;
    predictionText2 = prediction;


    stopwatch.Stop();
    labelExecutionTime.Text = "" + stopwatch.ElapsedMilliseconds + " ms";
    labelResult.Text = predictionText;
    TotalRatingText.Text = "" + predictionText2;
}

private void Form1_Load(object sender, EventArgs e)
{

}

private void labelResult_Click(object sender, EventArgs e)
{

}

private void labelResult_Click_1(object sender, EventArgs e)
{

}

private void button2_Click(object sender, EventArgs e)
{
    textBoxMagnitude.Clear();
    textBoxPotency.Clear();
    textBoxEnergy.Clear();
    EventNumberBox.Clear();
    EventDateBox.Clear();
    XBox.Clear();
    YBox.Clear();
    ZBox.Clear();
```

```
            labelResult.Text = "";
            labelExecutionTime.Text = "";
            TotalRatingText.Text = "";
        }

        private void labelExecutionTime_Click(object sender, EventArgs e)
        {

        }
    }
}
```

Appendix C.1: C++ code for G_RPT

```
#include <iostream>
using namespace std;
//Welcome to Geotechnical Based Rockburst Prediction Tool(G_RPT)
//This program predicts damage class based on the total ratings assigned to Geotechnical Parameters
//VARIABLE DECLARATION
double TensileStrength, TangentialStress, ElasticEnergy, PrincipalStress, quality, stress, prediction;
double RatingTensileStrength, RatingTangentialStrength, RatingElasticEnergy;
double RatingQuality, RatingStress, RatingPrincipalStress, Ratingprediction;
//MAIN PROGRAM
int main(){
    cout<< "Enter "<< endl;
   cin>> quality;
   cout<< "Enter Compressive Stress"<< endl;
   cin>> stress;
   cout<< "Enter Tensile Strength"<< endl;
   cin>> TensileStrength;
   cout<< "Enter Tangential Stress"<< endl;
   cin>> TangentialStress ;
   cout<< "Enter Linear Elastic Energy)"<< endl;
   cin>> ElasticEnergy;
   cout<< "Enter Principal Stress"<< endl;
   cin>> PrincipalStress;

   //COMPRESSIVE STRENGTH
   if(stress<74){
      RatingStress=1;
               } else if(stress>=74 && stress<202){
                 RatingStress=2;
                                        }
                          else if(stress>=202 && stress<330){
                          RatingStress=3;
                                                 }
```

```
                    else if(stress>=330){
                    RatingStress=4;
                                }
//ROCK QUALITY
if(quality<60){
    RatingQuality=1;
          } else if(quality>=60 && quality<74){
           RatingQuality=2;
                 }
                else if(quality>=74 && quality<88){
                RatingQuality=3;
                      }
                    else if(quality>=88 && quality<=1000){
                    RatingQuality=4;
                    }
 //TENSILE STRENGTH
  if(TensileStrength<6.5){
    RatingTensileStrength=1;
          } else if(TensileStrength>=6.5 && TensileStrength<18.5){
           RatingTensileStrength=2;
                      }
                else if(TensileStrength>=18.5 && TensileStrength<30.5){
                RatingTensileStrength=3;
                          }
                    else if(TensileStrength>=30.5){
                    RatingTensileStrength=4;
                    }
  //TANGENTIAL STRESS
  if(TangentialStress<37){
    RatingTangentialStrength=1;
          } else if(TangentialStress>=37 && TangentialStress<101){
           RatingTangentialStrength=2;
                      }
                else if(TangentialStress>=101 && TangentialStress<165){
```

```
                    RatingTangentialStrength=3;
                                        }
                                else if(TangentialStress>=165){
                                RatingTangentialStrength=4;
                                }
      //LINEAR ELASTIC ENERGY
   if(ElasticEnergy<5.1){
     RatingElasticEnergy=1;
            } else if(ElasticEnergy>=5.1 && ElasticEnergy<5.9){
              RatingElasticEnergy=2;
                                        }
                     else if(ElasticEnergy>=5.9 && ElasticEnergy<6.4){
                    RatingElasticEnergy=3;
                                        }
                                else if(ElasticEnergy>=6.4){
                                RatingElasticEnergy=4;
                                }
    //PRINCIPAL STRESS
   if(PrincipalStress<19){
     RatingPrincipalStress=1;
            } else if(PrincipalStress>=19 && PrincipalStress<26){
              RatingPrincipalStress=2;
                                        }
                     else if(PrincipalStress>=26 && PrincipalStress<32){
                    RatingPrincipalStress=3;
                                        }
                                else if(PrincipalStress>=32){
                                RatingPrincipalStress=4;
                                }
//RESULT
 prediction                                                                                    =
RatingElasticEnergy+RatingPrincipalStress+RatingQuality+RatingStress+RatingTange
ntialStrength+RatingTensileStrength;
if(prediction<6){
      cout << "Rockburst prediction is No damage: " << prediction << endl;
            } else if(prediction>=6 && prediction<15){
              cout << "Rockburst prediction is weak: " << prediction << endl;
                                        }
                     else if(prediction>=15 && prediction<20){
                     cout << "Rockburst prediction is Moderate: " << prediction <<
endl;
                                                }
                                else if(prediction>=20 && prediction<24){
                                cout << "Rockburst prediction is Strong: " <<
prediction << endl;
                                                        }
                                        else if(prediction>=24){
```

```
                                        cout << "Rockburst prediction is Extra Strong:
" << prediction << endl;
                                                }
    return 0;
}
```

Appendix C.2: GUI Code for G_RPT

```
using System;
using System.Diagnostics;
using System.Windows.Forms;
namespace GeotechnicalRockburstPredictionApp12
{
   public partial class Form1 : Form
   {
      public Form1()
      {
         InitializeComponent();
      }
      private double CalculateRating(double value, double range1, double range2,
double range3, double range4)
      {
         if (value < range1)
         {
            return 1;
         }
         else if (value >= range1 && value < range2)
         {
            return 2;
         }
         else if (value >= range2 && value < range3)
         {
            return 3;
         }
         else if (value >= range3 && value <= range4)
         {
            return 4;
         }
         else
         {
            return 0;
         }
      }
      private void button1_Click(object sender, EventArgs e)
      {
      }
      private void button1_Click_1(object sender, EventArgs e)
      {
         Stopwatch stopwatch = new Stopwatch();
         stopwatch.Start();
         if (!double.TryParse(textBoxQuality.Text, out double quality) ||
            !double.TryParse(textBoxStress.Text, out double stress) ||
            !double.TryParse(textBoxTensile.Text, out double tensileStrength) ||
            !double.TryParse(textBoxTangential.Text, out double tangentialStress) ||
```

```
            !double.TryParse(textBoxElasticEnergy.Text, out double elasticEnergy) ||
            !double.TryParse(textBoxPrincipal.Text, out double principalStress))
        {
            MessageBox.Show("Invalid input. Please enter valid numeric values.", "Input
Error", MessageBoxButtons.OK, MessageBoxIcon.Error);
            return;
        }
        double ratingQuality = CalculateRating(quality, 60, 74, 88, 1000);
        double ratingStress = CalculateRating(stress, 74, 202, 330, double.MaxValue);
        double ratingTensileStrength = CalculateRating(tensileStrength, 6.5, 18.5, 30.5,
double.MaxValue);
        double ratingTangentialStrength = CalculateRating(tangentialStress, 37, 101,
165, double.MaxValue);
        double ratingElasticEnergy = CalculateRating(elasticEnergy, 5.1, 5.9, 6.4,
double.MaxValue);
        double ratingPrincipalStress = CalculateRating(principalStress, 19, 26, 32,
double.MaxValue);
        double totalRating = ratingQuality + ratingStress + ratingTensileStrength +
ratingTangentialStrength + ratingElasticEnergy + ratingPrincipalStress;
        string predictionText;
        if (totalRating == 6)
        {
            predictionText = "No damage";
        }
        else if (totalRating > 6 && totalRating < 15)
        {
            predictionText = "Minor";
        }
        else if (totalRating >= 15 && totalRating < 20)
        {
            predictionText = "Moderate";
        }
        else if (totalRating >= 20 && totalRating < 24)
        {
            predictionText = "Strong";
        }
        else
        {
            predictionText = "Extra Strong";
        }
        double predictionText2;
        predictionText2 = totalRating;

        stopwatch.Stop();
        labelExecutionTime.Text = "" + stopwatch.ElapsedMilliseconds + " ms";
        labelResult.Text = predictionText;
        TotalRatingText.Text = "" + totalRating;
```

```
        }
        private void buttonClear_Click(object sender, EventArgs e)
        {
        }
        private void Form1_Load(object sender, EventArgs e)
        {
        }
        private void label12_Click(object sender, EventArgs e)
        {
        }
        private void label13_Click(object sender, EventArgs e)
        {
        }
        private void button2_Click_1(object sender, EventArgs e)
        {
            // Clear button click logic
            textBoxQuality.Clear();
            textBoxStress.Clear();
            textBoxTensile.Clear();
            textBoxTangential.Clear();
            textBoxElasticEnergy.Clear();
            textBoxPrincipal.Clear();
            DataSetBox.Clear();
            DateBox.Clear();
            XBox.Clear();
            YBox.Clear();
            ZBox.Clear();
            labelResult.Text = "";
            labelExecutionTime.Text = "";
            TotalRatingText.Text = "";
        }
    }
}
```